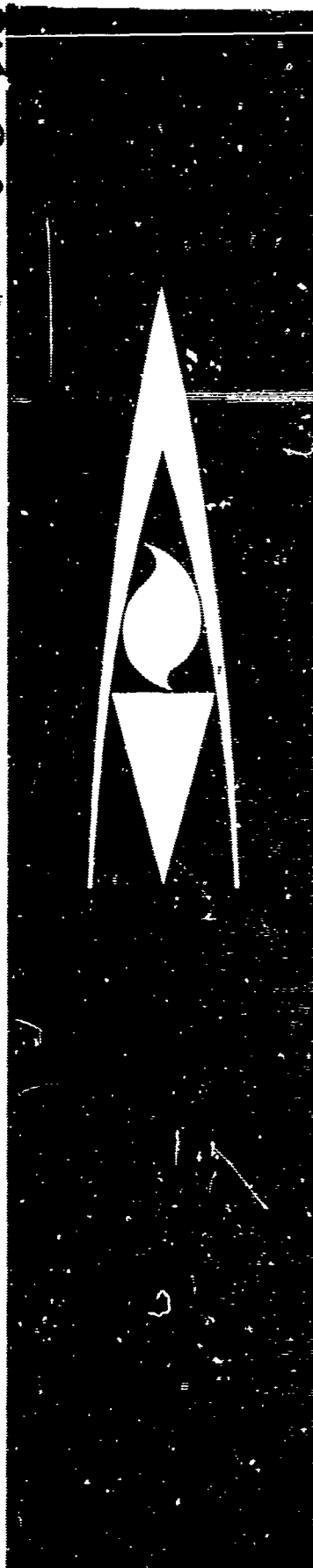
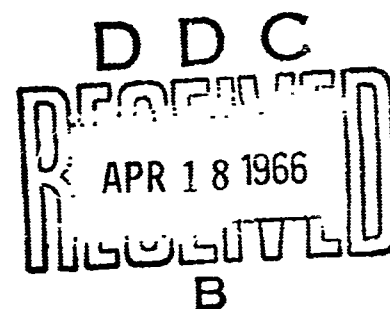


AD630932



FINAL REPORT
DEVELOPMENT OF THE FRANGIBLE ARCAS
METEOROLOGICAL ROCKET VEHICLE

G. K. OSS



Contract No. AF 19(628)-4033
 Project No. 6670
 Task No. 667003

April 1964 — December 1965

Prepared for:
 Air Force Cambridge Research Laboratories
 Office of Aerospace Research
 United States Air Force
 Bedford, Massachusetts

15 February 1966

Atlantic Research Corporation
 Shirley Highway at Edsall Road
 Alexandria, Virginia

ATLANTIC RESEARCH
 CORPORATION

CLEARINGHOUSE
 FOR FEDERAL SCIENTIFIC AND
 TECHNICAL INFORMATION

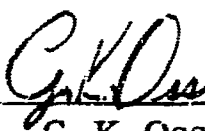
Hardcopy 27738

Microfiche

1,25 247,00

ARCHIVE COPY Code 1

FINAL REPORT
DEVELOPMENT OF THE FRANGIBLE ARCAS
METEOROLOGICAL ROCKET VEHICLE

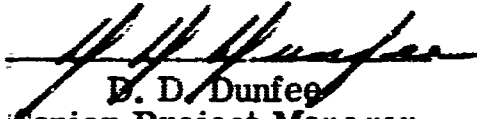

G. K. Oss
Project Manager
Sounding Rocket Systems

For:
Air Force Cambridge Research Laboratories
Office of Aerospace Research
United States Air Force
Bedford, Massachusetts

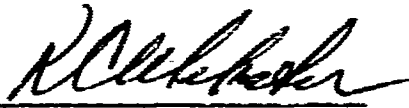
Contract AF 19(628)-4033
Project 6670
Task 67003

April 1964 - December 1965

Approved by:


B. D. Dunfee
Senior Project Manager
Sounding Rocket Systems

Approved by:


R. C. Webster
Head, Project Management Group
Production Division

Atlantic Research Corporation
Shirley Highway at Edsall Road
Alexandria, Virginia

15 February 1966

FOREWORD

This final technical report on the development of the Frangible ARCAS rocket vehicle system summarizes the efforts of Phase III of a three-phase program to develop and demonstrate the feasibility of a frangible meteorological rocket vehicle through systems flight test evaluation. This report is submitted pursuant to the requirements of Contract No. AF 19(628)-4033, dated 15 April 1964, under which the program was conducted for the Air Force Cambridge Research Laboratories, Office of Aerospace Research.

Phases I and II, development of the glass filament wound motor case and other major systems components, were conducted under the Bureau of Naval Weapons Contract NOw 62-1106-c between September 1962 and March 1963. These phases were documented in Progress Reports 1 through 5 entitled "Qualification, Documentation, Development and Delivery of EX 6 ARCAS Systems." Phase III, conducted between April 1964 and December 1964, is documented in monthly Progress Reports 1 through 16 entitled "Frangible ARCAS Meteorological Rocket Feasibility Program."

The author acknowledges the sincere cooperation of those individuals who contributed to the successful completion of the Frangible ARCAS program including Messrs. Robert Leviton, John Wright, George McLean and USAF Captain Thomas Smith of AFCRL, Dr. Thomas C. Poulter of Stanford Research Institute and personnel of the Pacific Missile Range, as well as numerous members of the Atlantic Research Corporation organization.

ABSTRACT

Development of the Frangible ARCAS vehicle and its explosive fragmentation system were successfully completed and demonstrated during this program. Of the seven static firings conducted with the flight design rocket motor during Phase III, all were successful. Two of these static tests included successful fragmentation of the spent rocket motor assembly to particle sizes yielding impact kinetic energy levels well below the 10 ft-lb limit specified for the program. Impact kinetic energy levels less than 3.0 ft-lb were achieved using an unshaped explosive charge in the forward section of the vehicle and 0.042-inch-thick sheet explosive overwrap. Further analysis of the system showed that fragmentation to levels of 1.5 ft-lb or less could be achieved using the same explosive configuration with only minor modification of the nozzle section.

The program included four flight tests. Two Frangible ARCAS vehicles, less the fragmentation system, were successfully flight tested at the Pacific Missile Range with a telemetry payload designed to monitor motor case skin temperatures during flight. These two diagnostic flight tests established the motor case skin temperature profile required to finalize the explosive fragmentation system design, demonstrated successful aerodynamic performance of the basic vehicle and allowed determination of a characteristic drag curve for the vehicle configuration using actual flight test data.

The first systems flight test vehicle was launched May 1965 and considered a 'No Test' because of a malfunction of the PMR modified launcher. After considerable postponement because of adverse weather conditions at the launch site, the program was concluded with the successful flight test of the second and final systems vehicle in December 1965. The major objective of the program was achieved with this successful flight test. All systems functioned as programmed and fragmentation was experienced subsequent to payload deployment at apogee, thereby demonstrating the feasibility of a frangible meteorological rocket system.

TABLE OF CONTENTS

	<u>Page</u>
FOREWORD	ii
ABSTRACT	iii
INTRODUCTION	vi
 I. VEHICLE SYSTEMS DESIGN AND DEVELOPMENT .	 1
A. Vehicle Description	1
B. Sequence of Events	2
C. Vehicle Design and Development	3
Rocket Motor Development	3
Fin Assembly	5
Dimple Motor	6
Payload Section	6
Payload Separation Gas Generator	7
Mechanical Timer	8
Redundant Initiator	10
 II. FRAGMENTATION SYSTEM DEVELOPMENT	 12
A. Initial Fragmentation Tests	12
B. Determination of Particle Free-Fall Drag Coefficients	14
C. Determination of Impact Kinetic Energy	15
D. Fragmenting Module Concept	17
E. Shock Tube Technique	19
F. Modular Charge/External Explosive Technique	20
G. Final Configuration	21
External Explosive Retention	23
H. Firing Train Development	23
I. Static Firing/Fragmentation Systems Test	25
Abbreviated Systems Test	26
 III. VEHICLE FINAL ASSEMBLY AND LAUNCH	 26
IV. VEHICLE STATIC AND DYNAMIC STABILITY	27

TABLE OF CONTENTS (Continued)

	<u>Page</u>
V. WIND WEIGHTING AND DISPERSION.	28
VI. DIAGNOSTIC FLIGHT TESTS.	29
A. Diagnostic Payload.	29
B. Flight Test Results.	30
C. Temperature Data	31
VII. SYSTEMS FLIGHT TESTS	33
A. Payload	33
B. Flight Test Results.	34
VIII. VEHICLE NOMINAL FLIGHT PERFORMANCE	35
IX. PROPOSED MODIFICATIONS FOR IMPROVED PERFORMANCE	36
A. Propellant Substitution	37
X. CONCLUSIONS.	38
LIST OF SYMBOLS.	40
LIST OF TABLES.	41
LIST OF FIGURES	42
APPENDIX I - Longitudinal Acceleration Effects on the Redundant Initiator	
APPENDIX II - Analysis of the Dynamic Pressure Effects of the Redundant Initiator Pressure Sensing Mechanism During Vehicle Descent	
APPENDIX III - Frangible ARCAS Flight Performance Analysis (Diagnostic Vehicles)	
APPENDIX IV - Frangible ARCAS Flight Test Results (Systems Vehicles)	

INTRODUCTION

Today's understanding of the structure and state of the earth's atmosphere is the result of major developments in synoptic meteorology. All major advances in this science have resulted from technological breakthroughs and discoveries attending observation. The continuing growth of the meteorological network has introduced the foreseeable requirement for a new development in meteorological rocket technology; namely, the ability to carry instrumented payloads to altitudes of approximately 60 kilometers over semi-populated geographical areas without inducing undue hazards to human life and property by the spent rocket vehicle or related falling objects.

Atlantic Research Corporation began investigation of the feasibility of a frangible vehicle concept to satisfy these requirements in September 1962 under Bureau of Naval Weapons Contract NOW 62-1106-c. This approach to the problem consists of fragmenting the spent rocket vehicle assembly, subsequent to payload ejection, to sufficiently small particle sizes to provide very low impact kinetic energy. The required fragmentation is achieved by means of an explosives system contained as an integral part of the vehicle. Development of the vehicle, designated Frangible ARCAS, continued through March 1963 and encompassed the development of most of the rocket motor hardware and vehicle subsystems. Program funding was expended, however, without the opportunity to evaluate the proposed fragmentation concepts.

Additional funding was made available in April 1964 by the Air Force Cambridge Research Laboratories, Office of Aerospace Research, under Contract No. AF 19(628)-4033 to continue the Frangible ARCAS development work which began in September 1962. The primary objective of the Frangible ARCAS program was to demonstrate the feasibility of a frangible meteorological rocket system comparable in performance to the standard ARCAS vehicle, but capable of self-induced fragmentation during flight subsequent to payload ejection. The degree of frangibility to be demonstrated by this program was specified as an impact kinetic energy of 10 ft-lb or less for the fragmented pieces at their terminal velocity. It should be noted,

however, that the magnitude of 10 ft-lb of kinetic energy at impact was arbitrarily selected for the purposes of this program and is not to be interpreted as a lethal impact energy limit.

The design approach originally selected during this program to achieve the required fragmentation capability was that of a single modular charge to be located in the forward section of the rocket vehicle. This approach was selected because of the advantages afforded by its simplicity, but program activities were designed to allow modification of this fragmentation approach in the event that test results indicated the need for relocation or addition of explosive material to achieve fragmentation within the specified limits. Subsequent testing and evaluation of the single modular charge showed the inability to fragment the center section of the motor case. Additional tests incorporating external placement of linear shaped charge and sheet explosive material showed improved fragmentation of the rocket assembly, with sheet explosive providing fragmentation well below the 10 ft-lb impact kinetic energy level. Program efforts, beginning in August 1964, were directed primarily toward the testing and evaluation of externally placed sheet explosive material in combination with a primary explosive charge in the forward section of the rocket motor. The same concept utilizing linear shaped charge in lieu of sheet explosive was evaluated as a backup, but the sheet explosive material was found to provide better fragmentation.

This final report presents a characterization of the Frangible ARCAS vehicle and a comprehensive summary of the development of the rocket vehicle, its performance, stability and flight test results. The report emphasizes the development of the fragmentation system, a major objective and requirement of the program.

FINAL REPORT
DEVELOPMENT OF THE EX 6 MOD 3 FRANGIBLE
ARCAS METEOROLOGICAL ROCKET VEHICLE

I. VEHICLE SYSTEMS DESIGN AND DEVELOPMENT

The Frangible ARCAS vehicle design was based largely on the design of the standard ARCAS vehicle since its performance was to be comparable. The vehicle, therefore, essentially constituted a redesign of the standard ARCAS unit to provide lightweight components to maximize vehicle performance and provide structures susceptible to explosive fragmentation. The development of most of these components and subsystems was completed during Phases I and II of the program. The efforts expended during Phase III of the program were directed primarily toward completion of component development, development of the fragmentation system and flight test evaluation of the vehicle.

A. VEHICLE DESCRIPTION

The Frangible ARCAS rocket vehicle, shown on Figure 1, incorporates a glass filament wound motor case, an integral canister magnesium fin assembly and the standard ARCAS propellant grain, igniter and nose cone. The solid propellant grain configuration provides thrust over a relatively long period of time and thus minimizes acceleration loads. The end-burning technique provides a greater degree of conversion of rocket thrust into vehicle velocity because a greater portion of the thrust is generated in a less-dense region of the atmosphere and results in lower drag losses. Because of the higher loading density, this technique also provides the smallest vehicle for a given performance requirement and permits the use of a slender rocket which provides relatively low aerodynamic drag.

The unit contains an explosive charge between the rocket motor headplate which is initiated by a mechanical timer unit at a time predetermined and set prior to launch. Initiation of the primary explosive charge

subsequent to payload ejection results in fragmentation of the forward section of the spent rocket motor assembly and induces sympathetic detonation of the 0.042-inch-thick sheet explosive material attached to the exterior of the motor case. Detonation propagation of the sheet explosive provides fragmentation of the motor case and fin assembly. Full-scale static firing/fragmentation tests conducted during the program provided fragmentation of the rocket motor assembly to impact kinetic energy levels of less than 10 ft-lb.

A photographic description of the Frangible ARCAS vehicle is presented on Figure 2. A comparison of the Frangible ARCAS vehicle with the standard ARCAS is presented by the photograph on Figure 3 and comparative dimensional and weight data are presented on Table I. A detailed weight breakdown of the Frangible ARCAS systems vehicle, less payload, is shown in Table II.

B. SEQUENCE OF EVENTS

The sequence of events from launch through fragmentation are outlined as follows in the order in which they occur. Upon launch, the rocket motor provides a sustained thrust for a period of approximately 30 seconds. As the propellant is consumed, a dimple motor incorporated in the headplate is exposed to the hot propellant gases in the rocket chamber during about the last one-half second of burning. Upon experiencing an elevated temperature, a pyrotechnic material contained in the core of the dimple motor tube provides sufficient pressure to form a convex dimple at the forward end of the tube. This movement imparted by the dimple motor is transmitted by a push rod to the mechanical timer unit which is preset to eject the payload at apogee by means of a gas generating cartridge activated by the timer unit. At a fixed time interval of 20 seconds after payload ejection, the primary firing mechanism, incorporated in the mechanical timer unit, initiates fragmentation of the spent rocket vehicle. In the event that a failure is experienced with the primary fragmentation initiation system, a secondary, independent initiator armed and activated by changes in atmospheric pressure will initiate fragmentation.

The vehicle flight events sequence is presented by the illustration on Figure 4.

C. VEHICLE DESIGN AND DEVELOPMENT

Of primary importance during development of the various rocket components was the maintenance of lightweight structures to maximize vehicle performance and provide components susceptible to explosive fragmentation. Presented below is a comprehensive summary of the development of the major vehicle components.

Rocket Motor Development

The Frangible ARCAS rocket motor incorporates a glass filament wound motor case containing a tapered Tayloron 5031* insulator, the standard ARCAS graphite throat insert with Tayloron PA-6* backup insulation, a laminated fiberglass headplate and the standard ARCAS propellant grain and igniter. An illustration of the rocket motor assembly is presented on Figure 5. Development of the lightweight fiberglass motor case was completed during Phase II of the program, during which time static firings of the motor at -50 and +130°F were successfully completed.

Since the standard ARCAS propellant grain and throat insert are incorporated in the rocket motor design, the internal ballistic performance is not changed. The design parameters and nominal performance ratings of the rocket motor at an operating temperature of 70°F are summarized below.

Nozzle Throat Area, in ²	0.197
Nozzle Exit Area, in ²	2.550
Expansion Ratio	13
Average Chamber Pressure, psia	975
Average Thrust, lb	325
Maximum Chamber Pressure, psia	1080
Maximum Thrust, lb	360
Total Impulse, lb-sec	9400
Burning Time, sec	30

* Taylor Corporation.

A nominal thrust-time curve is presented on Figure 6.

Development of an igniter for the rocket motor was precluded by using the standard ARCAS igniter. This pyrotechnic igniter incorporates 5.0 grams of ignition composition which is initiated by a 1.0 amp - no-fire . 3.5 amp - all-fire 105A squib. The standard igniter resistance is 1.0 to 1.3 ohms.

Although the motor case was developed during Phase II of the program, additional static firings of the rocket motor were conducted during Phase III to evaluate surface temperatures resulting from heat transfer through the motor case wall. The requirement for these data were foreseen in the event that external placement of explosive material was needed to effect adequate fragmentation of the rocket assembly. Seven static firings of the flight design filament wound motor case were successfully completed during Phase III of the program in as many attempts. A static firing summary is presented on Table III.

Motor case skin temperatures were monitored during two of the static firings for 150 seconds after motor ignition, which was the predicted flight time prior to fragmentation. The thermocouple locations and temperature data for the two tests, AFST-11 and AFST-12, are presented on Figures 7 and 8, respectively. As observed from these data, the greatest effect of internal motor temperatures on the motor case skin, due to heat transfer through the wall, was experienced subsequent to motor burning. The change in skin temperature along the length of the motor case at various times from rocket motor burnout to the approximate time of fragmentation is shown on Figure 9. These temperature data proved beneficial during development of the fragmentation system. A comparison of motor case skin temperatures during flight with the static firing temperature data also allowed a determination of the aerodynamic heating contribution to the vehicle temperature profile in flight.

The rocket motor headplate was redesigned during Phase III of the program, providing for a significant reduction in inert weight. This

weight reduction was accomplished by decreasing the flange thickness forward of the O-ring groove and "dishing" the headplate as illustrated in Figure 10. The inert weight was reduced from 1.25 pounds to 0.75 pound, representing a weight reduction of 40 per cent.

Since the headplate was designed to house a dimple motor which is activated by rocket motor flame temperature near motor burnout in order to start the mechanical timer, laboratory pressure tests were conducted to determine maximum headplate deflection as well as the structural integrity of the component. Although the maximum chamber pressure that is experienced under normal operating conditions with a 110° F firing temperature is 1350 psia, the headplate was pressurized to 2000 psig to determine structural integrity. A plot of maximum headplate deflection as a function of test pressure is presented on Figure 11. Although the weight reduction achieved by the Phase III design resulted in about twice the deflection as the original design, the magnitude of deflection (0.017 inch at 1350 psig) was acceptable for design purposes.

The headplate was also designed to provide a mechanical interlock with the propellant grain assembly by means of an overwrap of the propellant inhibitor as illustrated on Figure 12. This method of propellant retention proved highly successful in the Sparrow-HV ARCAS vehicle and provides potential growth for the system. Laboratory tests show this configuration to be capable of withstanding about 80g longitudinal acceleration at 70° F before yielding. This propellant retention system has also been successfully employed in the standard ARCAS vehicle.

Fin Assembly

The Frangible ARCAS fin assembly is an integral canister design manufactured of magnesium alloy. This single unit, hollow fin assembly is attached to the rocket motor case by six socket head cap screws as shown in Figure 13. The fin design consists of four conventional double-wedge blades with a 55° swept leading edge providing a total fin area of 119 in². The assembly is manufactured by forming the blades in four quarter section panels

which are subsequently welded together along each leading edge, tip and trailing edge to form a single, fixed cant fin assembly. The primary advantage of this type of fin construction is that the blades are pre-set for a particular roll rate which precludes the necessity of fin alignment during rocket motor assembly.

The Frangible ARCAS fin assembly was adapted to a standard ARCAS vehicle and successfully flight tested at Eglin Air Force Base in April 1963. This fin assembly was later successfully flight tested on the Frangible ARCAS diagnostic and systems vehicles at the Pacific Missile Range during Phase III of the program.

Dimple Motor

Development of the heat-activated dimple motor was accomplished at Atlantic Research Corporation's Flare-Northern Division. This device was designed to initiate the mechanical timer unit by means of an expanding dimple chamber upon sensing burnout of the rocket motor.

A total of sixteen dimple motors of the final design configuration have been tested under conditions that permitted post-test evaluation. Of these units tested, only one failed to initiate. This failure resulted from an insulating coating of epoxy on the pin. All other units performed successfully. The dimple motor configuration is shown on Figure 14. A post-test photograph showing five dimple motors in the expanded position is shown on Figure 15.

Payload Section

The payload section consists of a parachute container, which houses the parachute and serves as the forward portion of the vehicle air frame, and the standard ARCAS secant ogive nose cone. This assembly is essentially the same as that of the standard ARCAS vehicle except that the parachute assembly was modified to incorporate a nylon lanyard, a leather aft closure and relocation of the lanyard attachment point. These design changes were effected to substitute components in the parachute assembly that would perform the same function, but be more likely to provide low kinetic energy levels upon impact.

The parachute is prepacked in a split fabric bag contained within an outer aluminum barrel. The outer container is attached to the forward section of the primary module/retaining sleeve assembly. The nose cone, with an interlocked instrument base plate, is connected to the forward parachute closure which is secured in the barrel by three aluminum shear pins. Separation is accomplished by expelling the inner parachute assembly from the barrel by piston action created by a gas generating cartridge. This design, illustrated on Figure 16, was successfully tested in conjunction with the separation device.

Payload Separation Gas Generator

The Frangible ARCAS payload separation device is a pyrotechnic gas generating cartridge which is activated by a mechanical timer unit which initiates a percussion primer. A sectioned view of the gas generator is shown on Figure 17. The cartridge contains a charge of boron potassium nitrate pellets and has successfully ejected full-scale parachute assemblies with a simulated payload weight attached. The pressure-time trace produced by this gas generator in the free volume behind the payload is presented on Figure 18 in comparison with that of the standard ARCAS vehicle pyrogen generator system. As evidenced by this comparison, the maximum expulsion pressure experienced with the Frangible ARCAS cartridge is considerably lower than that of the standard ARCAS generator. This difference is attributed to the greater initial free volume in the Frangible ARCAS configuration. Although the magnitude of acceleration experienced during payload ejection has not been monitored with the Frangible ARCAS system, the resulting pressure-time history indicates that the shock loads experienced are less than those experienced with the standard ARCAS vehicle. It should be noted, however, that the reduced pressure peak also results in a decreased payload ejection velocity. The Frangible ARCAS system imparts a relative velocity of about 35 to 40 ft/sec to the payload as compared to about 55 ft/sec for the standard ARCAS system. The parachute ejection tests conducted during the program and previous ARCAS history, however, show that this velocity increment is sufficient for successful parachute deployment.

A pyrogen gas generator incorporating the standard ARCAS propellant grain, Figure 19, was successfully tested during this program. Although the unit performed well, the relatively heavy wall required for this generator was not susceptible to fragmentation and it was dropped from further consideration.

Mechanical Timer

The Frangible ARCAS mechanical timer unit, shown on Figure 20, was developed by Raymond Engineering Laboratory, Inc., Middletown, Connecticut. The purpose of the mechanical timer is to provide two important functions during the flight of the vehicle: (1) to activate the pyrotechnic gas generating cartridge at a preselected time for the purpose of ejecting the payload, and (2) to initiate the fragmentation explosive system 20 seconds after payload ejection.

Selection of a time subsequent to payload ejection for initiation of the fragmentation system was based on two factors: (1) allowance of enough time to permit the payload and spent rocket vehicle to become sufficiently separated so that fragmentation could be effected without incurring damage to the payload, and (2) design considerations for a redundant initiating mechanism to provide high systems reliability. An analysis was performed to determine a timer setting after payload ejection that would provide sufficient distance between the payload and vehicle at the time of fragmentation to prevent payload damage. Radar data from standard ARCAS flight incorporating Arcasonde payloads were used to establish a payload descent trajectory. By superimposing this trajectory profile on the predicted descent trajectory of the spent vehicle at various launch angles, it was possible to predict the distance between the two bodies at any time after payload ejection (apogee). A comparison of these data showed that a time interval of 20 seconds after payload ejection provided a separation distance of about 0.75 mile at the higher launch elevation angles as shown on Figure 21. The distance between the objects was found to increase to about 1.8 miles at a launch angle of 84° as

shown on Figure 22. This separation distance was considered adequate and thus constituted the selection of the 20-second time interval between payload ejection and fragmentation. The predicted distance between the payload and spent rocket at 20 seconds after payload ejection for various effective launch angles is shown by the graph on Figure 23. This inverse relationship between separation distance and elapsed time after payload separation was observed to be nearly linear beginning at about 86° QE and the distance between the bodies at the time of fragmentation is increased about 0.5 mile/degree decrease in launch angle below that point.

Because of the nature of the system and the functions required of the mechanical timer, several safety features were included in the unit as described below:

1. A manual safing pin was incorporated in the unit to prevent either function from occurring until its removal. Removal of this pin, which must be accomplished prior to installation of the payload, provides a commit-to-arm condition for the primary firing system which will initiate the fragmentation explosive charges.
2. A visual Safe/Arm indicator is provided to show the position of the primary firing train in the timer unit upon removal of the manual safing pin. This indicator is visible until the payload is installed.
3. A time-integrating Safe/Arm mechanism is incorporated in the firing system of the timer unit. This device consists of an acceleration sensing element designed to require 15g to 20g longitudinal acceleration for a period of 0.100 to 0.140 second in order for the rotor arm housing the initiating detonator to move to the in-line position. These conditions of longitudinal acceleration will permit the primary fragmentation system firing unit to become armed as the vehicle is ejected from the launcher.

The units incorporated in the final flight tests were subjected to shock and vibration tests to verify that the units would not become armed or actuated by these conditions. The results of these are presented on Table IV.

Redundant Initiator

Because of the reliability required with the fragmentation system, a secondary fragmentation initiation device was developed by the Space/Arm Division of Wallace O. Leonard Corporation, Pasadena, California. This unit was designed to become armed and initiate fragmentation by sensing changes in atmospheric pressure and is independent of all other systems aboard the vehicle.

Details of the redundant, pressure sensing initiator unit are shown by the illustration in Figure 24. The unit was designed to become armed at an ambient pressure equivalent to an altitude of 70,000 to 100,000 feet during vehicle ascent and initiate fragmentation at a pressure equivalent to an altitude of 50,000 to 70,000 feet during vehicle descent by means of an expanding bellows. This system allows fragmentation initiation by the pressure sensing unit only in the event of a failure of the mechanical timer mechanism. The minimum fragmentation altitude of 50,000 feet was selected in order to stay above the altitude levels currently used by commercial and most military aircraft.

The redundant initiator unit was designed to incorporate the following safety features:

1. A manual safing pin must be removed in order to allow the unit to initiate fragmentation. The pin was designed such that it could not be removed if the firing pin had been prematurely released.
2. The unit must experience the required pressure cycling to function.

The units were subjected to environmental testing to determine the effect of shock, vibration, etc., on the function of the unit. All units functioned within the prescribed pressure limits after all phases of the environmental test program. Test results are presented on Tables V and VI.

An analysis was performed by the manufacturer of the redundant initiator unit to determine the effect of high longitudinal acceleration loads on the unit. This analysis, presented in Appendix I, showed that a steady state acceleration of 245g is required to displace the arming system from the safe position and that a steady state acceleration of 330g would be required to arm the mechanism. Since the maximum longitudinal acceleration normally experienced during the operation of the Frangible ARCAS vehicle is only about 125g (during ejection from the closed breech launcher), the unit cannot be inadvertently armed by the acceleration loads imposed during its launch or flight.

An analysis of the dynamic pressure effects on the redundant initiator pressure sensing mechanism during vehicle descent was performed because of the vehicle attitudes that are encountered subsequent to payload ejection. The gyroscopic stabilizing effect induced by the vehicle burnout roll rate (Figure 25) in combination with the instability induced by loss of the forward vehicle weight upon ejection of the payload results in a tumbling motion of the spent vehicle during its descent. Since the sensing of dynamic pressure cannot be distinguished from ambient pressure by the redundant sensing element, it was important to determine the resulting effect of dynamic pressure upon the system. The results of this analysis, presented in Appendix II, showed that the effects of dynamic pressure would increase the altitude at which fragmentation by the redundant initiator is experienced from a nominal altitude of 60,000 feet to about 90,000 feet. The analysis also showed that the maximum possible altitude at which fragmentation could be effected by the redundant unit during vehicle descent (under pure dynamic pressure conditions) was 112,000 feet.

Although this analysis showed that the altitude at which fragmentation was likely to occur was increased by the effects of dynamic pressure, the limits of 112,000 feet maximum to 50,000 feet minimum did not interfere with the operation of the primary fragmentation system and provided a minimum altitude sufficiently high to avoid safety hazards to aircraft, etc. Since there

was no apparent reason for reducing the fragmentation altitude limits, the design was considered adequate regardless of the dynamic pressure effects.

II. FRAGMENTATION SYSTEM DEVELOPMENT

The major effort of the program was the development of an explosive fragmentation system capable of reducing the spent rocket vehicle to particle sizes yielding impact kinetic energies of 10 ft-lb or less. The necessity of maintaining lightweight components and minimizing vehicle drag while requiring fragmentation of the entire assembly imposed stringent requirements upon the design of the system. Because of the effect of externally placed components on the vehicle drag and the possible effect of aerodynamic heating on the component, the most desirable approach to the problem of fragmentation was that of a system wholly contained within the vehicle. In view of the possible difficulties foreseeable with such a system, however, the ultimate use of external components was considered as a back-up method of fragmentation.

A comprehensive summary of the development of the Frangible ARCAS explosive fragmentation system is presented below.

A. INITIAL FRAGMENTATION TESTS

The design approach originally selected during this program to achieve the required fragmentation was that of a single modular shaped charge located in the forward section of the rocket vehicle. This approach was selected because of the many advantages afforded by its simplicity, but program activities were designed to allow modification of this fragmentation approach in the event that test results indicated the need for relocation or addition of explosive material to achieve fragmentation within the specified limits. The preliminary design of the single modular shaped charge concept envisioned a system similar to that shown on Figure 26.

The initial fragmentation tests incorporating the shaped charges illustrated on Figure 27 were completed on June 18 under simulated altitude conditions representing a pressure environment of 100,000 feet. The motor cases used for these tests were the cases which were successfully static fired in tests AFST-9 and AFST-10 on May 13. A photograph showing the inert rocket motor assembly with grid markings for post-test identification and the bifocal shaped charge module is shown on Figure 28. A photograph of the pre-test set-up with the rocket motor assembly suspended from the ceiling of the simulated altitude chamber is presented on Figure 29.

High speed photographic coverage of the fragmentation sequence was obtained with a Fastex camera. The camera was mounted outside the test cell in a photographic port and was started just prior to detonation of the explosive module. The fragmentation sequence was obtained, but the flame resulting from the detonation engulfed the inert motor assembly before complete fragmentation was experienced (see Figure 30). Results of these two initial fragmentation tests are shown on Figures 31 and 32. As observed from these photographs, the shaped charges tested were effective in fragmenting the forward and aft section of the rocket assembly, but the center section of the motor case was left intact. Fragmentation of the nozzle section was accomplished by the focusing effect of the shaped charge and wave propagation through the empty motor case which served as a shock tube as illustrated on Figure 33.

Post-test analysis of the unit containing the bifocal shaped charge showed that the annular shaped wave was directed outboard more than anticipated because of vector effects resulting from central initiation as illustrated on Figure 34. Consequently, wave intersection with the motor case wall occurred farther forward than anticipated, as shown on Figure 35.

Fragments recovered from these initial tests were utilized in tests to determine characteristic drag coefficients for the determination of terminal velocity and impact kinetic energy. The determination of these aerodynamic coefficients for various shapes was necessary for evaluation of the particles produced during subsequent fragmentation tests.

B. DETERMINATION OF PARTICLE FREE-FALL DRAG COEFFICIENTS

The allowable particle sizes produced during fragmentation of the spent vehicle were defined in terms of impact kinetic energy,

$$E = \frac{W}{2g} V^2 \quad (1)$$

The maximum allowable limit was specified as an impact energy of 10 ft-lb for the resulting fragments at their terminal velocity. It should be noted, however, that the magnitude of 10 ft-lb of kinetic energy at impact was arbitrarily selected for the purposes of this program and is not to be interpreted as a lethal impact energy limit.

Because impact kinetic energy is indirectly dependent upon the coefficient of drag, as a result of its influence on velocity, tests were conducted to determine actual free-fall drag coefficients of the fragments obtained from the initial fragmentation tests. Although most of the fragments used for these tests were larger than the particle sizes anticipated as the system was developed further, they were adequate to determine characteristic drag coefficients of the various shapes for subsequent use in the program. The actual free-fall drag coefficients were determined experimentally by water tank tests. By recording the time required for each piece to free-fall through 8.75 feet of water and using these data to determine the average velocity for the particle in water, it was possible to utilize the equation for aerodynamic drag in determining the drag coefficient for each piece.

Using the drag equation for the conditions of terminal velocity (drag = weight), the relationship may be expressed as:

$$D = W = C_D \left(\rho \frac{V^2}{2} \right) S \quad (2)$$

The drag coefficient then becomes

$$C_D = \frac{2W_w}{\rho V_a^2 S} \quad (3)$$

where:

- W_w = sample weight in water, lb
- ρ = density of water, lb-sec²/ft⁴
- V_a = average free-fall velocity, ft/sec
- S = drag reference area, ft²

Ten drop tests of each sample were used to determine the average free-fall velocity for each fragment. The results of these tests are tabulated on Table VII. These data were used to calculate characteristic free-fall drag coefficients for the fragments as shown on Table VIII. Based on the maximum and minimum velocities recorded for each piece during the water tank tests, limit drag coefficients were determined, for reference, as shown on Table IX. Photographs of the rocket motor fragments used in the experimental determination of characteristic drag coefficients are shown in Figures 36, 37, and 38.

C. DETERMINATION OF IMPACT KINETIC ENERGY

Having determined a drag coefficient characteristic of each of the test fragments, it was possible to calculate their terminal velocity and resulting impact kinetic energy. Using Equation (2) for the conditions of terminal velocity, V_T , (drag = weight),

$$V_T = \sqrt{\frac{2W}{C_D \rho S}} \quad (4)$$

or

$$V_T = \sqrt{\frac{2W}{C_D(0.001756)S}} \quad \text{at 10,000 feet altitude*}$$

then

$$V_T = \sqrt{\frac{1140 W}{C_D S}} = 33.8 \sqrt{\frac{W}{C_D S}} \quad (4')$$

The terminal velocity and resulting impact kinetic energy for the test pieces were calculated as shown on Table X. These calculations show that, with the exception of the remaining motor case, all fragments tested provided an impact kinetic energy of less than 10 ft-lb.

Since the fragments from each subsequent fragmentation test conducted during the program were to be evaluated, a more convenient method of determining impact kinetic energy was derived by combining the above equations in such a manner as to express kinetic energy at impact directly in terms of fragment weight, coefficient of drag and drag reference area. The general expression was obtained by substituting Equation (4) into Equation (1), which allowed impact kinetic energy to be expressed as

$$E = \frac{W}{2g} V^2 = \frac{W}{2g} \left(\frac{2W}{C_D \rho S} \right)$$

or

$$E = \frac{W^2}{g C_D \rho S} = k \frac{W^2}{C_D S} \quad (5)$$

* An altitude of 10,000 feet was used to determine terminal velocity and impact energy, rather than sea level, to provide a factor of safety in the calculations.

where

$$k = \frac{1}{g\rho}$$

For an altitude of 10,000 feet, $\rho = 0.001756 \text{ lb-sec}^2/\text{ft}^4$, therefore,

$$k = \frac{1}{32.17 (0.001756)} = 17.7 \text{ ft}^3/\text{lb}$$

and

$$E = 17.7 \frac{W^2}{C_D S} \quad (6)$$

where

W = fragment weight, lb

C_D = free-fall coefficient of the fragment

S = drag reference area of the fragment, ft^2

The use of the impact kinetic energy equation in this form precluded the necessity of determining the magnitude of terminal velocity separately. This equation was used to determine the impact kinetic of particles produced in subsequent fragmentation tests during development of the system and was found to be considerably more convenient.

D. FRAGMENTING MODULE CONCEPT

Although full-scale tests of the various shaped charges showed their inability to fragment the entire rocket motor assembly, the potential advantages offered by a single modular charge were sufficient to justify additional investigation before the concept was dropped from consideration. A review of the test results obtained with the shaped charges, however, provided conclusive evidence that the effects of shaping the module were concentrating the detonation wave in a manner such that only localized areas of the

unit were effected by the charge. Additional tests also showed that low impingement angles did not provide adequate penetration. In summary, it was concluded that if fragmentation of the full length of the motor case was to be accomplished with a single modular charge, dispersion of the energy produced by the charge was necessary.

Since the effect of the shaped charge is to concentrate rather than disperse the resulting detonation products, the concept was reversed. The new concept was to provide dispersion of high velocity metal particles for penetration along the length of the motor case wall. Dispersion of the particles was accomplished by reversing the conical end of the shaped module and fabricating the end from cast metal to provide a large number of fragments.

Two inverted cone module designs, illustrated on Figures 39 and 40, were fabricated for test purposes. Target tests, as shown in Figure 41, were conducted to determine particle sizes and trajectories subsequent to penetration of the rocket motor headplate. The test set-up of the module assembly is illustrated on Figure 42.

Results of these tests showed that the Type I module provided particle dispersion sufficient to cover the entire motor case length, while the Type II module concentrated nearly all particles in a 4-inch diameter circle on the target 5 feet away. Typical particle sizes obtained are shown by the photograph in Figure 43.

A full-scale test of the Type I fragmenting module was conducted with a simulated motor case. Results of this test showed that the particles produced during detonation of the module failed to penetrate the glass filament wound tube of 0.110-inch wall thickness. Post-firing analysis of the remaining tube showed evidence of particle impact on the inside wall, but the low impingement angle resulted in deflection of the metal fragments rather than penetration of the fiberglass wall. Failure of both the shaped and fragmentating charges to effect fragmentation of the motor case resulted in the single charge concept being dropped from further consideration as a method of vehicle fragmentation.

E. SHOCK TUBE TECHNIQUE

Although the single modular charges tested during the program failed to provide complete fragmentation of the rocket motor assembly, test results showed reproducible fragmentation of the nozzle section and fin assembly to impact kinetic energy levels below 10 ft-lb. Since the test results also showed that the shape of the modular charge had no appreciable effect on the results attained, it was concluded that the most significant contribution to the effective aft end fragmentation experienced was that of the empty motor case, which acted as a shock tube for the modular charge and directed the resulting detonation wave to the nozzle section. These test results disclosed the fact that complete fragmentation of the rocket assembly could be effected if an external explosive material could be sympathetically initiated by the shock experienced during fragmentation of the aft section by the primary detonation wave. By allowing the motor case to remain intact to act as a carrier for the primary detonation wave from the internal explosive charge, fragmentation of the nozzle section would be completed prior to sympathetic detonation of the external explosive which would fragment the remaining motor case. This shock tube fragmentation concept is illustrated on Figure 44.

The first full-scale static firing/fragmentation test, conducted on September 22, incorporated this concept. A photograph of the test set-up is shown on Figure 45. The primary explosive charge consisted of 1.0 pound of Comp. "B" which was contained and initiated as illustrated on Figure 46. The external charge consisted of 0.030-inch-thick sheet explosive material. Test results showed that the external sheet explosive material was not sympathetically initiated during fragmentation of the nozzle section. Consequently, the test results were nearly identical to those attained with the single conical shaped charge (Figure 31).

A similar test was conducted to determine the ability of the primary shock to sympathetically initiate 100 grain/ft linear shaped charge from the aft end during fragmentation of the nozzle area. Figures 47 and 48

show the motor case with linear shaped charge incorporated in such a manner as to simulate being covered by the fin assembly. Test results of this combination also showed failure of the aft end fragmentation to impart sympathetic detonation of the external explosive.

F. MODULAR CHARGE/EXTERNAL EXPLOSIVE TECHNIQUE

The test results described above showed the inability to induce sympathetic detonation during fragmentation of the nozzle section, but the concept of motor case fragmentation by means of externally placed explosive material offered the greatest potential of any technique attempted. The ability to attain sympathetic detonation of the external explosive material was extremely desirable in order to avoid the necessity of a secondary ignition system for the external charge. The most positive means of inducing sympathetic initiation was to extend the external explosive material farther forward on the motor case to bring it into close proximity to the primary charge as illustrated in Figure 49. The disadvantage of initiating the external charge at the forward end was that fragmentation of the aft end of the motor would not benefit from the shock tube effect produced by the primary charge. The detonation rate of the external charge, about 7000 meters/second, is considerably greater than the wave velocity produced through the motor tube by the primary charge, which is more on the order of 3000 meters/second. This velocity difference was sufficient to allow advanced fragmentation or collapse of the motor case, thereby preventing the primary charge wave from reaching the nozzle section. By precluding the use of the motor case as a shock tube, fragmentation of the nozzle/fin section is dependent upon the external explosive material.

A full-scale fragmentation test was conducted on October 26 to evaluate the concept described above and the particle sizes resulting from this technique of fragmentation using 0.030-inch-thick sheet explosive. A photograph of the pre-test set-up is shown on Figure 50. Sympathetic detonation of the sheet explosive was successfully achieved and all sections of the rocket motor assembly were fragmented to sizes providing impact kinetic

energy levels less than 10 ft-lb except the throat insert back-up insulation section, as anticipated. It should be noted, however, that the motor case used for this initial test had not been static fired. Consequently, the insulation material in the motor case was uncharred and considerably stronger than the insulation in a fired motor case. A photograph of the fragments from this test is presented on Figure 51.

A similar test was conducted using eight strips of 100 grain/foot linear shaped charge in lieu of sheet explosive material (see Figure 52). Sympathetic detonation of the linear shaped charge was also achieved, but fragmentation of the unit was less effected than with the sheet explosive as evidenced by the test results shown on Figure 53. Post-test evaluation of the fragments produced showed the best fragmentation that could be expected with this technique incorporating linear shaped charges to be unacceptable with respect to impact kinetic energy unless substantially more shaped charge strips or larger strips were employed. An increase in number or size of these charges was undesirable with respect to vehicle weight and aerodynamic drag considerations. Consequently, the use of linear shaped charges as a method of motor case fragmentation was dropped from further consideration and all efforts were directed toward improving the modular charge/sheet explosive technique which appeared most promising.

G. FINAL CONFIGURATION

In order to provide more complete fragmentation of the nozzle section, the thickness of the sheet explosive material was increased from 0.030 inch to 0.042 inch, which is the minimum standard thickness commercially available at this time. This increase in thickness and weight of explosive material was believed to be adequate to provide fragmentation of the entire rocket assembly within the specified limit of 10 ft-lb of kinetic energy for the fragments upon impact.

A major milestone was achieved on October 26 with the successful static firing and subsequent fragmentation of a Frangible ARCAS rocket motor

assembly. A pre-firing photograph is presented in Figure 54 showing the rocket motor assembly mounted in a vertical firing position. No thrust or chamber pressure data were recorded because of the nature of the test. The primary objectives of the test were:

1. To evaluate the performance of the sheet explosive after subjection to full-time heat transfer temperature environment.
2. To evaluate the fragmentation capabilities of the 0.042-inch-thick sheet explosive when sympathetically initiated from the forward end by the primary charge.

The test was conducted in accordance with the sequence shown on Figure 55.

Approximately 120 seconds after rocket motor burnout, the primary explosive charge was initiated, effecting sympathetic detonation of the sheet explosive and fragmentation of the entire rocket motor assembly. The results of the fragmentation achieved with the single modular charge and 0.042-inch-thick sheet explosive is shown by the photograph in Figure 56. The temperature environment to which the sheet explosive was subjected as a result of heat transfer through the motor case wall had no deteriorating effect on its performance.

Subsequent analysis of the fragmented pieces with regard to impact kinetic energy showed the largest motor case fragment to provide an impact kinetic energy of less than 3 ft-lb as tabulated below:

<u>Fragment</u>	<u>Weight (gm)</u>	<u>Weight (lb)</u>	<u>C_D</u>	<u>Drag Ref. Area (ft²)</u>	<u>$\frac{W}{C_D S}$</u>	<u>Energy (ft-lb)</u>
Largest Motor Case Piece	35.0	0.077	1.00	0.082	0.94	1.28
Largest Fin Piece	27.3	0.110	1.24	0.165	0.54	0.49
Largest Insulation Piece	17.9	0.080	1.07	0.033	2.26	1.77
Largest Retaining Sleeve Piece	13.5	0.030	1.07	0.010	2.80	1.50
Fin Retaining Screw	6.0	0.013	1.00	0.001	13.00	2.98

It should be noted from the tabulation on page 22, that the maximum energy level experienced resulted from the fin retaining screws. Substitution of nylon or aluminum screws for the steel socket head cap screws currently used would reduce this impact energy to about 0.54 ft-lb. Minor modification of the nozzle section would also reduce the impact energy level of the insulation pieces. Hence, a maximum impact energy of about 1.5 ft-lb could be achieved with only minor modification of the nozzle section.

The test results obtained with the 0.042-inch-thick sheet explosive material demonstrated the success of the modular charge/sheet explosive technique and constituted its incorporation in the final design of the fragmentation system, illustrated on Figure 57. Two static firing/fragmentation tests were successfully conducted during the program incorporation 0.042-inch-thick sheet explosive material. All three tests showed similar results, with impact kinetic energy levels of the resulting fragments well below the limit of 10 ft-lb.

The sheet explosive material incorporated in the fragmentation system is DuPont's "Detasheet" C material. The manufacturer's specifications for this material are presented on Table XI.

External Explosive Retention

Calculations were performed to determine the maximum vehicle boundary layer shear stress at various times during flight. These calculations, tabulated on Table XII, indicated a maximum shear stress of only about 2 lb/ft² during flight. This relatively low magnitude of shear stress indicated that the external sheet explosive material could be retained with a temperature resistant, pressure sensitive tape, which was ultimately incorporated. A pressure sensitive base wrap was used to retain the sheet explosive to the motor case. An aluminized fiberglass tape was used as an overwrap.

H. FIRING TRAIN DEVELOPMENT

The successful results obtained with the modular charge/sheet explosive technique defined the basic fragmentation system. Test results

showed acceptable fragmentation of the motor case by sympathetic detonation of the sheet explosive. The task remained, however, to develop an explosive initiating train that could be incorporated in the modular charge and initiated by both the mechanical timer unit and the pressure sensing redundant initiator. Since the design and function of both these units had been completed, it was necessary to select a suitable initiator to provide reliable detonation of the primary explosive charge.

Laboratory tests of the mechanical timer fragmentation system firing mechanism showed repeatable high order detonation of the primary charge booster with a MK 125 stab primer. The initial test of a full-scale timer assembly, however, showed the inability of the MK 125 primer to induce high order detonation across the existing 0.092-inch gap under actual conditions. An M55 stab detonator was substituted for the MK 125 primer to increase the shock velocity from the output end. Although the M55 stab detonator is somewhat smaller in size, the output end contains RDX rather than lead azide which results in a shock velocity of about 8400 meters/second as compared to 4000-5000 meters/second for lead azide. An illustration of the mechanical timer firing train is presented on Figure 58.

Additional laboratory tests, incorporating lead sample plates, were conducted to compare the relative energy output of these initiators. The test results, shown on Figure 59, showed the M55 stab detonator to have about 2 to 3 times the penetrating effect.

A full-scale mechanical timer system fragmentation test incorporating the M55 stab detonator was successfully conducted at a simulated altitude of 100,000 feet. The test set-up is illustrated on Figure 60. Post-test analysis of the timer unit showed adequate fragmentation of all components. Successful completion of this test constituted the selection of the M55 stab detonator for use in both the mechanical timer and redundant initiator systems.

I. STATIC FIRING/FRAGMENTATION SYSTEMS TEST

The Frangible ARCAS rocket motor AFST-15 was incorporated in a full-scale systems test utilizing the final explosive fragmentation configuration described above. The test also incorporated the mechanical timer firing system. The unit was tested in the vertical firing position. No thrust or chamber pressure data were recorded because of the nature of the test.

The static firing portion of the test was completed with no apparent abnormalities. This static test marked the seventh and final successful static firing of the flight design motor case during Phase III of the program in as many attempts. The rocket motor was subjected to heat transfer temperatures for 120 seconds after rocket motor burnout. This time increment represented the approximate time, after rocket motor burnout, for the vehicle to coast 20 seconds past apogee. At this preselected time the stab detonator, which was to have induced fragmentation of the rocket assembly, was not initiated. After a time lapse of six minutes, the primary explosive charge was initiated by a back-up system (an electrically initiated blasting cap and RDX booster), effecting sympathetic detonation of the sheet explosive and fragmentation of the entire rocket motor assembly. Results of the fragmentation achieved with the 0.0042-inch-thick sheet explosive were similar to that of the unit AFST-14, shown on Figure 56. Subsequent analysis of the fragmented pieces with regard to impact kinetic energy showed the largest rocket motor fragments to provide an impact energy of less than 10 ft-lb as tabulated below.

<u>Fragment</u>	<u>Weight (lb)</u>	<u>C_D</u>	<u>Drag Ref. Area (ft²)</u>	<u>Energy (ft-lb)</u>
Largest Insulation Piece	0.080	1.07	0.033	3.22
Largest Fin Piece	0.110	1.24	0.165	1.05

The cause of the fragmentation initiation system failure was not readily apparent. However, in view of the fact that all system components were checked independently prior to the test and found to function satisfactorily, it was concluded that the failure was attributed to a disengagement of

the stab detonator resulting from shock and/or vibration during the test. It should be noted that the timer assembly was inverted since the rocket motor was static fired in the vertical position.

Abbreviated Systems Test

An abbreviated systems test was successfully completed at Atlantic Research's Pine Ridge test facility on December 21. This test incorporated a four-second burning time, heavywall rocket motor containing: (1) five Frangible ARCAS dimple motors in the headplate, and (2) the final design mechanical timer assembly incorporating an M55 stab detonator. The purpose of this test was to check the functioning of the system from rocket motor burnout through initiation of the M55 stab detonator by the mechanical timer firing pin and check a number of dimple motors for reliability. The test was designed to allow activation of the dimple motor by actual rocket motor temperature environment which would, in turn, start the timer unit.

The test was successfully concluded by initiation of the stab detonator by the mechanical timer unit firing pin. Post-firing examination of the assembly showed that all systems performed satisfactorily. All five of the dimple motors were activated during rocket motor burnout. Successful performance of this test motor and the fragmentation initiation systems substantiated the conclusion that the malfunction experienced during the full-scale systems test resulted from the disengagement of the stab detonator from the rotor arm housing during the static firing portion of the test.

III. VEHICLE FINAL ASSEMBLY AND LAUNCH

The Frangible ARCAS vehicle was designed to be launched from the standard LAU-41/A closed breech launcher. Final assembly and launch operations for the vehicle follow nearly the same procedures applicable to the standard ARCAS.

Subsequent to applying the external sheet explosive material, the propellant grain retaining sleeve used for shipping purposes is removed and replaced by the explosive module assembly, shown on Figure 61. After

removing the mechanical timer manual safing pin and attaching the payload, the vehicle is installed into the launcher as shown on Figure 62 using the standard ARCAS Styrofoam spacers. The launch piston, shown on Figure 63, is fitted to the aft end of the vehicle and the spring straps are positioned to engage the fin shroud to lock the piston assembly to the vehicle. The spring action of the straps provides release of the assembly upon ejection of the vehicle from the launch tube. The method of retention provided by the launcher piston assembly is illustrated in Figure 64.

Upon final installation of the vehicle into the launcher and elevation of the launcher in preparation for vehicle flight, final commit-to-arm of the fragmentation initiation system is accomplished by removing the manual safing pin from the redundant initiator through a small access door in the launch tube.

Although this final procedure in the sequence of launch operations was not mandatory and required a minor modification to the existing launch tube, as illustrated on Figure 65, it was recommended to provide maximum safety. This procedure precludes the requirement of handling the vehicle, whether loading or unloading from the launcher, with the redundant initiator manual safing pin removed.

IV. VEHICLE STATIC AND DYNAMIC STABILITY

Aerodynamic evaluation of the Frangible ARCAS vehicle configuration showed excellent static stability characteristics. The results of this analysis, presented on Figure 66, show the vehicle to be relatively insensitive to payload weight and center of gravity location throughout the range of reasonable payload weights and launch angles. As observed from this plot, at least one caliber of stability is maintained with a payload weight of 8.0 pounds regardless of the payload center of gravity location. Variation of the vehicle center of gravity during flight is presented on Figure 67.

The dynamic stability is presented by a comparison of vehicle pitch frequency and roll rate as a function of flight time on Figure 68.

As observed from the comparison of these parameters, the vehicle is designed to provide "crossover" early in flight. Although the fin assembly was originally designed to provide a nominal roll rate of 20 rps at rocket motor burnout, the final vehicle configuration was several pounds heavier than anticipated, resulting in a slight decrease in vehicle burnout velocity and a corresponding decrease in maximum roll rate to about 16.3 rps with the existing fin assemblies. Although this reduction in roll rate had no detrimental effect on vehicle performance, the roll rate of future vehicles may be increased by increasing the cant of the fin blades, thereby allowing a potential growth of the system by permitting the use of heavier payloads. The vehicle pitching frequency for various payload weights and center of gravity locations is shown as a function of time on Figure 69.

V. WIND WEIGHTING AND DISPERSION

Because of the similarity between the Frangible ARCAS and the standard ARCAS vehicles and the limited number of flight tests involved, the standard ARCAS wind weighting and dispersion data were used for the flights during the program. Wind sensitivity and weighting factors for the standard ARCAS vehicle are presented on Figure 70 and Table XIII, respectively.

Current dispersion statistics for the standard ARCAS vehicle show that 95 per cent of all impacts will be within a radius of 6.5 nautical miles of the predicted impact point. The tabulation below shows the impact error experienced with the Frangible ARCAS flight vehicles.

<u>Flight Test</u>	<u>QE (degree)</u>	<u>Predicted Impact Range (NM)</u>	<u>Actual Impact Range (NM)</u>	<u>Impact Error (NM)</u>
AFFT-1	84.5	23.4	23.5 ^a	0.1 ^a
AFFT-2	77.0	41.0	35.6	5.4
AFFT-3	b	b	b	b
AFFT-4	c	c	c	c

a. No radar track. Impact range determined by extrapolating early portion of trajectory and telemetry data.

b. No test. Launcher malfunction induced severe reduction of vehicle performance.

c. Fragmented in flight as programmed. No impact range.

These data show the impact location to be within the area predicted.

VI. DIAGNOSTIC FLIGHT TESTS

The Frangible ARCAS program included the flight testing of two diagnostic vehicles. These units, shown in Figure 71, were of the same configuration as the systems vehicle except for the omission of the fragmentation system. The purpose of the diagnostic flight tests was threefold:

- a. To evaluate the general aerodynamic characteristics and flight performance of the vehicles.
- b. To determine a drag curve by flight data analysis which would accurately characterize the vehicle configuration so that the systems vehicle performance could be accurately predicted.
- c. Monitor motor case skin temperatures during flight to determine the temperature environment to which the external explosive material would be subjected.

A. DIAGNOSTIC PAYLOAD

A payload to monitor motor case and payload section temperature during flight was designed and built by the Electro-Mechanics Division of Atlantic Research Corporation. The locations of interest were selected as shown on Figure 72, based on temperature data obtained from static firings. Thermistors were desired for this application because their use would preclude the need for payload signal preamplification. A study was conducted, however, which determined that available thermistors would not provide satisfactory readout resolution over the range of vehicle temperatures that were expected (see Figures 73 and 74). Laboratory tests indicate no permanent alteration of the thermistors tested to temperatures of 1600° F, but resolution obtained at temperatures above about 400° F was insufficient to achieve temperature data to even 20 per cent accuracy. For this reason, motor case temperatures were monitored with thermocouples. Thermistors were used as a temperature reference and to monitor temperatures in the payload section.

The diagnostic payload, shown on Figures 75 and 76, was designed to sample thermocouple data by means of a motor driven communicator for 0.75 second sequentially. The thermistors were commutated at the same rate and in such a manner as to make frame identification possible. The selected thermocouples were connected to a magnetic amplifier for signal preamplification. Four hundred cycle power was supplied by an ERA Transpac solid-state inverter. A block diagram of the telemetry system is shown on Figure 77.

B. FLIGHT TEST RESULTS

Performance of the diagnostic vehicles was predicted based on the standard ARCAS drag data. The units were launched without the auxiliary gas generator boost to minimize the shock loads imparted to the telemetry payload. A comparison of the predicted and actual performance attained is presented on Figure 78. This comparison shows that the predicted performance was somewhat optimistic as compared to the flight performance attained. Since the parameters such as vehicle weight, propellant weight, and total impulse were known to be accurate, it was concluded that the optimistic prediction was primarily attributed to the vehicle drag data. The apogee performance of the vehicles, particularly that of the initial flight, showed the actual performance to be reasonably close to that predicted. This observation indicated that the drag data assumed would require only minor modification to improve the accuracy of the predicted performance and was substantiated by a comparison of predicted and actual vehicle roll rate during flight, shown on Figure 79. Since the vehicle roll rate is directly proportional to its velocity, the agreement of these data indicated that the velocity of the vehicle AFFT-1 was close to that predicted.

The drag data characterizing the basic vehicle configuration was established by utilizing the data obtained from these initial flight tests. The resulting characteristic drag curve is presented on Figure 80. A detailed analysis of the flight performance data and the modification required to the

assumed drag curve to provide agreement between the actual and predicted data are presented in Appendix III. The revised drag data resulting from this analysis provided predicted performance that agreed well with the flight data obtained, as evidenced by the trajectory profiles on Figure 81. A comparison of actual and predicted times to impact, tabulated below, also showed relatively good agreement between the revised predicted performance and that achieved.

Flight Test	Time From Launch to Impact (seconds)		
	Predicted*	Radar Data	Telemetry Data
AFFT-1	247	No Data	248
AFFT-2	210	202	205

* Based on revised performance data.

C. TEMPERATURE DATA

During the initial flight, the motor case thermocouples failed to respond immediately after launch and only a 420 cps frequency was recorded with no deviation. This failure was apparently induced by "lock-in" of the voltage control oscillator with the power inverter. The thermistors in the payload section, however, were not affected and provided temperature data throughout the flight. The maximum temperatures recorded were about 180° F as shown on Figure 82.

It should be noted that although the motor case skin temperatures were not recorded during flight, the frequency output of the payload indicated that the motor temperatures did not exceed 575° F. This determination was made by observing the output frequency of the voltage control oscillator. Calibration of the payload during its manufacture showed that temperature differences of approximately 500° F between the motor case thermocouples and the reference thermistor produced an increase in the output frequency of the voltage control oscillator. Analysis of the telemetry data showed that no frequency change was experienced. Since the maximum reference temperature

was about 75°F, it was concluded that the motor case skin temperatures did not exceed 575°F during the flight. This conclusion was substantiated by the results of the second flight test.

The second flight test vehicle, AFFT-2, was instrumented with four thermistors in the payload section and eight thermocouples in the skin of the glass filament wound motor case. The thermistors in the payload section failed to respond shortly after launch, resulting in the absence of the positive signal on the commutated data trace. The motor case skin thermocouples were not affected and motor temperature data were recorded throughout the flight, but loss of the positive signal precluded identification of eight thermocouples with respect to their position on the motor case. Analysis of the temperature data, however, showed the inability to identify the individual locations of the thermocouples to be inconsequential since the difference in the temperatures was only about 50°F. The motor case skin temperatures during flight are presented on Figure 83 in comparison with the maximum skin temperatures recorded during several static firings of the motor earlier in the program. As observed from this plot, the maximum skin temperatures recorded were about 500°F. A comparison of the rate of temperature increase experienced during static and flight tests showed the aerodynamic heating contribution to the temperature environment experienced during flight to be prevalent. Since the sheet explosive incorporated in the fragmentation system had performed successfully after exposure to motor case temperatures of about 500°F for six minutes (static firing/fragmentation test AFST-15, November 25, 1964), the flight data showed that the system would not be adversely affected by the temperature environment experienced during flight.

The lower temperatures experienced during flight beginning at about apogee, as compared to those experienced during static firing, were attributed to the lower ambient temperatures experienced at the higher altitudes and to transfer of the residual heat source from the rocket motor chamber. This transfer is induced by the differential pressures experienced between the rocket motor chamber residual gases subsequent to burnout and the local atmosphere.

VII. SYSTEMS FLIGHT TESTS

The Frangible ARCAS program included two flight tests of the complete systems vehicle. These units, one of which is shown being loaded into the closed breach launcher on Figure 84, incorporated 0.042-inch-thick sheet explosive material from the forward edge of the fiberglass motor case to the leading edge of the fin assembly. The explosive material was not extended under the fin assembly to effect fragmentation of the nozzle/fin section because it was not considered necessary to fragment the aft section in order to demonstrate the feasibility of the system in flight. Based on the results of the fragmentation tests conducted earlier in the program, the degree of fragmentation anticipated with the two systems vehicles was as shown on Figure 85. The purpose of the systems flight tests was as follows:

- a. To demonstrate the feasibility of a frangible meteorological rocket system in flight.
- b. To evaluate the general aerodynamic characteristics and flight performance of the systems vehicle.
- c. To determine the difference, if any, in the drag characteristics of the systems vehicle as compared to the basic vehicle configuration (less fragmentation system).

The systems flight tests were conducted on San Nicolas Island. The Launch Hazard Area and Maximum Impact Area which were prescribed by PMR Range Safety are shown on Figures 86 and 87, respectively.

A. PAYLOAD

The systems flight test vehicles carried the standard Arcasonde 1A telemetry payload and the standard ARCAS silk parachute, 15-feet in diameter. The parachutes used in these flights, however, did not incorporate the normal silverized surface to aid in radar tracking. The reflective surface was omitted to aid in radar tracking of the rocket motor in lieu of the payload, which was to be tracked by GMD-1 ground equipment.

B. FLIGHT TEST RESULTS

The first of two systems vehicles was launched on May 20, 1965. This vehicle was intended primarily for evaluation of the redundant fragmentation initiation system. During ejection of the vehicle from the government modified launcher, the cover plate to the access port was ejected, resulting in loss of the required launch pressure. Analysis of the flight data showed the ejection velocity of the vehicle from the launcher to be only about 60 ft/sec instead of the usual 230 ft/sec. Consequently, the vehicle reached an abnormally low apogee altitude of only 69,000 feet which was less than the minimum altitude of 70,000 feet required to arm the redundant fragmentation mechanism. The first systems flight test was therefore considered a "No Test."

During analysis of the flight data, it was observed that the altitude-velocity and velocity-time relationship were somewhat below the predicted, although the reduced ejection velocity was considered. A comparison of the predicted and actual data indicated an increase in either the characteristic vehicle drag or the drag reference area. Since the drag curve was established for the basic vehicle configuration during the initial diagnostic flight tests, a series of trajectories were computed with increased drag reference area. Further analysis showed good agreement between the actual and predicted performance data when the drag reference area was increased from 0.126 ft^2 to 0.151 ft^2 . This effective increase in drag reference area was most likely attributed to turbulent flow conditions and skin friction effects related to the sheet explosive overwrap. A more detailed presentation of the flight data analysis, and determination of launch velocity experienced and effective drag reference area increase is provided in Appendix IV.

The second and final systems vehicle was successfully flight tested on December 21, 1965 without a launch tube access port. The delay experienced between the two final flights was attributed to a combination of range scheduling of the single flight test and adverse weather conditions at the launch site.

Radar data showed normal flight performance through an apogee altitude of 130,000 feet at which time payload ejection was observed. The payload telemetry signal was lost during vehicle ascent, consequently no GMD-1 data were obtained during payload descent. However, successful payload ejection was determined by both radar observation and physical recovery of the payload. Successful radar coverage of the descending rocket motor assembly was maintained subsequent to payload ejection. Fragmentation was induced by the primary system (mechanical timer unit) at about $T + 121$ seconds and an altitude of 123,000 feet, or payload ejection plus 20 seconds, as programmed. The fragmentation event was observed by both island and main-land radars. One piece, undoubtedly the nozzle/fin section of the motor assembly, was tracked to impact at the normal descent velocity. With the exception of this piece, which was not expected to fragment, radar observation showed a "cloud" of particles with varying rates of descent. Radar track of various particles was maintained at intervals and the "cloud" was observed to disperse as it descended. Except for the extreme aft end of the vehicle, which was not prepared for fragmentation on this final unit, all indications were that the degree of fragmentation attained was the same as that achieved during tests conducted earlier in the program, see Figure 56.

A Flight Test Summary for the Frangible ARCAS Program is shown on Table XIV. The actual sequence of events for flight AFFT-4 is illustrated on Figure 88. A more detailed presentation of the flight data is presented in Appendix IV.

VIII. VEHICLE NOMINAL FLIGHT PERFORMANCE

The basic Frangible ARCAS rocket vehicle is comparable in performance to the standard ARCAS. However, addition of the 5.7-pound fragmentation system and the increase in vehicle drag resulting from the slightly larger body diameter (see Table I), reduced the apogee altitude of the systems vehicle by about 65,000 feet.* Trajectory profiles for the vehicle with

* For 10.5-pound payload, sea level launch, $QE = 84^\circ$.

and without the fragmentation system are presented on Figure 89 in comparison with the standard ARCAS. Trajectory profiles for the systems vehicle at various effective launch angles are shown on Figure 90. Nominal trajectory data for the basic and systems vehicle are presented in Tables XV and XVI, respectively. Other pertinent systems vehicle performance data are presented as follows:

- a. Apogee Altitude and Ranges versus Effective Launch Angle, Figure 91.
- b. Apogee Altitude versus Apogee Range, Figure 92.
- c. Apogee Altitude versus Payload Weight, Figure 93.
- d. Vehicle Velocity versus Flight Time, Figure 94.
- e. Burnout Mach Number versus Burnout Weight, Figure 95.

A comparative performance summary of the standard ARCAS and Frangible ARCAS vehicles is presented on Table XVII. As observed from the above data, the Frangible ARCAS vehicle performance was considerably reduced by the required systems weight and configuration. Although the apogee altitudes attainable with the Phase III configuration were somewhat less than desired, the vehicle performance was sufficient to demonstrate the feasibility of the frangible rocket system. Various modifications which will provide apogee altitudes of approximately 200,000 feet are presented below.

IX. PROPOSED MODIFICATIONS FOR IMPROVED PERFORMANCE

Preliminary studies have been completed to determine the increase in apogee altitude that could be achieved by increasing the length of the existing vehicle to provide additional total impulse and burning time. These data show that the corresponding increase in vehicle weight and the effects of gravity turn on longer burning time for the same magnitude of thrust soon overcome the contribution of increased total impulse. The data, however, show that substitution of a more energetic propellant and an increase in motor length of approximately 9.0 inches would provide the desired performance.

The following sections present a brief discussion of the performance that could be achieved with various configurations.

A. PROPELLANT SUBSTITUTION

In order to significantly increase vehicle performance without necessitating a major redesign of the motor, the substitution of a higher energy propellant was considered. The propellant used for this comparative analysis was Arcadene, an aluminized carboxy terminated polybutadiene (CTPB) formulation which is manufactured by Atlantic Research Corporation. In addition to its high performance and good physical properties, this propellant has excellent bonding characteristics and is ideally suited to a motor such as the Frangible ARCAS. Polybutadiene type propellant systems have been in routine use for a number of years and are currently employed in missile systems such as Minuteman, Pershing and Sparrow.

Preliminary analysis of vehicle performance with Arcadene propellant and various motor total impulses show that an increase in motor length is required to provide the desired increase in performance. Figure 96 shows apogee altitude performance as a function of total impulse and motor length. As observed from this data, an increase in motor length of 8.5 inches will provide an apogee altitude of 200,000 feet.¹ The motor length required to achieve this performance corresponds to a burning time of 33 seconds, which is the maximum ambient burning time desirable with the current motor case insulation thickness. The tabulation presented below compares vehicle performance.

<u>Parameter</u>	<u>Phase III Vehicle</u>	<u>Extended Vehicle</u>
Motor Length, in	69.5	78.0
Liftoff Weight, lb ²	68.4	75.9
Burnout Weight, lb ²	25.4	26.9
Total Impulse, lb-sec	9400	11,200
Burning Time, sec	30	33
Apogee Altitude, ft ¹	119,000	200,000

1. For 10.5-pound payload, sea level launch, QE = 84°.

2. Excluding payload weight.

A comparative illustration of the Phase III and extended vehicle is presented on Figure 97. Apogee performance of the modified vehicle is shown on Figure 98 for various payload weights and launch angles.

It should be noted that while the desired altitude is achieved with the extended motor described above, the performance might be further increased by a greater total impulse for the same burning time. This could be accomplished by increasing the motor operating pressure which would, in turn, increase the propellant burning rate and maintain the 33 second burning time.

X. CONCLUSIONS

The successful performance of the final systems flight test vehicle satisfactorily demonstrated the feasibility of a frangible meteorological rocket system. Furthermore, the degree of fragmentation demonstrated with a complete vehicle during this program and the successful operation of this system in flight constitute a significant technological advance in the state-of-the-art of meteorological rocket systems and rocketry in general.

Although the performance of the Phase III Frangible ARCAS vehicle was somewhat less than desired, its performance could be significantly improved by substituting an existing higher energy propellant such as Arcadene or incorporating a short boost phase. Substitutions of a higher energy propellant could be accomplished utilizing the basic motor design and would provide an apogee altitude of 200,000 feet¹, thereby providing acceptable altitudes for an operational frangible meteorological rocket system.

Although fragmentation of the vehicle to particle sizes yielding a maximum of about 3.0 ft-lb of impact kinetic energy was demonstrated, fragmentation to 1.5 ft-lb or less could be achieved with the same explosive configuration with only minor modification of the nozzle section.

1. 10.5-pound payload, sea level launch, QE = 84°.

Sheet explosive 0.042-inch-thick provides fragmentation of the vehicle to particle sizes yielding less than 3.0 ft-lb of impact kinetic energy when incorporated along the entire length of the motor case in combination with a modular explosive charge in the forward section of the vehicle. The shape of the modular charge has no appreciable effect on the degree of fragmentation achieved when used in this configuration. Furthermore, it may be concluded that complete fragmentation to the required particle sizes cannot be achieved with a single modular charge of conventional explosive material, regardless of the shape of the module.

Results of the fragmentation tests conducted during this program show the need for a better definition of allowable particle sizes if this or similar concepts are to be employed with regard to "lethal limit." Definition of acceptable particle sizes in terms of impact kinetic energy appears to be inadequate with respect to "lethal limit" since kinetic energy alone does not account for all factors which contribute to this limit.

LIST OF SYMBOLS

A_e	= nozzle exit area, in ²
A_t	= nozzle throat area, in ²
C_D	= coefficient of drag
D	= drag, lb
E	= kinetic energy, ft-lb
F	= thrust, lb
F_{max}	= maximum thrust, lb
h	= altitude, ft
k	= kinetic energy constant, 1/g ρ , ft ³ /lb
g	= gravitational acceleration, ft/sec ²
NM	= nautical miles
P	= ambient pressure, psia
P_{max}	= maximum pressure, psia
$P_{c max}$	= maximum chamber pressure, psia
P_t	= total pressure, $P_a + q$, psia
q	= dynamic pressure, $\rho V^2/2$, psi
QE	= effective launch angle, deg
R	= Reynold's number
S	= drag reference area, ft ²
t	= time, sec
t_a	= action time, sec
T_b	= burning time, sec
T_{max}	= maximum temperature, °F
V	= velocity, ft/sec
V_a	= average velocity, ft/sec
V_{max}	= maximum velocity, ft/sec
V_{min}	= minimum velocity, ft/sec
V_T	= terminal velocity, ft/sec
W	= weight, lb
W_w	= weight in water, lb
X	= characteristic length, ft
ρ	= density, lb-sec ² /ft ⁴
τ_o	= boundary layer shear stress, lb ft ⁻²

LIST OF TABLES

<u>Table</u>	<u>Description</u>
I	ARCAS and Frangible ARCAS Dimensional and Weight Comparisons
II	Nominal Component Weights
III	Static Firing Summary (Phase III Program)
IV	Environmental Test Data, Mechanical Timer Unit
V	Functional Test Results of Redundant Initiators
VI	Functional Test Results of Redundant Initiators
VII	Water Tank Test Data for Particle C_D Determination
VIII	Particle C_D Calculations Using Experimental Data
IX	Maximum and Minimum Particle C_D Using Experimental Data
X	Particle Impact Kinetic Energy Calculations
XI	"Detasheet" Sheet Explosive Manufacturer's Specifications
XII	Calculations of Maximum Boundary Layer Shear Stress
XIII	Frangible ARCAS Wind Weighting Factors
XIV	Flight Test Summary
XV	Trajectory Data (Basic Vehicle)
XVI	Trajectory Data (Systems Vehicle)
XVII	Comparative Performance Summary

LIST OF FIGURES

<u>Figure</u>	<u>Description</u>
1	Frangible ARCAS Assembly Drawing
2	Vehicle Configuration
3	Photographic Comparison of Standard ARCAS and Frangible ARCAS
4	Nominal Flight Events Sequence
5	Frangible ARCAS Rocket Motor Assembly
6	Frangible ARCAS Nominal Thrust Versus Time
7	Motor Case Skin Temperature Versus Time (Static Firing AFST-11)
8	Motor Case Skin Temperature Versus Time (Static Firing AFST-12)
9	Motor Case Skin Temperature Profile
10	Headplate Configuration
11	Maximum Headplate Deflection Versus Chamber Pressure
12	Propellant Grain Retention Method
13	Photo Showing Method of Fin Attachment
14	Illustration of Dimple Motor
15	Post-Test Photograph of Actuated Dimple Motors
16	Frangible ARCAS Parachute Assembly
17	Pyrotechnic Gas Generator Assembly
18	Payload Ejection Pressure Versus Time
19	Pyrogen Gas Generator Assembly
20	Mechanical Timer Assembly Photograph
21	Payload and Rocket Body Trajectories After Apogee (88° QE)
22	Payload and Rocket Body Trajectories After Apogee (84° QE)
23	Payload and Rocket Body Relative Distance Versus Launch Angle
24	Redundant Initiator Illustration
25	Illustration of Vehicle Attitude in Flight Trajectory
26	Single Modular Shaped Charge Configuration
27	Shaped Charge Fragmentation Modules
28	Motor Assembly with Bifocal Fragmentation Module
29	Simulated Altitude Fragmentation Test Set-Up
30	Photographic Sequence of Fragmentation Test

LIST OF FIGURES (Continued)

<u>Figure</u>	<u>Description</u>
31	Conical Shaped Charge Pre- and Post-Test Comparison
32	Bifocal Shaped Charge Pre- and Post-Test Comparison
33	Illustration of Fragmentation Module Propagation
34	Illustration of Bifocal Charge Wave Propagation
35	Wave Paths of Bifocal Charge
36	Photo of Drag Coefficient Test Pieces
37	Photo of Drag Coefficient Test Pieces
38	Photo of Drag Coefficient Test Pieces
39	Fragmenting Cone Assembly (Type I)
40	Fragmenting Cone Assembly (Type II)
41	Target Test Set-Up
42	Module Assembly Test Set-Up
43	Photo Showing Fragments Produced by Inverted Cone Modules
44	Shock Tube Fragmentation Concept
45	Static Firing Fragmentation Test Set-UP
46	Forward Motor Assembly Illustration
47	Linear Shaped Charge Pre-Test Photograph
48	Linear Shaped Charge Pre-Test Photograph
49	Sympathetic Detonation Fragmentation Concept
50	Photo of Pre-Test Set-Up Using Sheet Explosive
51	Test Results Obtained with 0.030-Inch-Thick Sheet Explosive
52	Pre-Test Photo of Fragmentation Model with Linear Shaped Charge
53	Fragmentation Test Results Using Linear Shaped Charge
54	Static Firing/Fragmentation Test Set-Up
55	Static Firing/Fragmentation Sequence Diagram
56	Test Results Using 0.042-Inch-Thick Sheet Explosive
57	Final Fragmentation System Assembly
58	Primary Firing Train (Mechanical Timer)
59	Firing Train Detonation Test Results
60	Set-Up for Mechanical Timer Fragmentation Test

LIST OF FIGURES (Continued)

<u>Figure</u>	<u>Description</u>
61	Explosive Module Assembly
62	Loading of Vehicle into Launcher
63	Launcher Piston Assembly
64	Launcher Piston Attachment
65	Launch Tube Modification for Systems Flight Tests
66	Vehicle Static Stability
67	Vehicle Center of Gravity Versus Flight Time
68	Vehicle Nominal Pitch Frequency and Roll Rate Versus Time
69	Vehicle Pitching Frequency Versus Payload Weights
70	Vehicle Wind Sensitivity Versus Altitude
71	Photo of Diagnostic Flight Test Vehicles
72	Thermocouple Locations for Diagnostic Flight Tests
73	Predicted Motor Case Skin Temperature Versus Flight Time
74	Predicted Fin Temperature Versus Flight Time
75	Frangible ARCAS Diagnostic Payload
76	Diagnostic Payload Assemblies
77	Block Diagram of Diagnostic Payload Telemetry System
78	Trajectory Profiles for Diagnostic Flight Vehicles
79	Vehicle Roll Rate Versus Flight Time (Flight AFFT-1)
80	Vehicle Drag Coefficient Versus Mach Number
81	Trajectory Profiles for Diagnostic Flight Vehicles (Critique No. 1)
82	Payload Section Temperatures Versus Flight Time
83	Motor Case Skin Temperature Versus Flight Time
84	Loading of Systems Vehicle into Launcher
85	Anticipated Fragmentation of Phase III Systems Vehicles
86	Launch Hazard Area for Systems Flight Tests
87	Allowable Impact Area for Systems Flight Tests
88	Actual Sequence of Events (Systems Flight Test AFFT-4)
89	Comparative Nominal Trajectory Profiles to Apogee
90	Nominal Trajectory Profiles (Phase III Systems Vehicle)

LIST OF FIGURES (Continued)

<u>Figure</u>	<u>Description</u>
91	Systems Vehicle Performance Curves
92	Apogee Performance (Phase III Systems Vehicle)
93	Apogee Altitude Versus Payload Weight
94	Vehicle Velocity Versus Flight Time
95	Burnout Mach Number Versus Vehicle Burnout Weight
96	Apogee Altitude Versus Motor Length and Corresponding Total Impulse
97	Comparison of Phase III and Modified Phase III Vehicle
98	Apogee Altitude Performance of Modified Phase III Vehicle

Table I

Frangible ARCAS Vehicle Dimensional and Weight Comparisons

Parameter	Standard ARCAS	Frangible ARCAS		Frangible ARCAS With Fragmentation System
	Mod 0	Without Fragmentation System	Mod 3	
A. Dimensions (inches)				
Nose Cone	18.1	18.1		18.1
Parachute Container	11.5	11.5		11.5
Rocket Motor Assembly	60.7	64.5		69.5
Over-all Length	90.3	94.1		99.1
Maximum Body Diameter	4.5	4.7		4.8
Minimum Body Diameter	4.5	4.4		4.5
Fin Span	13.0	13.0		13.0
B. Weights (pounds)				
Loaded Motor Assembly	66.4	62.7		68.4
Payload Weight ^a	10.7	10.4		10.4
Total Launch Weight (Nominal)	77.1	73.1		78.8
Vehicle Weight at Motor Eurnout (Less Payload Weight)	23.3	19.7		25.4

^aIncludes parachute assembly, Arcasonde I, nose cone and ballast.

Table II

Detailed Weight Breakdown of the Frangible ARCAS Vehicle (Less Payload)

<u>Component</u>	<u>Nominal Weight at Lift-Off (lbs)</u>	<u>Nominal Weight at Burnout (lbs)</u>
Motor Case Assembly	16.50	15.20
Fin Assembly	1.69	1.69
Fin Screws	0.03	0.03
Propellant Assembly*	42.70	1.00
Retaining Sleeve	1.49	1.49
Explosive Module Fwd. Plate	0.32	0.32
Explosive Module Aft Plate	0.29	0.29
Push Rod	0.02	0.02
Mechanical Timer Assembly	0.70	0.70
Redundant Initiator	0.30	0.30
Primary Explosive Charge	2.06	2.06
Sheet Explosive Charge & Overwrap	<u>2.30</u>	<u>2.30</u>
	68.40 lbs.	25.40 lbs.

* Includes propellant, headplate, O-ring, dimple motor and inhibitor

Table II
Frangible ARCAS Phase III Static Firing Summary

Motor Data				Proof Pressure Test Results		Static Firing Test Results						
Sequence Number	Date Fired	Unit Designation	Configuration	Proof Pressure (psi)	Comments	Test Number	Conditioning Temperature (°F)	P _{max} (psia)	t _a (sec)	F _{max} (lb)	T _{max} (°F)	Comments
1	5-13-64	Residual	ED-04-26-45-8 Tayloron 5031 Motor Insulation with PA-6 Nozzle Backup Insulation	1700	Acceptable	AFST-9	+70	1088	28.5	356	••	Successful
2	5-13-64	Residual		1700	Acceptable	AFST-10	+70	1071	28.8	357	Lost Data	Successful
3	5-13-64	Residual		1700	Acceptable	AFST-11	+70	1080	28.1	360	428	Successful
4	6-11-64	Residual		1700	Acceptable	AFST-12	+75	1096	27.5	365	500	Successful
5	9-22-64	T-III-1A	T-III-2B T-III-3	1700	Acceptable	AFST-13*	+84	••	••	••	---	Successful
6	10-28-64	T-III-2B		1700	Acceptable	AFST-14*	+70	••	••	••	••	Successful
7	11-28-64	T-III-3		1700	Acceptable	AFST-15*	+55	••	••	••	••	Successful

*Static firing/fragmentation test.

**Not recorded.

43
44
45

Table IV

Drop, Shock, Acceleration and Vibration Test Results of the
Mechanical Timer Unit, Model 1758

Arming Time at 20 g's
Longitudinal Acceleration*

Test No.	Time (ms)
1	101
2	102
3	109
4	123
5	108
6	113

Shock Tests: The Unit Experienced 80 g's Shock Along the Longitudinal Axis and 50 g's Shock Along the Transverse Axis for a Duration of 6 ms Without Becoming Armed.

Vibration Tests: Sweep - 2 to 500 cps at 5 g's Resonant Point at 300 cps Unit Was Vibrated in Two Planes at the Resonant Point for 15 Minutes. No Abnormalities Were Observed.

*Requirement of 15 to 20 g's for 100 to 140 ms Was Specified

Drop Tests: The Units Were Dropped 3.5 Feet Into Soft Sand While Oriented in a Position Most Conducive to Arming. The Units did not Become Armed. It Should be Noted that this Drop Condition Was Considered More Severe than would be Expected During Normal Handling of the Units During Launch.

Table V. Manufacturer's Functional Test Results of the Redundant Initiators

Unit Serial Number	Test No. 1		Test No. 2		Test No. 3		Test No. 4	
	Altitude (thousands of feet)		Altitude (thousands of feet)		Altitude (thousands of feet)		Altitude (thousands of feet)	
	Armed	Fired	Armed	Fired	Armed	Fired	Armed	Fired
001	70-100	57.0	70-100	56.8	70-100	57.0	70-100	57.0
002	70-100	57.0	70-100	57.0	70-100	57.0	70-100	57.2
003	70-100	57.0	70-100	57.1	70-100	57.3	70-100	57.7
004	70-100	56.0	70-100	56.0	70-100	55.2	70-100	55.3
005	70-100	53.0	70-100	52.3	70-100	52.7	70-100	52.6
006	70-100	53.9	70-100	54.1	70-100	54.3	70-100	54.0

Note: Functional Specification: Arm between 70,000 and 100,000 feet during ascent.
Fire between 50,000 and 70,000 feet during descent.

Table VI
Atlantic Research Corporation's Functional Test Results of the Redundant Initiators

Unit Serial Number	Test No. 1		Test No. 2		Test No. 3	
	Altitude (thousands of feet)		Altitude (thousands of feet)		Altitude (thousands of feet)	
	Armed	Fired	Armed	Fired	Armed	Fired
001	70-80	58.0	70-80	57.0	a	a
002	70-80	57.5	90-100	58.5	80-90	59.5
003	90-100	59.5	90-100	59.5	90-100	60.0
004	70-80	56.7	70-80	58.5	70-80	57.5
005	70-80	56.0	70-80	56.7	70-80	56.0
006	70-80	56.0	70-80	56.0	70-80	56.0

Notes: Functional Specification: Arm between 70,000 and 100,000 feet during ascent.
Fire between 50,000 and 70,000 feet during descent.

a. Unit damaged during third test. No additional tests attempted.

Table VII

Tabulation of Time Required (in seconds) for Test Piece to Free-Fall Through 8.75 ft of Water

Test Piece	Test Number										t_{\min} (sec)	t_{\max} (sec)	t_a (sec)
	1	2	3	4	5	6	7	8	9	10			
Fin Flange	12.2	12.8	12.8	12.5	13.2	12.5	13.1	13.1	12.9	13.2	12.2	13.2	12.8
Fin Piece Number 1	19.5	10.0	16.7	16.5	10.6	19.0	8.1	7.6	17.2	21.1	7.6	21.1	14.6
Fin Piece Number 2	11.8	8.2	15.0	8.8	12.3	8.4	11.2	10.5	10.0	15.0	8.2	15.0	11.1
Fin Piece Number 3	21.5	20.4	20.0	20.0	17.9	20.4	18.5	17.7	20.0	18.7	17.7	21.5	19.5
Fin Piece Number 4	22.1	13.9	20.6	20.6	21.5	20.7	20.6	15.4	21.6	21.2	13.9	22.1	19.8
Fin Piece Number 5	17.1	18.0	16.6	17.0	17.0	16.4	16.6	16.4	15.9	16.7	15.9	18.0	16.7
Fin Rib	11.2	13.9	11.7	9.6	7.6	11.6	9.6	6.7	9.6	9.5	6.7	13.9	10.1
Motor Case Section Number 1	8.6	7.6	7.8	7.4	7.8	7.3	8.0	8.0	7.7	7.4	7.4	8.6	7.8
Motor Case Section Number 2	11.8	11.2	10.5	10.3	12.7	12.8	13.3	11.8	11.2	12.4	10.3	13.3	11.8
Motor Case Section Number 3	10.8	10.0	9.6	9.1	9.1	9.9	9.4	9.2	9.2	9.6	9.1	10.8	9.6
Motor Case Section Number 4	29.8	29.2	28.3	28.2	29.2	28.2	29.0	29.2	29.8	28.5	28.2	29.8	28.9
Motor Case Section Number 5	12.8	11.5	11.2	11.4	13.7	11.6	12.7	11.9	12.1	12.2	11.2	13.7	12.1
Large Insulation	5.5	6.0	6.2	6.0	6.4	6.3	6.3	6.4	6.0	5.6	5.5	6.4	6.1
Small Insulation	11.9	11.5	9.6	8.9	11.6	10.2	12.0	11.3	11.5	11.2	8.9	12.0	11.0
Parachute Canister Piece Number 1	6.5	7.0	6.2	6.8	11.0	6.6	6.5	7.3	5.9	6.9	5.9	11.0	7.1
Parachute Canister Piece Number 2	13.6	11.5	10.0	14.6	11.5	10.0	12.5	14.7	12.6	13.6	10.0	14.7	12.5
Fin Retaining Screw	2.7	2.8	2.9	2.6	2.7	2.9	2.7	2.2	2.7	2.3	2.2	2.9	2.6

 t_{\min} = Minimum time required for sample to free-fall through a depth of 8.75 feet of water during 10 tests. t_{\max} = Maximum time required for sample to free-fall through a depth of 8.75 feet of water during 10 tests. t_a = Average time required for sample to free-fall through a depth of 8.75 feet of water during 10 tests.

$$V_g = \frac{8.75}{t_a}, V_{\max} = \frac{8.75}{t_{\min}} \text{ and } V_{\min} = \frac{8.75}{t_{\max}}$$

Table VIII
Tabulation of Calculations to Determine Average Free-Fall
Drag Coefficients Using Experimental Data

Test Piece	W_w (lb)	t_a (sec)	D (ft)	$V_a = \frac{D}{t_a}$ (ft/sec)	S (ft ²)	$1.034 W_w$	V_a^2	$V_a^2 S$	C_D
Fin Flange	0.029	12.8	8.75	0.684	0.0591	0.0300	0.467	0.0276	1.09
Fin Piece Number 1	0.168	14.6	8.75	0.600	0.3890	0.1740	0.360	0.1400	1.24
Fin Piece Number 2	0.142	11.1	8.75	0.788	0.1910	0.1470	0.620	0.1182	1.24
Fin Piece Number 3	0.030	19.5	8.75	0.449	0.1050	0.0310	0.201	0.0211	1.47
Fin Piece Number 4	0.014	19.8	8.75	0.441	0.0452	0.0145	0.1951	0.0088	1.65
Fin Piece Number 5	0.012	16.7	8.75	0.524	0.0278	0.0124	0.274	0.0076	1.63
Fin Rib	0.010	10.1	8.75	0.866	0.0160	0.0103	0.750	0.0120	0.86
Motor Case Section Number 1	0.287	7.8	8.75	1.121	0.1470	0.2970	1.260	0.1850	1.61
Motor Case Section Number 2	0.162	11.8	8.75	0.741	0.1990	0.1675	0.550	0.1095	1.53
Motor Case Section Number 3	0.049	9.6	8.75	0.913	0.0320	0.0506	0.834	0.0267	1.90
Motor Case Section Number 4	0.010	28.9	8.75	0.303	0.0415	0.0103	0.092	0.0038	2.71
Motor Case Section Number 5	0.600	12.1	8.75	0.723	1.1950	0.6200	0.523	0.6250	0.99
Large Insulation	0.044	6.1	8.75	1.435	0.0206	0.0455	2.060	0.0425	1.07
Small Insulation	0.022	11.0	8.75	0.795	0.0242	0.0228	0.631	0.0147	1.55
Parachute Canister Piece Number 1	0.011	7.1	8.75	1.230	0.0100	0.0114	1.510	0.0151	0.76
Parachute Canister Piece Number 2	0.002	12.5	8.75	0.700	0.0035	0.0021	0.490	0.0017	1.23
Fin Retaining Screw	0.011	2.6	8.75	3.370	0.0010	0.0114	11.350	0.0114	1.00

Using the drag equation $D = W = C_D \frac{\rho V_a^2}{2} S$,

$$C_D = \frac{2W_w}{\rho V_a^2 S} = \frac{2W_w}{\left(\frac{62.4}{32.2}\right) V_a^2 S} = \frac{1.034 W_w}{V_a^2 S}$$

W_w = Weight of piece in water

t_a = Average time to fall through 8.75 feet of water

D = Depth of water through which each piece was dropped

V_a = Average velocity in water

C_D = Average drag coefficient

Table IX

Tabulation of Calculations to Determine Maximum and Minimum Free-Fall Drag Coefficients Using Experimental Data

Test Piece	t _{min} (sec)	t _{max} (sec)	D (ft)	V _{max} (ft/sec)	V _{min} (ft/sec)	V ² _{max}	V ² _{min}	S (ft ²)	1.034 W _w	V ² _{max} S	V ² _{min} S	C _D max	C _D min
Fin Flange	12.2	13.2	8.75	0.717	0.663	0.514	0.440	0.0591	0.0300	0.0304	0.0263	1.15	0.99
Fin Piece Number 1	7.6	21.1	8.75	1.151	0.415	1.329	0.172	0.3890	0.1740	0.5160	0.0075	2.60	0.34
Fin Piece Number 2	8.2	15.0	8.75	1.068	0.583	1.138	0.340	0.1910	0.1470	0.2170	0.0654	2.26	0.68
Fin Piece Number 3	17.7	21.5	8.75	0.494	0.407	0.244	0.166	0.1050	0.0310	0.0256	0.0094	1.78	1.31
Fin Piece Number 4	13.9	22.1	8.75	0.629	0.396	0.395	0.157	0.0452	0.0145	0.0179	0.0072	2.04	0.61
Fin Piece Number 5	15.9	18.0	8.75	0.550	0.486	0.302	0.236	0.0278	0.0124	0.0084	0.0013	1.88	0.46
Fin Rib	6.7	13.9	8.75	1.307	0.629	1.702	0.395	0.0160	0.0103	0.0272	0.0063	1.64	0.38
Motor Case Section Number 1	7.4	8.6	8.75	1.182	1.019	1.400	1.035	0.1470	0.2970	0.2060	0.1520	1.95	1.44
Motor Case Section Number 2	10.3	13.3	0.75	0.849	0.658	0.720	0.433	0.1990	0.1675	0.1433	0.0861	1.94	1.17
Motor Case Section Number 3	9.1	10.8	8.75	0.962	0.810	0.925	0.656	0.0320	0.0506	0.0296	0.0210	2.41	1.71
Motor Case Section Number 4	28.2	29.8	8.75	0.310	0.294	0.096	0.087	0.0415	0.0103	0.0040	0.0036	2.86	2.57
Motor Case Section Number 5	11.2	13.7	8.75	0.781	0.639	0.610	0.408	1.1950	0.6200	0.7290	0.4870	1.27	0.85
Large Insulation	5.5	6.4	8.75	1.590	1.369	2.530	1.870	0.0206	0.0455	0.0521	0.0038	1.20	0.87
Small Insulation	8.9	12.0	8.75	0.984	0.729	0.967	0.530	0.0242	0.0228	0.0234	0.0128	1.77	0.96
Parachute Canister Piece Number 1	5.9	11.0	8.75	1.483	0.796	2.200	0.635	0.0100	0.0114	0.0220	0.0064	1.78	0.52
Parachute Canister Piece Number 2	10.0	14.7	8.75	0.875	0.595	0.766	0.354	0.0035	0.0021	0.0027	0.0012	1.75	0.78
Fin Retaining Screw	2.2	2.9	8.75	3.980	3.020	15.820	9.100	0.0010	0.0114	0.0158	0.0091	1.25	0.72

Using the drag equation $D = W = C_D \frac{\rho V^2}{2} S$,

$$C_{D \min} = \frac{2W_w}{\rho V_{\max}^2 S} = \frac{1.034 W_w}{V_{\max}^2 S}$$

$$C_{D \max} = \frac{2W_w}{\rho V_{\min}^2 S} = \frac{1.034 W_w}{V_{\min}^2 S}$$

Table X
Calculations of Impact Kinetic Energy at Terminal Velocity
Using Experimentally Determined Drag Coefficients

Using the drag equation

$$D = W = C_D \frac{\rho V_T^2}{2} S \text{ for conditions of terminal velocity (drag = weight)}$$

$$V_T = \sqrt{\frac{2W}{C_D S}} \text{ or } V_T = \sqrt{\frac{2W}{C_D (0.001756) S}} \text{ at 10,000 feet altitude}$$

then

$$V_T = \sqrt{\frac{1140W}{C_D S}} = 33.8 \sqrt{\frac{W}{C_D S}}$$

Motor Part	W (gms)	W (lbs)	$\frac{W}{2g}$ (lb-sec ² /ft)	C _D ^{**}	S (ft ²)	$\frac{W}{C_D S}$	$\sqrt{\frac{W}{C_D S}}$	$V_T = 33.8 \sqrt{\frac{W}{C_D S}}$	V_T^2	$E = \frac{W}{2g} \frac{V_T^2}{(ft-lbs)}$
Largest Fin Piece	178	0.393	0.00610	1.24	0.400	0.495	0.704	30.2	912	5.55
Average Fin Piece	23	0.058	0.00090	1.24	0.070	0.087	0.297	27.6	760	0.68
Fin Rib	10	0.022	0.00035	0.86	0.017	0.015	1.469	41.0	1,680	0.59
Fin Retaining Screw	6	0.013	0.00020	1.00	0.001	0.001	13.000	122.0	14,880	2.98
Largest Parachute Container Piece	12	0.026	0.00040	0.76	0.021	0.016	1.626	43.0	1,830	0.74
Largest Glass Filament Piece*	45	0.100	0.00155	1.61	0.048	0.077	1.300	38.5	1,480	2.29
Largest Motor Case Insulation Piece	46	0.102	0.00160	1.07	0.022	0.024	4.250	69.5	4,830	7.70
Largest Graphite Throat Insert Piece	2	0.004	0.00060	1.07	0.002	0.002	2.000	47.8	2,280	1.37
Remaining Motor Case	-	8.750	0.13600	0.50	1.480	0.740	11.820	116.5	13,580	1,840.00

*Excluding the remaining motor case.

Table XI. "Detasheet" Specifications

Property	"Detasheet" C
Explosive Content & Material	63% PETN—8% NC
Detonation Velocity (meters/sec)	7000
Density (gms/cc)	1.48
Flexibility Range, (° F)	-65 to 160
Storage Life at Ambient Temperatures	Indefinite (a)
Thermal stability (° F)	
24 Hours	250
1 Hour	275
Hot Bar Ignition Temperature (° F)	
Instantaneous (extrapolated)	565
5 Seconds	456
15 Seconds	380
30 Seconds	353
Impact Sensitivity (5 Kg drop test)	56+ in
Static Sensitivity (joules)	>0.9(b)
Minimum Tensile Strength (psi)	
ASTM D-1566-60T	30(c)
Range of Per Cent Elongation	
ASTM D-412-61T	15 to 150
Minimum Propagation Thickness (in)	
Sheet (steel back-up plate)	—
Sheet (unconfined)	0.025
Cord	0.060(d)

- Notes:**
- a. "Detasheet" C has been stored at ambient temperatures for over four years to date with no change in performance or flexibility.
 - b. Failed to detonate at 30 Kv discharged through a capacitance of 2600 pf.
 - c. "Detasheet" flexible explosive will creep to rupture under continuous stress as low as 1½ psi. The reported tensile data was developed at 20 in/min crosshead travel.
 - d. This cord diameter corresponds to approximately 15 grains per foot explosive.

Table XII

Calculations of the Frangible ARCAS Maximum Boundary Layer Shear Stress

For turbulent boundary layer:

$$\tau_o = \frac{1.5 \rho V^2}{\sqrt{R}} \quad (\text{lb/ft}^2)$$

where

 ρ = ambient density (lb-sec²/ft⁴) V = vehicle velocity (ft/sec) R = Reynold's number

t (sec)	Altitude (ft)	ρ	V (ft/sec)	$\nu = \mu/\rho$	$\frac{R}{(ft)}$	Vx	$R = Vx/\nu$	\sqrt{R}	V^2	ρV^2	$1.5 \rho V^2$	τ_o
10	6,600	0.00198	1,263 x 10 ³	1.84 x 10 ⁻⁴	5	6.32 x 10 ³	3.44 x 10 ⁷	5.86 x 10 ³	1.60 x 10 ⁶	5.12 x 10 ³	4.68 x 10 ³	0.80
16	16,000	0.00145	1,907 x 10 ³	2.34 x 10 ⁻⁴	5	9.53 x 10 ³	4.06 x 10 ⁷	6.38 x 10 ³	3.63 x 10 ⁶	5.26 x 10 ³	7.90 x 10 ³	1.24
20	224,200	0.00110	2,353 x 10 ³	2.92 x 10 ⁻⁴	5	11.75 x 10 ³	4.02 x 10 ⁷	6.37 x 10 ³	5.52 x 10 ⁶	6.07 x 10 ³	9.10 x 10 ³	1.43
26	40,100	0.00088	3,207 x 10 ³	5.10 x 10 ⁻⁴	5	16.01 x 10 ³	3.14 x 10 ⁷	5.60 x 10 ³	10.29 x 10 ⁶	5.95 x 10 ³	8.92 x 10 ³	1.60
30	53,600	0.000804	3,564 x 10 ³	9.75 x 10 ⁻⁴	5	17.81 x 10 ³	1.83 x 10 ⁷	4.28 x 10 ³	12.70 x 10 ⁶	3.86 x 10 ³	5.79 x 10 ³	1.35
60	131,400	66 x 10 ⁻⁷	2,180 x 10 ³	5.64 x 10 ⁻²	5	10.9 x 10 ³	1.97 x 10 ⁵	4.44 x 10 ²	4.75 x 10 ⁶	3.13 x 10	4.69 x 10	0.11

**Table XIII. Frangible ARCAS Systems Flight Test Vehicles,
Wind Weighting Factors**

<u>Altitude Stratum (ft)</u>	<u>Wind Weighting Factors</u>
20-50	0.095
50-100	0.093
100-200	0.109
200-300	0.077
300-400	0.059
400-600	0.093
600-800	0.069
800-1,000	0.047
1,000-1,200	0.037
1,200-1,400	0.028
1,400-1,600	0.020
1,600-1,800	0.013
1,800-2,000	0.024
2,000-3,000	0.057
3,000-4,000	0.040
4,000-5,000	0.022
5,000-10,000	0.051
10,000-20,000	0.034
20,000-30,000	0.015
30,000-50,000	0.017

Unit Wind Effect: 1.57 NM/knot
Tower Tilt Effect: 3.2 NM/degree

Table XIV. Frangible ARCAS Phase III Flight Test Summary

Flight Test No.	Vehicle No.	Mission	Payload	Payload Weight (lb)	QE (degrees)	Predicted Apogee Altitude (ft)	Actual Apogee Altitude (ft)	Per Cent Error
AFFT-1	FAD-1	Diagnostic	Special TM	10.1	84.5	188,000	190,000 ^b	+1.1
AFFT-2	FAD-2	Diagnostic	Special TM	10.1	77.0	125,000	114,373	-8.6
AFFT-3	FAS-1	Systems Test	Arcasonde 1A	10.5	a	a	69,000 ^a	a
AFFT-4	FAS-2	Systems Test	Arcasonde 1A	10.5	84.9	127,500	129,800	+1.8

- a. No test. Loss of launcher pressure resulted in severe reduction of vehicle performance.
b. Based on TM data.

FAD: Frangible ARCAS Diagnostic Vehicle
FAS: Frangible ARCAS Systems Vehicle

Table XV.

INITIAL TRAJECTORY PARAMETER VALUES

TIME	ACC.	VEL.	ALT.	FL ANGLE	RANGE	DYN PRESS	MACH*	THRUST	FL. WGT.	DRAG/WT	DRAG LOSS
2.00000	99.0	393.1	611	82.57	73	1.847, 02	.36	294.4	70.77	.0907	3.5
4.00000	121.7	617.4	1604	81.54	212	4.343, 02	.56	338.9	67.85	.2246	13.1
6.00000	127.3	866.7	3069	80.77	441	8.159, 02	.79	349.5	64.70	.4588	34.5
8.00000	124.1	1120.6	5029	80.15	771	1.285, 03	1.02	364.3	61.45	1.0874	80.0
10.00000	102.0	1340.7	7459	79.63	1205	1.704, 03	1.23	366.8	58.13	2.1563	192.1
12.00000	97.5	1530.2	10291	79.16	1735	2.060, 03	1.43	367.4	54.82	2.6897	348.8
14.00000	98.7	1734.8	13504	78.73	2363	2.364, 03	1.63	368.0	51.54	3.0907	535.1
16.00000	100.8	1934.5	17099	78.33	3092	2.613, 03	1.84	364.8	48.30	3.4404	745.9
18.00000	106.3	2141.0	21086	77.96	3929	2.801, 03	2.07	358.9	45.13	3.6733	975.3
20.00000	116.2	2362.8	25484	77.62	4879	2.928, 03	2.33	352.6	42.04	3.8013	1216.5
22.00000	130.0	2607.7	30332	77.30	5957	2.993, 03	2.63	344.3	39.05	3.8024	1461.6
24.00000	157.5	2893.7	35687	77.01	7176	3.005, 03	2.98	344.7	36.11	3.6775	1703.4
26.00000	192.2	3242.2	41651	76.74	8565	2.858, 03	3.35	344.6	33.20	3.4361	1933.0
28.00000	125.0	3627.1	48345	76.50	10155	2.570, 03	3.73	242.4	30.56	3.0799	2144.2
30.00000	-66.7	3620.9	54444	76.26	11870	1.835, 03	3.73	34.2	29.83	2.2505	2317.8

STAGE 1 MISSILE PARAMETERS

WEIGHT	EXIT AREA	DRAG REF. AREA	MASS FLOW CONST.	STAGE TIME	INTEG. INT.
62.70	2.55	.1196	.00463000	30.00	.50

STAGE 2 MISSILE PARAMETERS

WEIGHT	EXIT AREA	DRAG REF. AREA	MASS FLOW CONST.	STAGE TIME	INTEG. INT.
19.70	.00	.1316	.00000000	1000.00	1.00

TIME	ACC.	VEL.	ALT.	FL ANGLE	RANGE	DYN PRESS	MACH*	THRUST	FL. WGT.	DRAG/WT	DRAG LOSS
30.00000	-109.9	3620.9	55444	76.26	11870	1.840, 03	3.74	.0	30.20	2.4507	2317.8
35.00000	-62.8	3210.4	71919	75.62	15979	6.711, 02	3.31	.0	30.20	.9891	2573.2
40.00000	-45.0	2947.0	84770	74.87	19872	2.768, 02	3.00	.0	30.20	.4425	2682.2
45.00000	-37.5	2743.5	100461	74.02	23662	1.229, 02	2.77	.0	30.20	.2124	2732.1
50.00000	-34.0	2505.6	113184	73.05	27399	.992, 01	2.54	.0	30.20	.1111	2757.2
55.00000	-32.3	2400.5	125023	71.96	31105	.5191, 01	2.34	.0	30.20	.0634	2770.6
60.00000	-31.1	2242.5	136019	70.72	34791	1.697, 01	2.14	.0	30.20	.0358	2778.0
65.00000	-30.4	2080.1	146195	69.29	38464	4.447, 00	1.96	.0	30.20	.0211	2782.3
70.00000	-29.7	1939.0	155563	67.64	42128	5.502, 00	1.80	.0	30.20	.0129	2784.9
75.00000	-29.1	1791.8	164129	65.73	45785	3.338, 00	1.66	.0	30.20	.0081	2786.5
80.00000	-28.5	1647.7	171898	63.48	49437	2.130, 00	1.52	.0	30.20	.0054	2787.6
85.00000	-27.7	1507.1	178873	60.80	53084	1.318, 00	1.40	.0	30.20	.0035	2788.3
90.00000	-26.8	1370.8	185054	57.58	56727	8.783, -01	1.29	.0	30.20	.0023	2788.4
95.00000	-25.5	1239.9	190645	53.68	60367	6.045, -01	1.17	.0	30.20	.0016	2789.1
100.00000	-23.8	1116.4	195045	48.88	64005	4.217, -01	1.05	.0	30.20	.0009	2789.3
105.00000	-21.5	1002.7	198856	42.95	67641	2.875, -01	.96	.0	30.20	.0005	2789.4
110.00000	-18.4	902.5	201877	35.61	71275	2.139, -01	.86	.0	30.20	.0003	2789.5
115.00000	-14.1	820.7	204151	26.63	74909	1.647, -01	.79	.0	30.20	.0002	2789.5
119.430	-9.6	770.5	205177	17.79	77960	1.351, -01	.74	.0	30.20	.0002	2789.5
119.600	-9.4	766.5	205424	17.34	78105	1.344, -01	.74	.0	30.20	.0002	2789.5
119.820	-8.9	766.9	205513	16.44	78396	1.331, -01	.74	.0	30.20	.0002	2789.5
120.000	-8.7	763.1	205556	15.99	78541	1.325, -01	.74	.0	30.20	.0002	2789.5
120.200	-8.5	761.4	205597	15.53	78686	1.319, -01	.73	.0	30.20	.0002	2789.5
120.400	-8.2	759.7	205637	15.07	78832	1.313, -01	.73	.0	30.20	.0002	2789.5
120.600	-8.0	758.1	205676	14.61	78977	1.308, -01	.73	.0	30.20	.0002	2789.6
120.800	-7.7	756.5	205714	14.15	79122	1.302, -01	.73	.0	30.20	.0002	2789.6
121.000	-7.5	755.0	205750	13.69	79268	1.297, -01	.73	.0	30.20	.0002	2789.6
121.200	-7.2	753.6	205789	13.22	79413	1.292, -01	.73	.0	30.20	.0002	2789.6
121.400	-7.0	752.1	205819	12.75	79558	1.287, -01	.73	.0	30.20	.0002	2789.6

Table XV. (Cont'd)

121.600	-6.7	750.8	205252	12.28	79703	1.282, -01	.72	.0	30.20	.0002	2789.6
122.000	-6.2	748.2	205913	11.34	79994	1.274, -01	.72	.0	30.20	.0002	2789.6
122.600	-5.4	744.7	205995	9.91	80430	1.262, -01	.72	.0	30.20	.0002	2789.6
123.000	-4.9	742.6	206044	8.96	80720	1.254, -01	.72	.0	30.20	.0002	2789.6
123.600	-4.1	739.9	206108	7.51	81156	1.246, -01	.71	.0	30.20	.0002	2789.6
124.000	-3.6	738.4	206144	6.54	81447	1.240, -01	.71	.0	30.20	.0002	2789.6
124.600	-2.6	736.4	206189	5.08	81883	1.234, -01	.71	.0	30.20	.0002	2789.6
125.000	-2.3	735.4	206212	4.10	82173	1.231, -01	.71	.0	30.20	.0002	2789.6
125.600	-1.5	734.3	206238	2.63	82609	1.227, -01	.71	.0	30.20	.0002	2789.6
126.000	-.9	733.8	206249	1.64	82900	1.225, -01	.71	.0	30.20	.0002	2789.6
126.600	-.1	733.5	206256	.17	83335	1.224, -01	.71	.0	30.20	.0002	2789.6
127.800	1.5	734.4	206236	-2.70	84207	1.229, -01	.71	.0	30.20	.0002	2789.6
APOGEE CONDITIONS											
128.80		736.6	206184		84933						
132.800	8.0	754.6	205663	-14.76	87839	1.311, -01	.73	.0	30.20	.0002	2789.6
137.800	13.6	813.2	204303	-25.57	91471	1.506, -01	.78	.0	30.20	.0002	2789.6
142.800	18.0	892.6	202154	-34.73	95103	1.944, -01	.86	.0	30.20	.0003	2789.7
147.800	21.2	931.0	199217	-42.24	98736	2.575, -01	.95	.0	30.20	.0004	2789.7
152.800	23.5	1103.2	195492	-48.31	102370	3.805, -01	1.05	.0	30.20	.0008	2789.8
157.800	25.2	1225.5	190978	-53.22	106005	5.492, -01	1.16	.0	30.20	.0014	2790.0
162.800	26.5	1355.0	185677	-57.21	109641	7.861, -01	1.27	.0	30.20	.0021	2790.3
167.800	27.4	1490.0	179587	-60.50	113279	1.195, 00	1.39	.0	30.20	.0031	2790.7
172.800	28.1	1628.8	172709	-63.23	116917	1.934, 00	1.51	.0	30.20	.0049	2791.4
177.800	28.6	1770.6	165045	-65.52	120555	2.967, 00	1.64	.0	30.20	.0073	2792.3
182.800	28.9	1914.5	156595	-67.48	124195	4.967, 00	1.77	.0	30.20	.0117	2793.8
187.800	29.0	2059.5	147362	-69.16	127833	8.357, 00	1.93	.0	30.20	.0189	2795.1
192.800	28.9	2204.6	137350	-70.61	131470	1.472, 01	2.10	.0	30.20	.0315	2799.9
197.800	28.4	2348.6	126569	-71.89	135102	2.707, 01	2.27	.0	30.20	.0548	2805.5
202.800	27.2	2488.7	115036	-73.01	138725	5.192, 01	2.46	.0	30.20	.0989	2817.9
207.800	24.7	2619.5	102784	-74.02	142328	1.019, 02	2.63	.0	30.20	.1838	2839.8
212.800	19.8	2731.9	89864	-74.92	145894	1.976, 02	2.78	.0	30.20	.3407	2880.9
217.800	8.7	2805.8	76469	-75.75	149390	4.153, 02	2.88	.0	30.20	.6930	2961.4
222.800	-11.2	2804.9	62810	-76.52	152750	7.913, 02	2.89	.0	30.20	1.3130	3117.4
227.800	-43.4	2675.7	49400	-77.26	155866	1.337, 03	2.76	.0	30.20	2.3182	3402.4
232.800	-84.2	2354.6	37031	-78.03	158572	1.864, 03	2.43	.0	30.20	3.5927	3880.0
237.800	-99.7	1876.4	26638	-78.89	160695	1.768, 03	1.86	.0	30.20	4.0775	4515.4
242.800	-81.5	1413.3	18593	-79.93	162203	1.330, 03	1.36	.0	30.20	3.5160	5136.2
247.800	-36.2	1106.0	12478	-81.15	163226	1.009, 03	1.05	.0	30.20	2.1119	5601.9
252.800	-16.3	1007.0	7288	-82.40	163976	9.601, 02	.92	.0	30.20	1.4972	5864.9
257.800	-11.7	933.2	2496	-83.56	164565	9.622, 02	.84	.0	30.20	1.3583	6093.3
..... IMPACT.....											
260.800	-9.7	901.0	-237	-84.21	164858	9.653, 02	.81	.0	30.20	1.2962	6221.6

Table XV. (Cont'd)

TRAJECTORY NO. 1

FRANGIBLE ARCS BASIC VEHICLE FEB 8, 66

TIME	THRUST	MACH =	CU
STAGE 1			
.000	250.00	.000	.28600
.100	250.00	.600	.29400
.300	242.00	.800	.30500
.800	254.00	1.000	.39200
1.300	249.00	1.100	.58800
1.800	286.00	1.200	.61700
2.300	305.00	1.400	.60400
2.800	316.00	1.600	.56800
3.800	336.00	1.800	.53900
4.800	340.00	2.000	.50600
5.800	345.00	2.500	.43100
6.900	348.00	3.000	.36700
7.800	357.00	3.500	.32060
8.800	362.00	4.000	.29000
9.800	358.00	5.000	.24500
14.800	352.00	6.000	.21500
19.800	330.00	8.000	.21500
21.800	318.00	.000	.00000
23.800	316.00	.000	.00000
25.800	314.00	.000	.00000
26.800	312.00	.000	.00000
27.300	296.00	.000	.00000
27.800	242.00	.000	.00000
28.300	161.00	.000	.00000
28.800	67.00	.000	.00000
30.000	.00	.000	.00000

STAGE 2			
.00	.286	.00	.286
.60	.294	.60	.294
.80	.305	.80	.305
1.00	.392	1.00	.392
1.10	.588	1.10	.588
1.20	.617	1.20	.617
1.40	.604	1.40	.604
1.60	.568	1.60	.568
1.80	.539	1.80	.539
2.00	.506	2.00	.506
2.50	.431	2.50	.431
3.00	.367	3.00	.367
3.50	.320	3.50	.320
4.00	.290	4.00	.290
5.00	.245	5.00	.245
6.00	.215	6.00	.215
8.00	.215	8.00	.215

FRANGIBLE AREAS SYSTEMS VALUE

INITIAL TRAJECTORY DATA, LINE VALUES									
RAIL LENGTH	ANGLE	VELOCITY	ALTITUDE	PAYLOAD	TIME				
0	6.0	230.0	0	10.0	0.00				
STAGE 1 MISSILE PARAMETERS									
WEIGHT	EXIT AREA	CRAG REF. AREA	MASS FLOW CONST.	STAGE TIME	INTEG. FRI.				
68.40	2.55	1500	0.0045000	30.00	0.50				
ACC.	VEL.	FL ANGLE	RANGE	DYN PRESS	MACH	TPUSI	FL WGT.	DRAG/WT	DRAG LOSS
80.8	375.8	82.54	71	1.681	02	294.4	76.54	0.060	3.9
108.8	576.8	81.43	204	3.757	02	338.8	73.70	0.264	13.7
113.0	798.9	80.54	419	6.765	02	349.3	70.66	0.451	34.7
113.6	1026.1	79.90	729	1.085	03	363.9	67.43	0.795	75.2
86.6	1230.2	79.32	1139	1.456	03	366.2	64.25	2.025	165.4
78.1	1392.6	78.72	1638	1.725	03	366.5	61.04	2.566	317.4
76.0	1545.6	78.29	2222	1.945	03	367.0	57.85	3.0025	458.4
76.4	1598.4	77.82	2893	2.120	03	363.5	54.70	3.2942	701.4
77.6	1851.9	77.31	3655	2.247	03	357.4	51.62	3.5401	921.8
82.4	2011.4	76.95	4513	2.332	03	351.0	48.61	3.6855	1154.8
89.0	2181.7	76.55	5472	2.377	03	342.4	45.71	3.7541	1394.7
105.7	2375.8	76.18	6544	2.400	03	342.8	42.86	3.7434	1636.3
126.8	2607.7	75.82	7747	2.396	03	342.7	40.02	3.6547	1874.7
68.3	2852.6	75.49	9101	2.221	03	340.6	37.46	3.3356	2102.0
-84.8	2786.9	75.17	10538	1.636	03	32.5	36.75	2.5578	2293.5

STAGE 2 MISSILE PARAMETERS									
WEIGHT	EXIT AREA	DRAG KFF.	AREA	MASS FLOW	CONST.	STAGE TIME	INTEG.	INT.	
25.40	.00	.1660		.00000000		1000.00	1.00		
ACC.	VEL.	ALT.	FL ANGLE	RANGE	DYN PRESS	MACH	FL. XGT.	DRAG/WT	ORAG LOSS
-124.3	2785.9	46919	15.17	10538	1.641, C3	2.88	35.90	2.9021	2293.2
-73.0	2315.2	59122	74.72	13862	6.347, C2	2.40	35.90	1.3111	2610.8
-52.1	2007.6	69451	73.03	15881	2.925, C2	2.07	35.90	.6701	2765.0
-42.7	1773.9	78440	71.56	19734	1.500, C2	1.82	35.90	.3718	2846.4
-37.0	1577.6	86337	65.75	22483	6.423, C1	1.61	35.90	.2207	2892.3
-33.6	1402.3	93271	67.52	25110	4.465, C1	1.42	35.90	.1295	2918.8
-31.7	1240.4	99311	64.73	27830	2.740, C1	1.25	35.90	.0777	2934.9
-29.4	1088.9	104498	61.17	30453	1.707, C1	1.09	35.90	.0453	2944.5
-27.1	948.0	108959	56.54	33054	9.935, C0	.93	35.90	.0170	2949.0
-24.8	817.9	112611	50.40	35654	6.541, C0	.81	35.90	.0094	2951.0
-21.5	701.4	115167	42.10	38244	4.104, C0	.69	35.90	.0057	2952.2
-16.4	609.6	117114	30.37	40030	2.892, C0	.60	35.90	.0037	2953.0
-10.4	564.7	118138	18.14	43106	2.216, C0	.54	35.90	.0030	2953.4
-9.7	544.7	118207	17.55	43207	2.184, C0	.54	35.90	.0030	2953.4
-9.3	542.8	118239	16.31	43310	2.167, C0	.53	35.90	.0029	2953.5
-9.0	541.0	118270	16.27	43413	2.154, C0	.53	35.90	.0029	2953.5
-8.7	539.2	119299	15.62	43517	2.140, C0	.53	35.90	.0029	2953.5
-8.3	537.5	118328	14.76	43620	2.127, C0	.53	35.90	.0029	2953.5
-8.0	535.9	118355	14.31	43723	2.114, C0	.53	35.90	.0029	2953.5
-7.6	534.3	118381	13.65	43826	2.101, C0	.53	35.90	.0028	2953.6
-7.2	532.8	118405	12.93	43930	2.090, C0	.52	35.90	.0028	2953.6
-6.9	531.4	118429	12.31	44033	2.077, C0	.52	35.90	.0028	2953.6
-6.5	530.1	118451	11.64	44136	2.065, C0	.52	35.90	.0028	2953.6
-6.1	528.8	118471	10.97	44239	2.053, C0	.52	35.90	.0028	2953.6
-5.4	526.5	118503	9.61	44342	2.041, C0	.52	35.90	.0027	2953.7
-4.3	523.6	118556	7.55	44755	2.017, C0	.51	35.90	.0027	2953.7
-3.5	522.0	118581	6.17	44967	2.004, C0	.51	35.90	.0027	2953.7
-2.1	520.3	118609	6.08	45270	2.000, C0	.51	35.90	.0027	2953.7

2953.2
2953.1
2953.0

35.90
35.90
35.90

.00
.00
.00

.51
.51
.51

1.99
1.99
1.99

2.00
2.00
2.00

4.57
4.57
4.57

6.17
6.08
6.08

1185.81
1186.00
1186.00

522.0
527.3
527.3

-3.5
-2.3
-2.3

94.0000
94.6000
95.8000

97.80

Table XVI. (Cont'd)

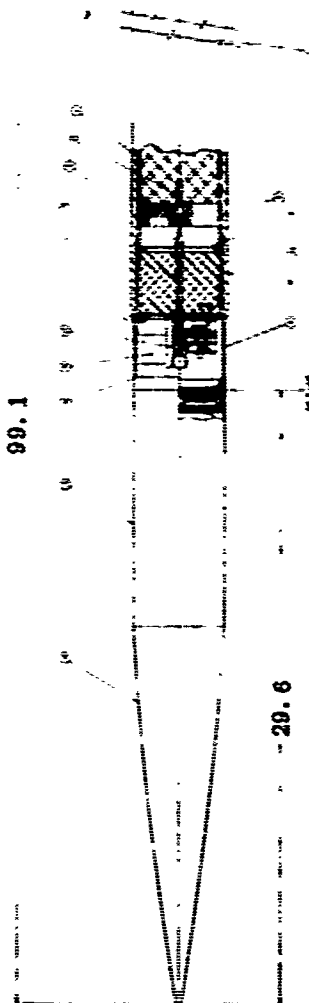
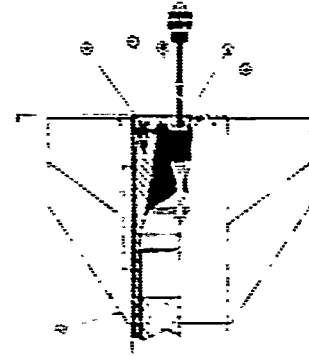
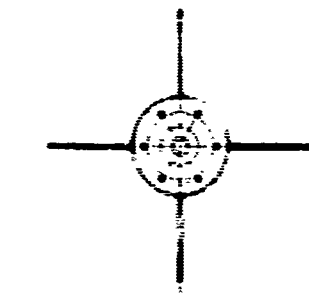
94.0000	-1.6	519.5	1186.21	2.63	45478	1.727, 00	.51	.0	35.90	.0027	2953.8
94.6000	-2.4	518.9	1186.30	.57	45788	1.742, 00	.51	.0	35.90	.0027	2953.9
95.8000	1.9	519.8	1186.14	-3.64	46407	1.992, 00	.51	.0	35.90	.0027	2954.0
97.80		527.5	1184.84		47438						
100.800	10.9	552.7	1180.51	-20.31	48909	2.236, 00	.54	.0	35.90	.0031	2954.5
105.800	17.7	525.4	1166.95	-34.10	51541	2.389, 00	.62	.0	35.90	.0039	2955.0
110.800	22.1	725.9	1145.45	-44.54	54135	4.421, 00	.72	.0	35.90	.0061	2955.5
115.800	24.8	843.9	1116.04	-52.25	56706	6.649, 00	.84	.0	35.90	.0099	2957.1
120.800	26.4	972.4	1078.74	-57.93	59274	1.026, 01	.97	.0	35.90	.0185	2958.5
125.800	26.7	1105.6	1033.62	-62.35	61632	1.772, 01	1.11	.0	35.90	.0484	2964.3
130.800	26.5	1238.9	980.86	-65.75	64375	2.746, 01	1.25	.0	35.90	.0779	2974.3
135.800	25.7	1369.4	920.77	-68.47	66893	4.432, 01	1.39	.0	35.90	.1239	2990.7
140.800	23.7	1493.2	853.66	-70.68	69376	7.354, 01	1.54	.0	35.90	.1980	3016.4
145.800	20.4	1603.5	780.10	-72.54	71806	1.193, 02	1.64	.0	35.90	.3115	3057.0
150.800	14.5	1690.2	701.09	-74.12	74153	1.990, 02	1.74	.0	35.90	.5039	3123.9
155.800	5.4	1740.3	618.14	-75.51	76400	3.178, 02	1.80	.0	35.90	.7930	3228.1
160.800	-6.5	1739.7	533.62	-76.76	78494	4.691, 02	1.80	.0	35.90	1.1706	3384.0
165.800	-21.3	1670.2	444.94	-77.93	80353	6.435, 02	1.72	.0	35.90	1.6358	3609.7
170.800	-35.2	1526.6	371.35	-73.07	81950	7.824, 02	1.57	.0	35.90	2.0316	3910.4
175.800	-39.7	1333.0	300.93	-80.22	83237	7.887, 02	1.34	.0	35.90	2.2154	4261.0
180.800	-32.8	1145.8	239.88	-81.40	84225	7.287, 02	1.23	.0	35.90	2.0044	4606.2
185.800	-11.2	1044.1	186.14	-82.58	84981	7.264, 02	1.00	.0	35.90	1.3367	4868.0
190.800	-9.9	993.1	135.59	-83.66	85590	7.734, 02	.93	.0	35.90	1.2994	5078.4
195.800	-9.0	945.9	87.39	-84.63	86084	8.174, 02	.87	.0	35.90	1.2744	5285.4
200.800	-0.1	903.3	41.35	-85.48	86482	8.583, 02	.82	.0	35.90	1.2466	5488.1
205.900	-7.9	863.8	-271	-86.23	86800	8.967, 02	.77	.0	35.90	1.2442	5689.1
		IMPACT.....								

Table XVI. (Cont'd)

FRANGIBLE ARCAS SYSTEMS VEHICLE				TRAJECTORY NO.
TYPE	THRUST	PACH =	EP 2 60	4
STAGE 1				
.000	250.00	.000	.28600	
.100	250.00	.600	.29400	
.300	242.00	.800	.30500	
.800	254.00	1.000	.39200	
1.300	249.00	1.100	.58200	
1.800	206.00	1.200	.61700	
2.300	305.00	1.400	.60400	
2.800	316.00	1.600	.56800	
3.800	336.00	1.800	.53900	
4.800	344.00	2.000	.50600	
5.800	345.00	2.500	.43100	
6.900	348.00	3.000	.36700	
7.800	357.00	3.500	.32000	
8.800	362.00	4.000	.29000	
9.800	358.00	5.000	.24500	
14.800	352.00	6.000	.21500	
19.800	330.00	8.000	.21300	
21.800	318.00	.000	.00000	
23.800	316.00	.000	.00000	
25.800	314.00	.000	.00000	
26.800	312.00	.000	.00000	
27.300	296.00	.000	.00000	
27.800	242.00	.000	.00000	
28.300	161.00	.000	.00000	
28.800	67.00	.000	.00000	
30.000	.00	.000	.00000	
STAGE 2				
.00	.00	.286		
.60	.60	.294		
.80	.80	.305		
1.00	1.00	.392		
1.10	1.10	.582		
1.20	1.20	.617		
1.40	1.40	.604		
1.60	1.60	.568		
1.80	1.80	.539		
2.00	2.00	.506		
2.50	2.50	.431		
3.00	3.00	.367		
3.50	3.50	.320		
4.00	4.00	.290		
5.00	5.00	.245		
6.00	6.00	.215		
8.00	8.00	.213		

**Table XVII. Comparative Performance Summary for the ARCAS and Frangible ARCAS Vehicles
(for 10.5 lb Payload, Sea Level Launch, 84° QE, Auxiliary Gas Generator Boost)**

Parameter	Standard ARCAS	Frangible ARCAS without Fragmentation System	Frangible ARCAS with Fragmentation System
	Mod 0	Mod 3	Mod 3
Apogee Altitude (ft)	210,000	206,000	119,000
Apogee Range (ft)	87,300	83,300	45,800
Impact Range (ft)	173,000	164,600	86,700
Time to Apogee (sec)	128	127	95
Time to Impact (sec)	258	260	205
Vehicle Velocity at Motor Burnout (ft/sec)	3,600	3,620	2,790
Altitude at Motor Burnout (ft)	55,000	55,400	47,000

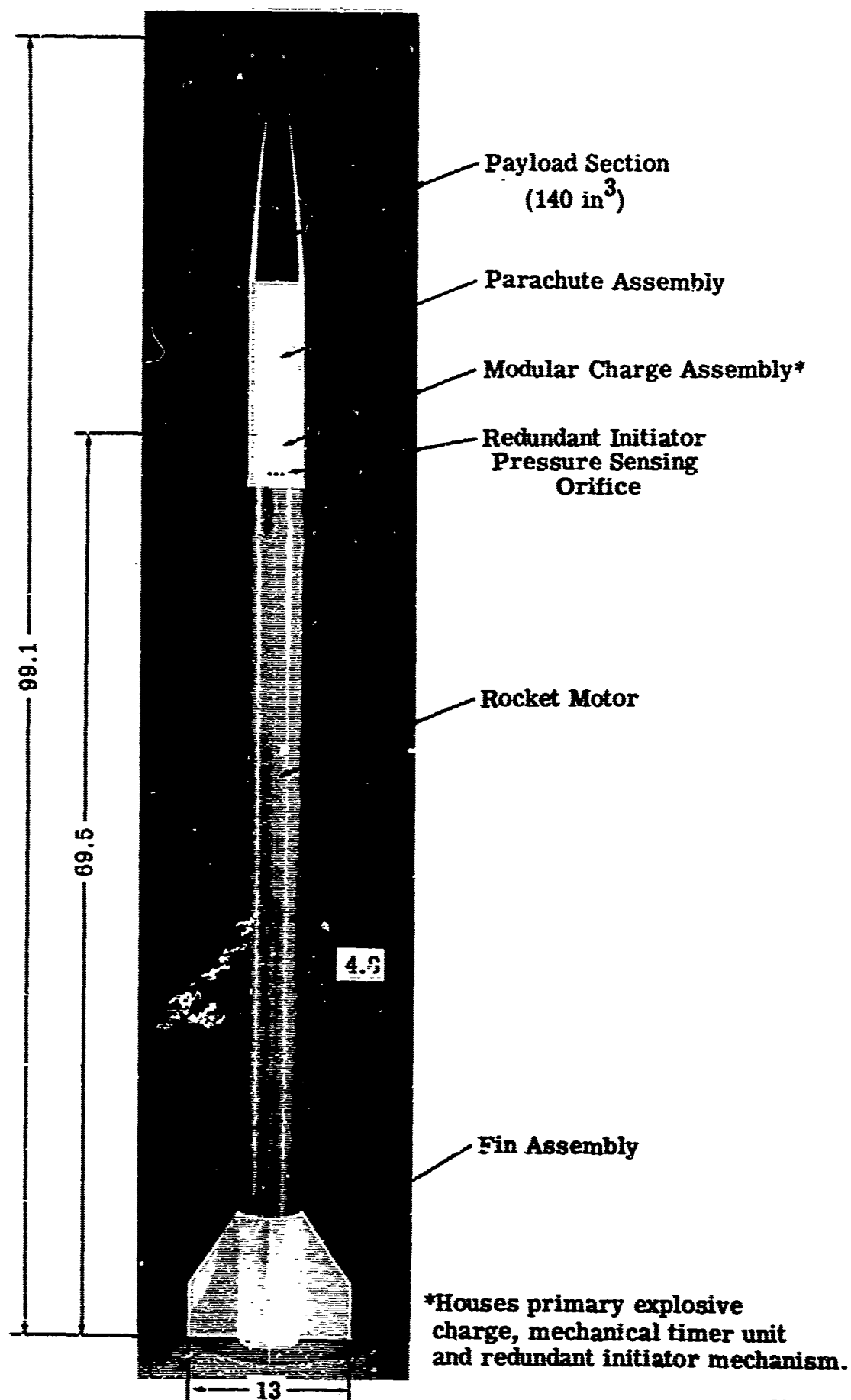


NO.	DESCRIPTION	QTY	UNIT	PRICE	TOTAL
1	VALVE	1	EA	10.00	10.00
2	SEAL	1	EA	5.00	5.00
3	ROD	1	EA	15.00	15.00
4	WASHER	1	EA	2.00	2.00
5	NUT	1	EA	3.00	3.00
6	SCREW	1	EA	4.00	4.00
7	SPRING	1	EA	6.00	6.00
8	PLATE	1	EA	8.00	8.00
9	GASKET	1	EA	1.00	1.00
10	HOUSING	1	EA	20.00	20.00
11	FLANGE	1	EA	12.00	12.00
12	BRACKET	1	EA	7.00	7.00
13	BEARING	1	EA	9.00	9.00
14	SHAFT	1	EA	11.00	11.00
15	KEY	1	EA	2.00	2.00
16	WASHER	1	EA	2.00	2.00
17	NUT	1	EA	3.00	3.00
18	SCREW	1	EA	4.00	4.00
19	SPRING	1	EA	6.00	6.00
20	PLATE	1	EA	8.00	8.00
21	GASKET	1	EA	1.00	1.00
22	HOUSING	1	EA	20.00	20.00
23	FLANGE	1	EA	12.00	12.00
24	BRACKET	1	EA	7.00	7.00
25	BEARING	1	EA	9.00	9.00
26	SHAFT	1	EA	11.00	11.00
27	KEY	1	EA	2.00	2.00
28	WASHER	1	EA	2.00	2.00
29	NUT	1	EA	3.00	3.00
30	SCREW	1	EA	4.00	4.00
31	SPRING	1	EA	6.00	6.00
32	PLATE	1	EA	8.00	8.00
33	GASKET	1	EA	1.00	1.00
34	HOUSING	1	EA	20.00	20.00
35	FLANGE	1	EA	12.00	12.00
36	BRACKET	1	EA	7.00	7.00
37	BEARING	1	EA	9.00	9.00
38	SHAFT	1	EA	11.00	11.00
39	KEY	1	EA	2.00	2.00
40	WASHER	1	EA	2.00	2.00
41	NUT	1	EA	3.00	3.00
42	SCREW	1	EA	4.00	4.00
43	SPRING	1	EA	6.00	6.00
44	PLATE	1	EA	8.00	8.00
45	GASKET	1	EA	1.00	1.00
46	HOUSING	1	EA	20.00	20.00
47	FLANGE	1	EA	12.00	12.00
48	BRACKET	1	EA	7.00	7.00
49	BEARING	1	EA	9.00	9.00
50	SHAFT	1	EA	11.00	11.00
51	KEY	1	EA	2.00	2.00
52	WASHER	1	EA	2.00	2.00
53	NUT	1	EA	3.00	3.00
54	SCREW	1	EA	4.00	4.00
55	SPRING	1	EA	6.00	6.00
56	PLATE	1	EA	8.00	8.00
57	GASKET	1	EA	1.00	1.00
58	HOUSING	1	EA	20.00	20.00
59	FLANGE	1	EA	12.00	12.00
60	BRACKET	1	EA	7.00	7.00
61	BEARING	1	EA	9.00	9.00
62	SHAFT	1	EA	11.00	11.00
63	KEY	1	EA	2.00	2.00
64	WASHER	1	EA	2.00	2.00
65	NUT	1	EA	3.00	3.00
66	SCREW	1	EA	4.00	4.00
67	SPRING	1	EA	6.00	6.00
68	PLATE	1	EA	8.00	8.00
69	GASKET	1	EA	1.00	1.00
70	HOUSING	1	EA	20.00	20.00
71	FLANGE	1	EA	12.00	12.00
72	BRACKET	1	EA	7.00	7.00
73	BEARING	1	EA	9.00	9.00
74	SHAFT	1	EA	11.00	11.00
75	KEY	1	EA	2.00	2.00
76	WASHER	1	EA	2.00	2.00
77	NUT	1	EA	3.00	3.00
78	SCREW	1	EA	4.00	4.00
79	SPRING	1	EA	6.00	6.00
80	PLATE	1	EA	8.00	8.00
81	GASKET	1	EA	1.00	1.00
82	HOUSING	1	EA	20.00	20.00
83	FLANGE	1	EA	12.00	12.00
84	BRACKET	1	EA	7.00	7.00
85	BEARING	1	EA	9.00	9.00
86	SHAFT	1	EA	11.00	11.00
87	KEY	1	EA	2.00	2.00
88	WASHER	1	EA	2.00	2.00
89	NUT	1	EA	3.00	3.00
90	SCREW	1	EA	4.00	4.00
91	SPRING	1	EA	6.00	6.00
92	PLATE	1	EA	8.00	8.00
93	GASKET	1	EA	1.00	1.00
94	HOUSING	1	EA	20.00	20.00
95	FLANGE	1	EA	12.00	12.00
96	BRACKET	1	EA	7.00	7.00
97	BEARING	1	EA	9.00	9.00
98	SHAFT	1	EA	11.00	11.00
99	KEY	1	EA	2.00	2.00
100	WASHER	1	EA	2.00	2.00

NO.	DESCRIPTION	QTY	UNIT	PRICE	TOTAL
1	VALVE	1	EA	10.00	10.00
2	SEAL	1	EA	5.00	5.00
3	ROD	1	EA	15.00	15.00
4	WASHER	1	EA	2.00	2.00
5	NUT	1	EA	3.00	3.00
6	SCREW	1	EA	4.00	4.00
7	SPRING	1	EA	6.00	6.00
8	PLATE	1	EA	8.00	8.00
9	GASKET	1	EA	1.00	1.00
10	HOUSING	1	EA	20.00	20.00
11	FLANGE	1	EA	12.00	12.00
12	BRACKET	1	EA	7.00	7.00
13	BEARING	1	EA	9.00	9.00
14	SHAFT	1	EA	11.00	11.00
15	KEY	1	EA	2.00	2.00
16	WASHER	1	EA	2.00	2.00
17	NUT	1	EA	3.00	3.00
18	SCREW	1	EA	4.00	4.00
19	SPRING	1	EA	6.00	6.00
20	PLATE	1	EA	8.00	8.00
21	GASKET	1	EA	1.00	1.00
22	HOUSING	1	EA	20.00	20.00
23	FLANGE	1	EA	12.00	12.00
24	BRACKET	1	EA	7.00	7.00
25	BEARING	1	EA	9.00	9.00
26	SHAFT	1	EA	11.00	11.00
27	KEY	1	EA	2.00	2.00
28	WASHER	1	EA	2.00	2.00
29	NUT	1	EA	3.00	3.00
30	SCREW	1	EA	4.00	4.00
31	SPRING	1	EA	6.00	6.00
32	PLATE	1	EA	8.00	8.00
33	GASKET	1	EA	1.00	1.00
34	HOUSING	1	EA	20.00	20.00
35	FLANGE	1	EA	12.00	12.00
36	BRACKET	1	EA	7.00	7.00
37	BEARING	1	EA	9.00	9.00
38	SHAFT	1	EA	11.00	11.00
39	KEY	1	EA	2.00	2.00
40	WASHER	1	EA	2.00	2.00
41	NUT	1	EA	3.00	3.00
42	SCREW	1	EA	4.00	4.00
43	SPRING	1	EA	6.00	6.00
44	PLATE	1	EA	8.00	8.00
45	GASKET	1	EA	1.00	1.00
46	HOUSING	1	EA	20.00	20.00
47	FLANGE	1	EA	12.00	12.00
48	BRACKET	1	EA	7.00	7.00
49	BEARING	1	EA	9.00	9.00
50	SHAFT	1	EA	11.00	11.00
51	KEY	1	EA	2.00	2.00
52	WASHER	1	EA	2.00	2.00
53	NUT	1	EA	3.00	3.00
54	SCREW	1	EA	4.00	4.00
55	SPRING	1	EA	6.00	6.00
56	PLATE	1	EA	8.00	8.00
57	GASKET	1	EA	1.00	1.00
58	HOUSING	1	EA	20.00	20.00
59	FLANGE	1	EA	12.00	12.00
60	BRACKET	1	EA	7.00	7.00
61	BEARING	1	EA	9.00	9.00
62	SHAFT	1	EA	11.00	11.00
63	KEY	1	EA	2.00	2.00
64	WASHER	1	EA	2.00	2.00
65	NUT	1	EA	3.00	3.00
66	SCREW	1	EA	4.00	4.00
67	SPRING	1	EA	6.00	6.00
68	PLATE	1	EA	8.00	8.00
69	GASKET	1	EA	1.00	1.00
70	HOUSING	1	EA	20.00	20.00
71	FLANGE	1	EA	12.00	12.00
72	BRACKET	1	EA	7.00	7.00
73	BEARING	1	EA	9.00	9.00
74	SHAFT	1	EA	11.00	11.00
75	KEY	1	EA	2.00	2.00
76	WASHER	1	EA	2.00	2.00
77	NUT	1	EA	3.00	3.00
78	SCREW	1	EA	4.00	4.00
79	SPRING	1	EA	6.00	6.00
80	PLATE	1	EA	8.00	8.00
81	GASKET	1	EA	1.00	1.00
82	HOUSING	1	EA	20.00	20.00
83	FLANGE	1	EA	12.00	12.00
84	BRACKET	1	EA	7.00	7.00
85	BEARING	1	EA	9.00	9.00
86	SHAFT	1	EA	11.00	11.00
87	KEY	1	EA	2.00	2.00
88	WASHER	1	EA	2.00	2.00
89	NUT	1	EA	3.00	3.00
90	SCREW	1	EA	4.00	4.00
91	SPRING	1	EA	6.00	6.00
92	PLATE	1	EA	8.00	8.00
93	GASKET	1	EA	1.00	1.00
94	HOUSING	1	EA	20.00	20.00
95	FLANGE	1	EA	12.00	12.00
96	BRACKET	1	EA	7.00	7.00
97	BEARING	1	EA	9.00	9.00
98	SHAFT	1	EA	11.00	11.00
99	KEY	1	EA	2.00	2.00
100	WASHER	1	EA	2.00	2.00

Figure 1

Frangible ARCAS Vehicle Configuration



9545-2

8841

Figure 2

Comparison of EX6 Mod 3
Frangible ARCAS With
Standard EX6 Mod 0 ARCAS



33339

Figure 3

Nominal Frangible ARCAS Flight Events Sequence Phase III Vehicle Configuration

33268

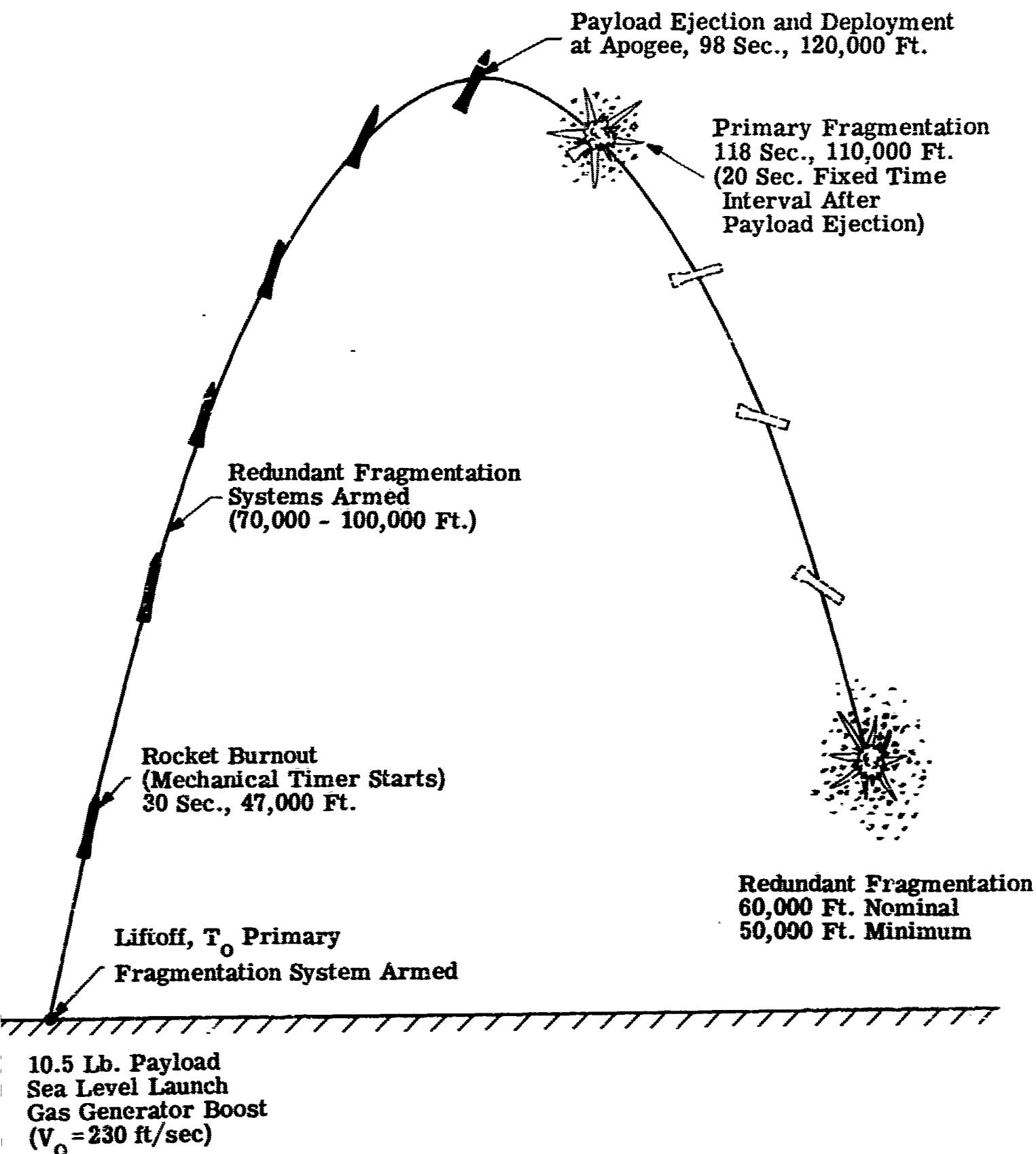


Figure 4

Frangible ARCAS Rocket Motor Assembly

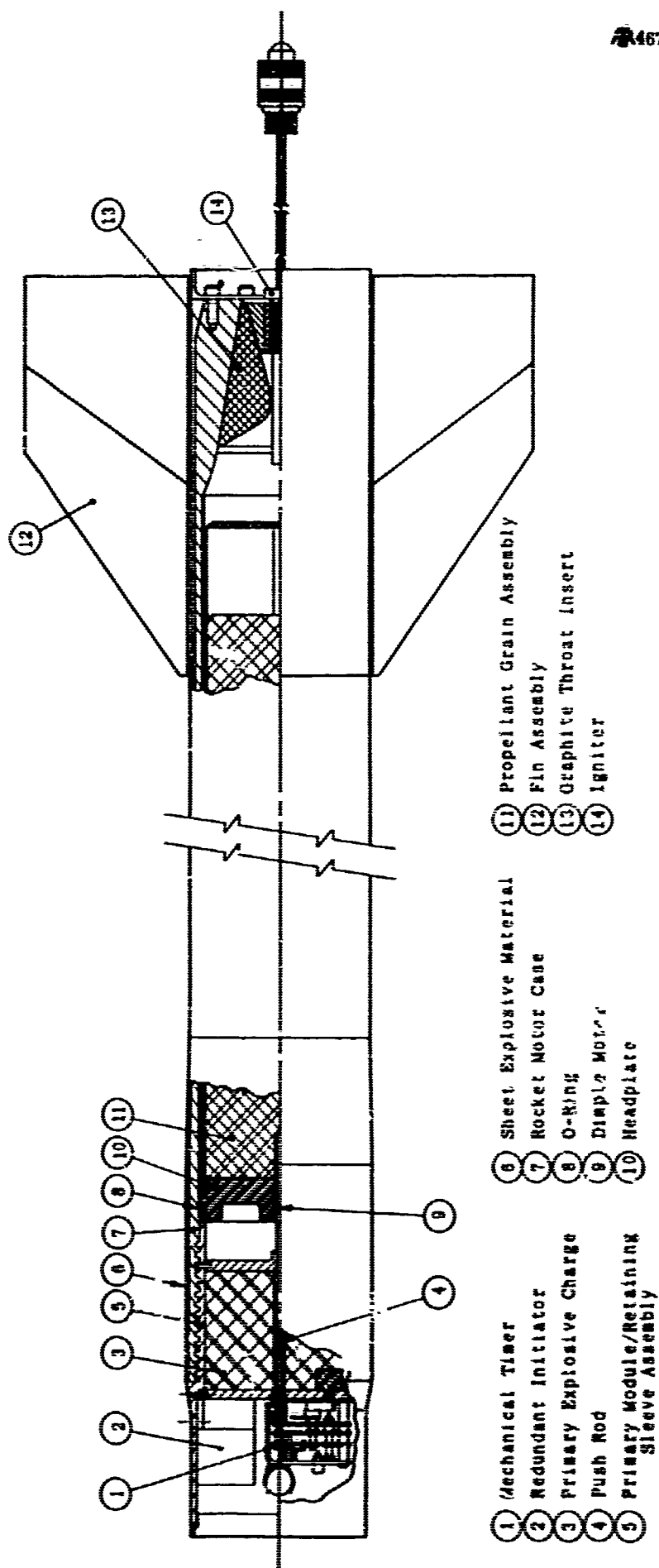


Figure 5

Nominal Thrust Versus Time for the Frangible ARCAS Rocket Motor

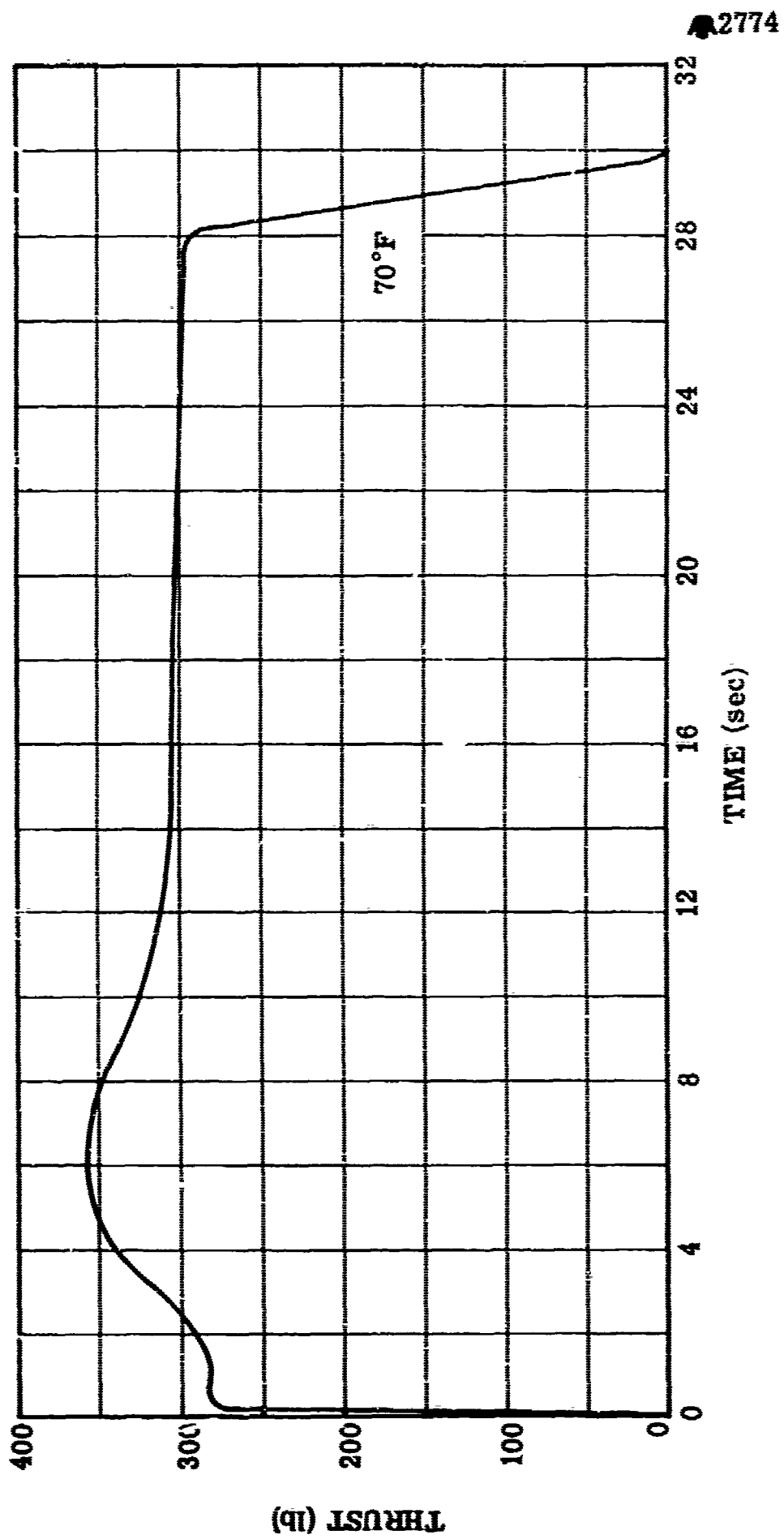


Figure 6

Frangible ARCAS Motor Case Skin Temperature Versus Time Static Firing AFST-11

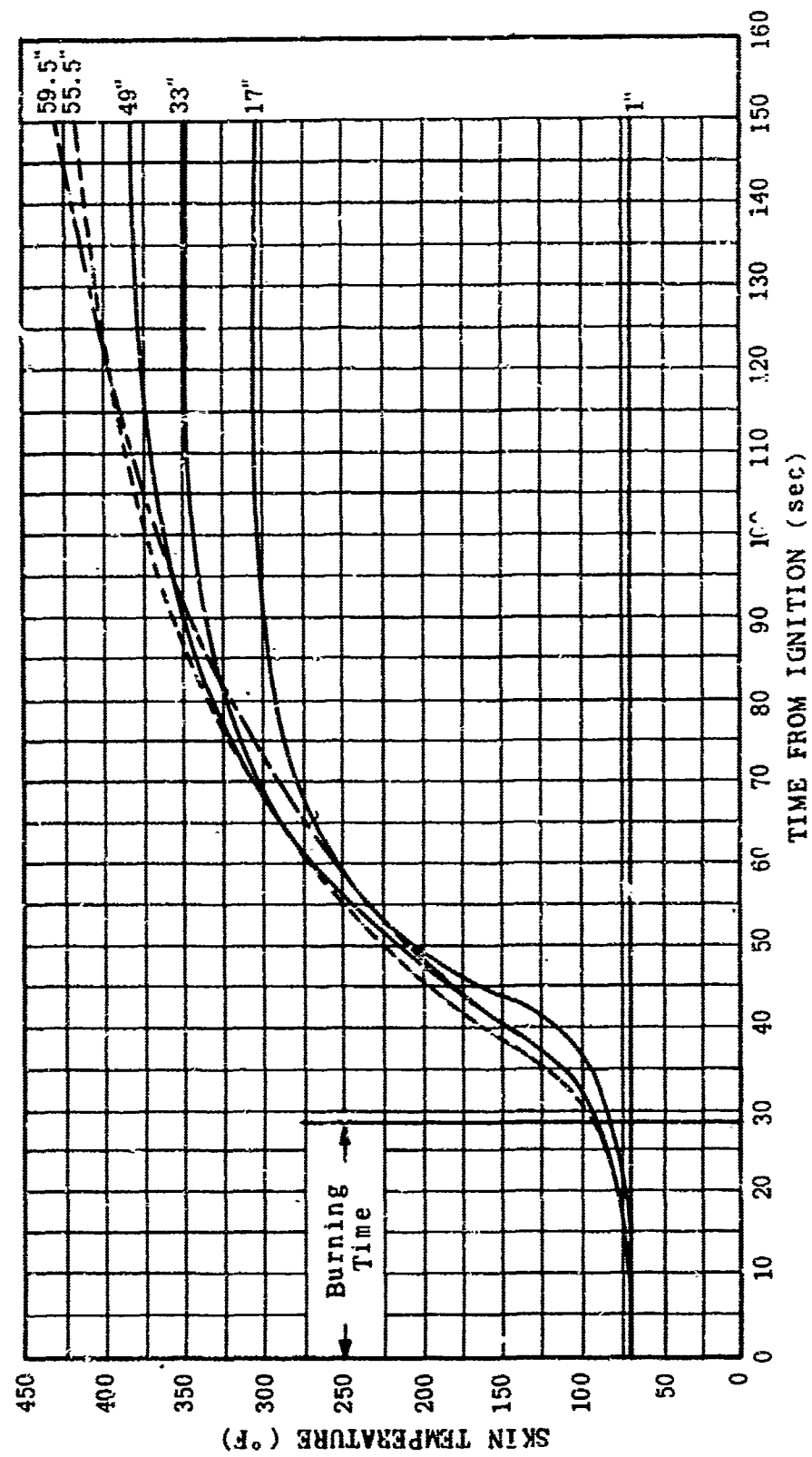
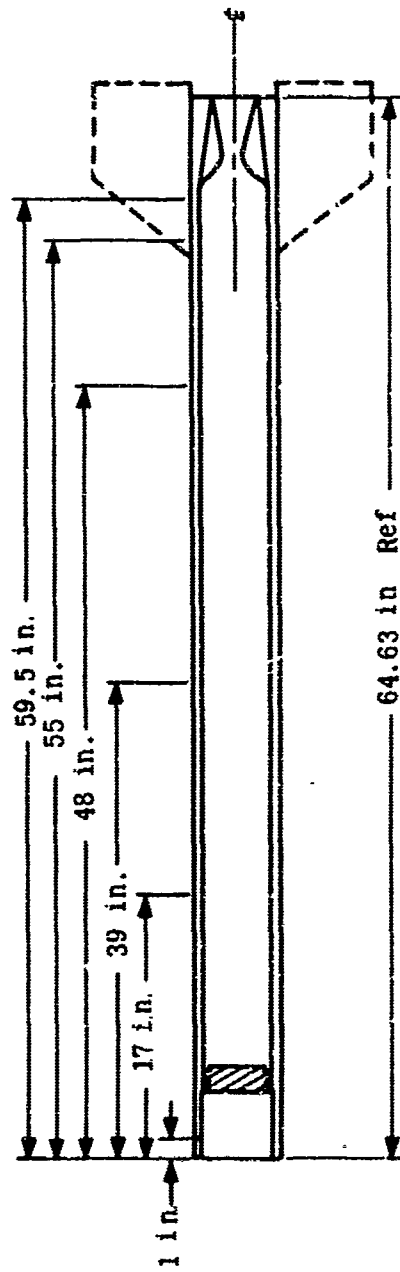
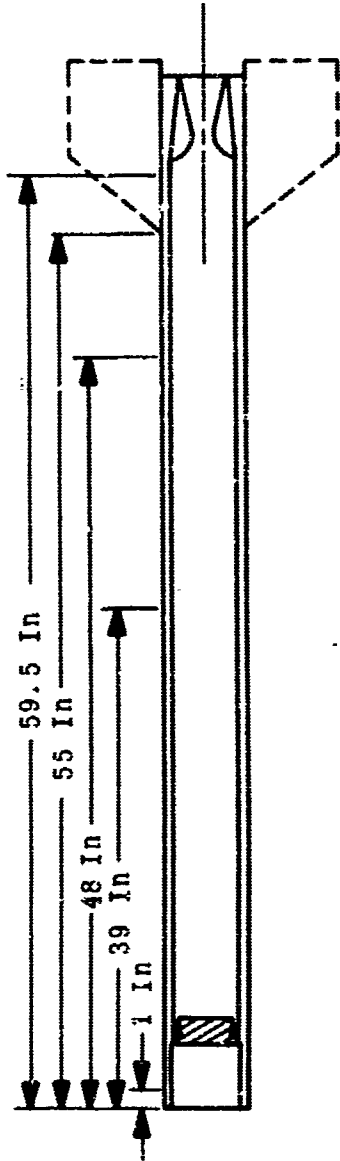


Figure 7

Frangible ARCAS Motor Case Skin Temperature
Static Firing AFST-12



33091

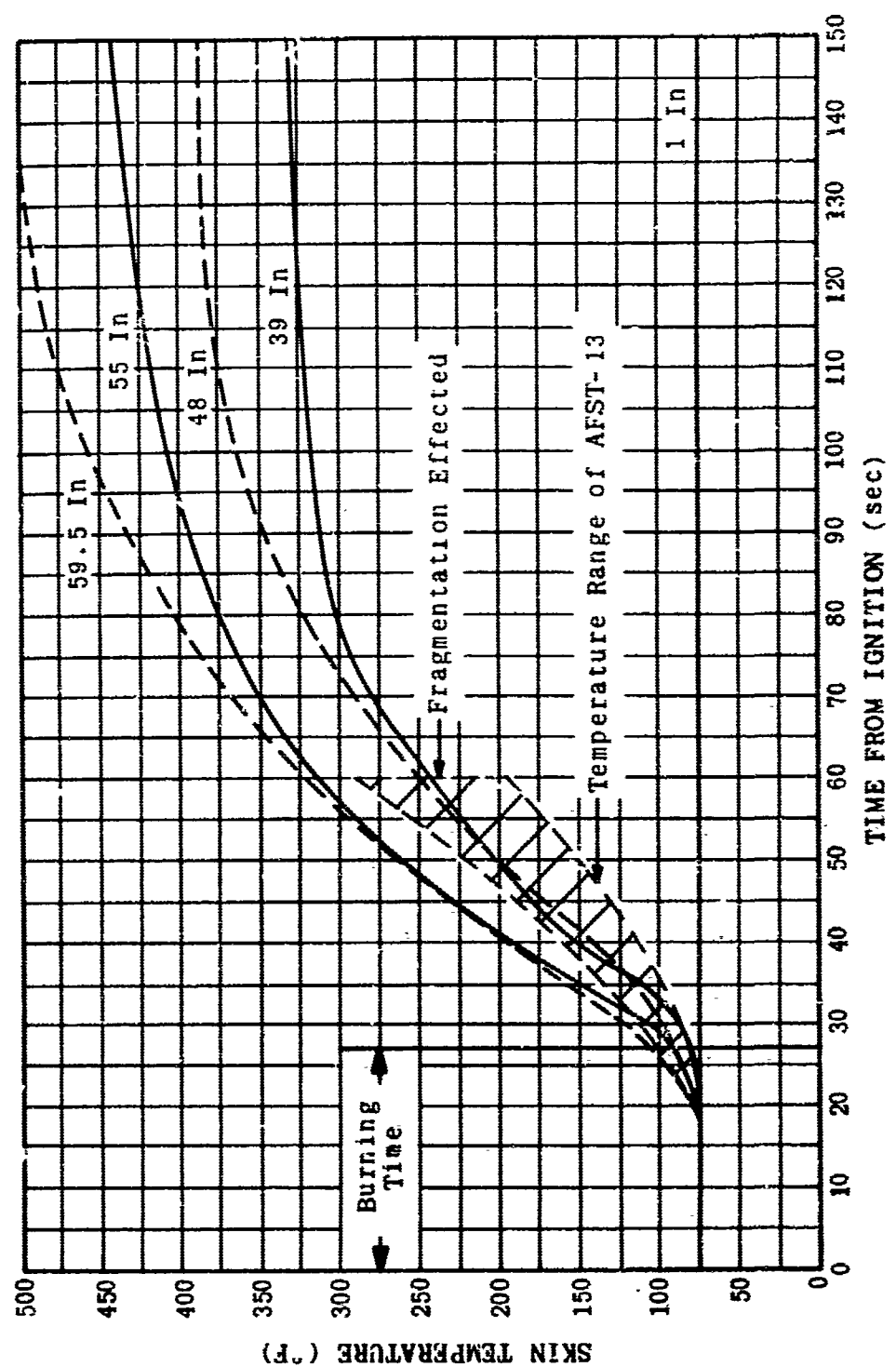


Figure 8

Approximate Motor Case Skin Temperature Profiles of the Frangible ARCAS Motor Case

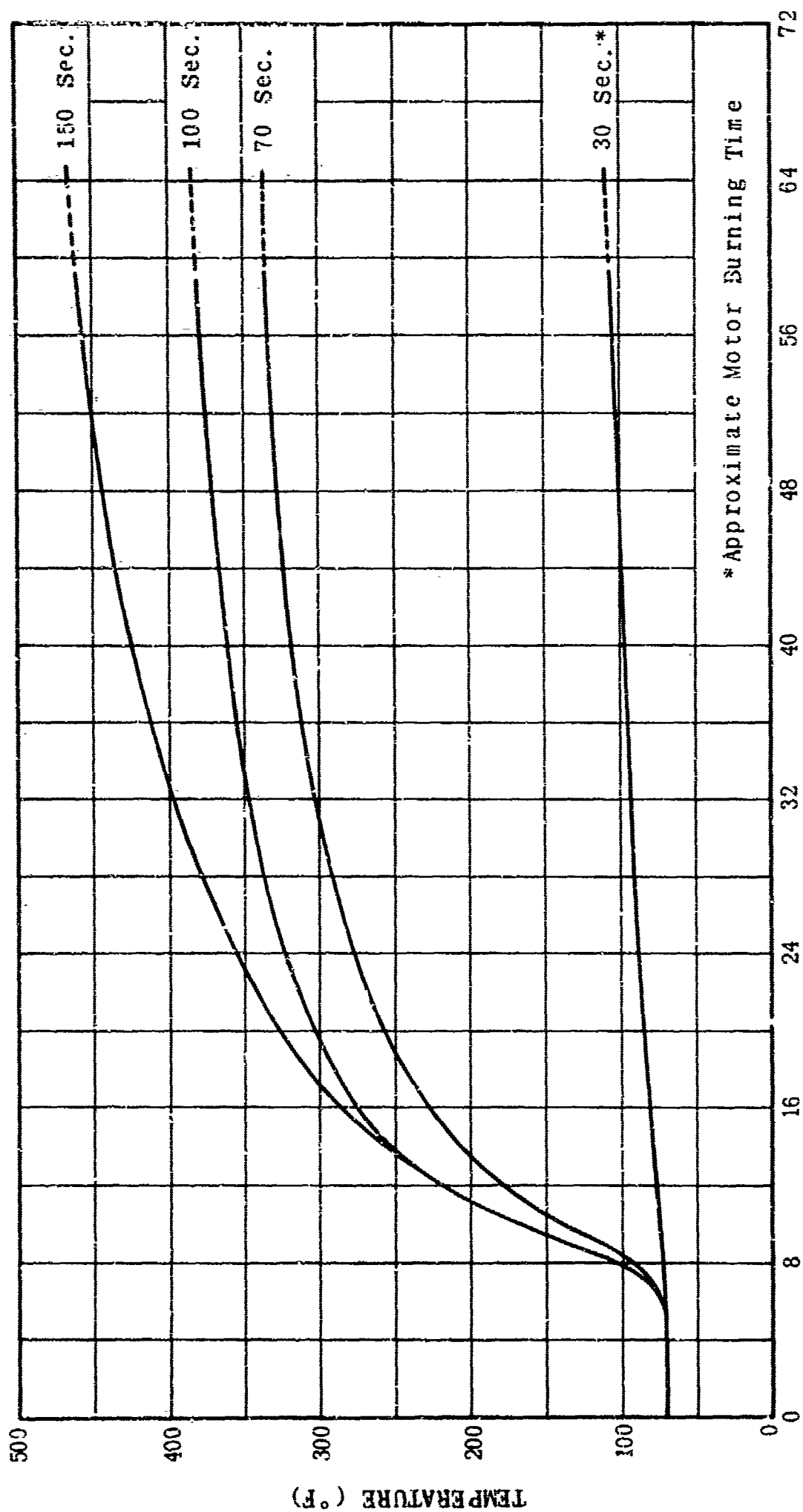
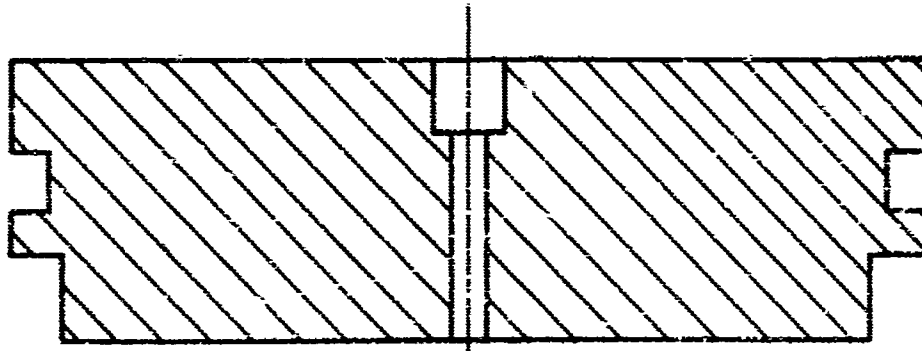


Figure 9

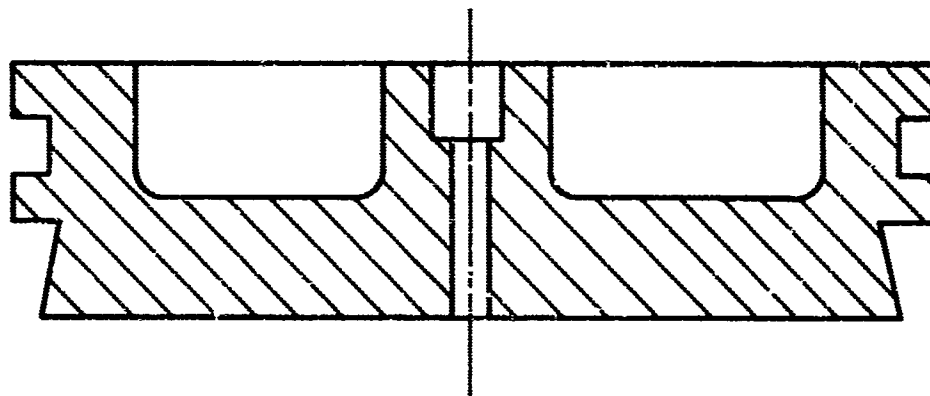


Headplate

DISTANCE FROM FORWARD EDGE OF MOTOR CASE (in)



Phase II Headplate, 1.25 Lbs.



Phase III Headplate, 0.75 Lbs.

Figure 10

Frangible ARCAS Maximum Headplate Deflection Versus Chamber Pressure

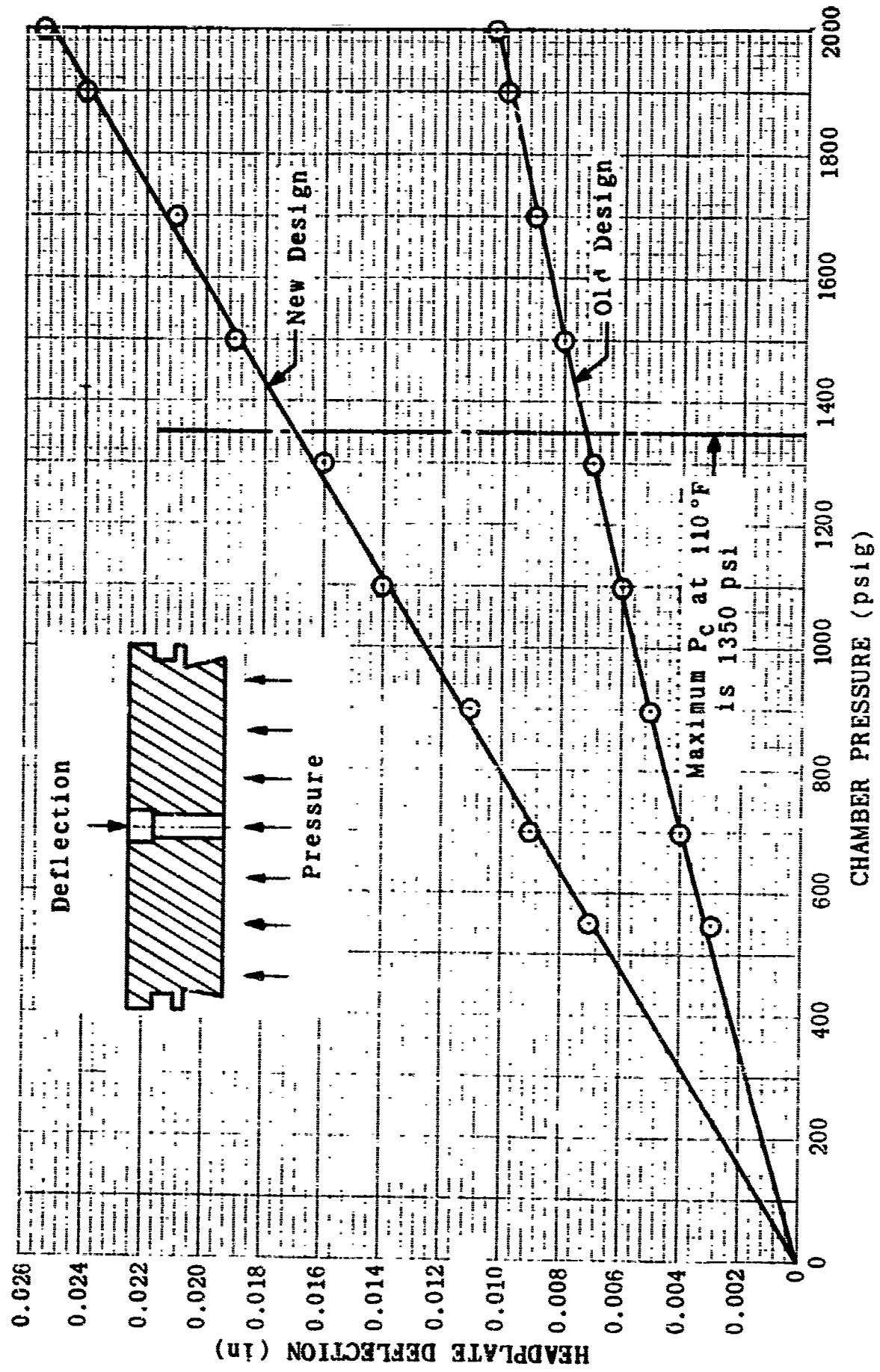


Figure 11

Frangible ARCAS Propellant Grain Retention Method

4729

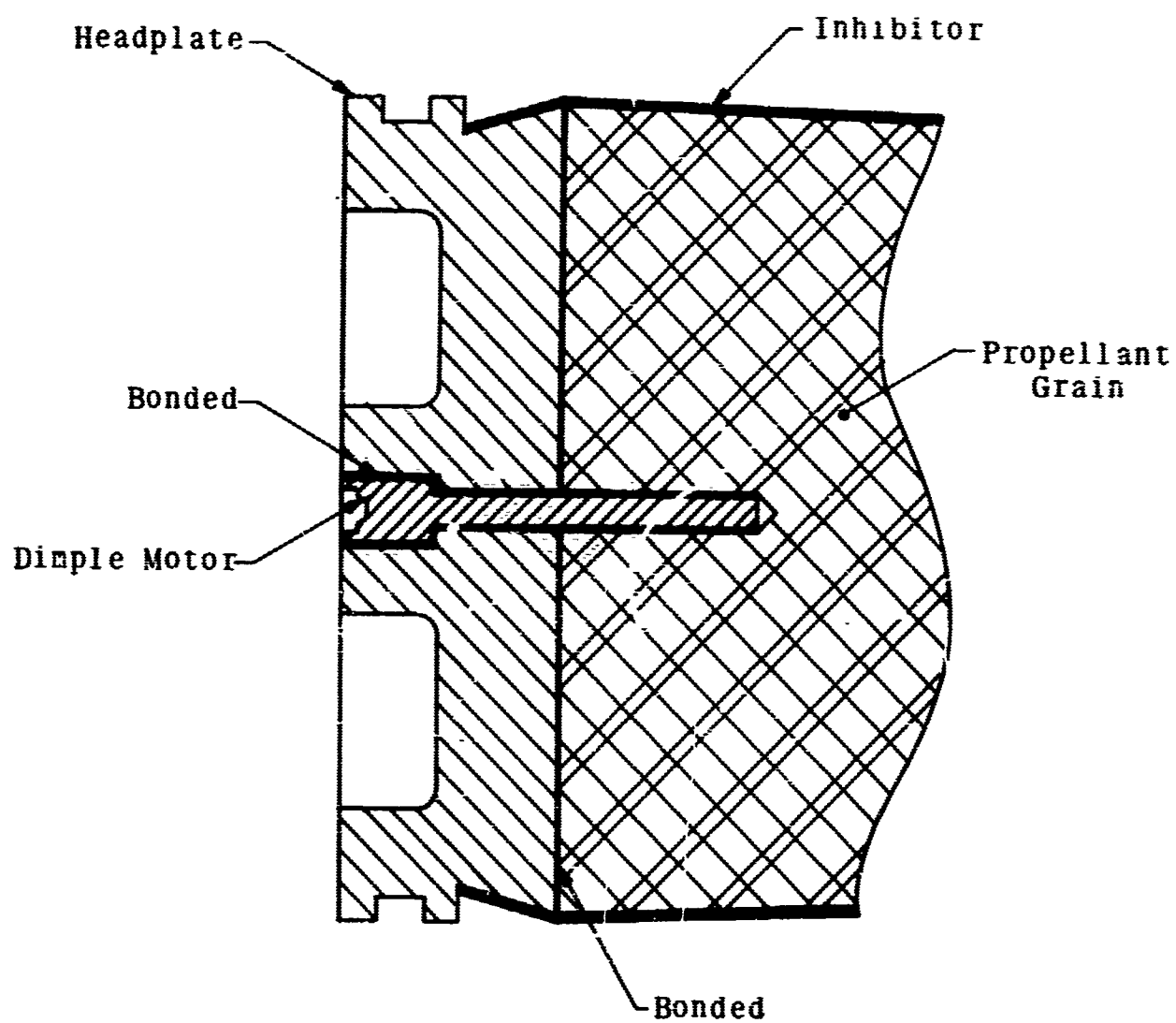
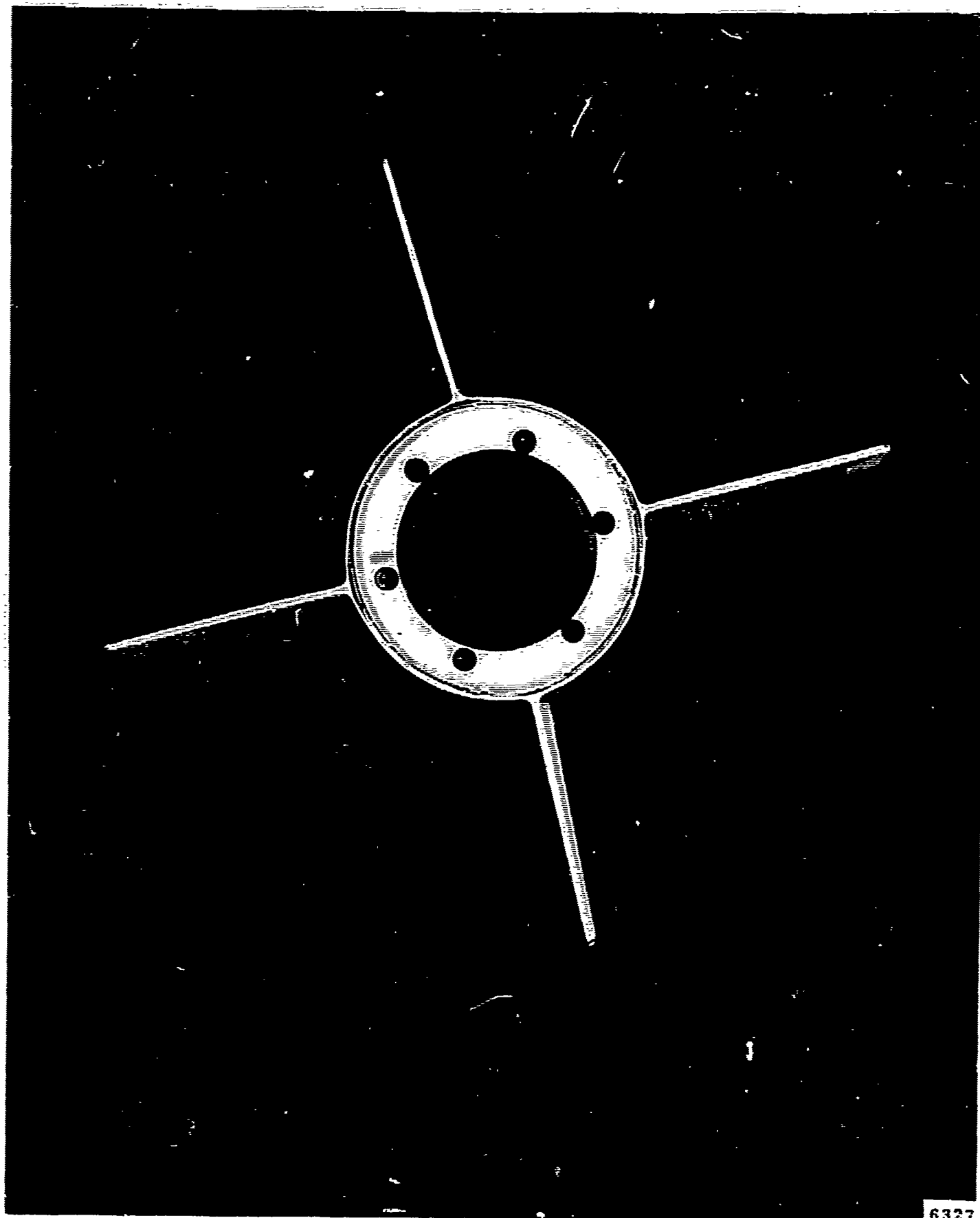


Figure 12

Aft View of the Frangible ARCAS Vehicle
Showing the Method of Fin Attachment



6327

4679

Figure 13

Heat Actuated Dimple Motor

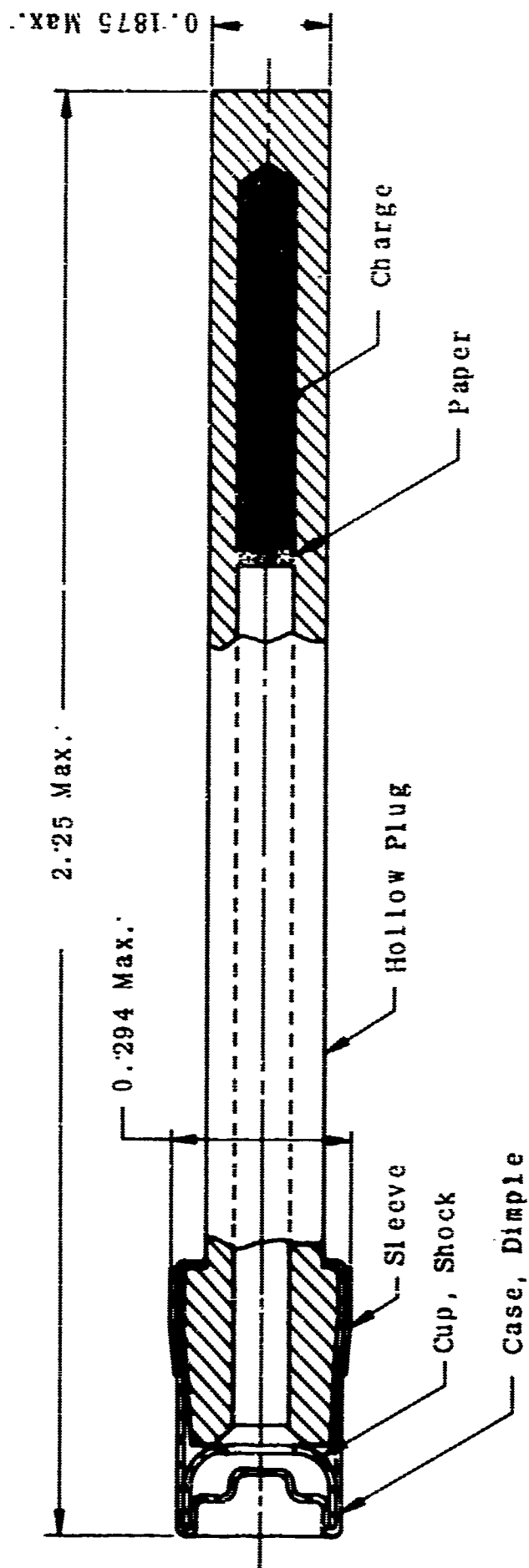
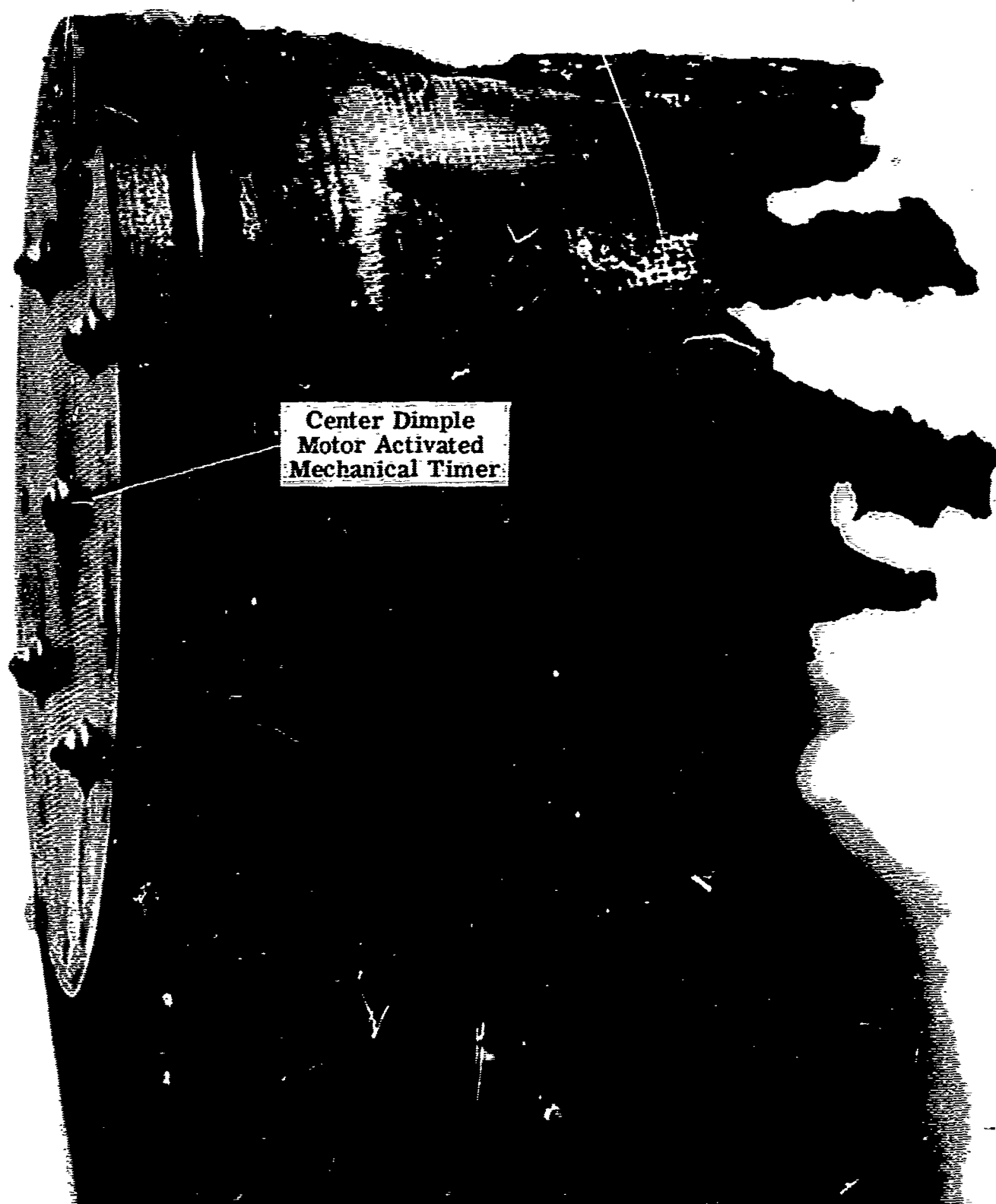


Figure 14

2113

Post-Firing Photograph of Headplate
Containing Heat Actuated Dimple Motors



Center Dimple
Motor Activated
Mechanical Timer

A2165

Figure 15

Frangible ARCAS Parachute Assembly

Frangible ARCAS Parachute Assembly

4730

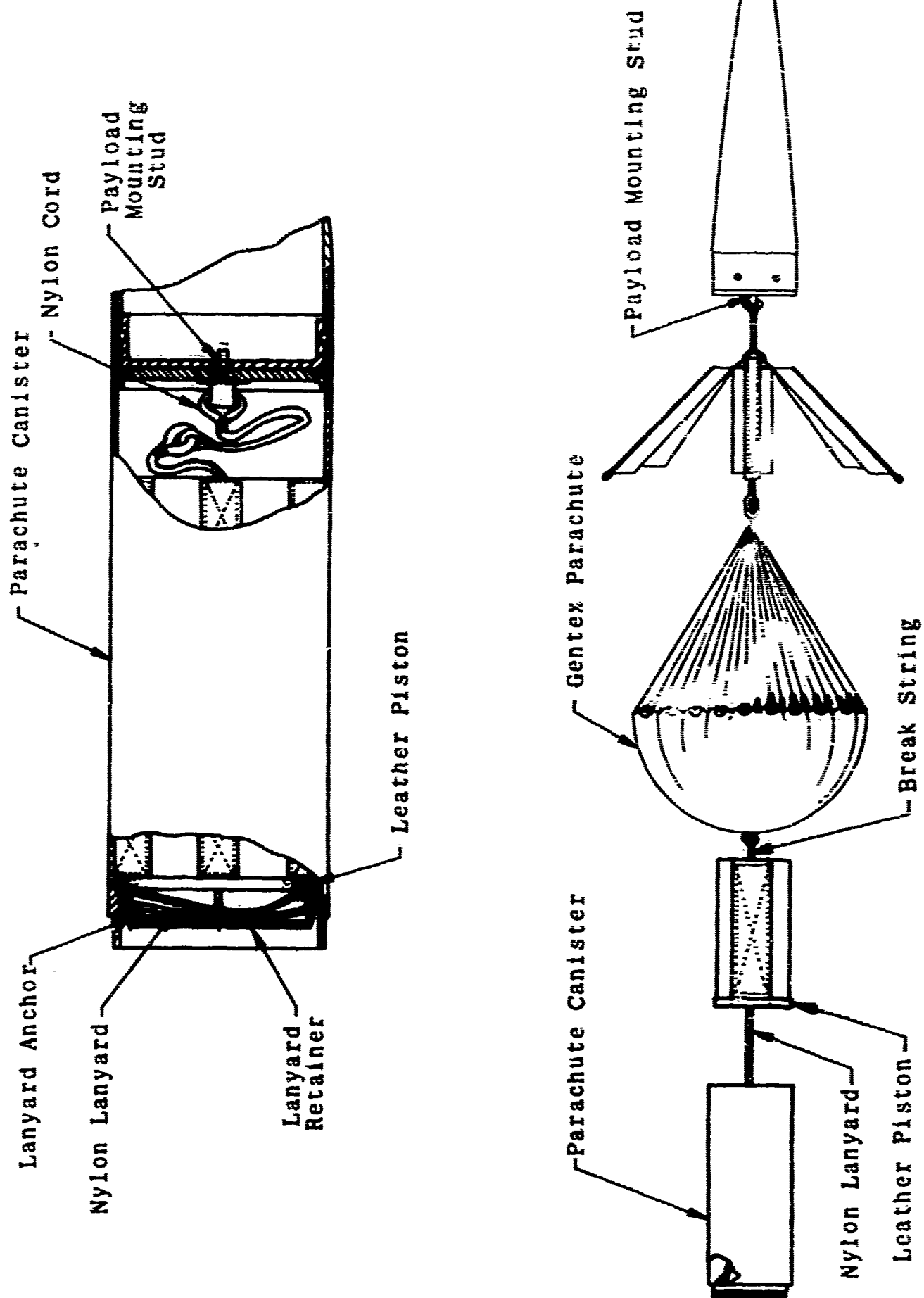


Figure 16

Phase III Frangible ARCAS Pyrotechnic Gas Generator Assembly

2112

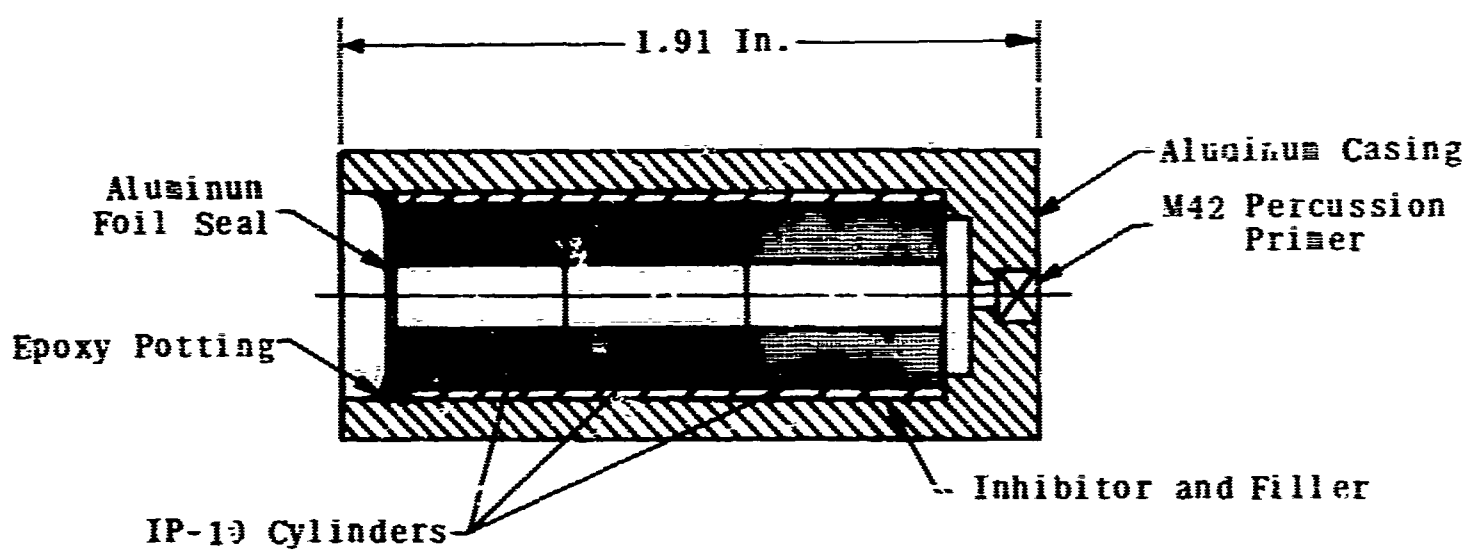


Figure 17

Payload Ejection Pressure Versus Time

2010

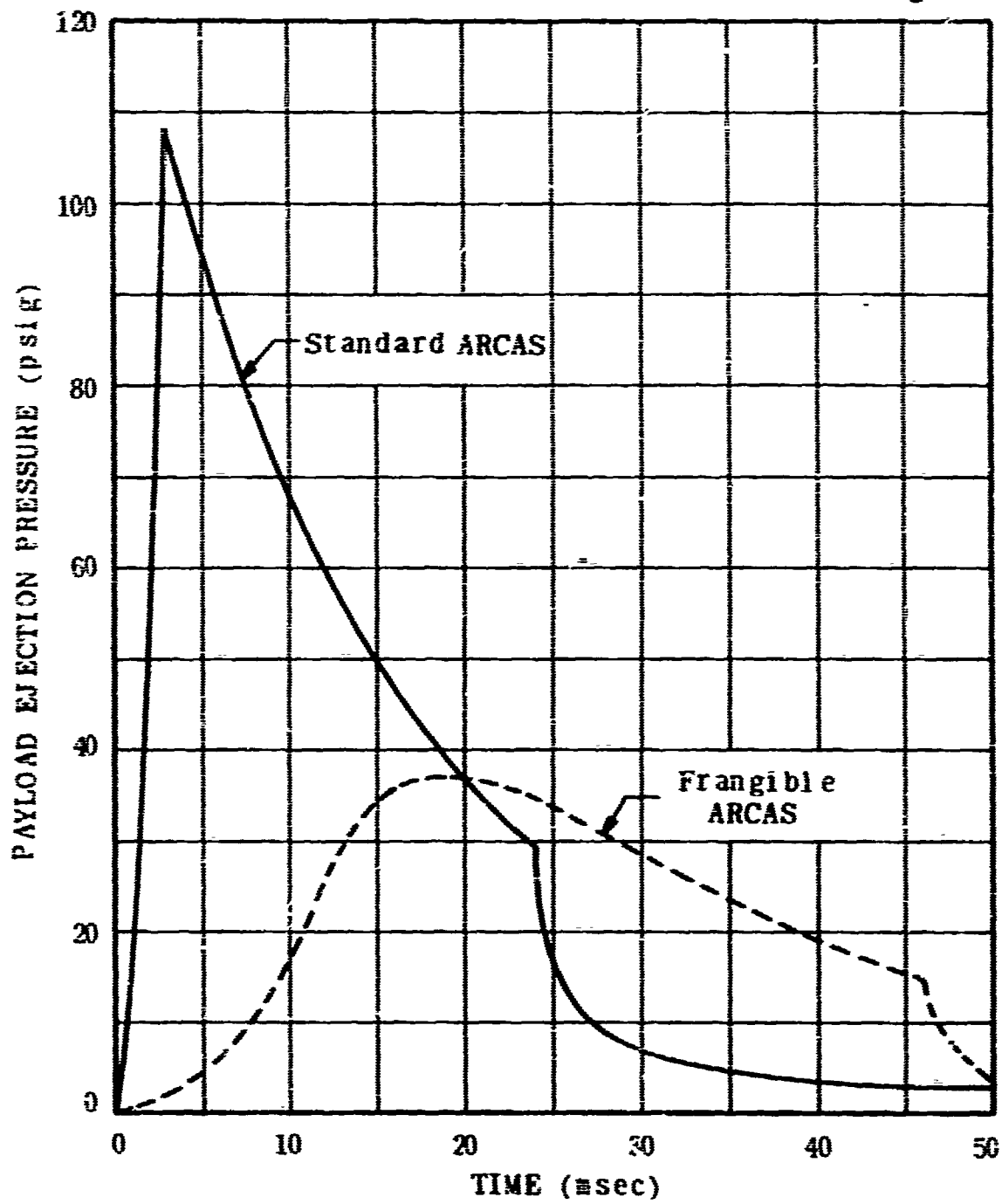


Figure 18

Frangible ARCAS Pyrogen Gas Generator Assembly

$P_{C_{max}} = 5000 \text{ psia}$
 $T_b = 0.150 \text{ sec}$

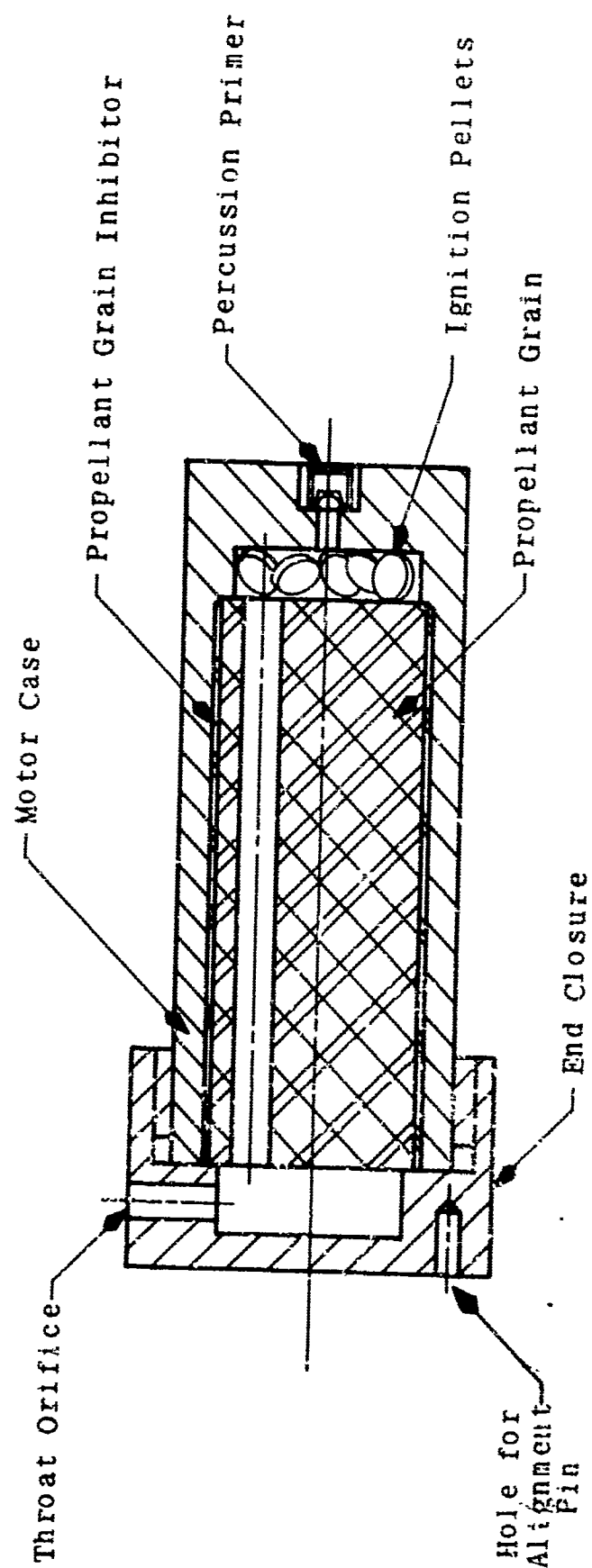


Figure 19

The Frangible ARCAS Mechanical Timer Assembly

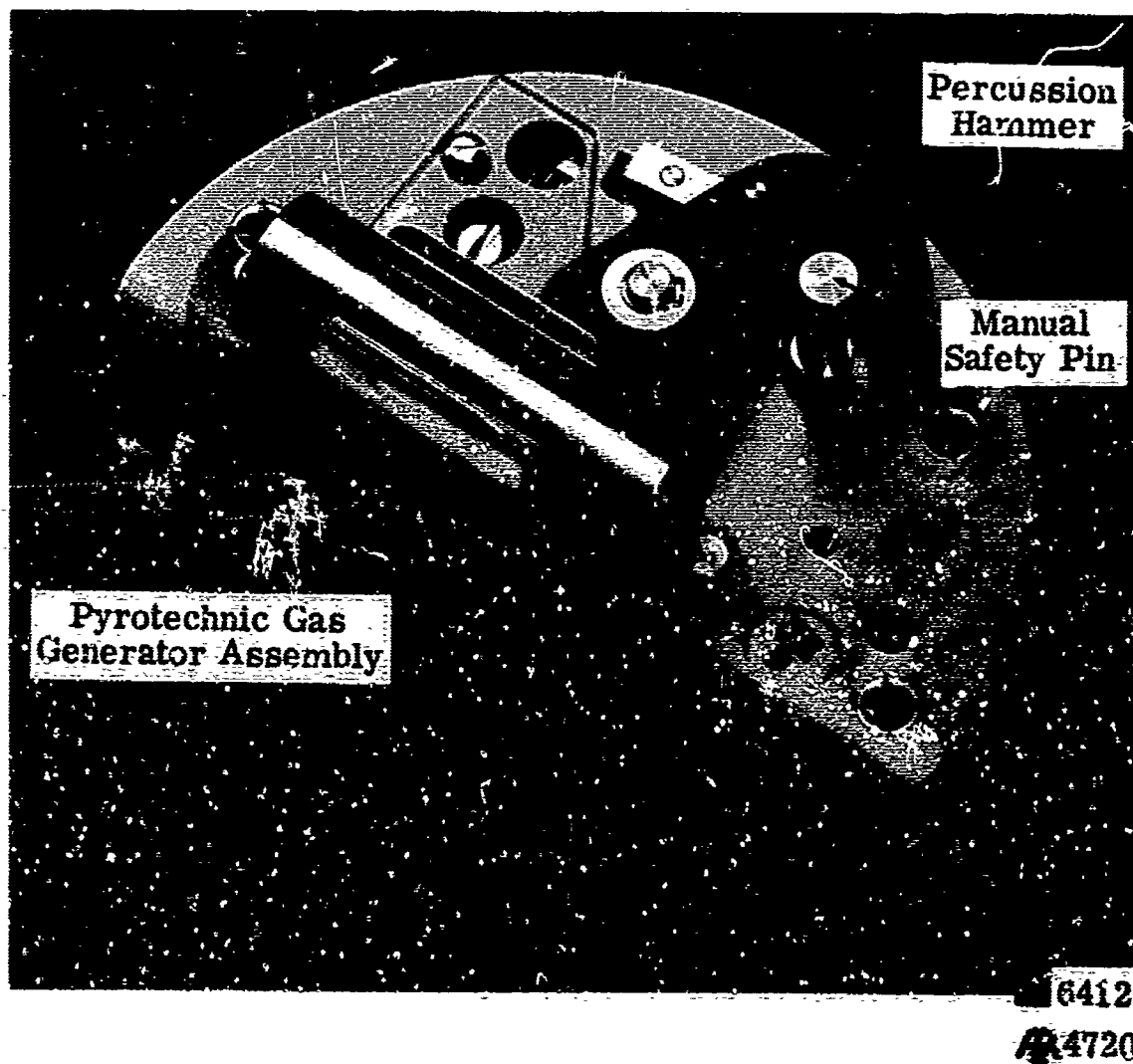


Figure 20

Nominal Payload and Rocket Body Trajectories for First 20 Seconds After Apogee

8852

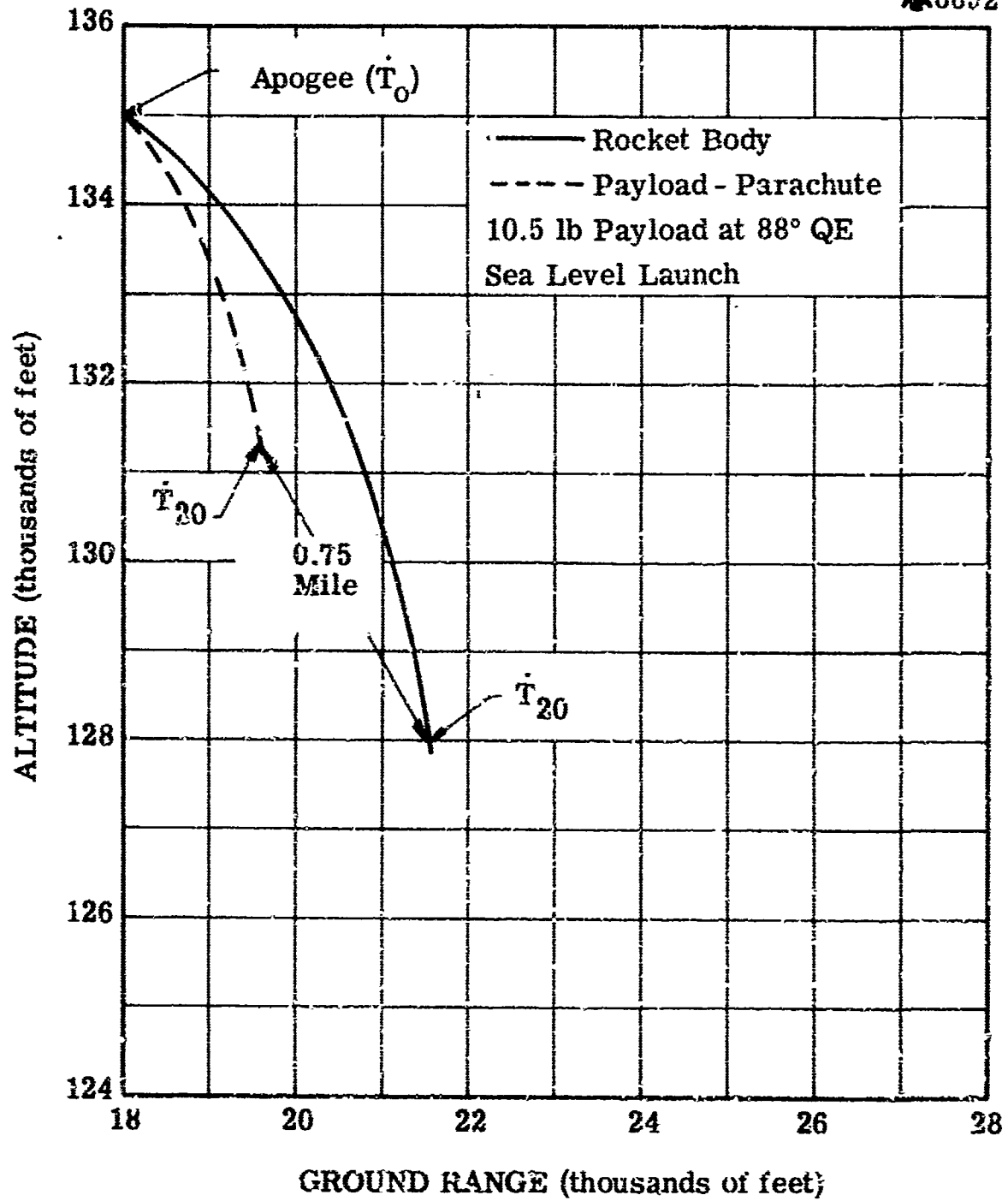


Figure 21

Nominal Payload and Rocket Body Trajectories for First 20 Seconds After Apogee

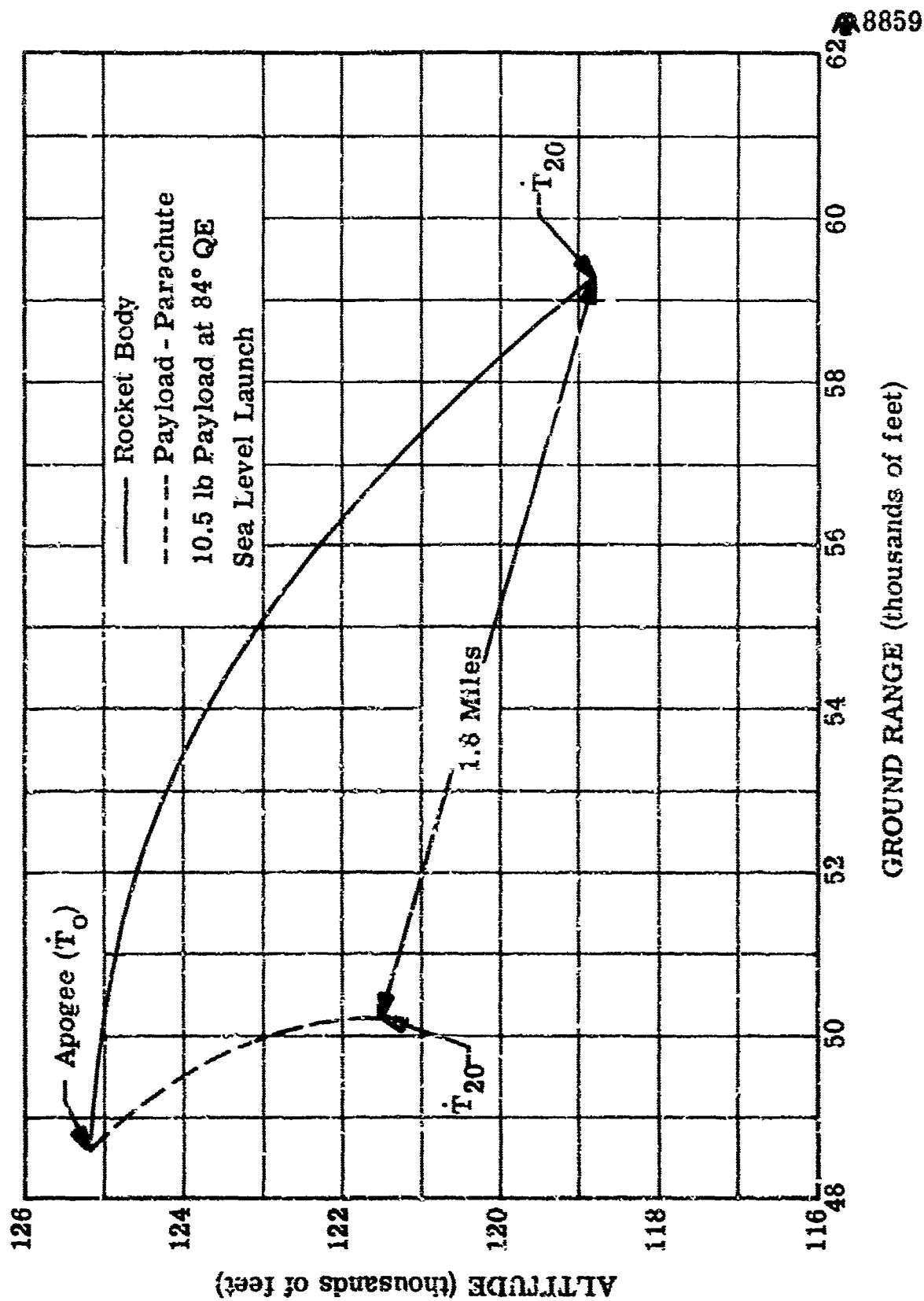


Figure 22

Nominal Distance Between Payload and Rocket Vehicle
20 Seconds After Apogee Versus Effective Launch Angle

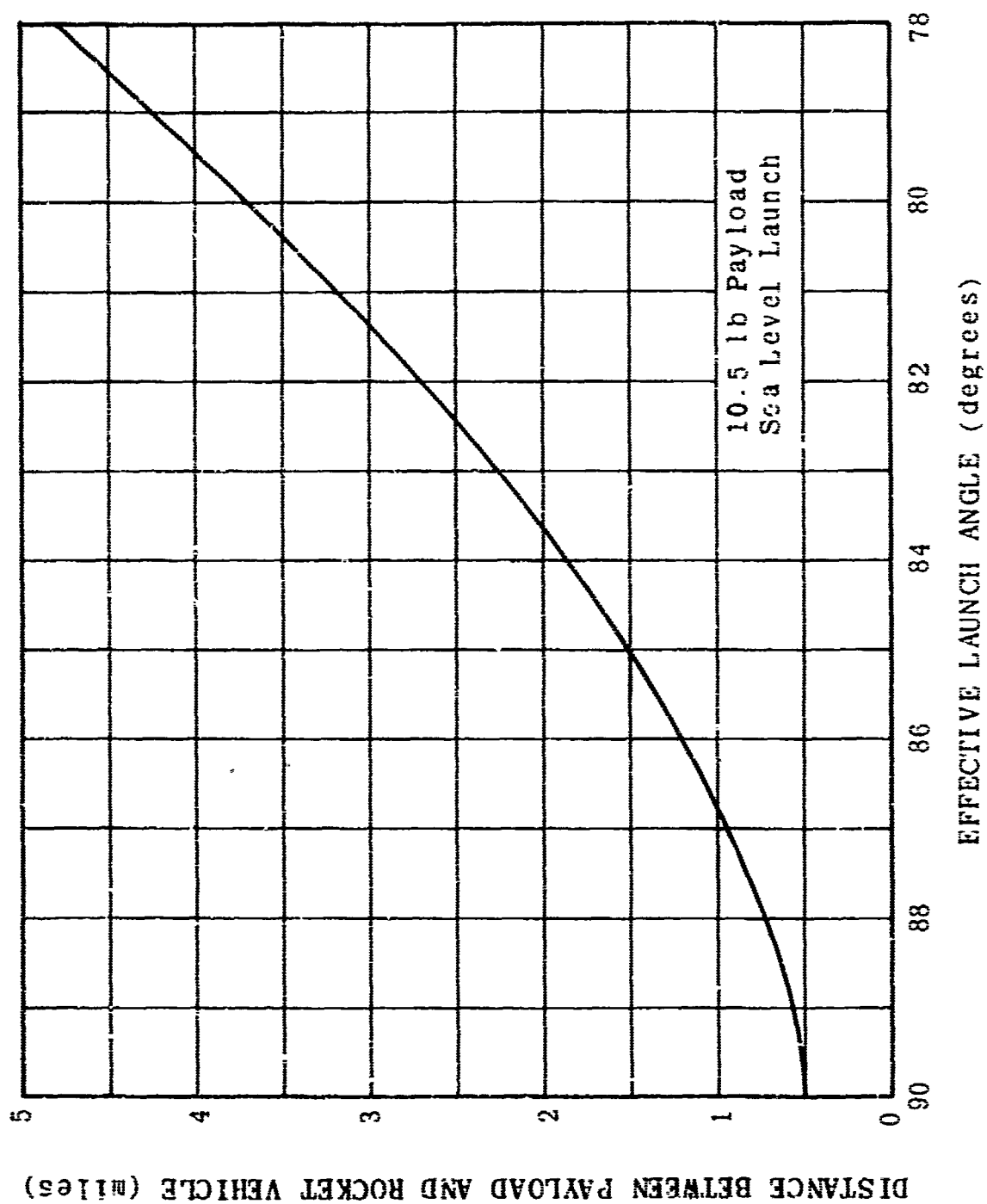


Figure 23

Illustration of Frangible ARCAS Redundant Initiator Assembly for Explosive Fragmentation System

4677

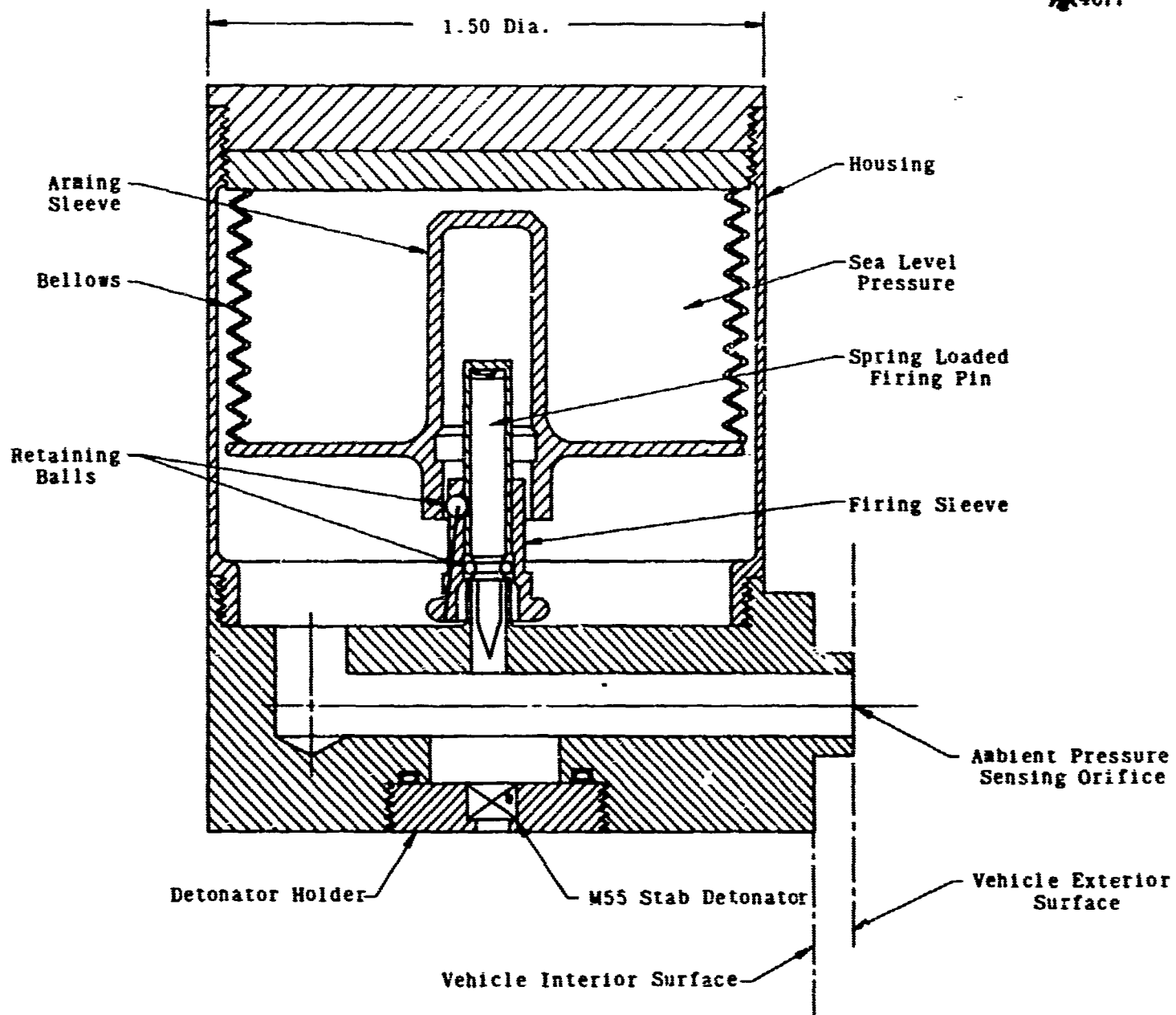


Figure 24

Illustration of Vehicle Attitude Along a
Free Flight Ballistic Trajectory

2709

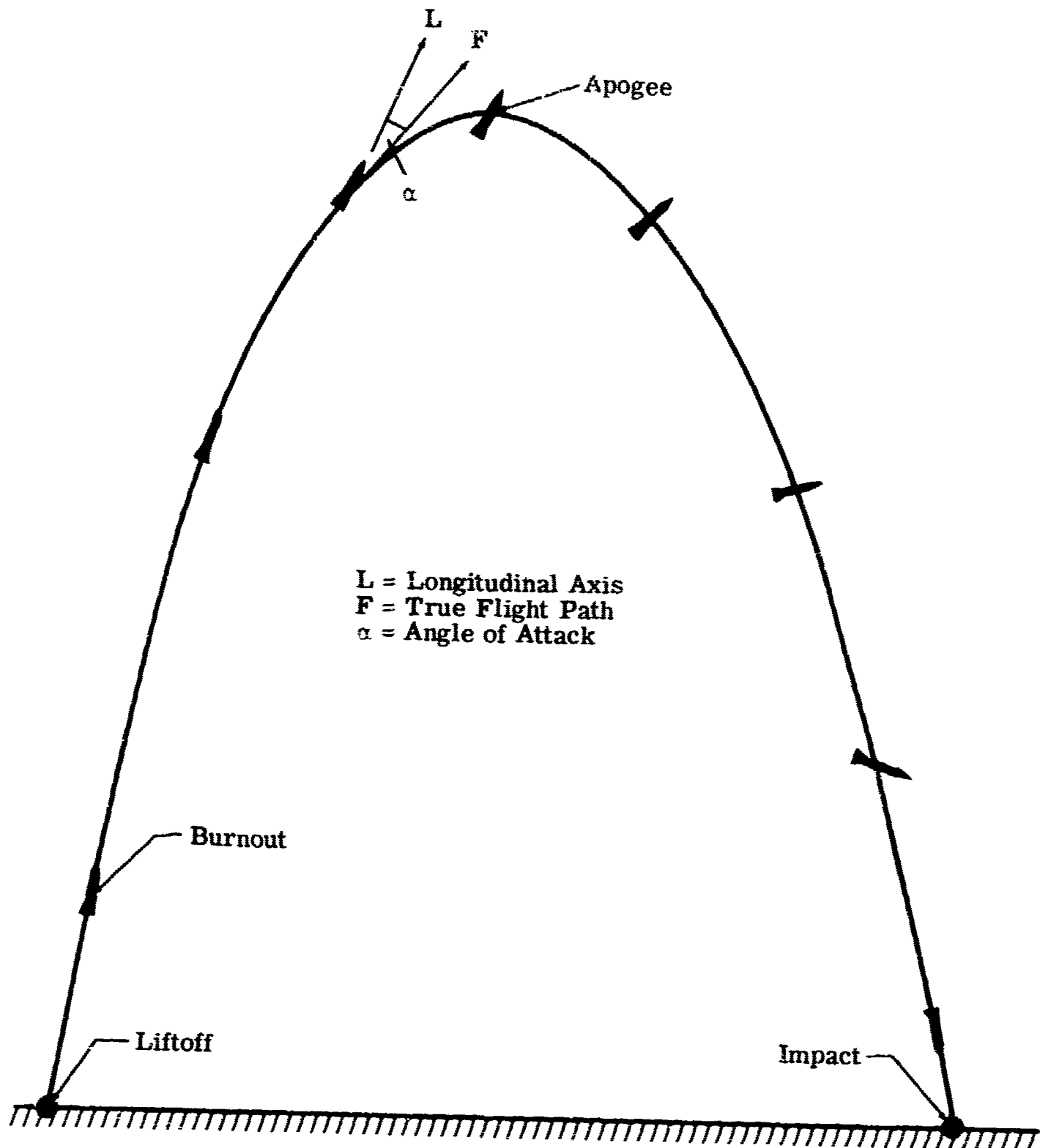


Figure 25

Single Modular Shaped Charge Fragmentation System Configuration

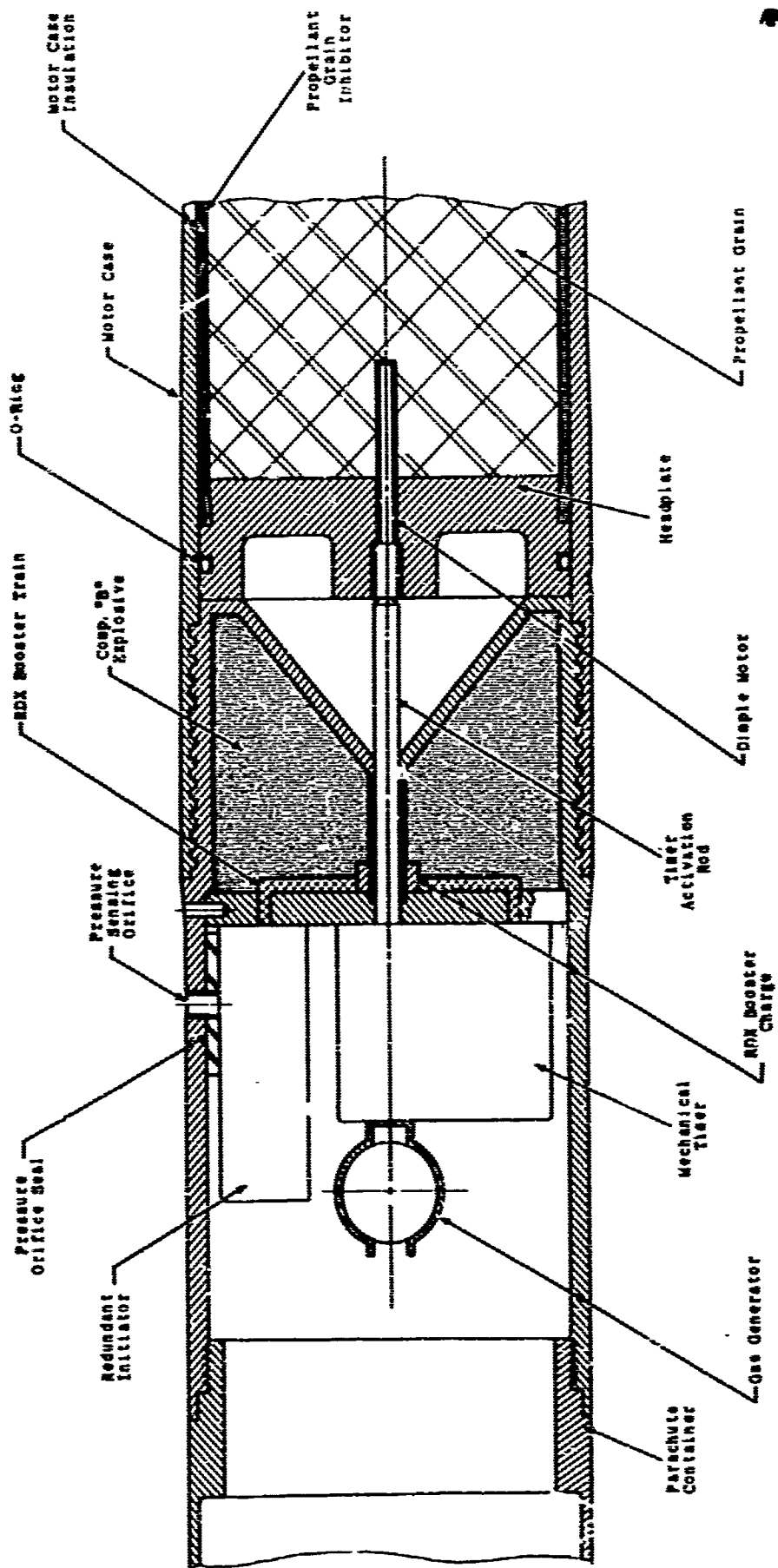


Figure 26

33282

Frangible ARCAS Shaped Charge Fragmentation Modules

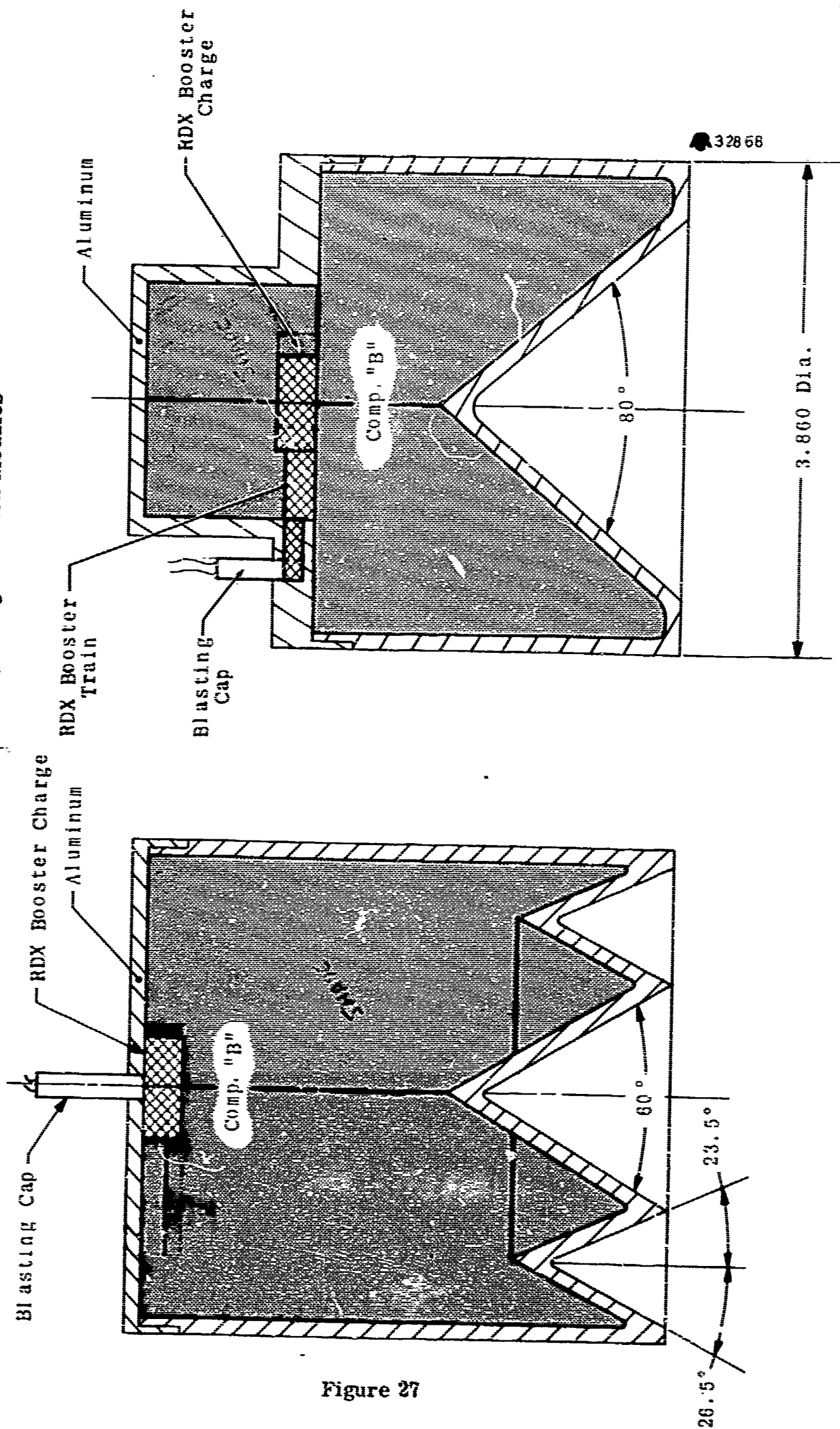


Figure 27

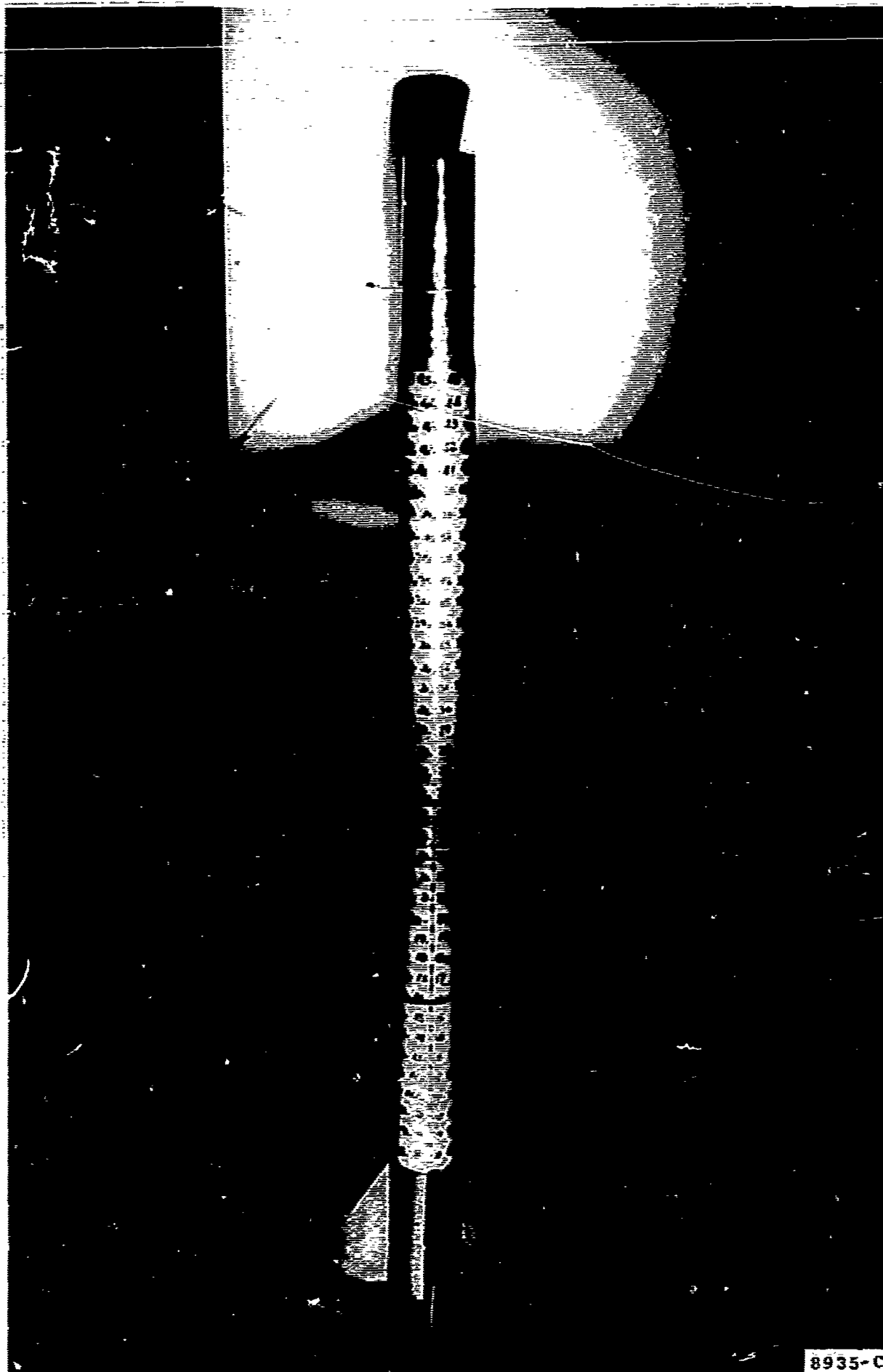
Frangible ARCAS Rocket Motor Assembly Showing
Grid Markings and Bifocal Fragmentation Module



8035-A
A3322

Figure 28

**Frangible ARCAS Rocket Motor Assembly Showing
Setup in Simulated Altitude Chamber**

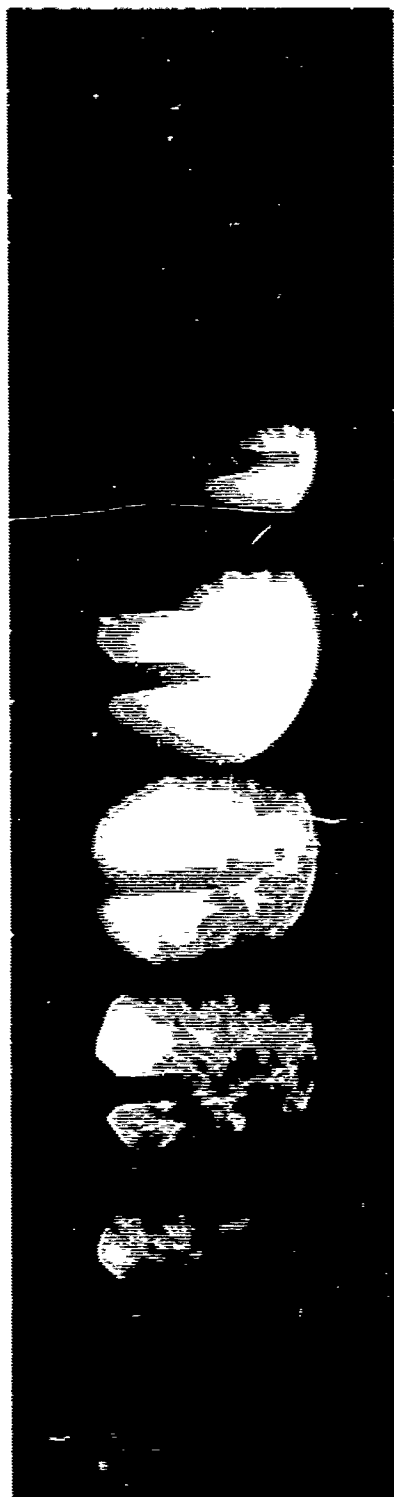


8935-C

33220

Figure 29

**Photographic Sequence of First Frangible ARCAS
Simulated Altitude Fragmentation Test**



A4713

Simulated Altitude: 100,000 Feet
Film Speed: 3,000 Frames/Sec
**Explosive Charge: Single Modular
Conical Shaped
Charge (Figure 27)**

Figure 30

Pre-Test and Post-Test Comparison of the
Frangible ARCAS Rocket Motor Assembly
Incorporating the Conical Shaped Charge

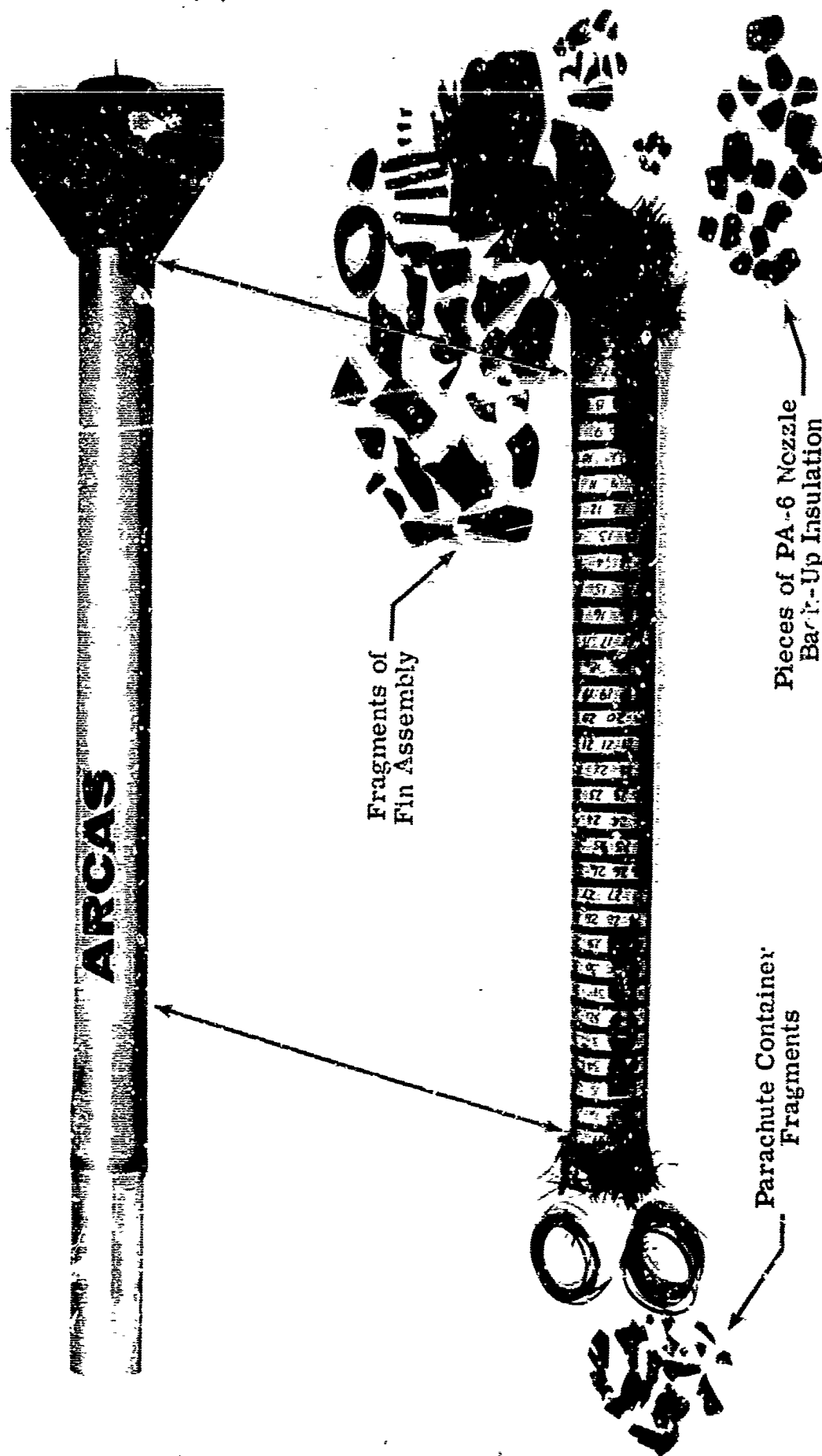


Figure 31



Conical Shaped Charge

Pre-Test and Post-Test Comparison of the
Frangible ARCAS Rocket Motor Assembly
Incorporating the Bifocal Shaped Charge

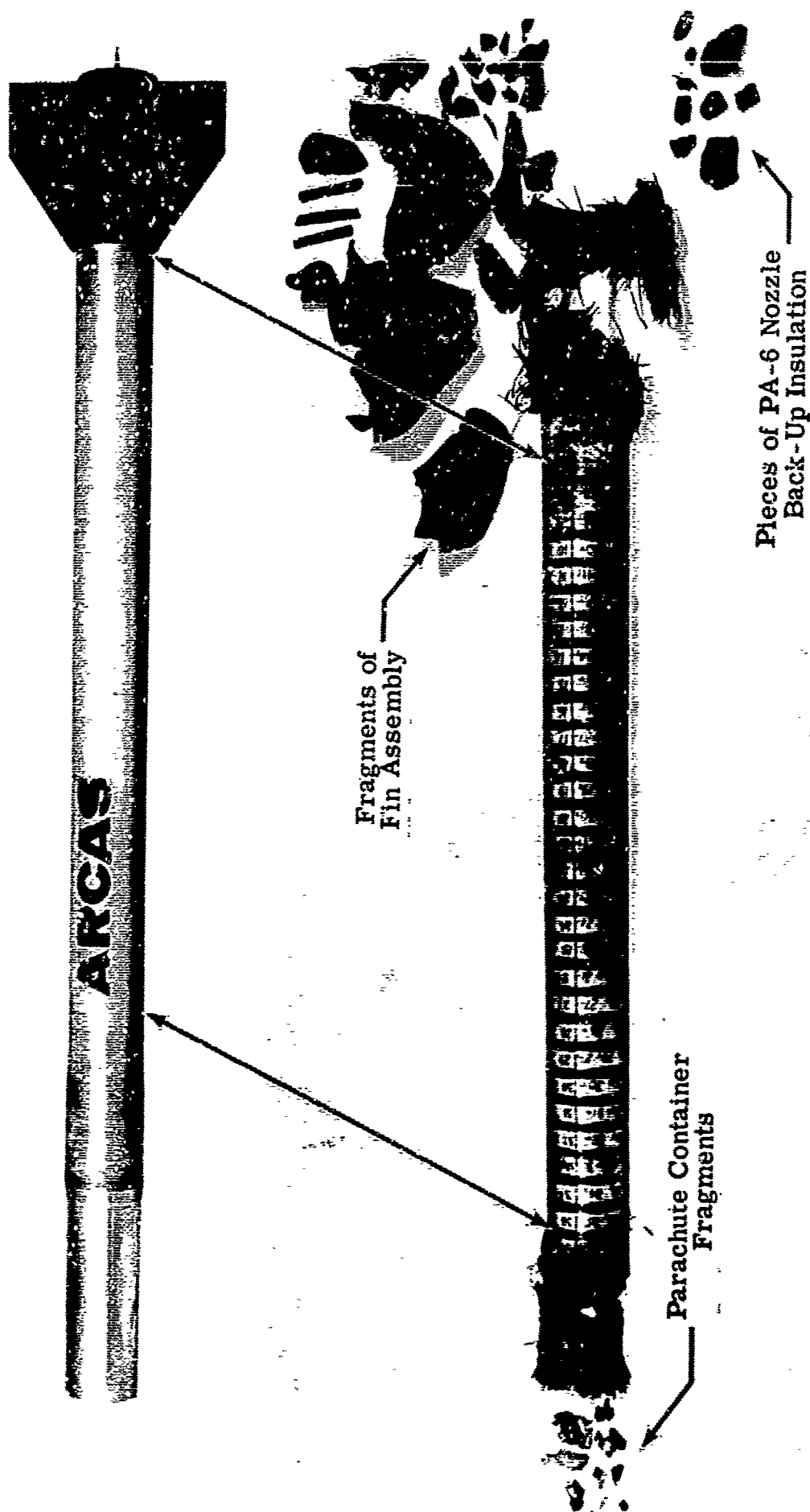


Figure 32

Illustration of Fragmentation Module Ignition, Focusing and Propagation

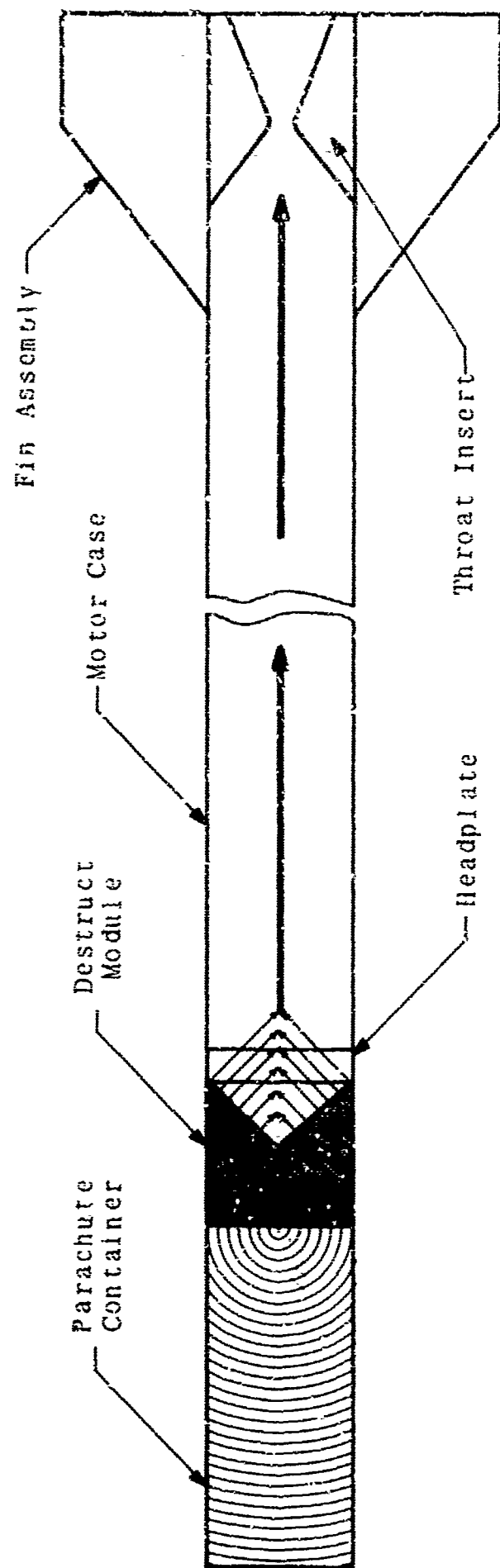


Figure 33

Illustration of Bifocal Charge Wave Propagation

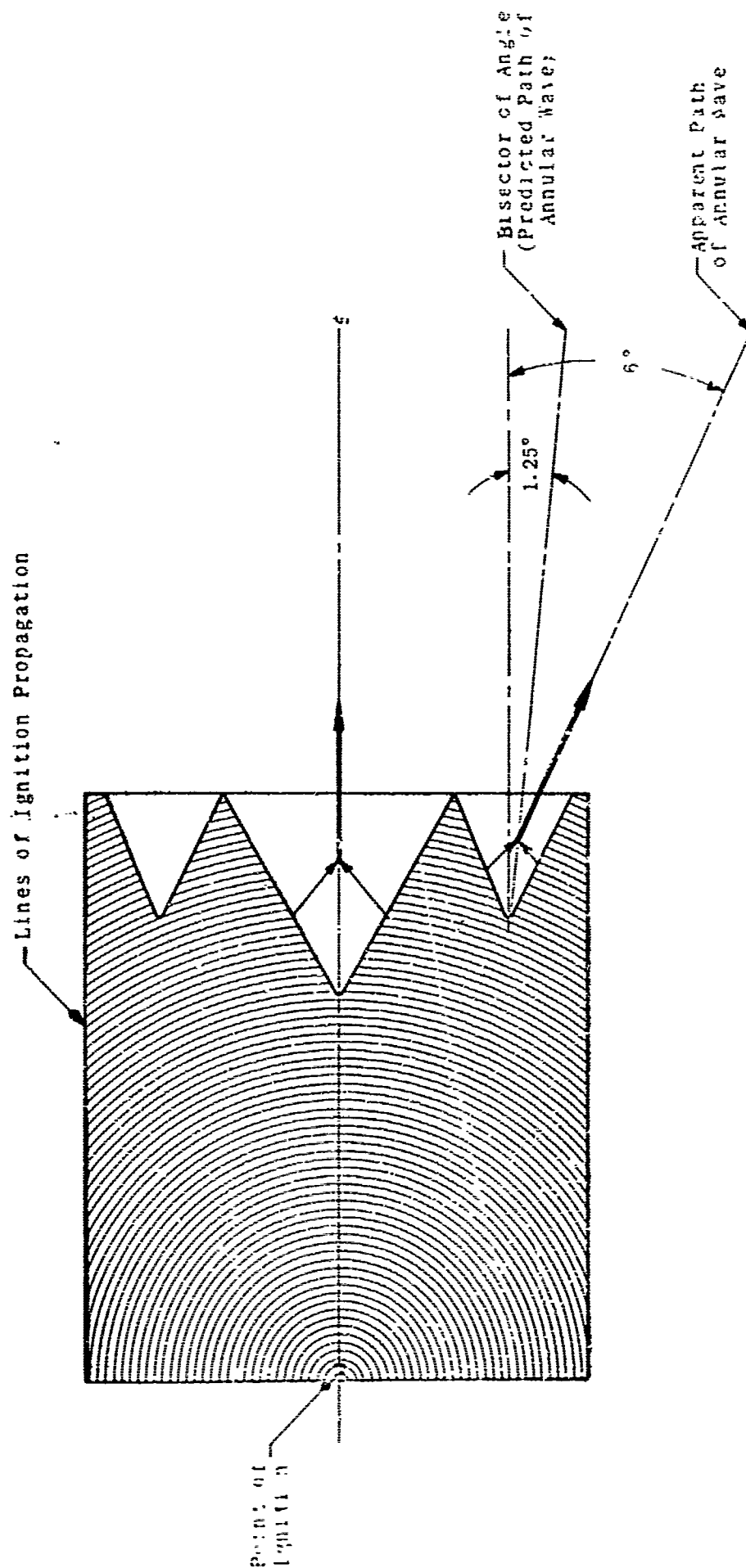


Figure 34

Predicted and Actual Wave Paths of Bifocal Fragmentation Charge

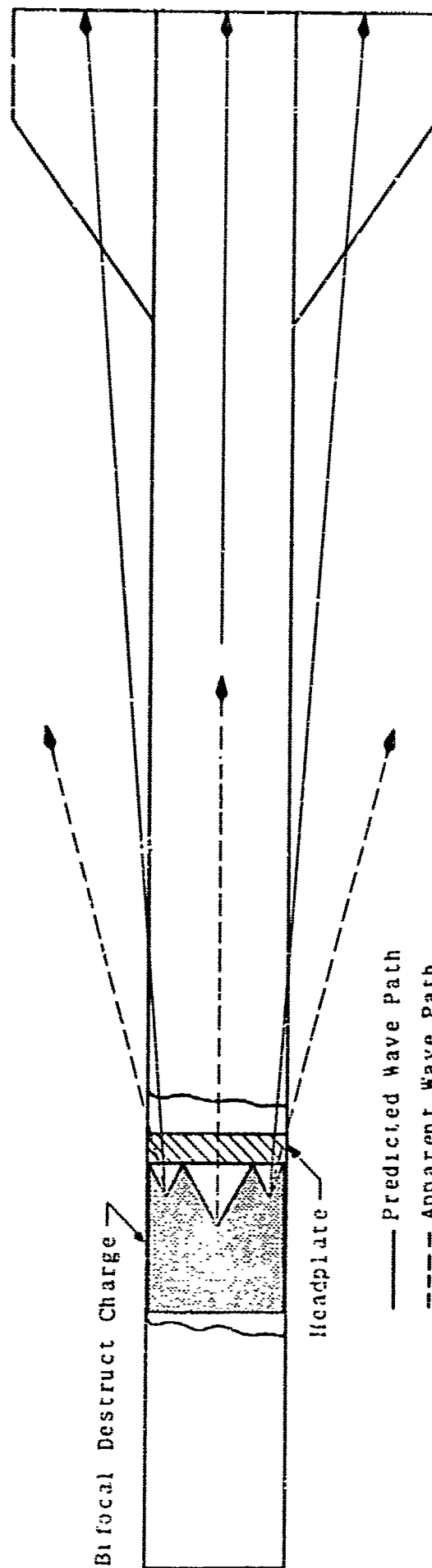


Figure 35

Drag Coefficients of Motor Case Pieces

Quarter Section of Remaining Motor Case (motor case section no. 5)
 $C_D = 0.99$

Motor Case Section No. 1
 $C_D = 1.61$

Motor Case Section No. 2
 $C_D = 1.53$

Motor Case Section No. 3
 $C_D = 1.90$

Large Insulation Piece
 $C_D = 1.07$

Motor Case Section No. 4
 $C_D = 2.71$

Small Insulation Piece
 $C_D = 1.55$

0 1 2 3 4 5
 SCALE (in)

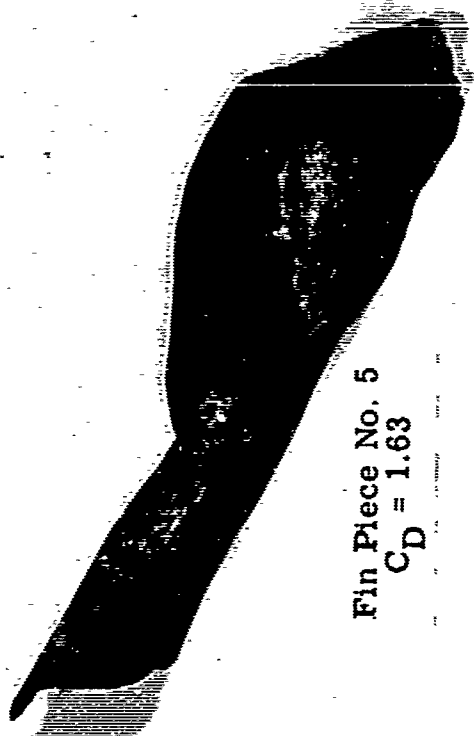
33531

Figure 36

Drag Coefficients of Rocket Motor Pieces



Parachute Container Piece No. 1
 $C_D = 0.76$



Fin Piece No. 5
 $C_D = 1.63$



Parachute Container Piece No. 2
 $C_D = 1.23$



Fin Retaining Screw
 $C_D = 1.00$

Fin Rib
 $C_D = 0.88$

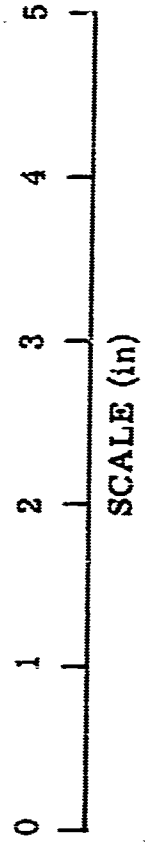


Figure 37

Drag Coefficients of Fin Pieces



Fin Piece No. 1
 $C_D = 1.24$



Fin Piece No. 3
 $C_D = 1.47$



Fin Piece No. 4
 $C_D = 1.65$



Fin Piece No. 2
 $C_D = 1.24$



Fin Flange
 $C_D = 0.09$

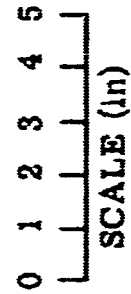


Figure 38

Inverted Fragmenting Cone Assembly - Type I

33473

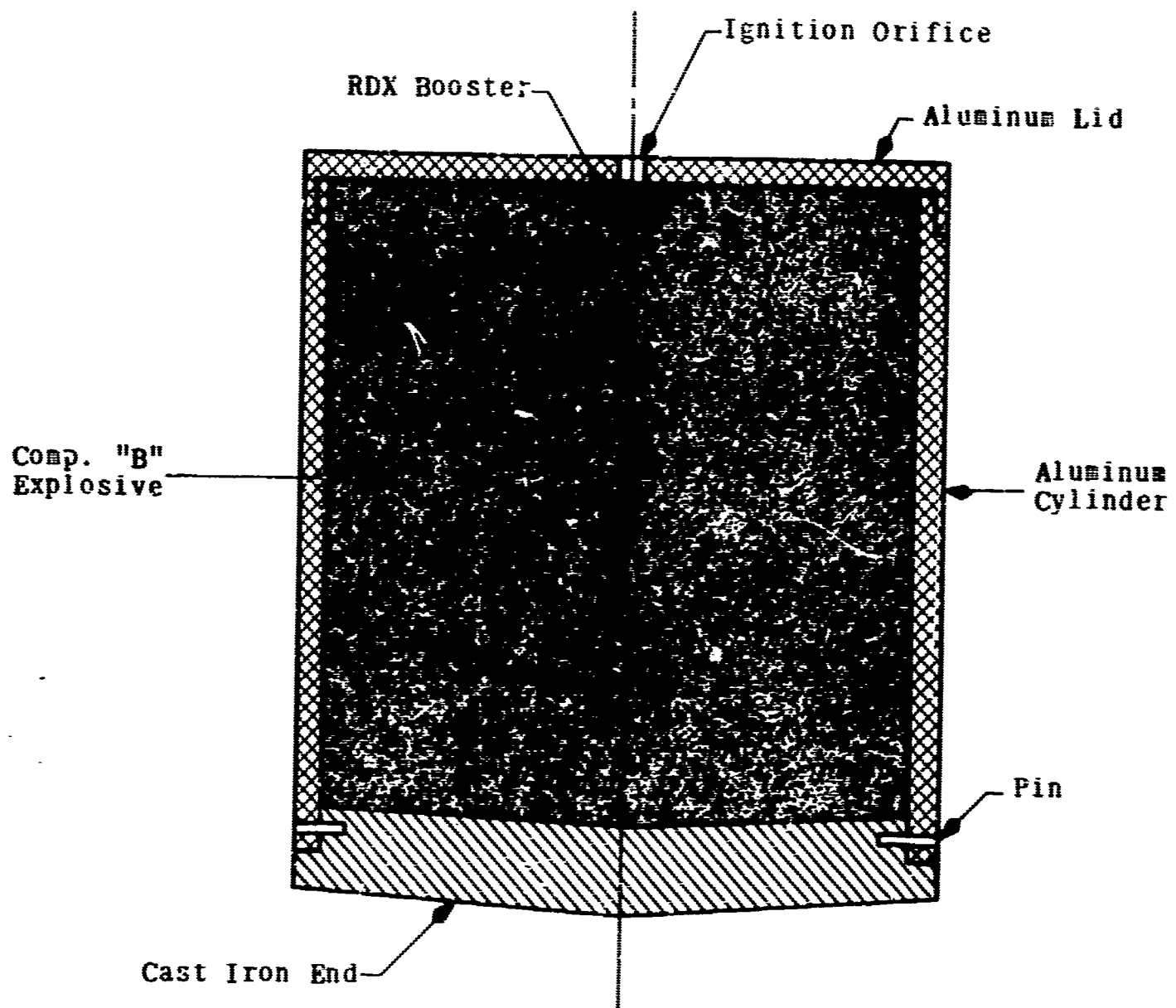


Figure 39

Inverted Fragmenting Cone Assembly - Type II

33470

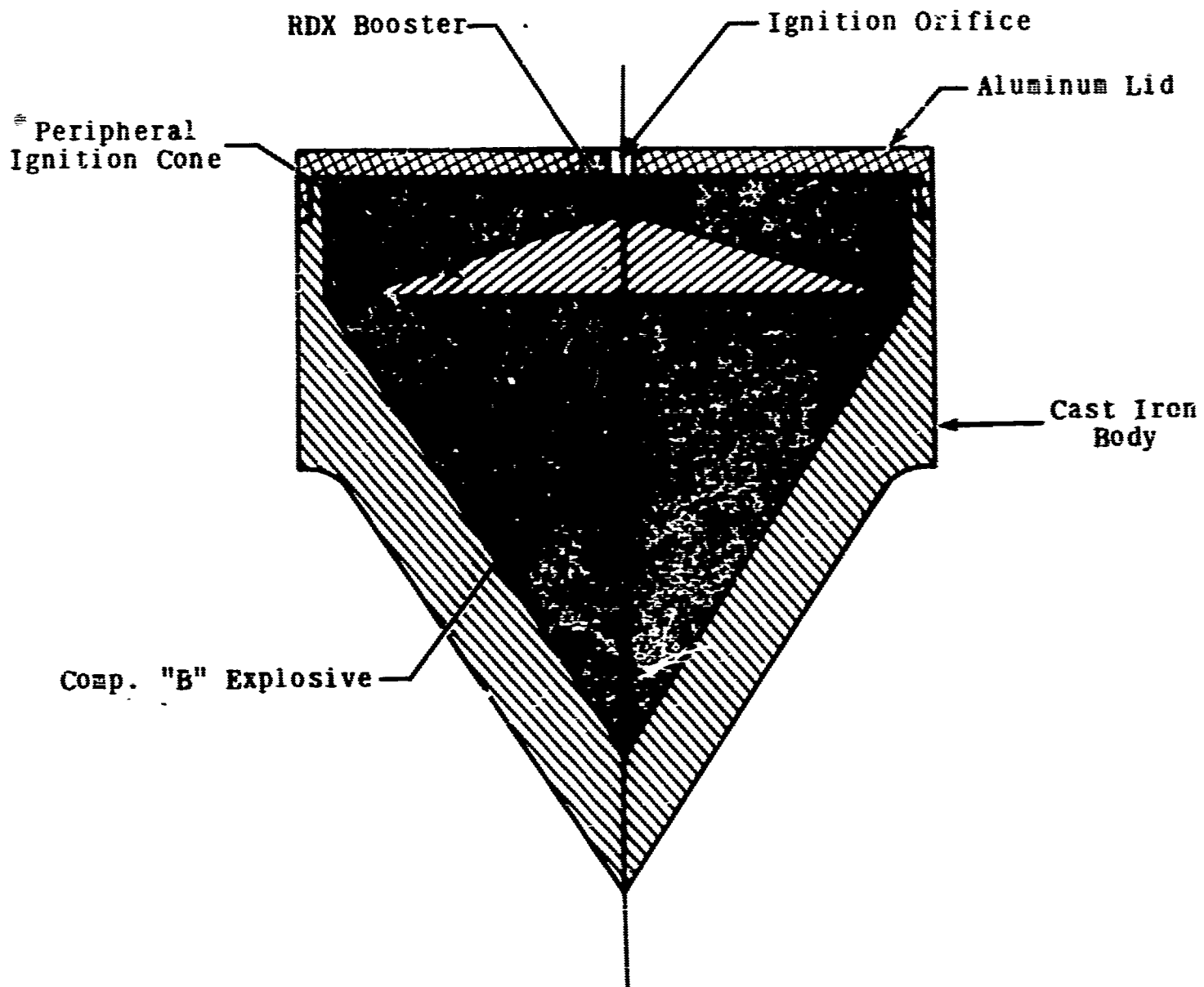


Figure 40

Fragmenting Module Target Test Setup

83471

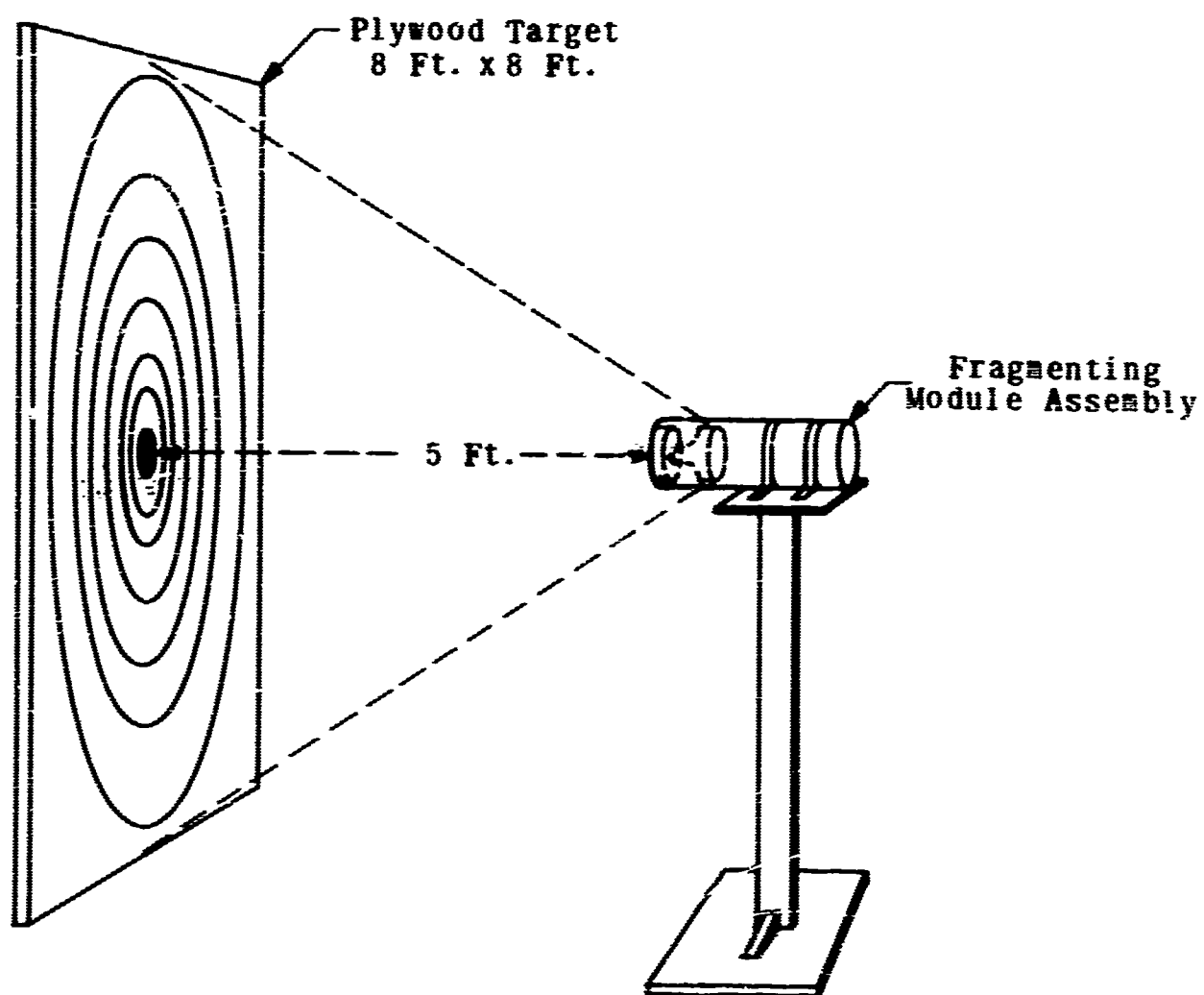


Figure 41

**Fragmenting Module Assembly for Target Tests
(Type II Module Shown)**

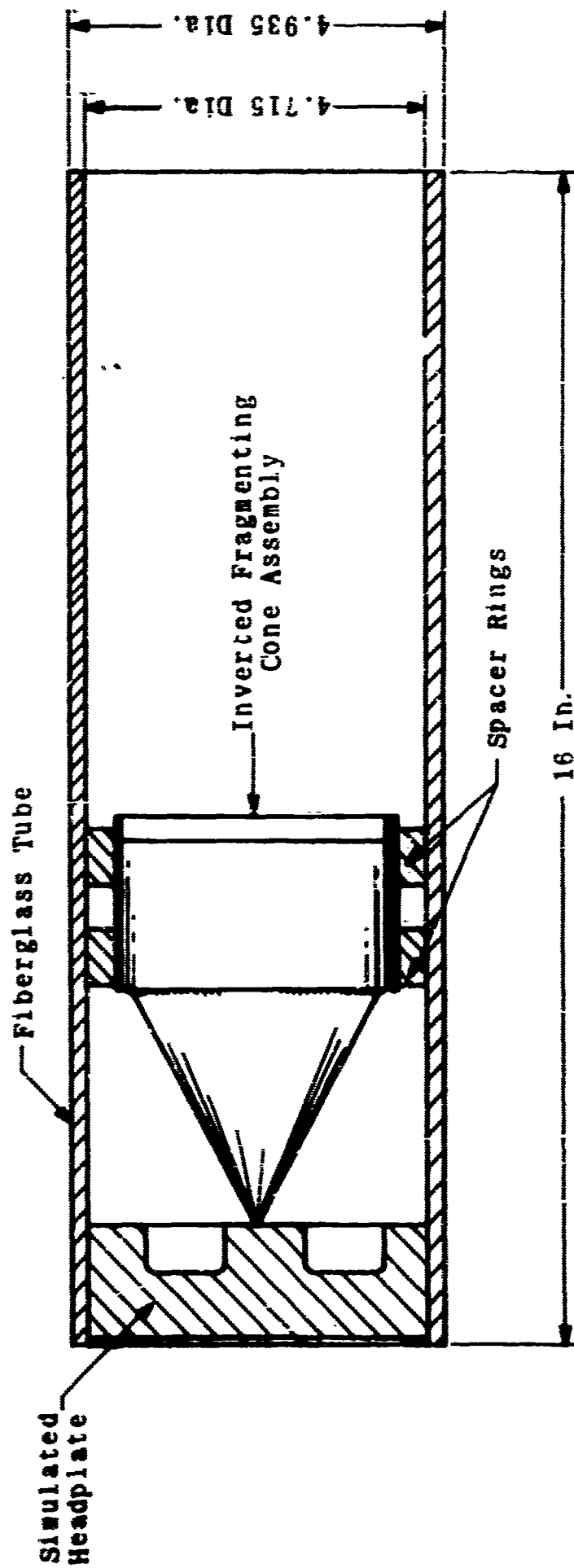


Figure 42

27468

Photograph Showing Particles Produced Upon
Detonation of the Fragmenting Module

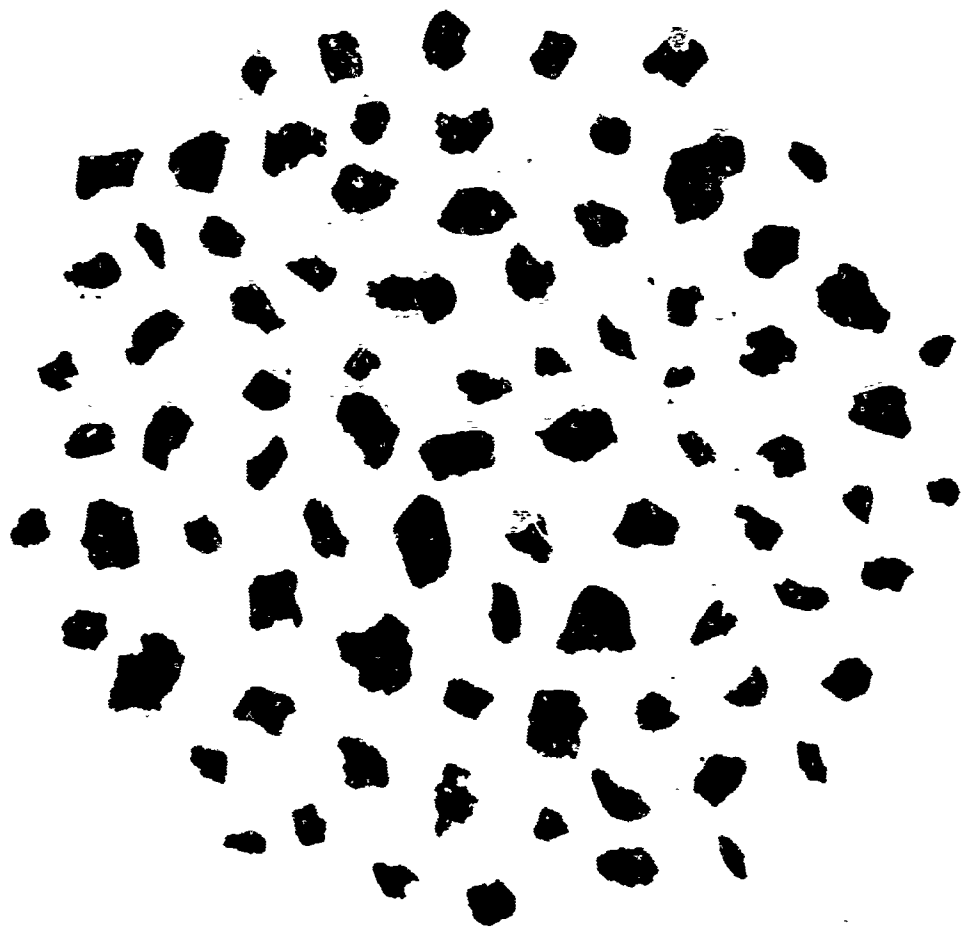
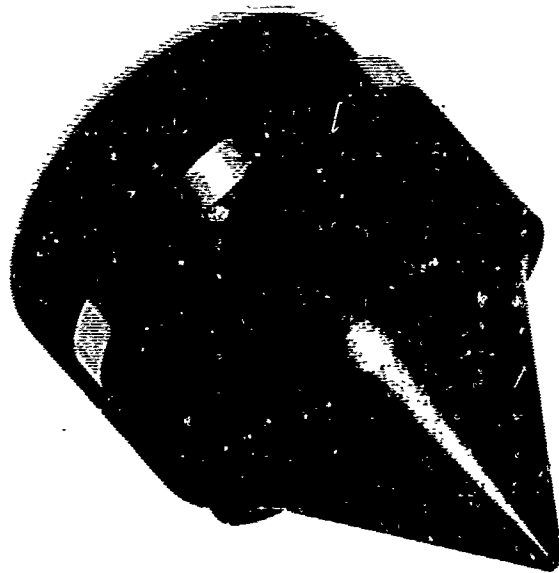


Figure 43

Illustration of Shock Tube Fragmentation Concept

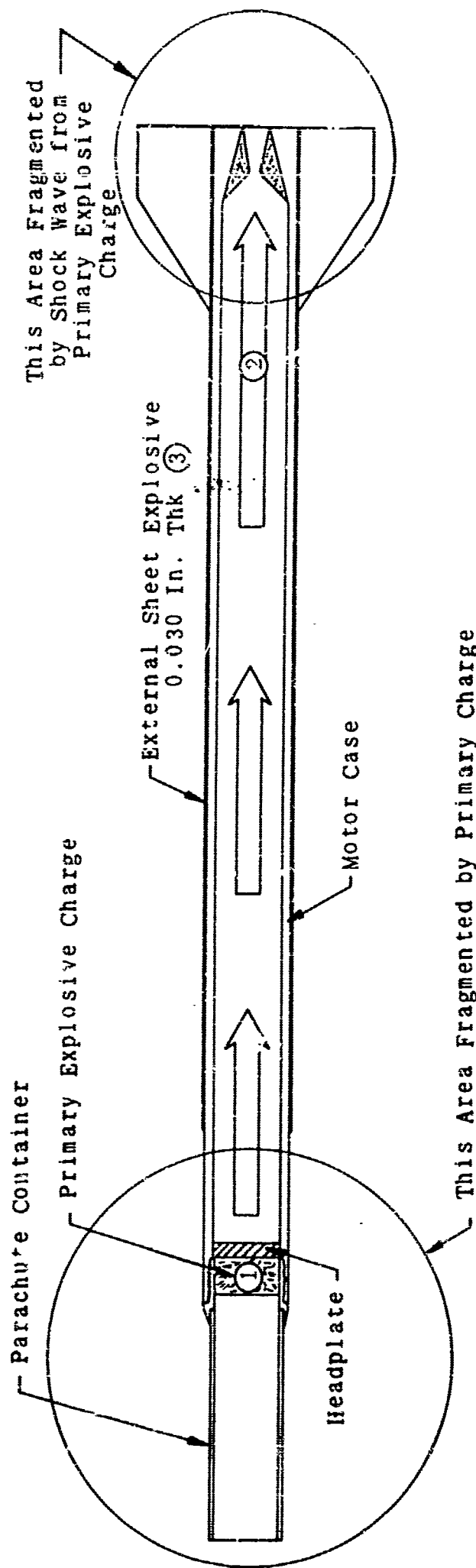


Figure 44

Sequence of Rocket Assembly Fragmentation

- ① Primary Charge Initiated, Fragmenting Area Shown and Transmitting Shock Wave Through Motor Case
- ② Aft Section Fragmented by Impact of Primary Shock Wave. External Sheet Explosive Initiated by Primary Wave Impact and Fragmentation at Aft Section.
- ③ External Sheet Explosive Detonates from Aft End Forward, Fragmenting Remaining Motor Case.

Frangible ARCAS AFST-13 Static Firing/Fragmentation Test Setup

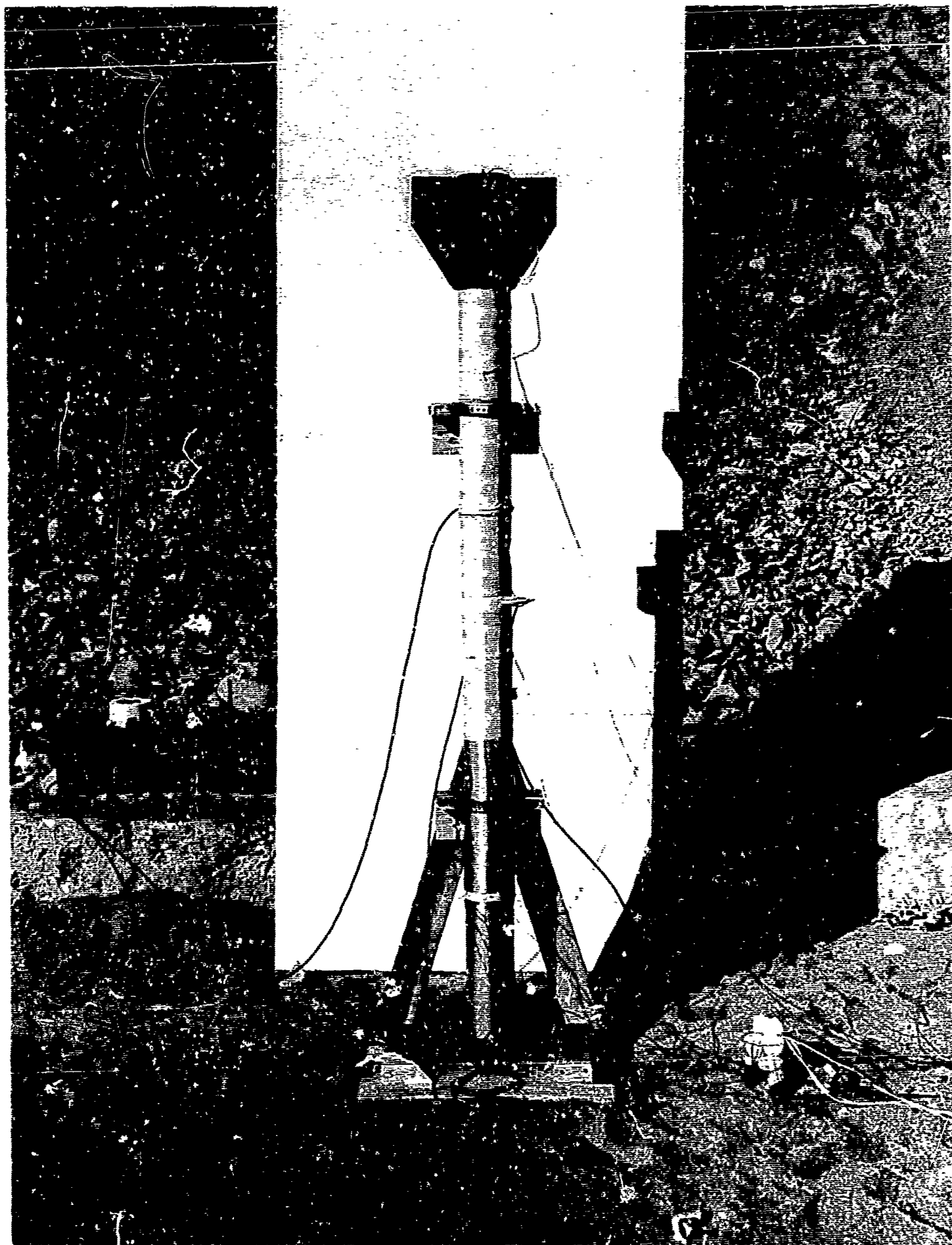


Figure 45

34192

Forward Section Assembly Showing Method of Retaining the Primary Explosive Charge
Static Firing/Fragmentation Test AFST-13

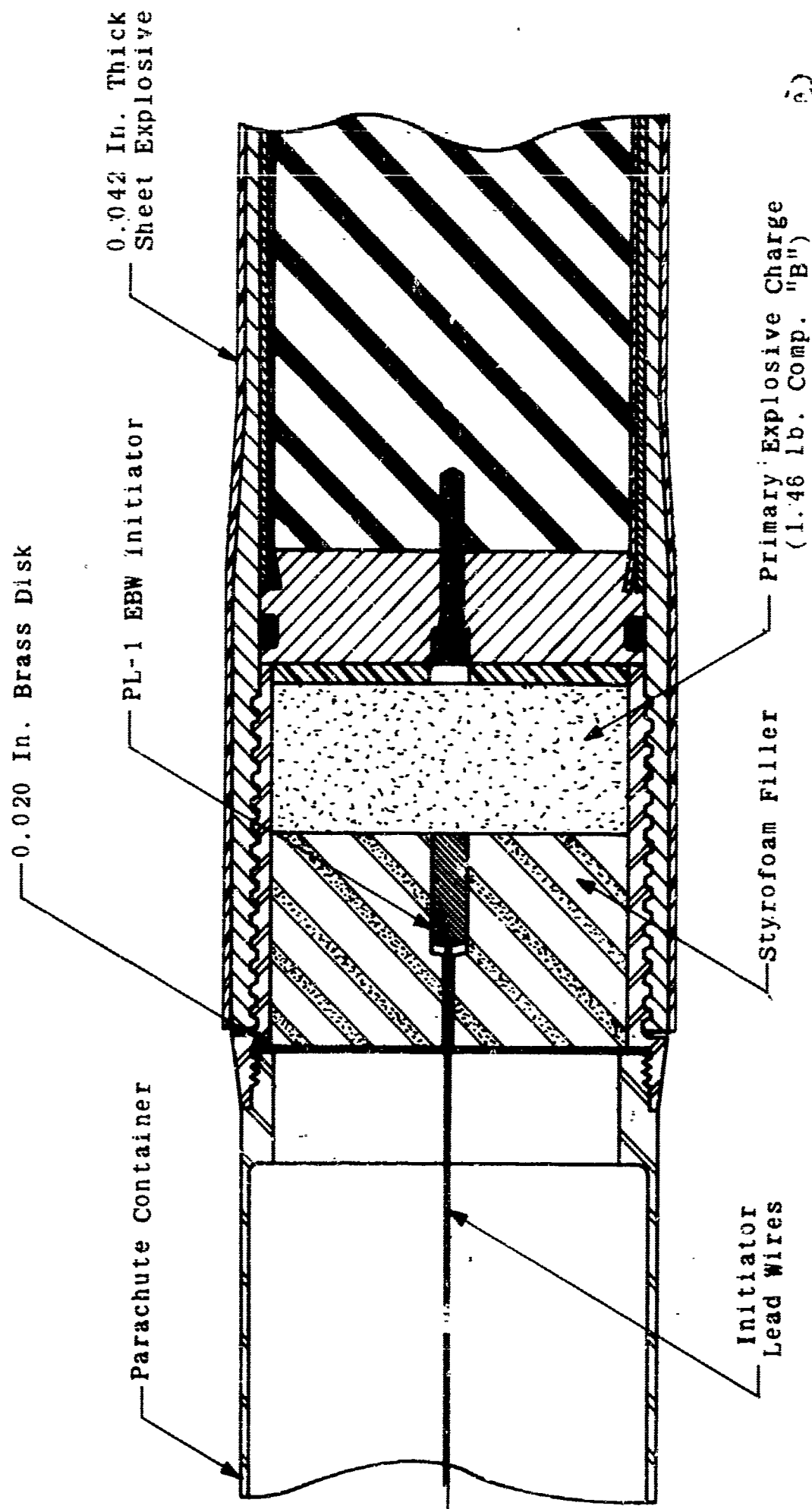


Figure 46

34228

Frangible ARCAS Rocket Motor Case Showing Linear Shaped Charge and Simulated Fin Cover

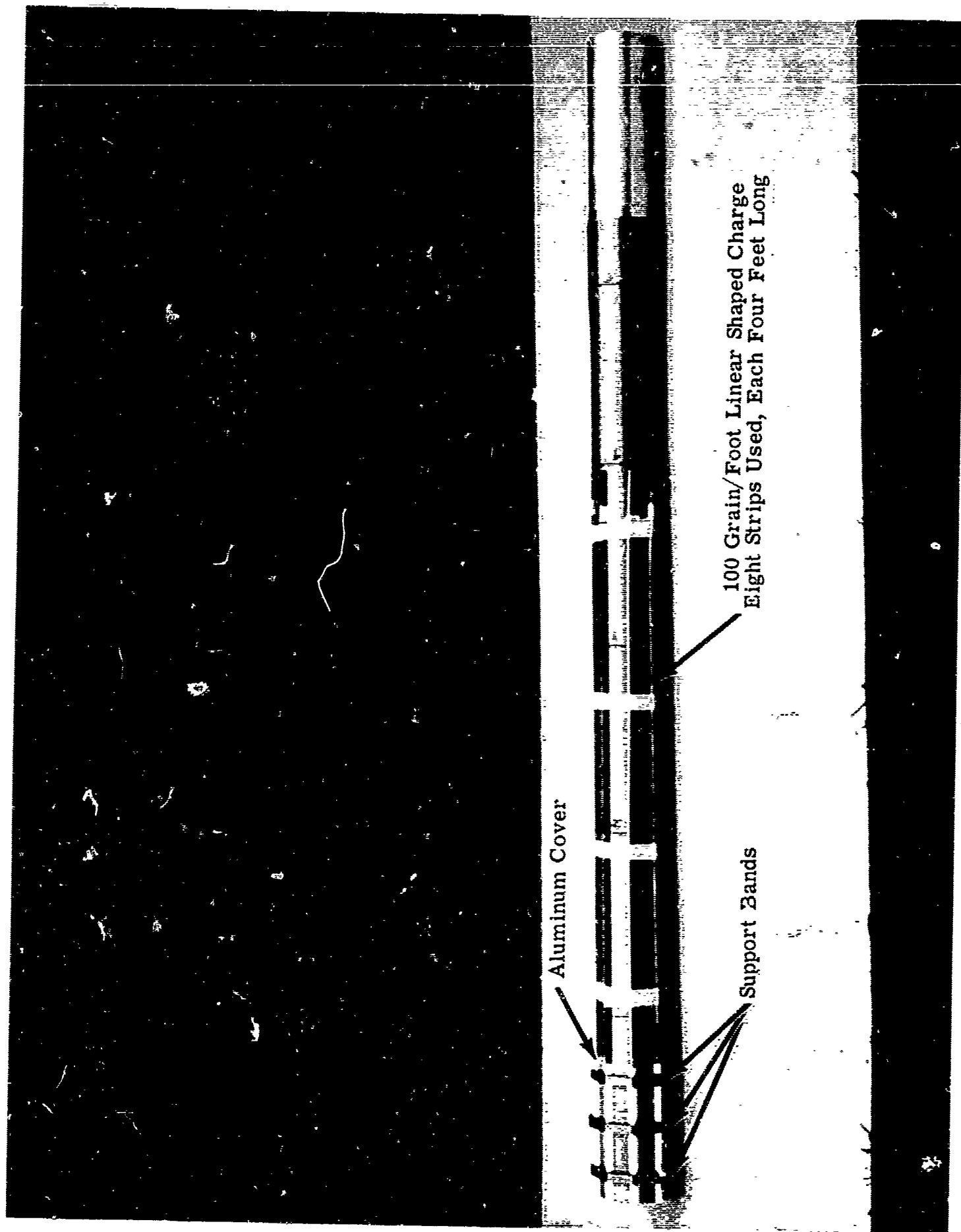


Figure 47

34195

Frangible ARCAS Rocket Motor Case Showing Cross-Section of 100 Grain/Foot Linear Shaped Charge with Simulated Fin Cover



R34196

Figure 48

Illustration of Sympathetic Detonation Fragmentation Concept

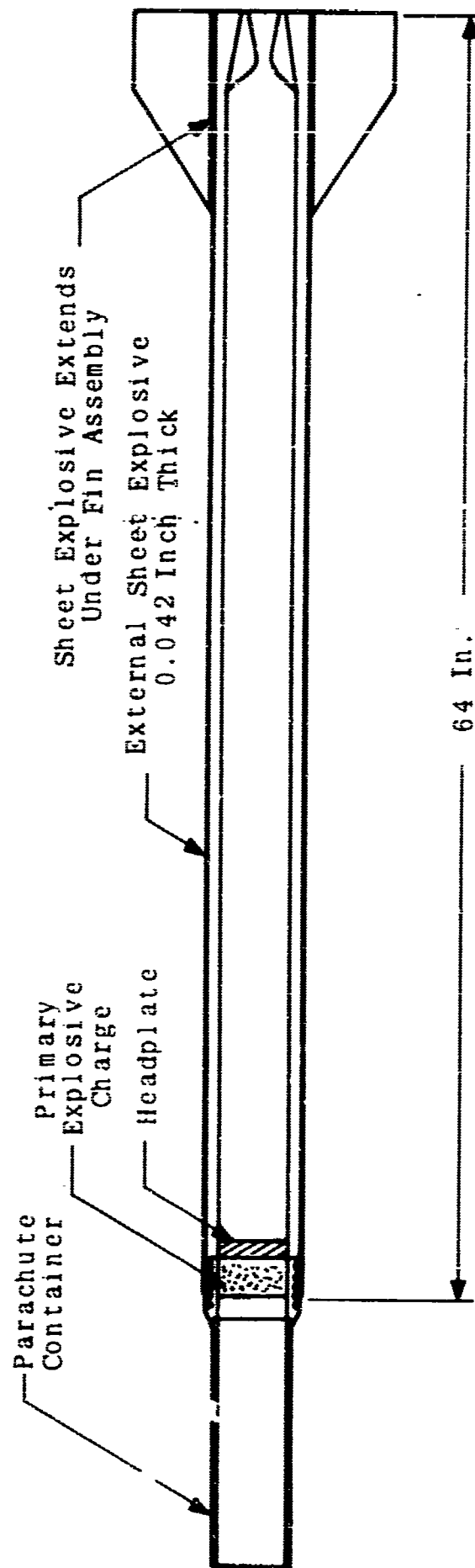


Figure 49

Frangible ARCAS Fragmentation Test Setup Incorporating
an Internal Explosive Charge and External Sheet
Explosive Material

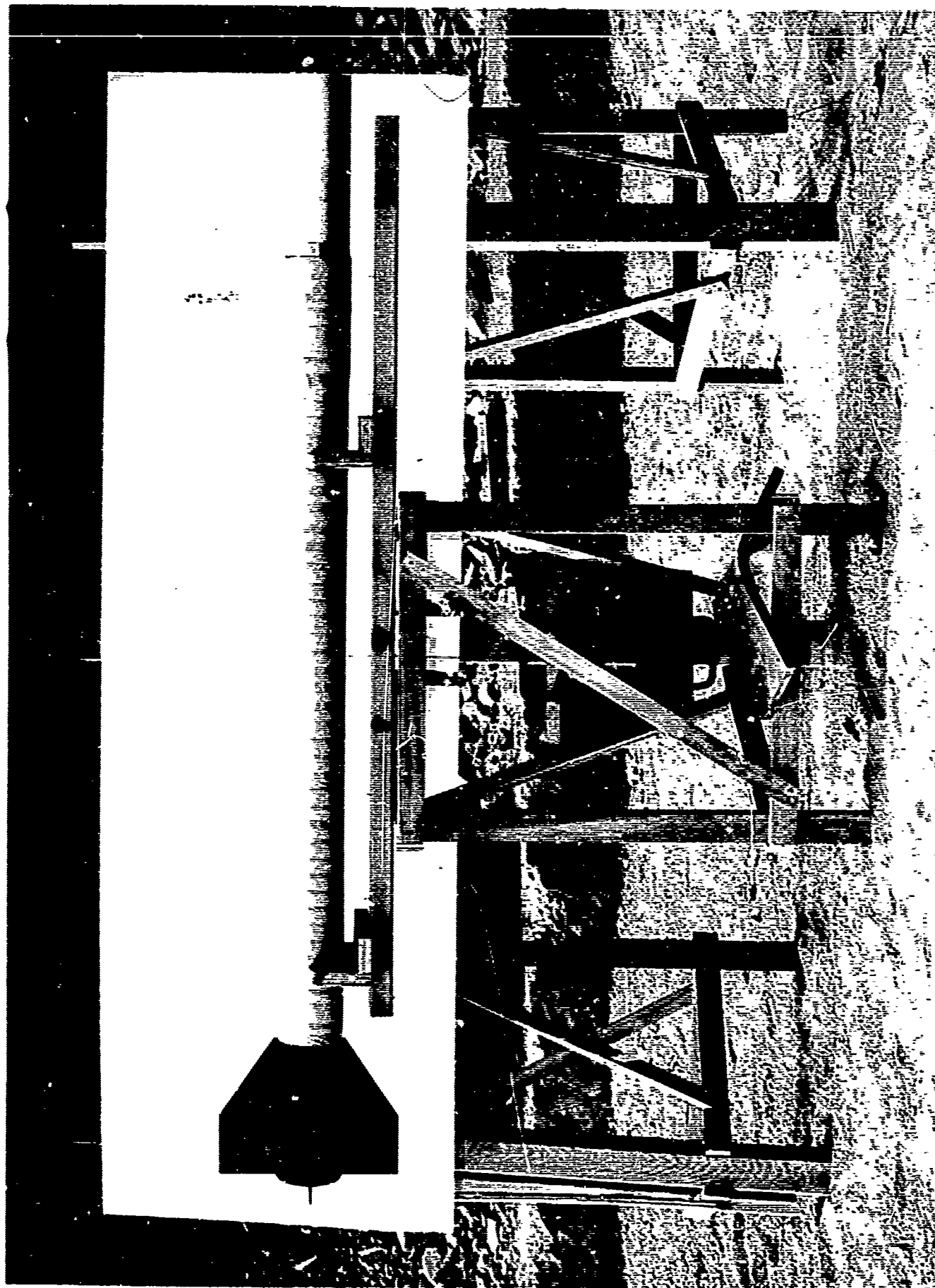


Figure 50

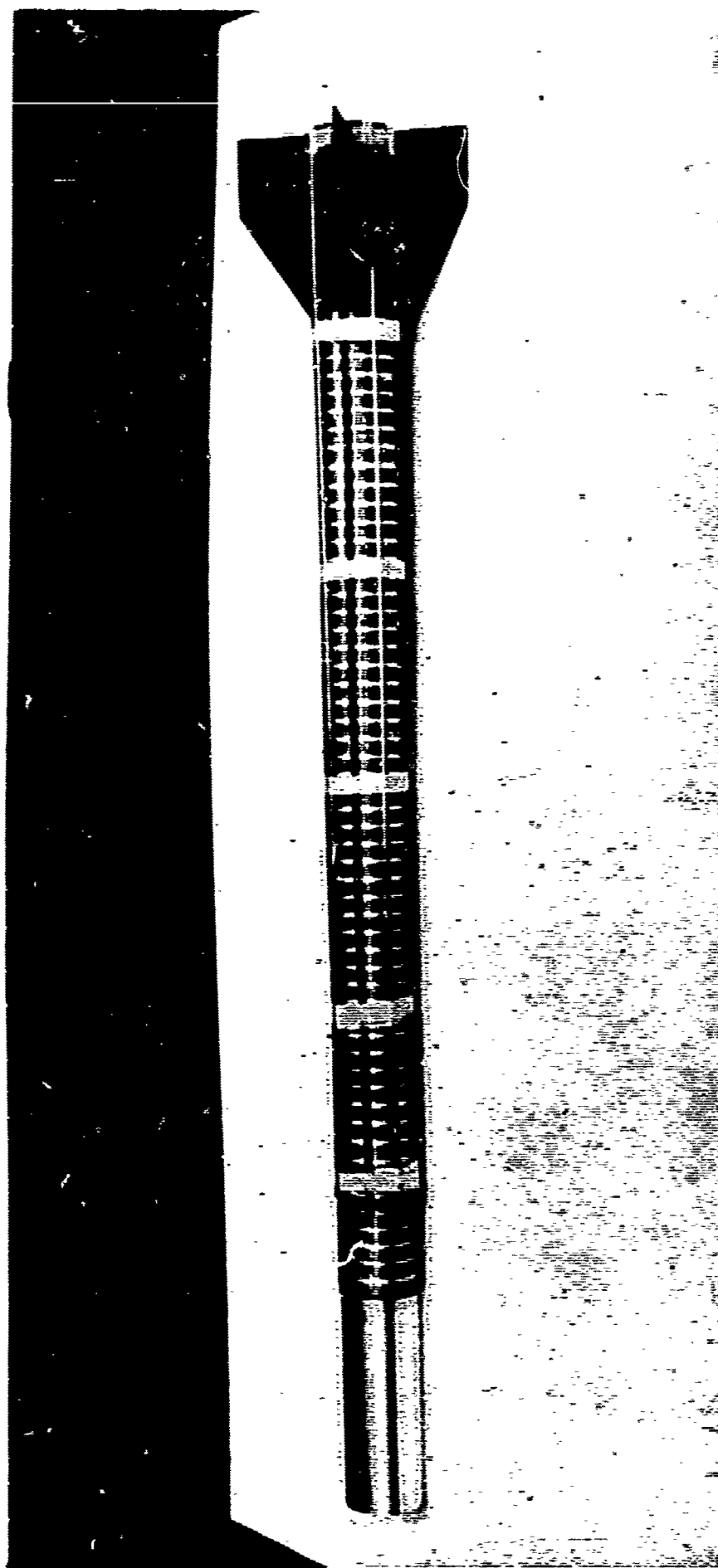
34507

Photograph. Showing Test Results Obtained With a Modular Explosive Charge and 0.030 Inch Thick External Sheet Explosive



Figure 51

Frangible ARCAS Rocket Motor Assembly Showing
Grid Markings and Linear Shaped Charge



AR 33831

Figure 52

Photograph Showing Test Results Obtained With a Modular Explosive Charge and Linear Shaped Charge (simultaneous detonation)

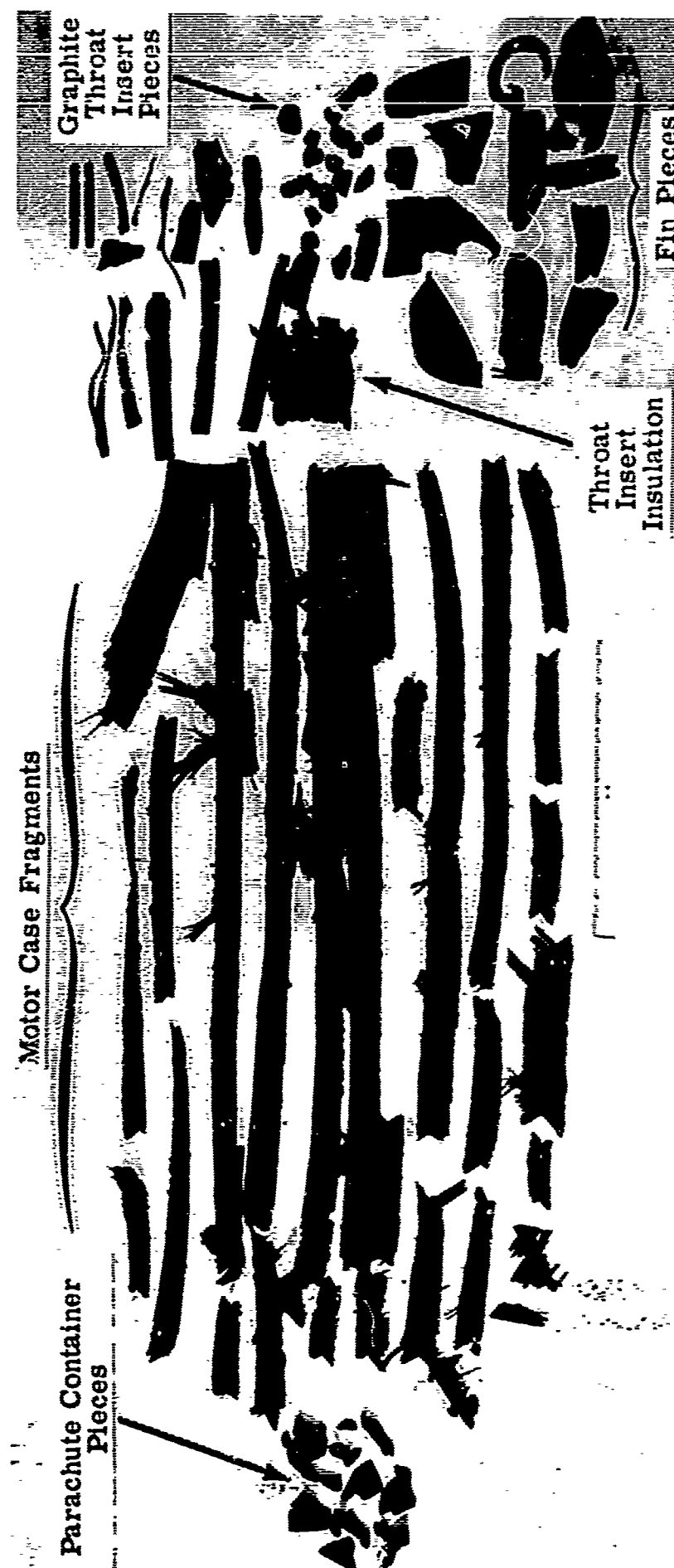


Figure 53

Frangible ARCAS AFST-14 Static Firing/Fragmentation Test Setup

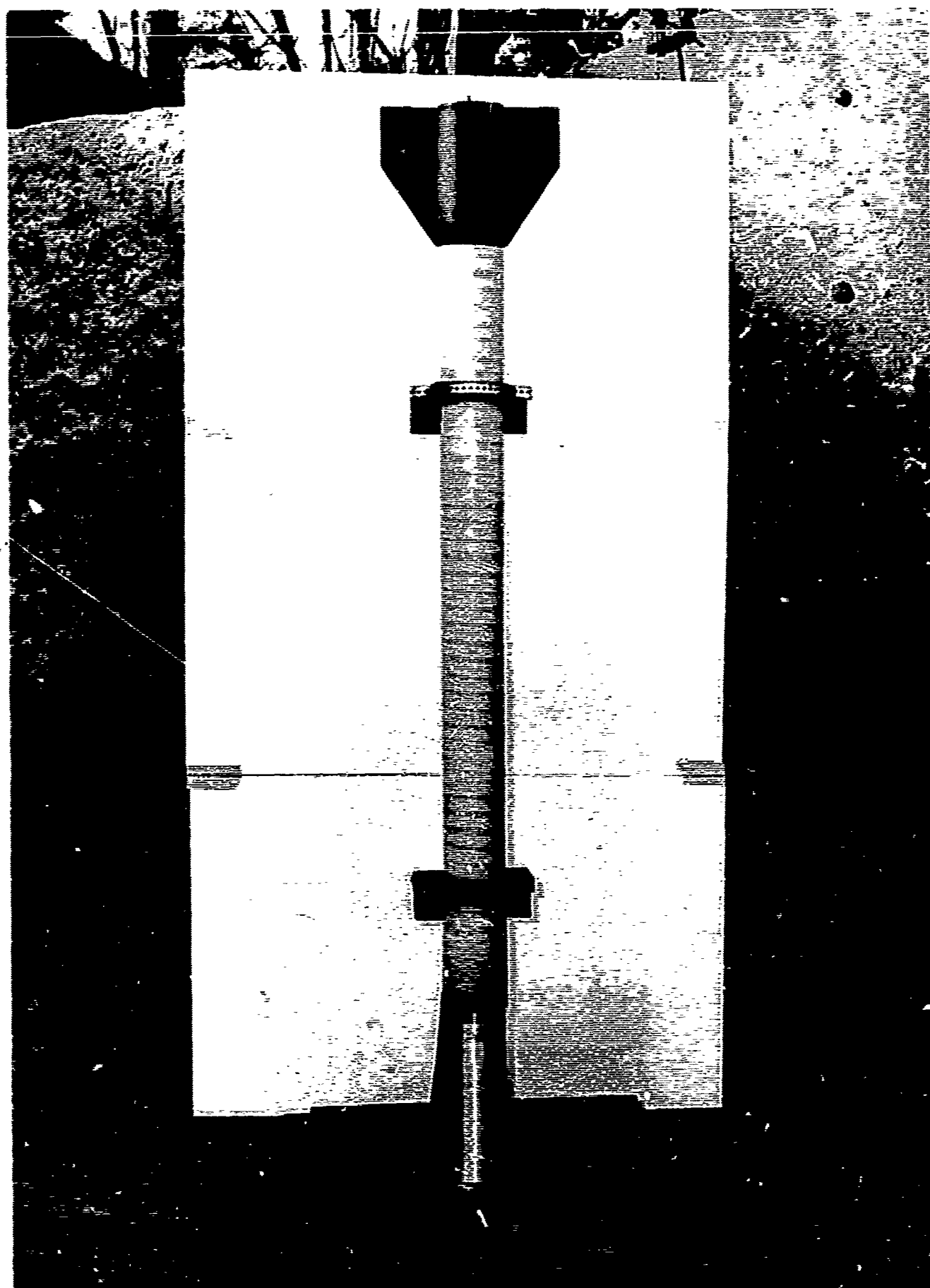


Figure 54

34508

AFST-14 Test Sequence Diagram

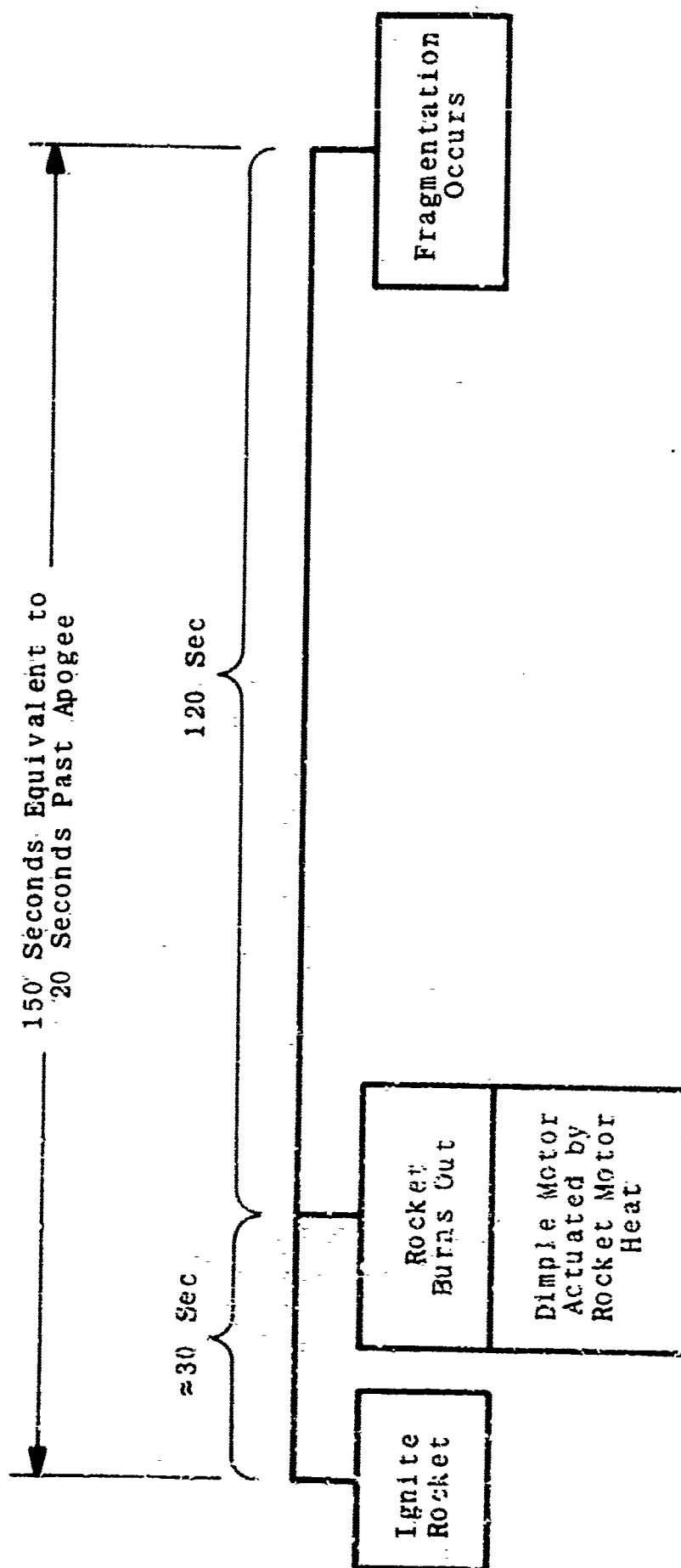


Figure 55

Pre-Test and Post-Test Comparison of the Frangible ARCAS
Rocket Motor Assembly Incorporating a Primary Explosive
Charge and 0.042-Inch Thick Sheet Explosive

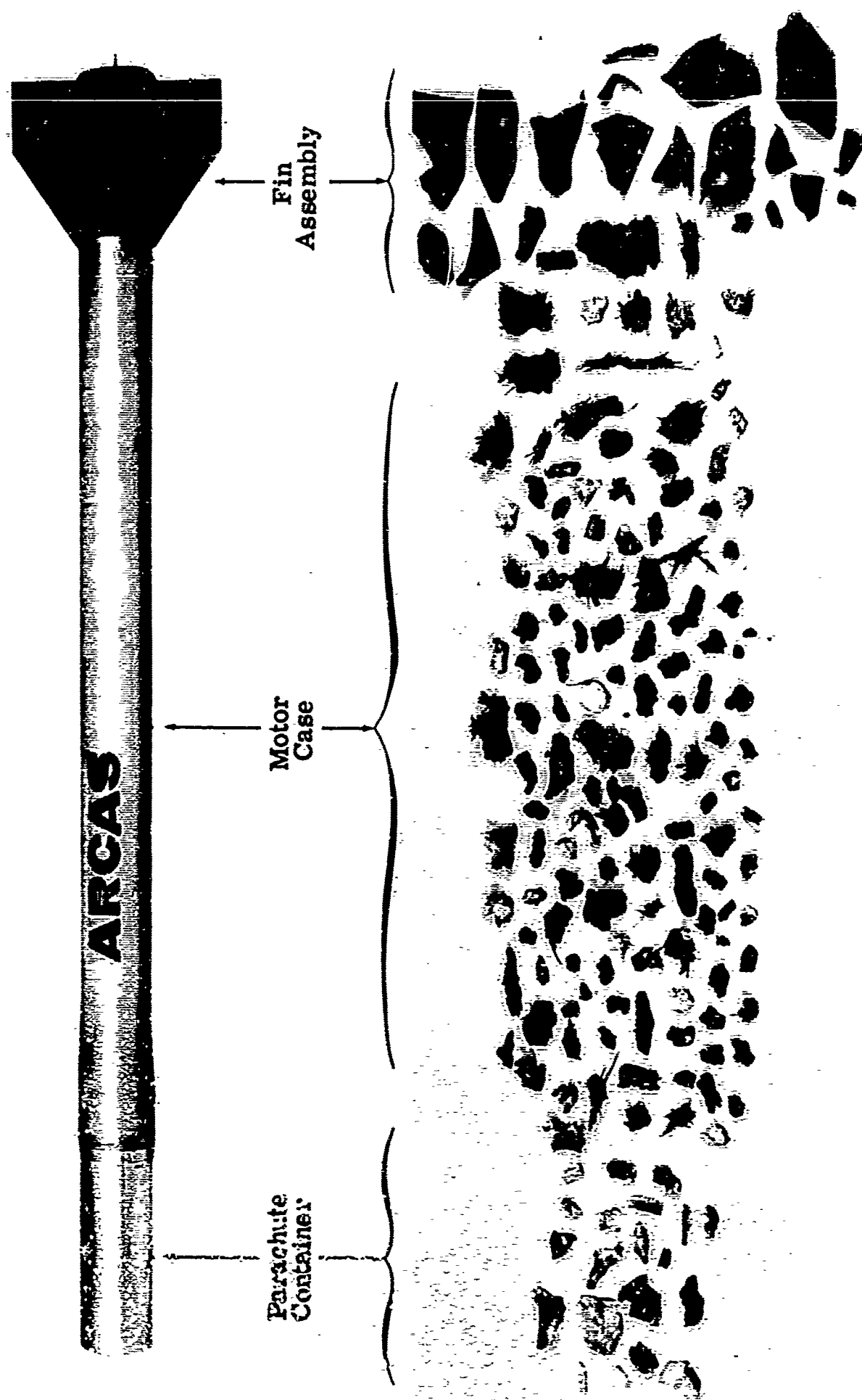


Figure 56

AR 34527

Frangible ARCAS Fragmentation System Assembly

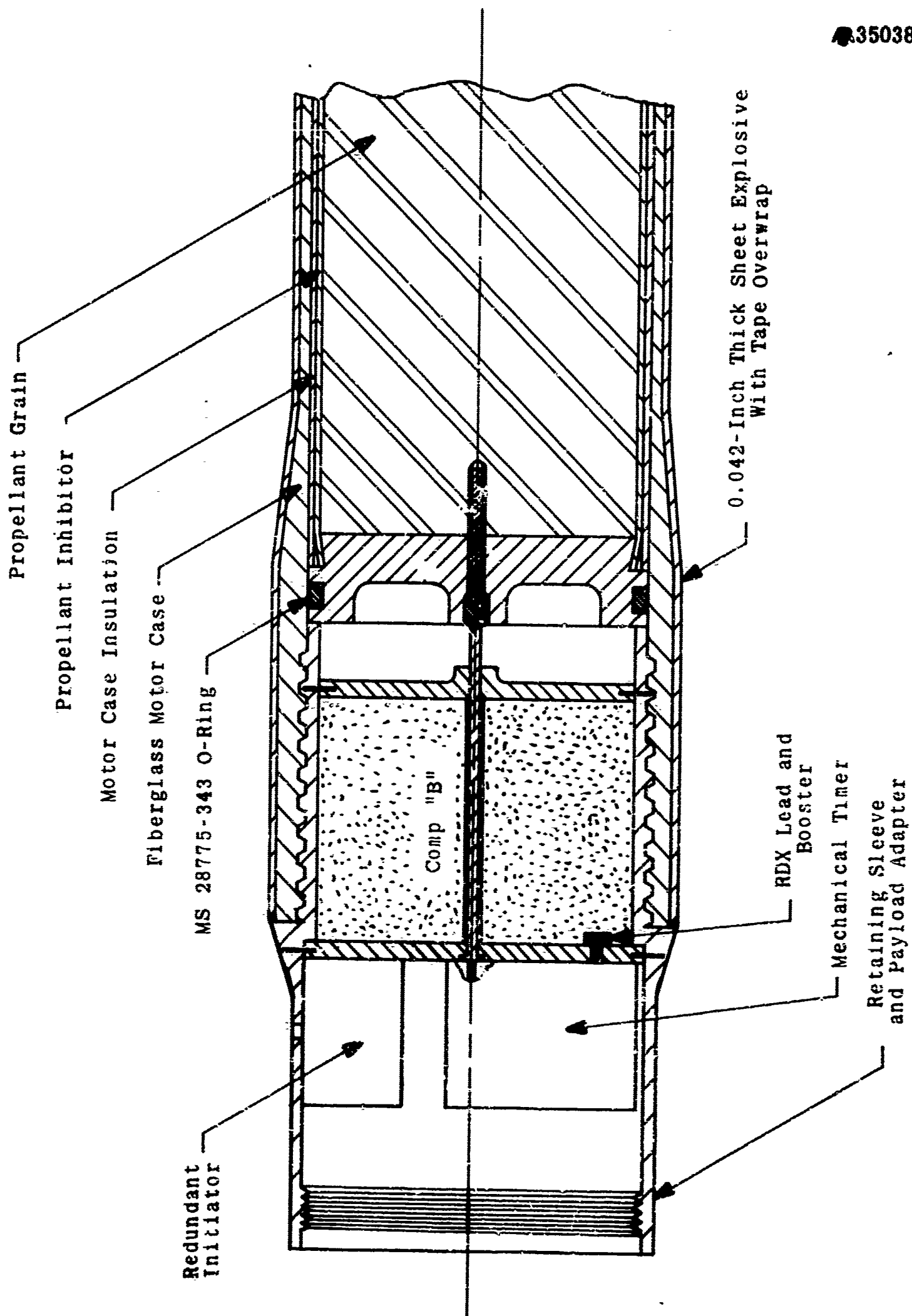


Figure 57

Primary Firing Train of Mechanical Timer

5040

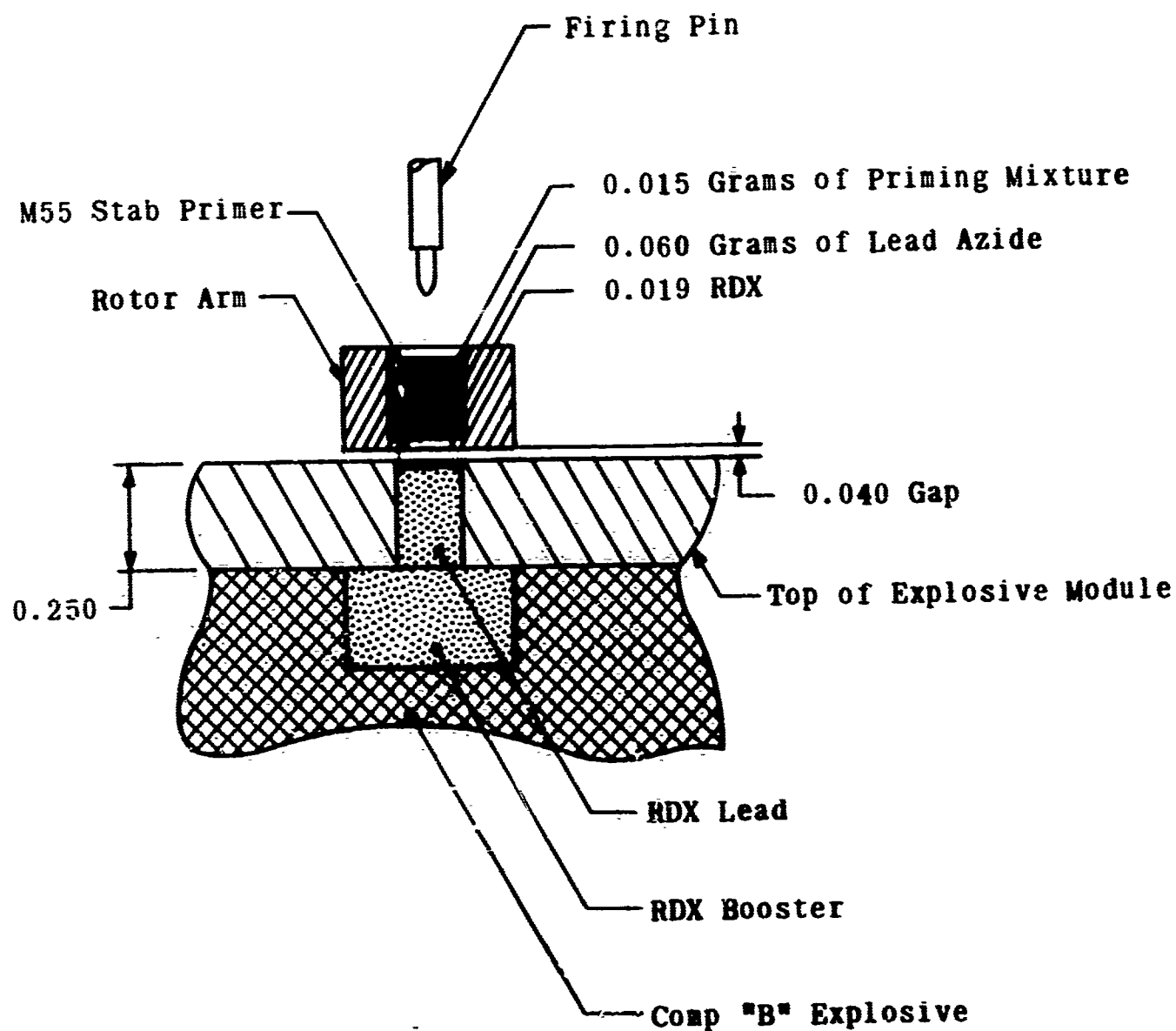
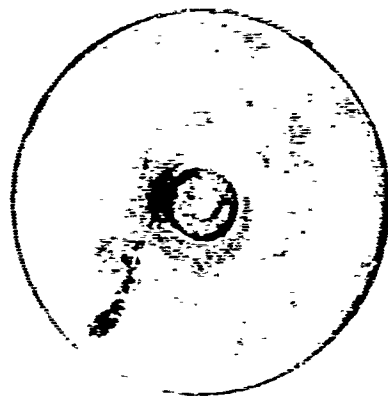
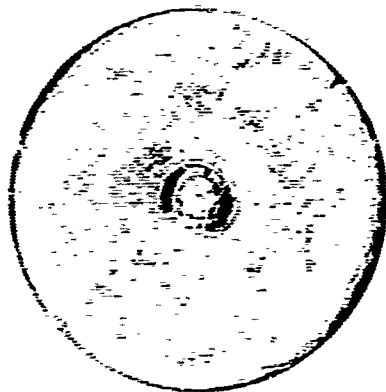


Figure 58

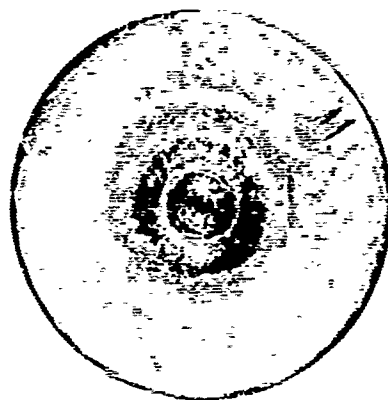
Results of Fragmentation Firing Train Detonation Tests Using 1/8-inch Thick Lead Sample Plates for Relative Comparison



Mk 125
Stab Primer

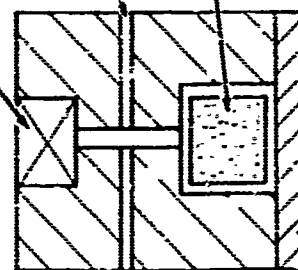


Modified Mk 125
(Stab Detonator)



M55 Stab Detonator
Note Full Penetration
at Center of Cavity

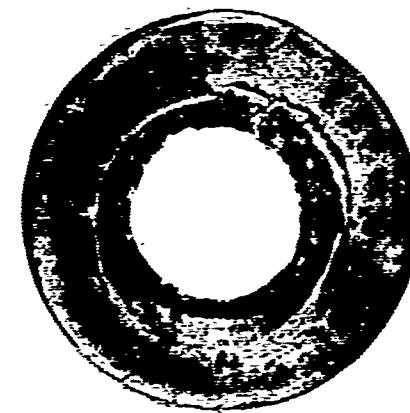
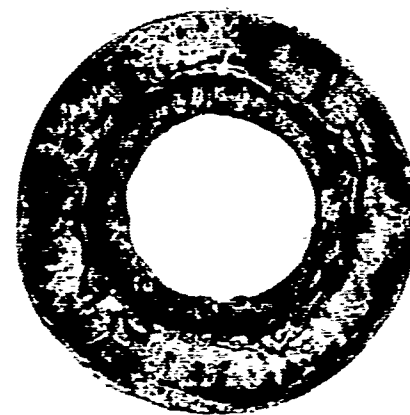
M55 Stab
Detonator



Vent
Hole

RDX
Lead

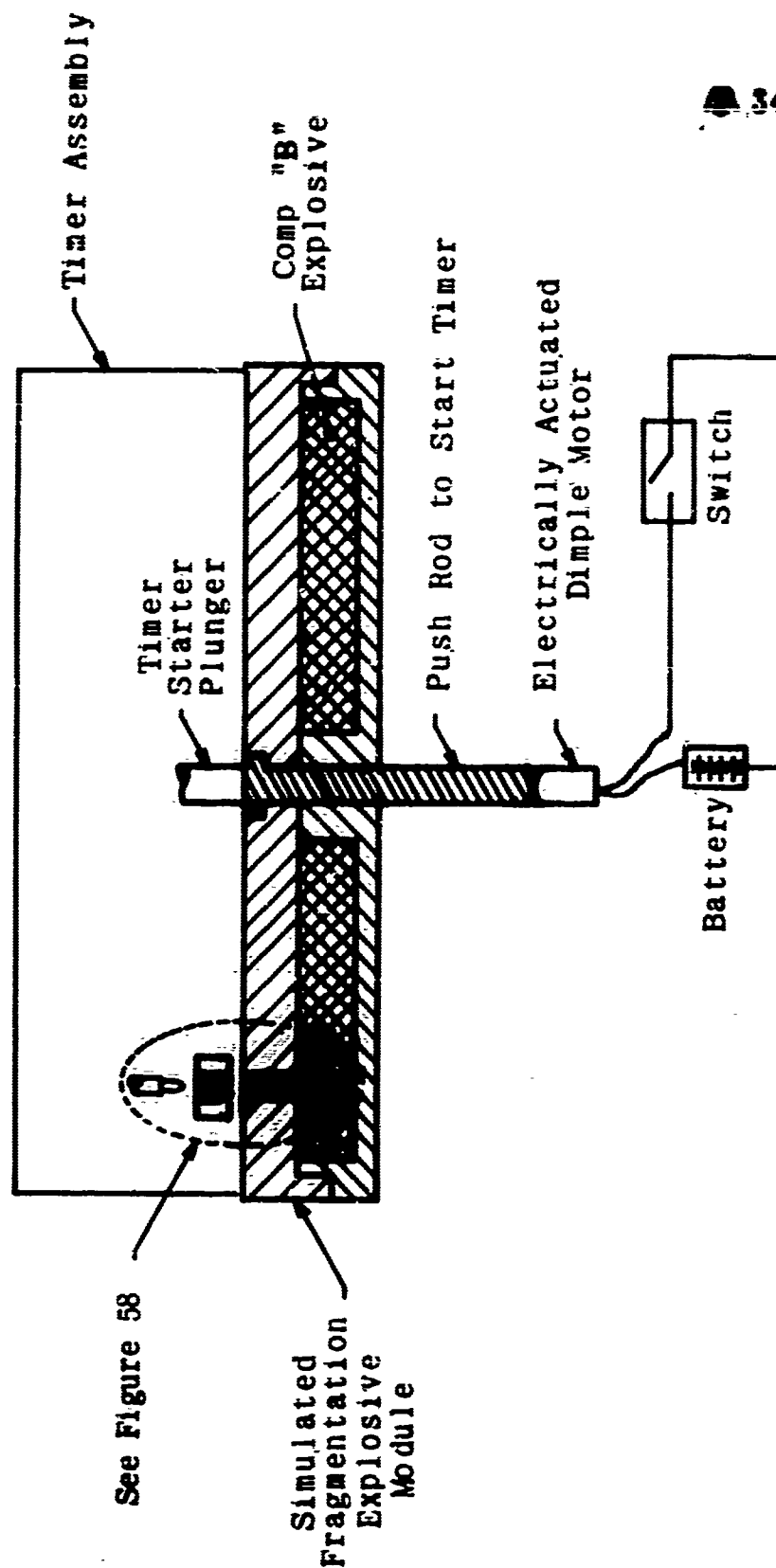
Lead Sample
Plate



Sample Plates Showing Results of High Order
Detonation of RDX Lead Through 0.092 Vented Gap

Figure 59

Setup for Mechanical Timer Initiation System Test



34514

Figure 60

Frangible ARCAS Explosive Module Assembly

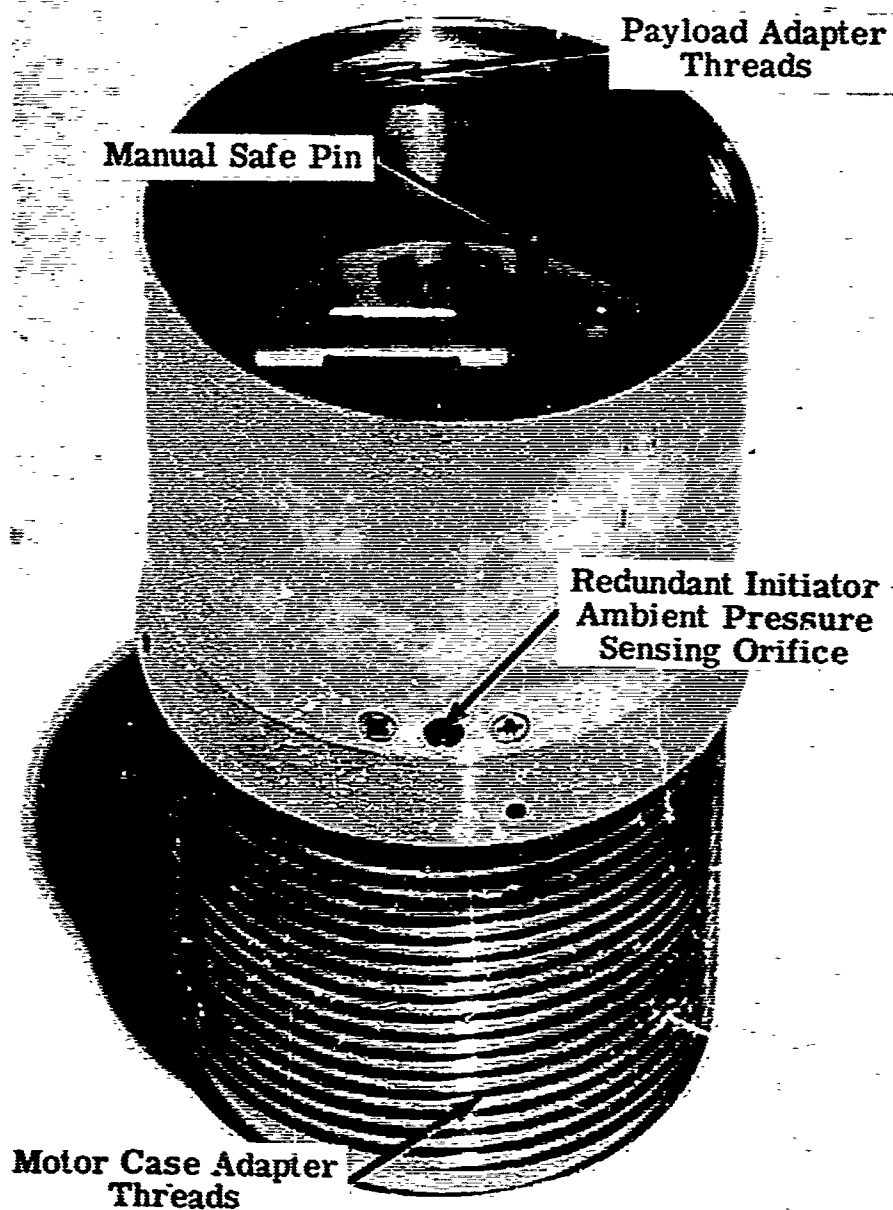
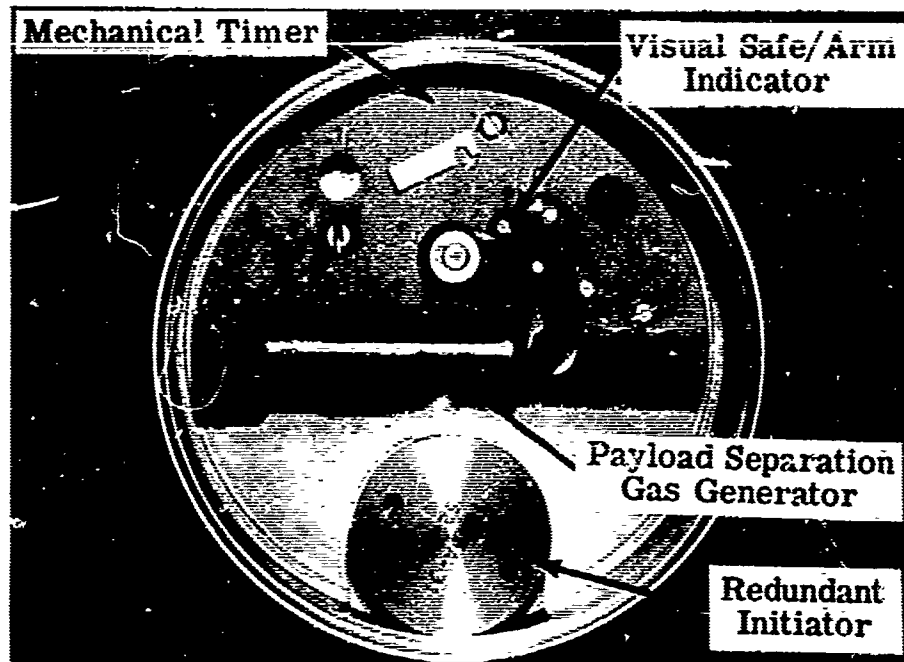


Figure 61

2404

4681

Photograph of the Frangible ARCAS Explosive Module Assembly

Frangible ARCAS Explosive Module Assembly

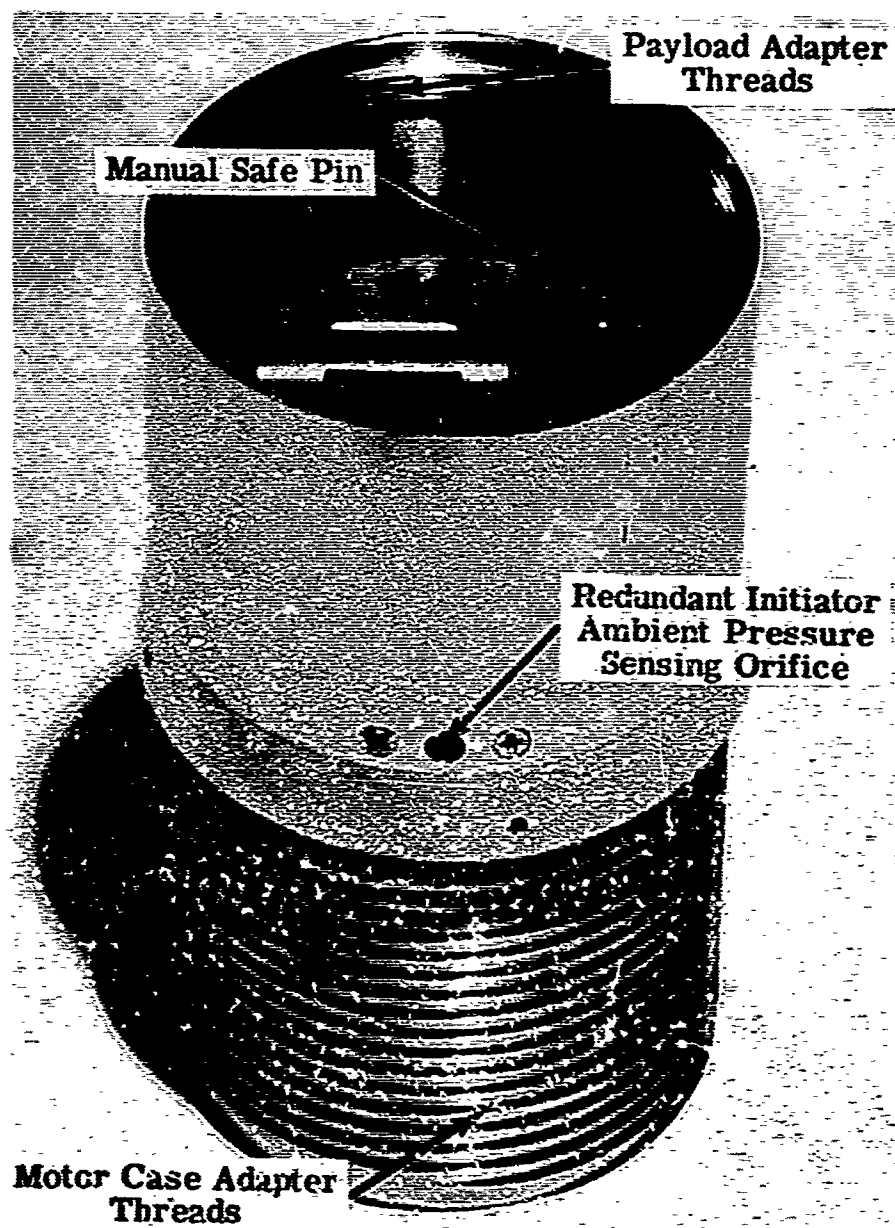
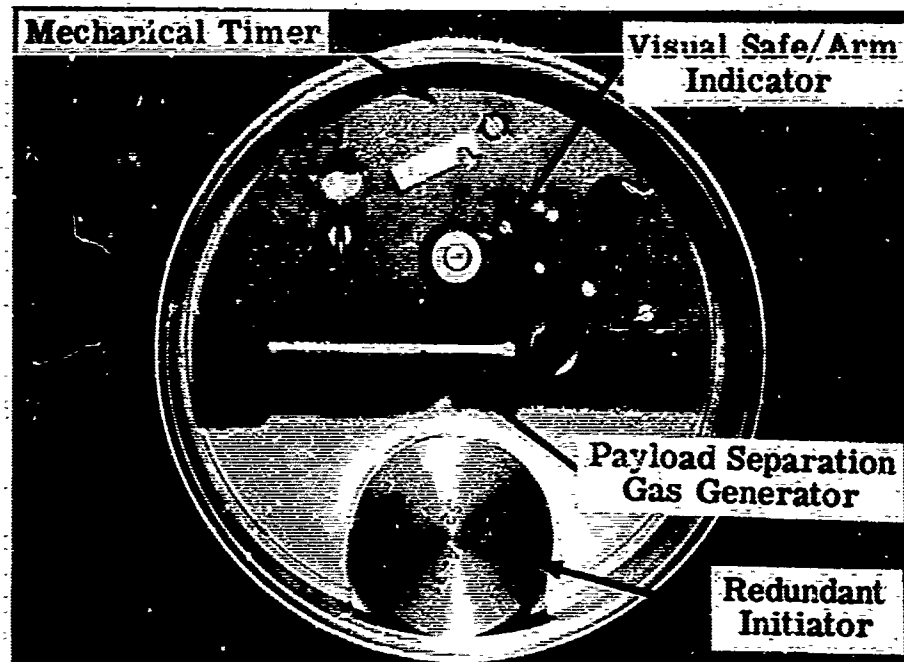
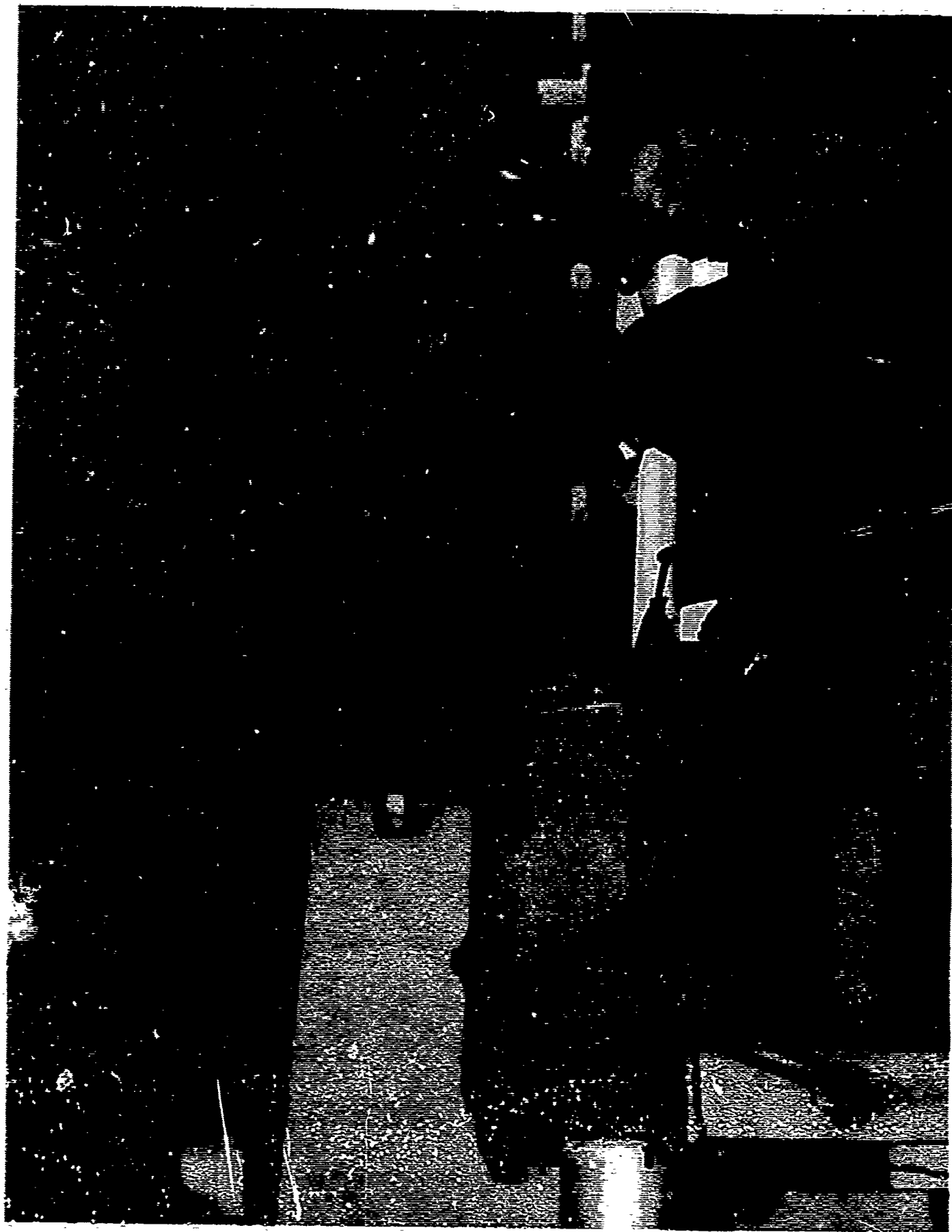


Figure 61

9404

4661

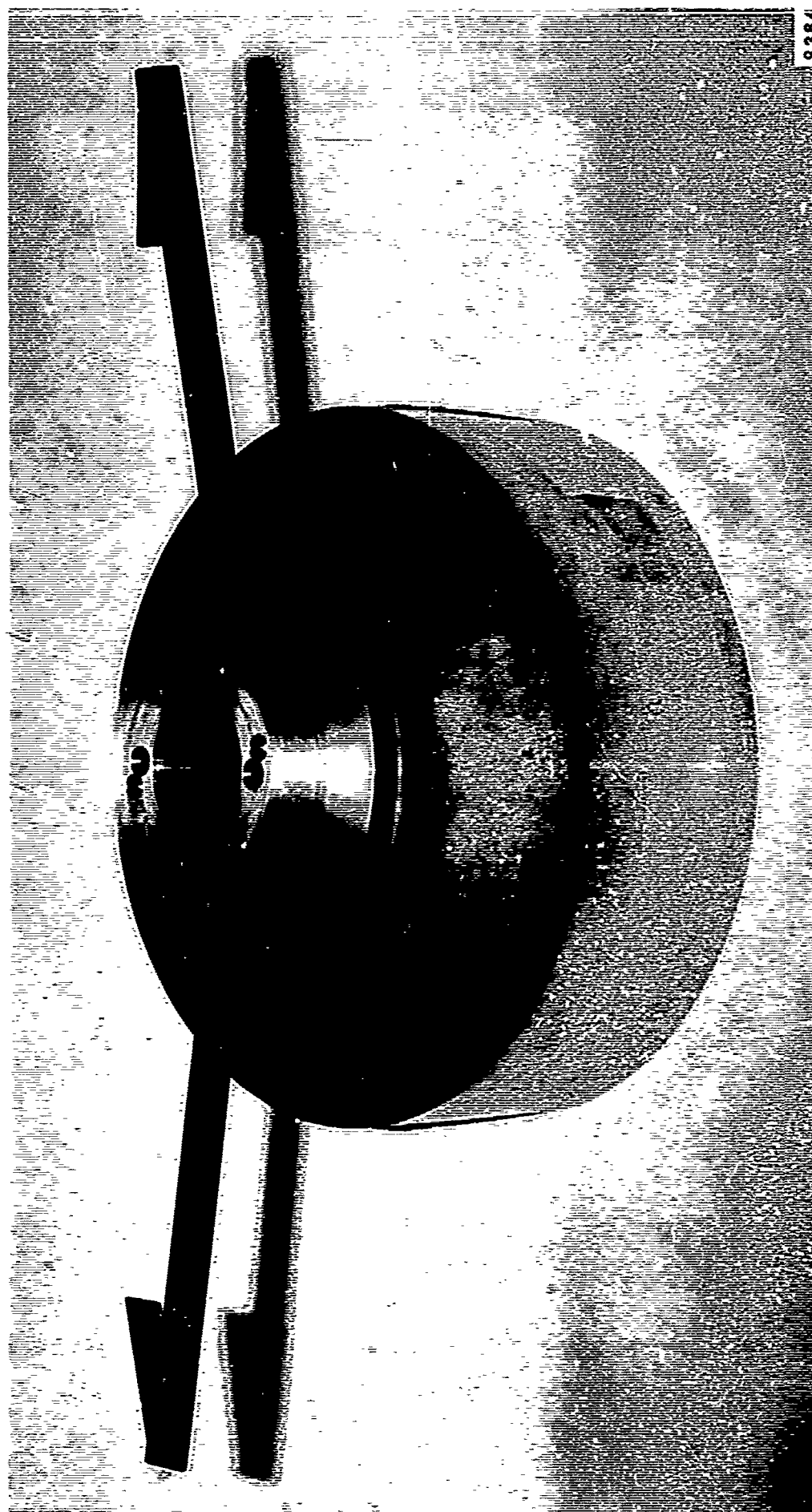
Photograph of the Frangible ARCAS Vehicle Being Loaded
into the LAU-41/A Closed Breech Launcher



88721

Figure 62

Frangible ARCAS Launcher Piston Assembly



9384
A 4680

Figure 63

**Modification of the Standard ARCAS Launcher Piston for
Adaptation to the MOD 3 Vehicle**

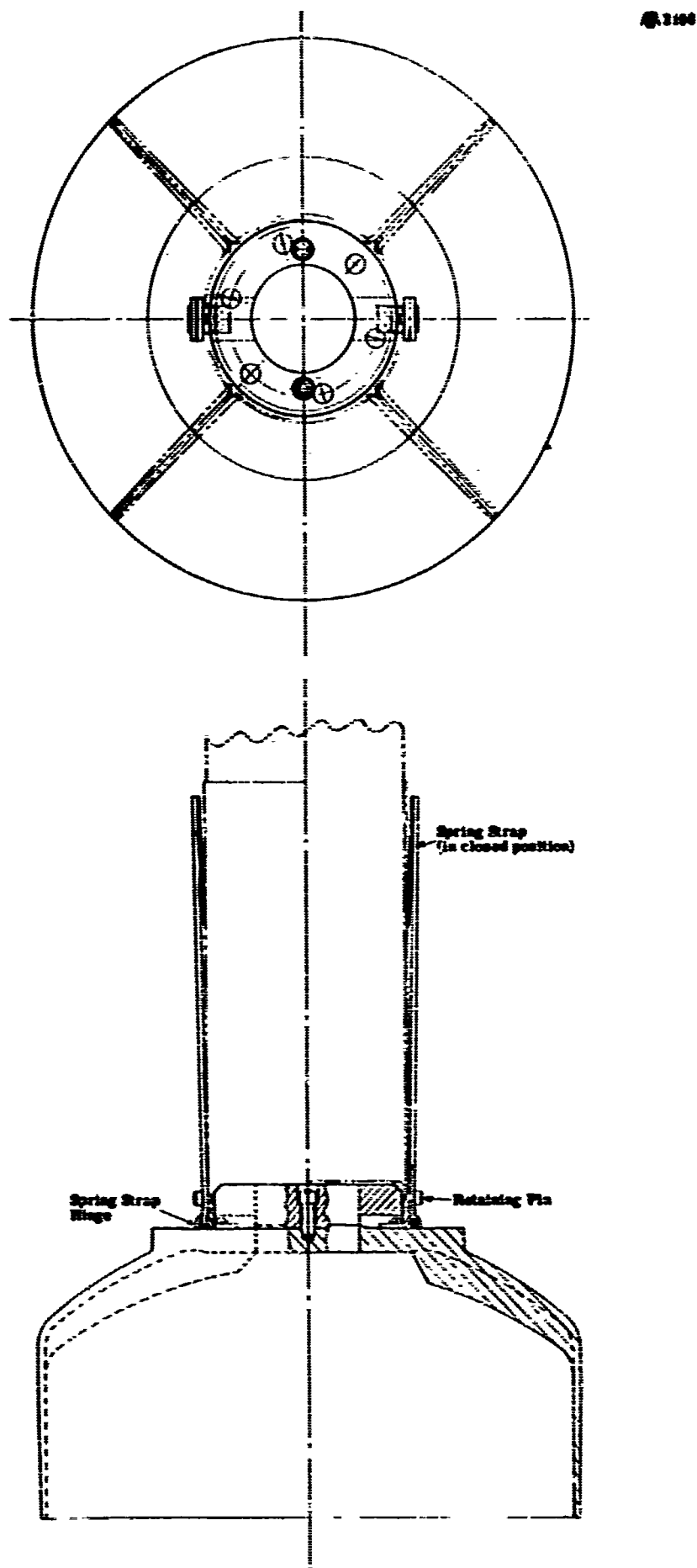


Figure 64

Illustration of Modification to the Standard ARCAS Launch Tube to Provide Access Port for the Frangible ARCAS Vehicle

2116

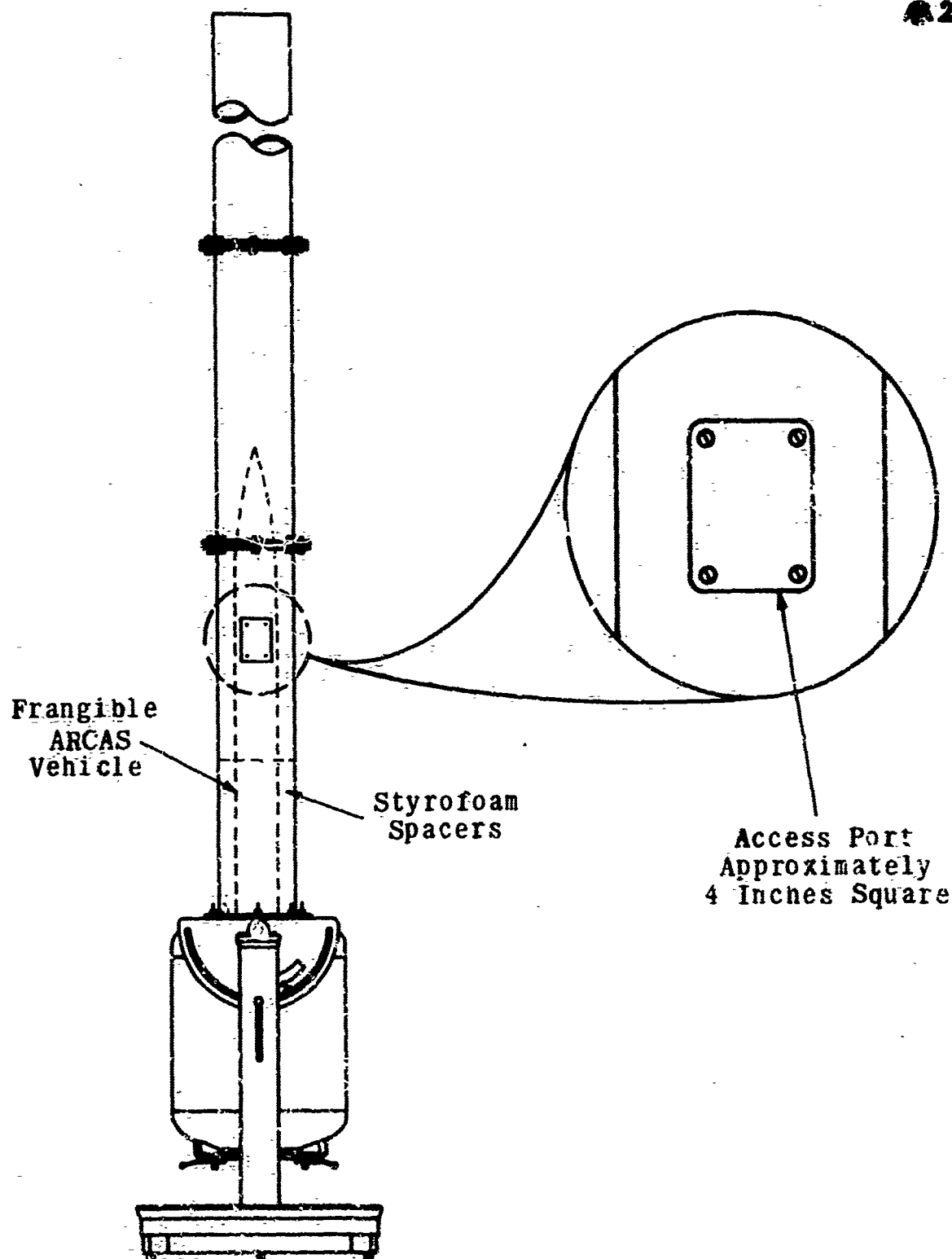


Figure 65

Frangible ARCAS Static Stability

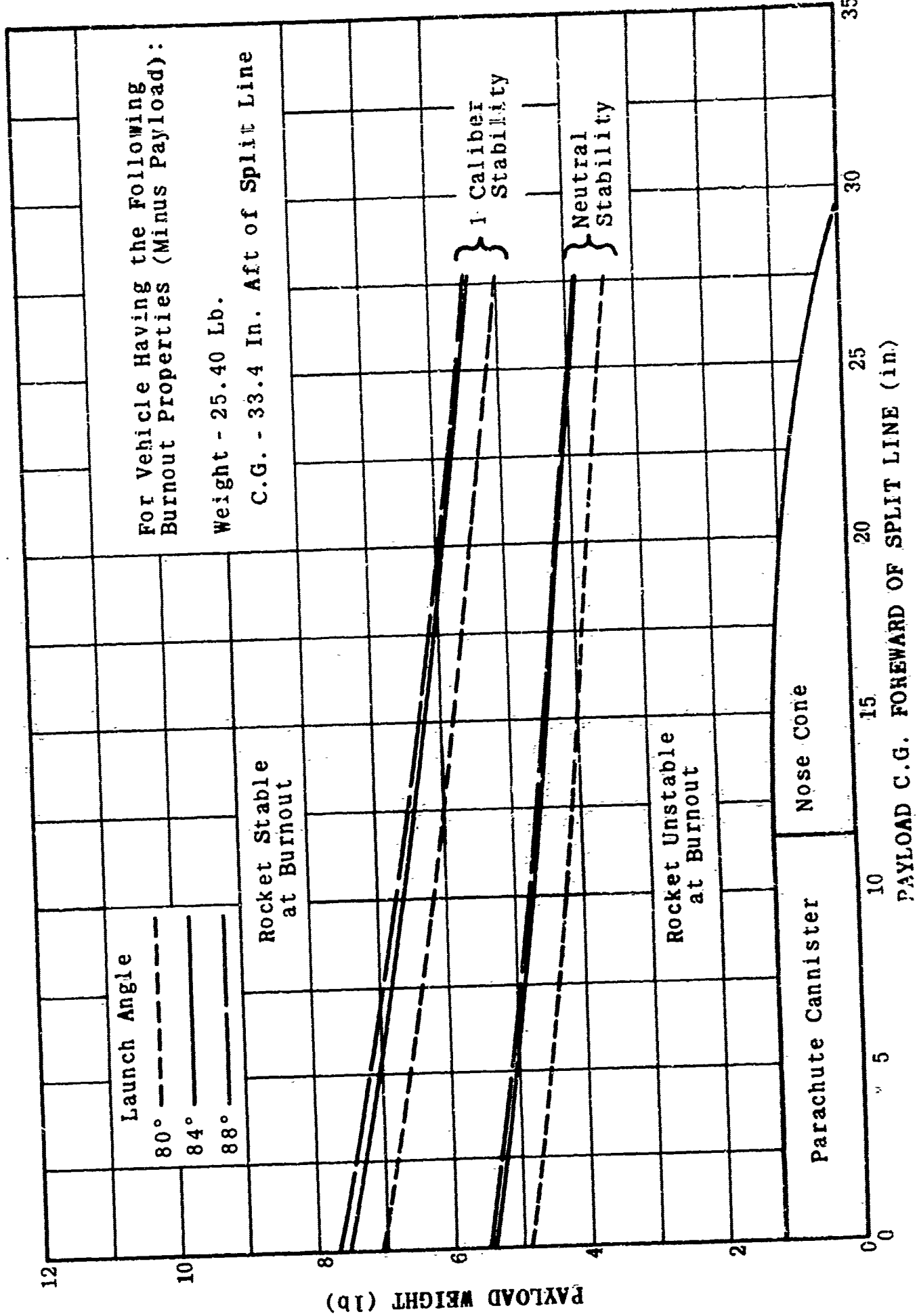


Figure 66

Frangible ARCAS Center of Gravity Versus Time with 10.38 lb Payload

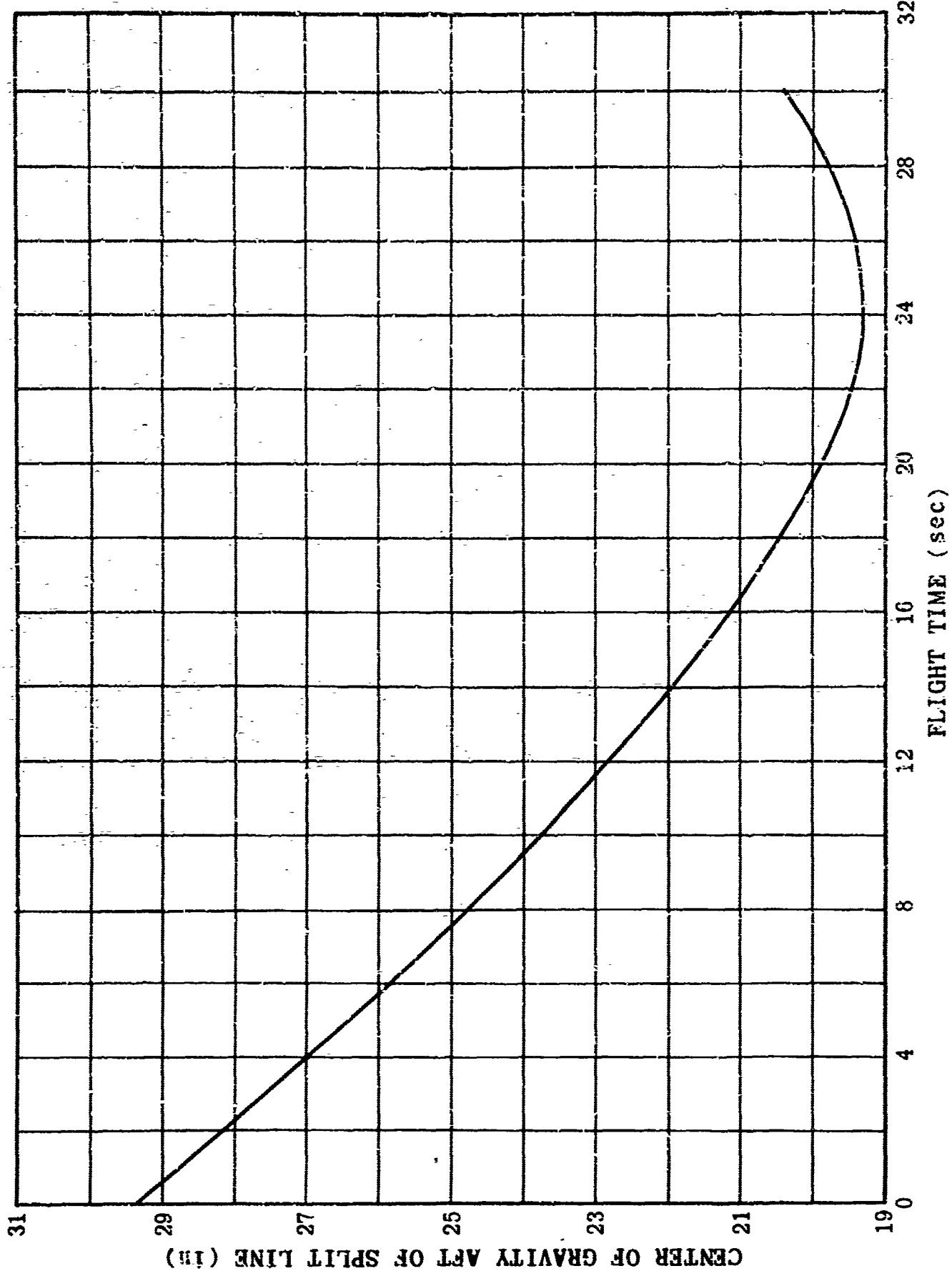


Figure 67

Frangible ARCAS Pitch Frequency and Roll Rate Versus Time for 10.7 lb Payload
84° QE - Sea Level Launch - Auxiliary Gas Generator Boost

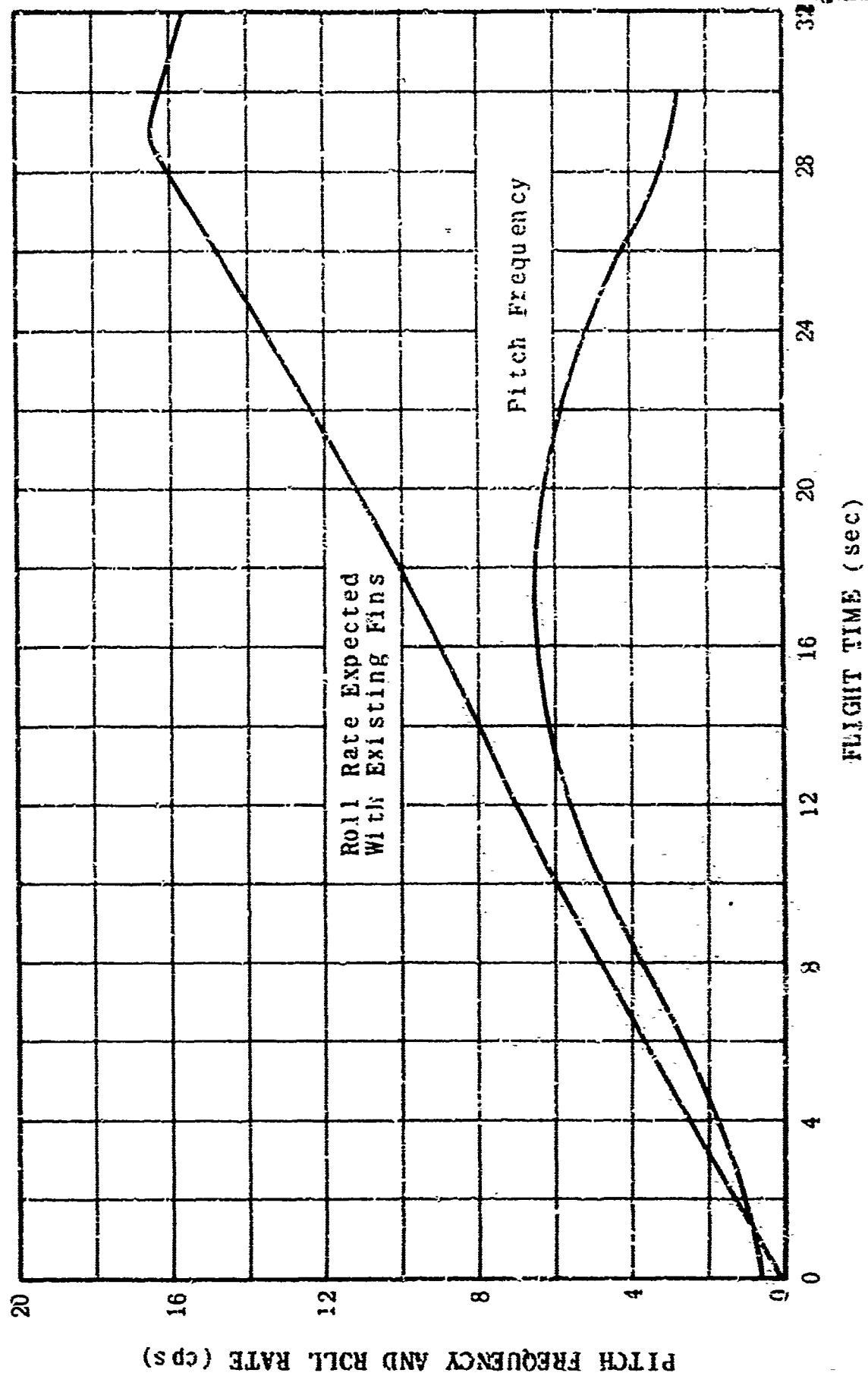
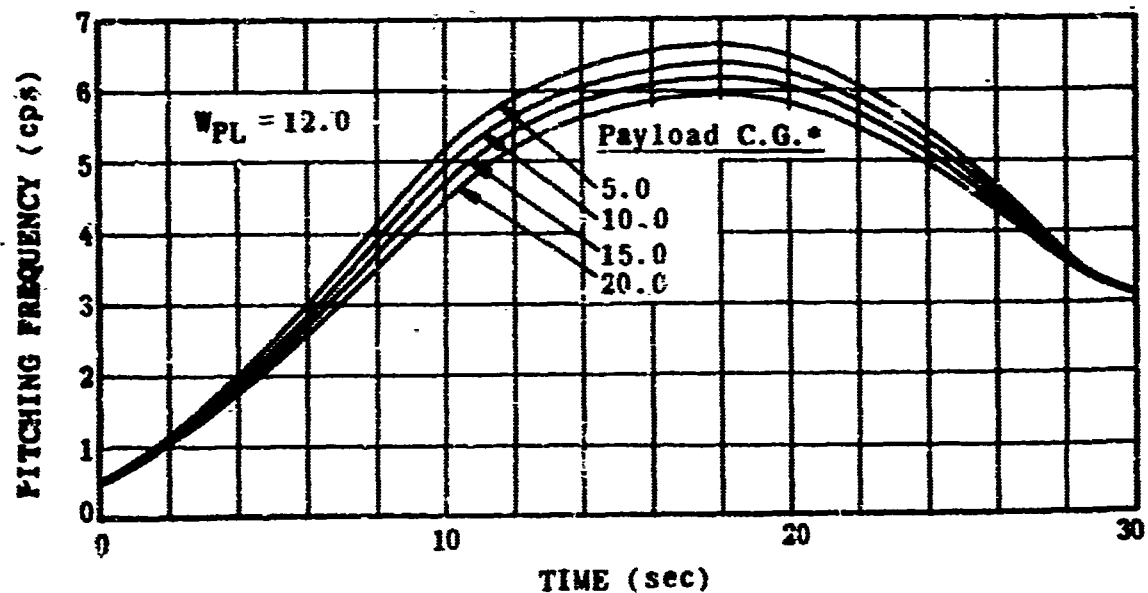
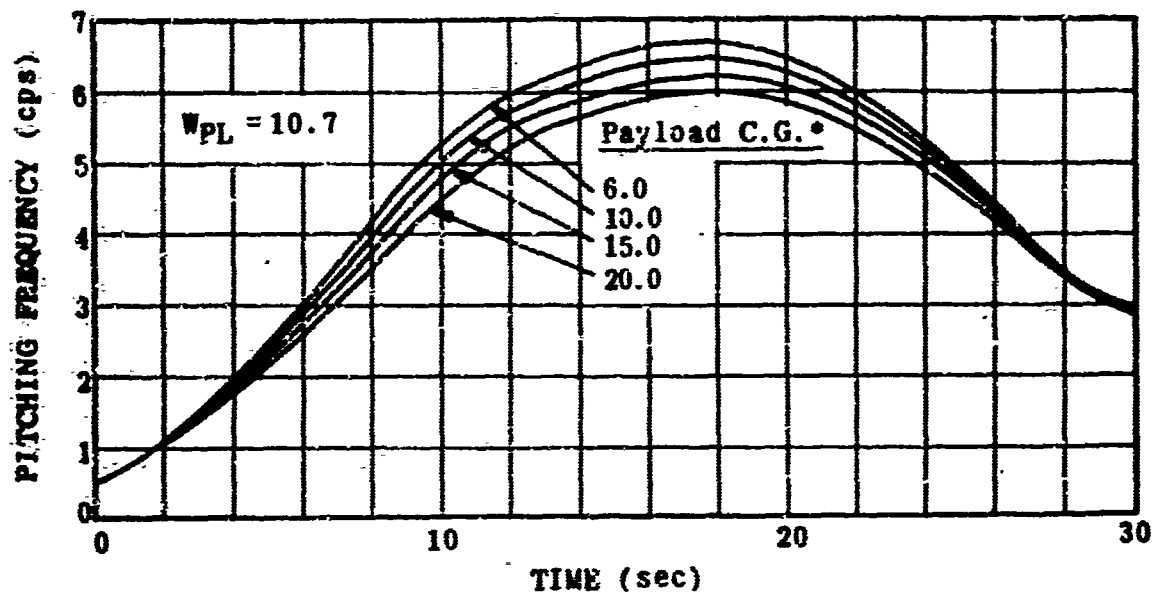
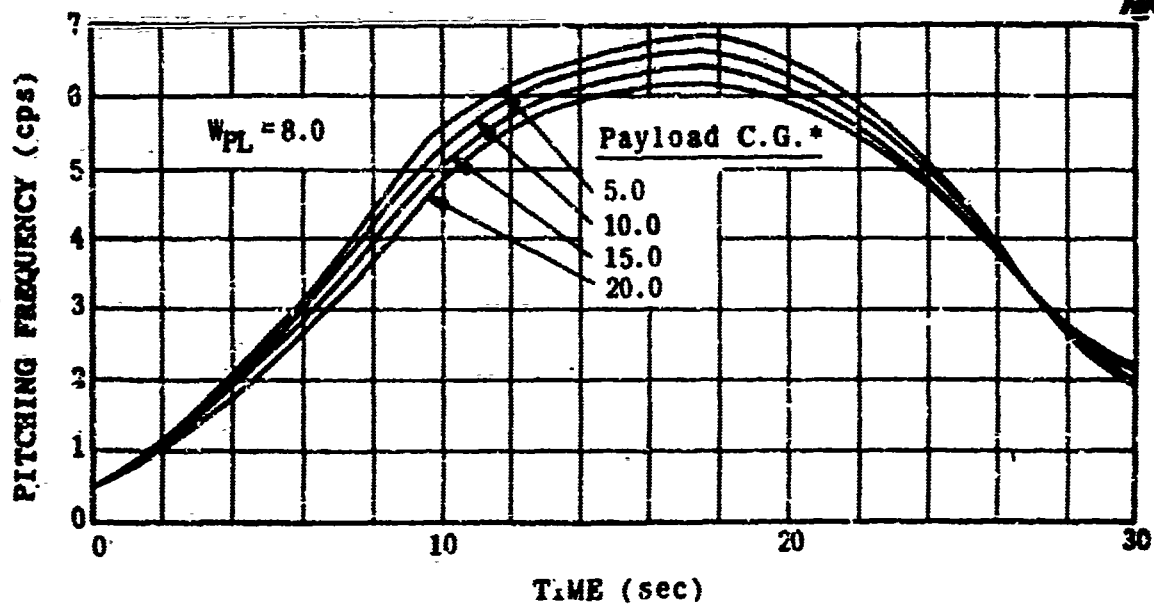


Figure 68

2117

Frangible ARCAS Pitching Frequency (Arcasonde Payload) for $QE = 84^\circ$

2403



*Inches Ahead of S.L.

Figure 69

Wind Sensitivity Versus Altitude for the PWN-6A and PWN-7A Vehicles

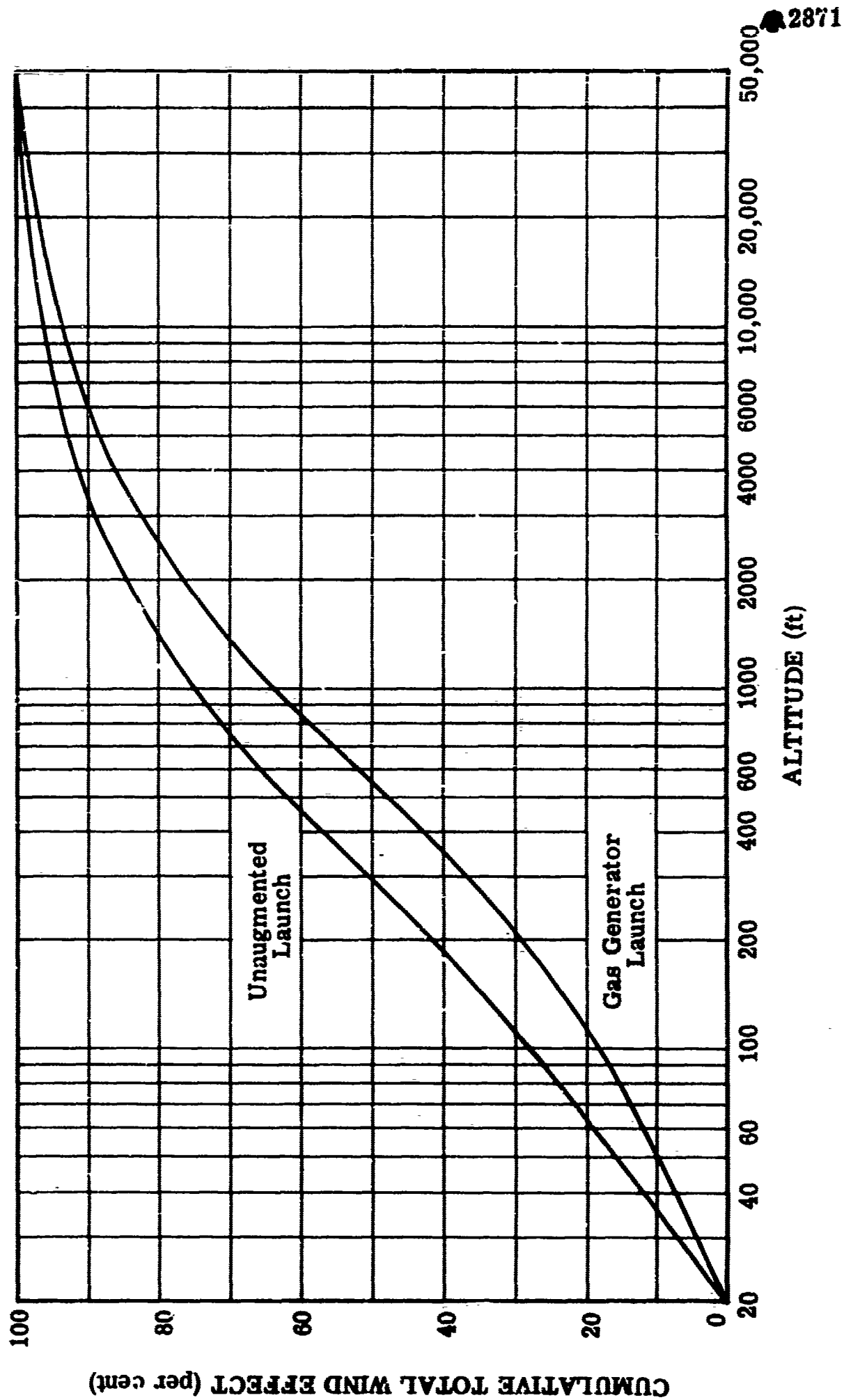


Figure 70

Photograph of the Frangible ARCAS Diagnostic Flight Test Vehicles

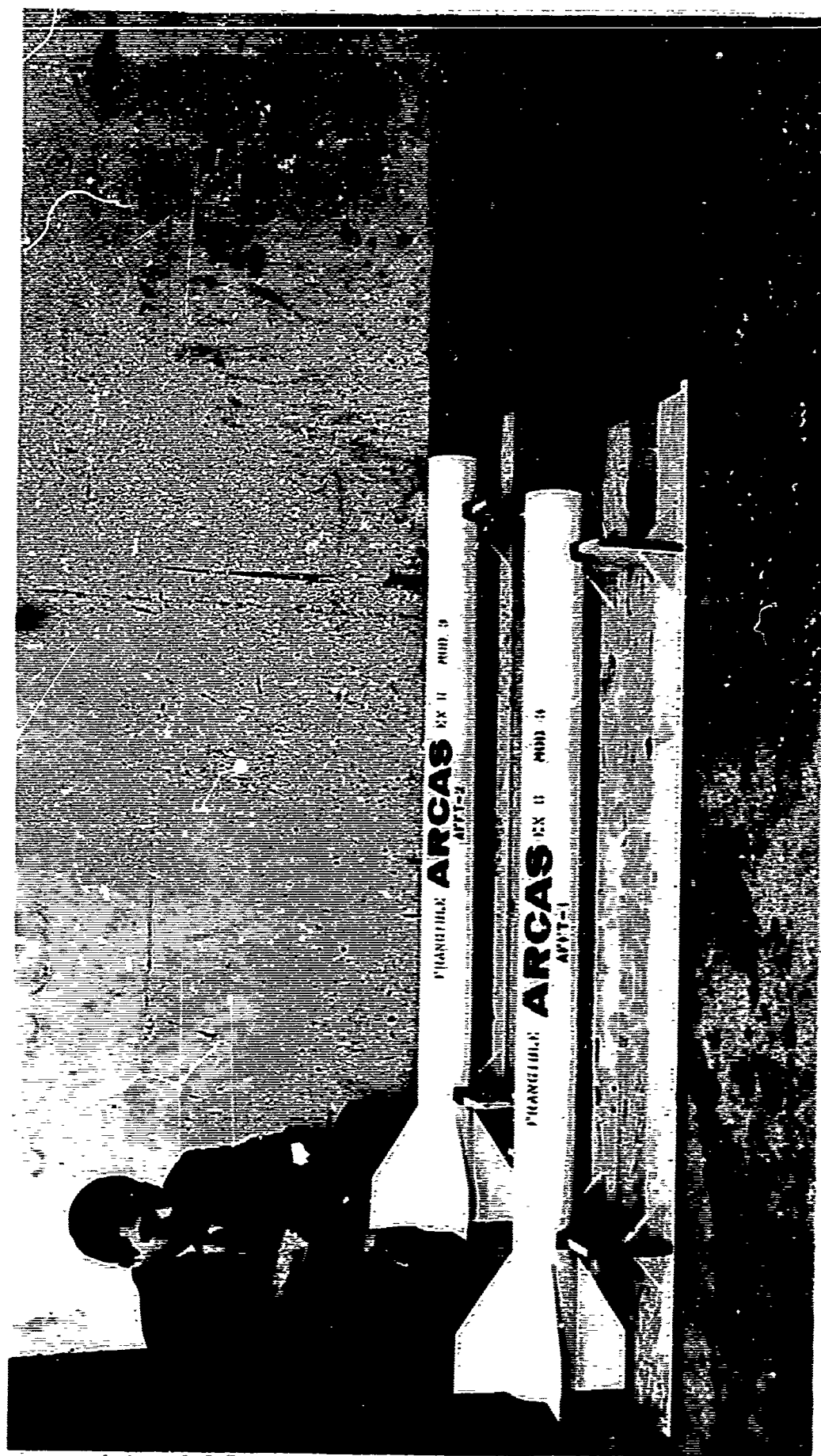
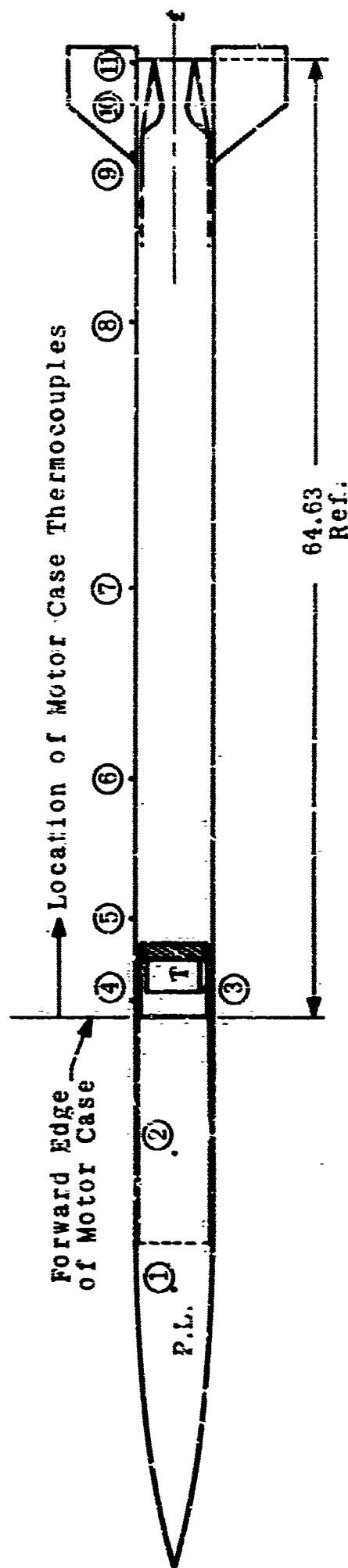


Figure 71

AR 34992

Thermocouple Locations for Frangible ARCAS Diagnostic Flight Tests



*Thermistors
T = Mechanical Timer

Number	Location of Thermocouple
T-1*	Payload (Ambient)
T-2*	Instrumentation Section (Ambient)
T-3*	Inner Surface (Destruct Module)
T-4	1.0 In.
T-5	5.0 In.
T-6	17.0 In.
T-7	33.0 In.
T-8	49.0 In.
T-9	55.5 In.
T-10	59.5 In.
T-11	64.6 In.

Figure 72

Predicted Frangible ARCAS Motor Case Skin Temperatures Induced by Aerodynamic Heating During Flight

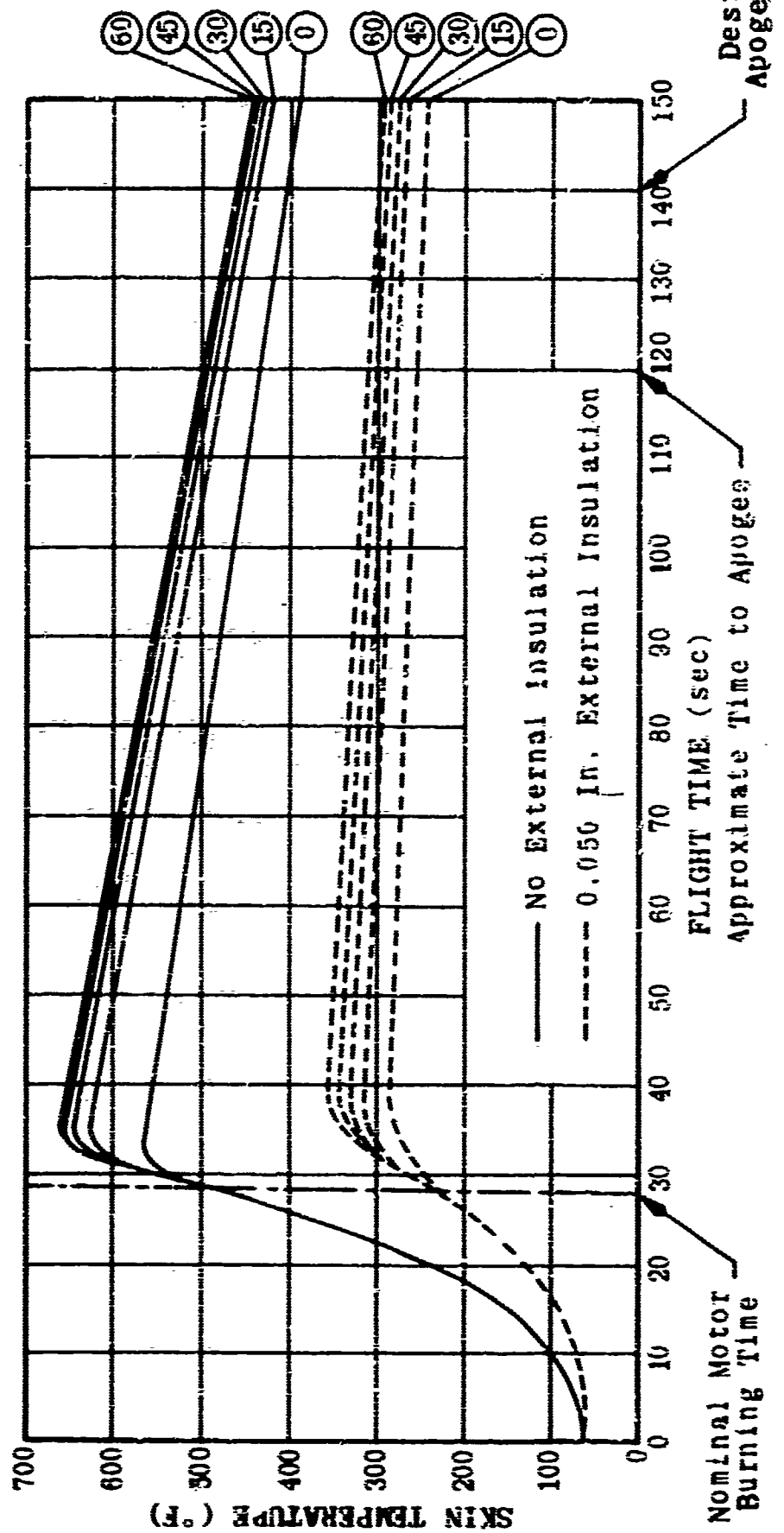
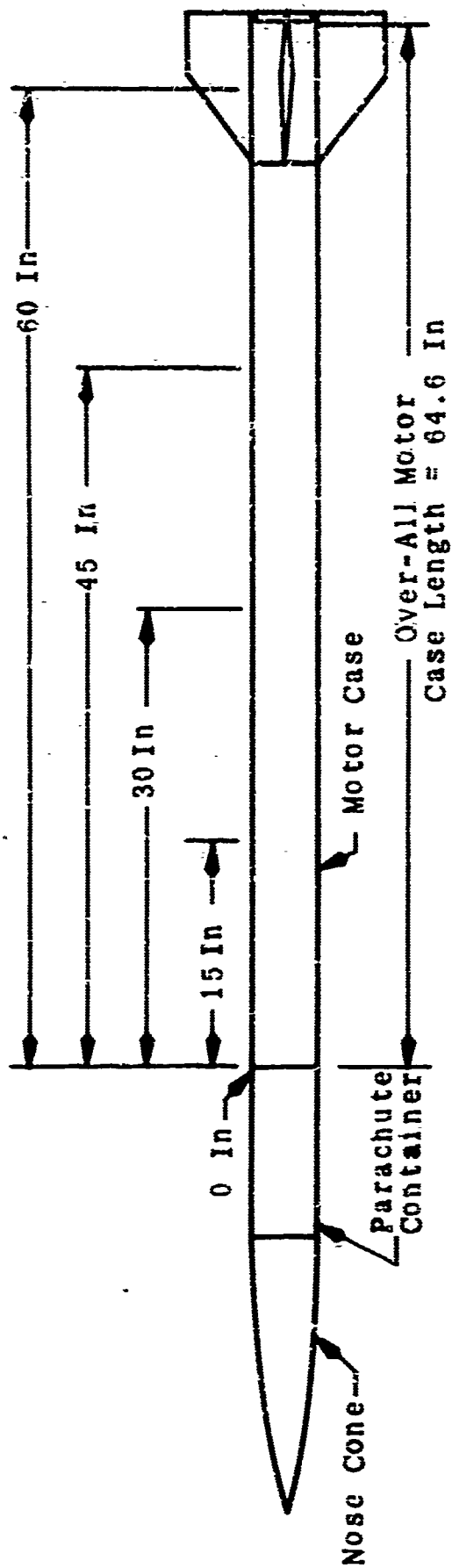


Figure 73

Predicted Frangible ARCAS Fin Temperatures

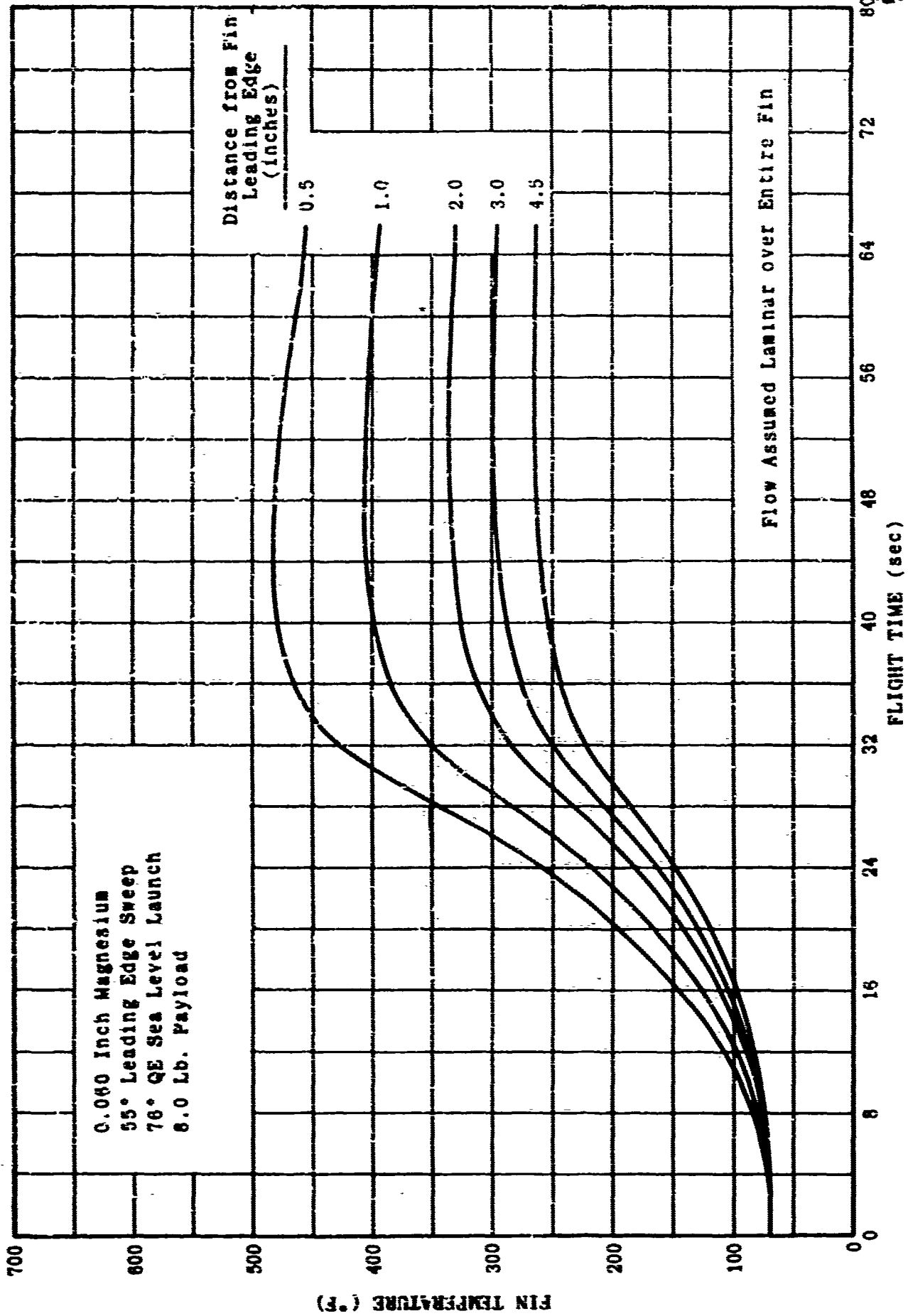


Figure 74

Frangible ARCAS Diagnostic Payload

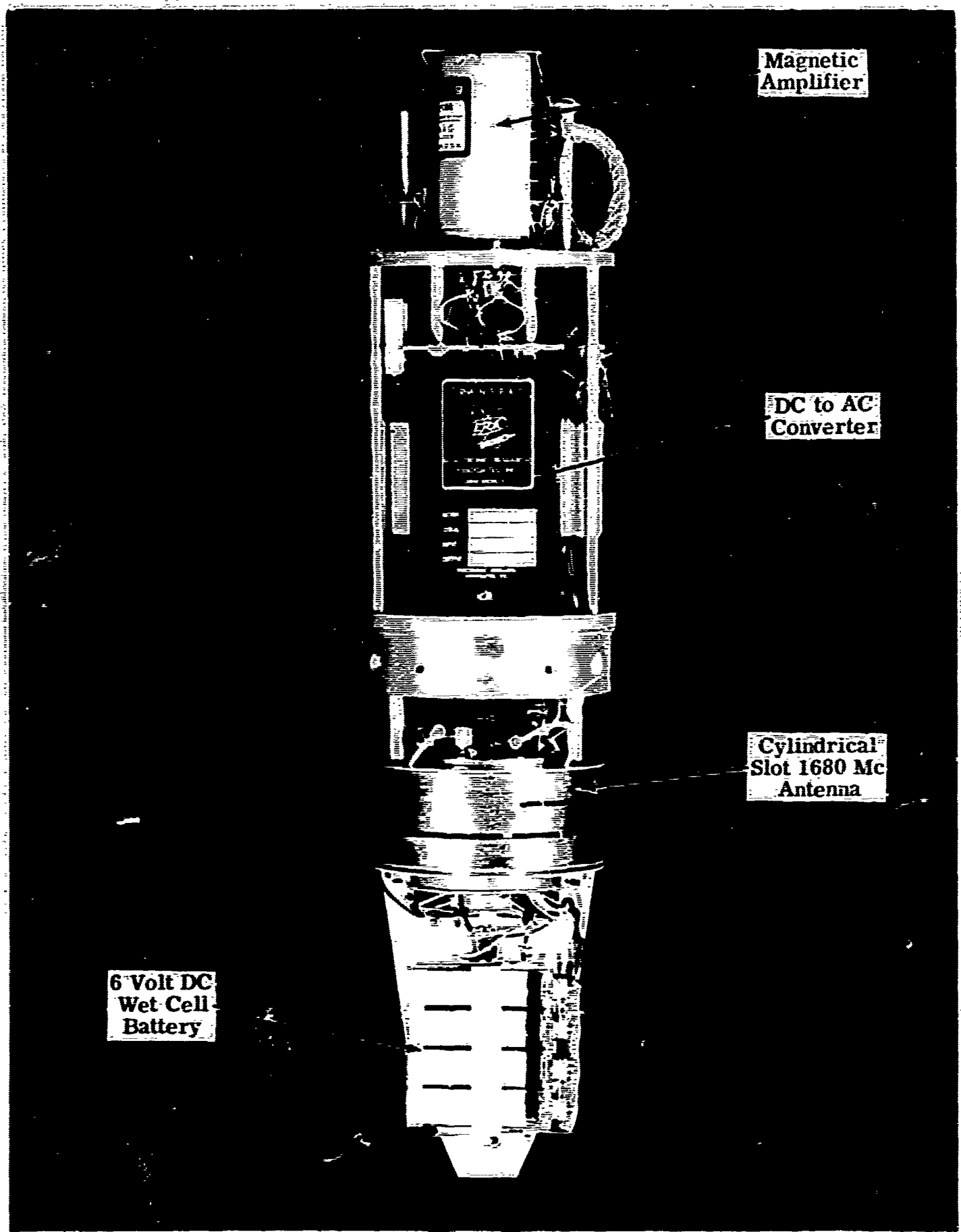


Figure 75

Frangible ARCAS Diagnostic Payload Assemblies

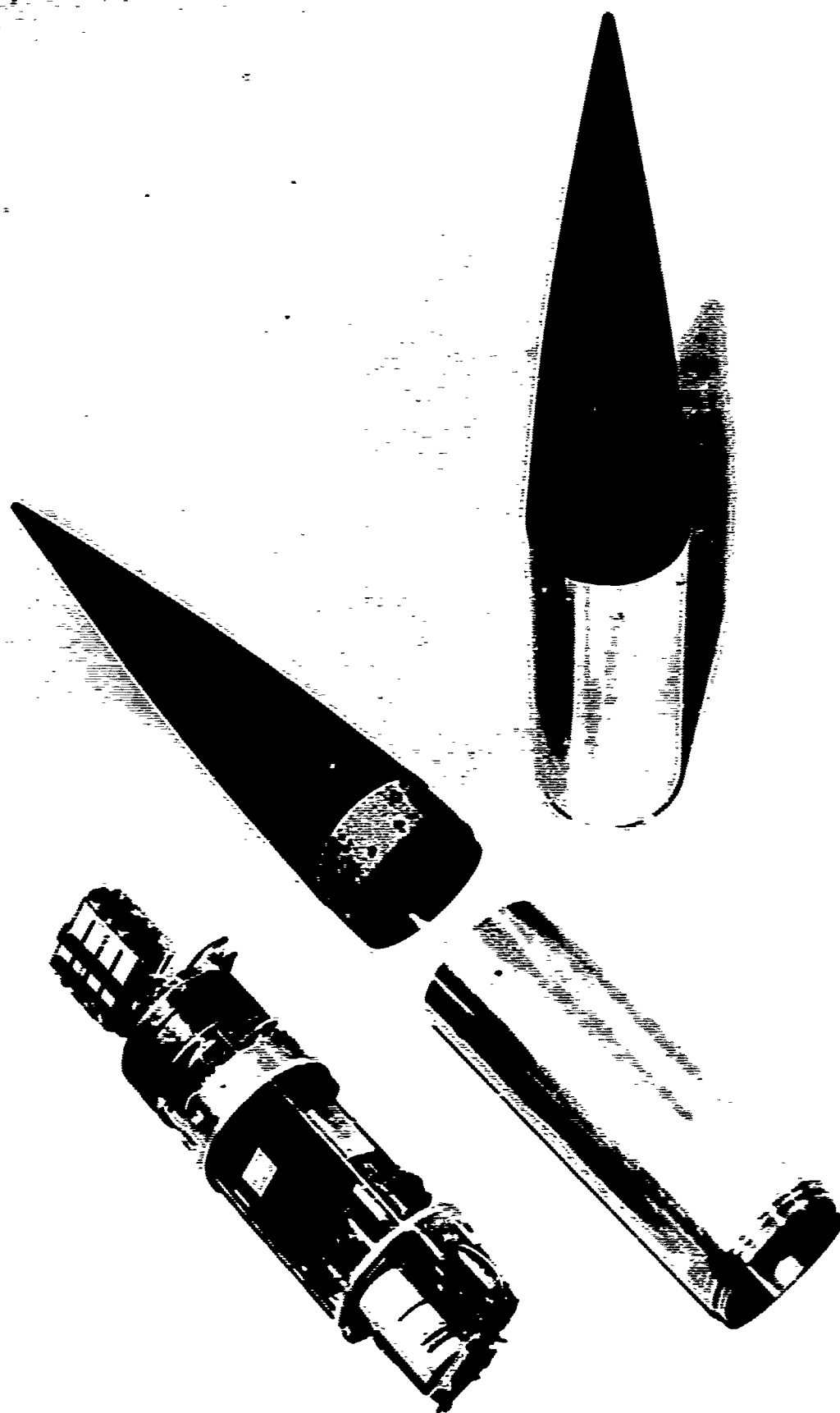


Figure 76

34526

Block Diagram of the Frangible ARCAS Diagnostic Telemetry System

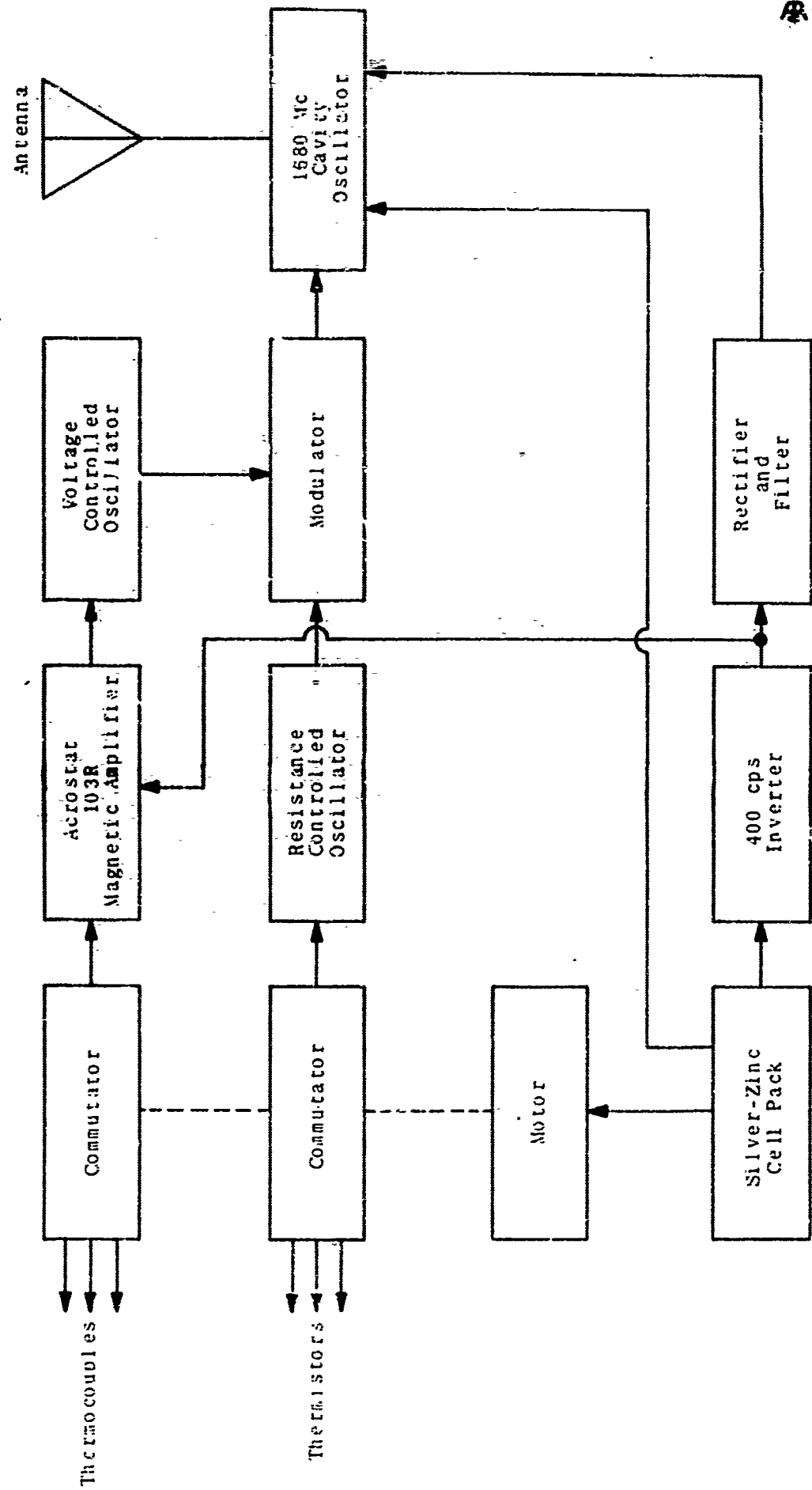


Figure 77

Frangible ARCAS Trajectory Profiles for 10.1 lb Payload Sea Level Launch
Diagnostic Vehicles AFFT-1 and AFFT-2 Without Auxiliary Gas Generator Boost

2553

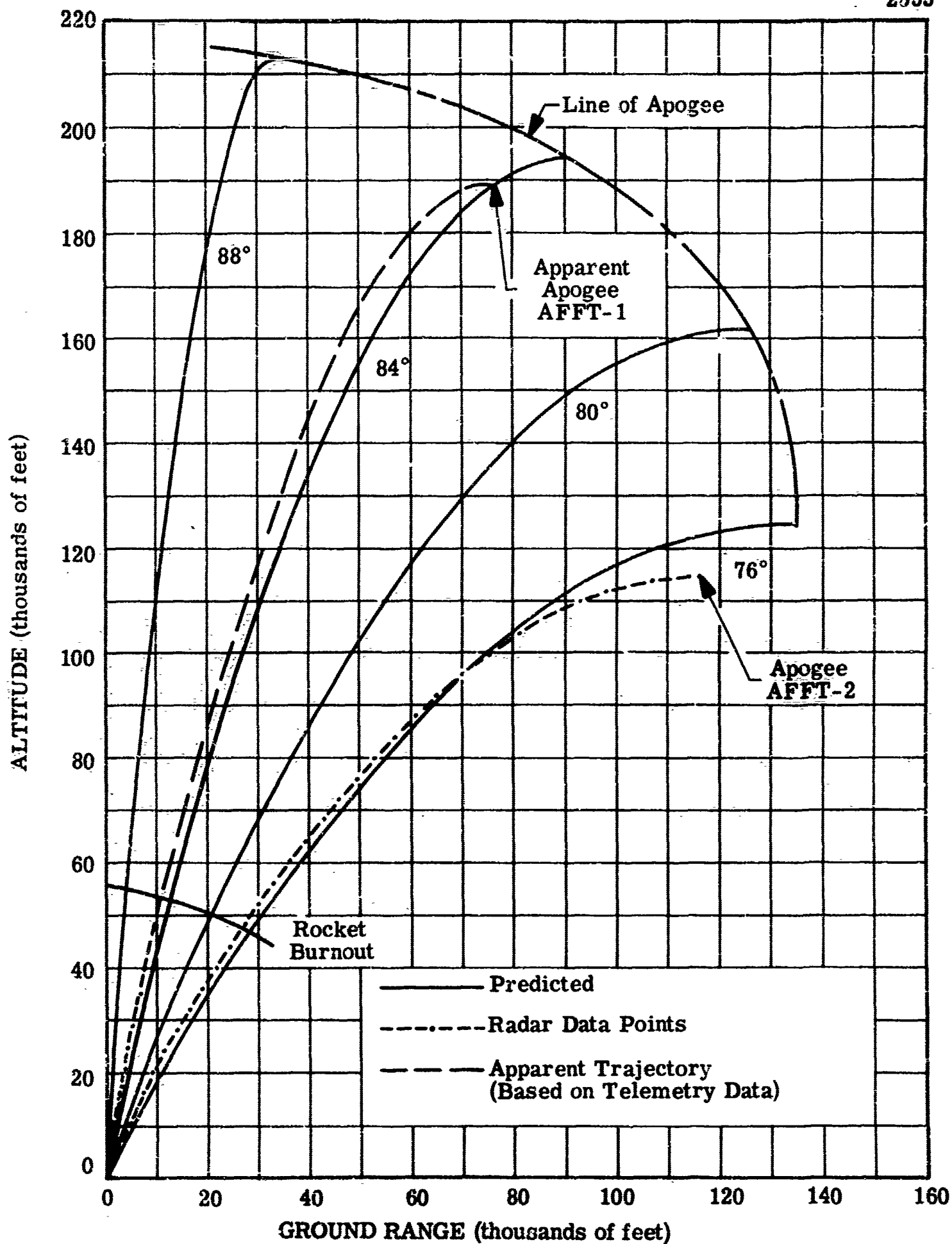


Figure 78

Roll Rate Versus Time Frangible ARCAS Diagnostic Flight Test AFFT-1

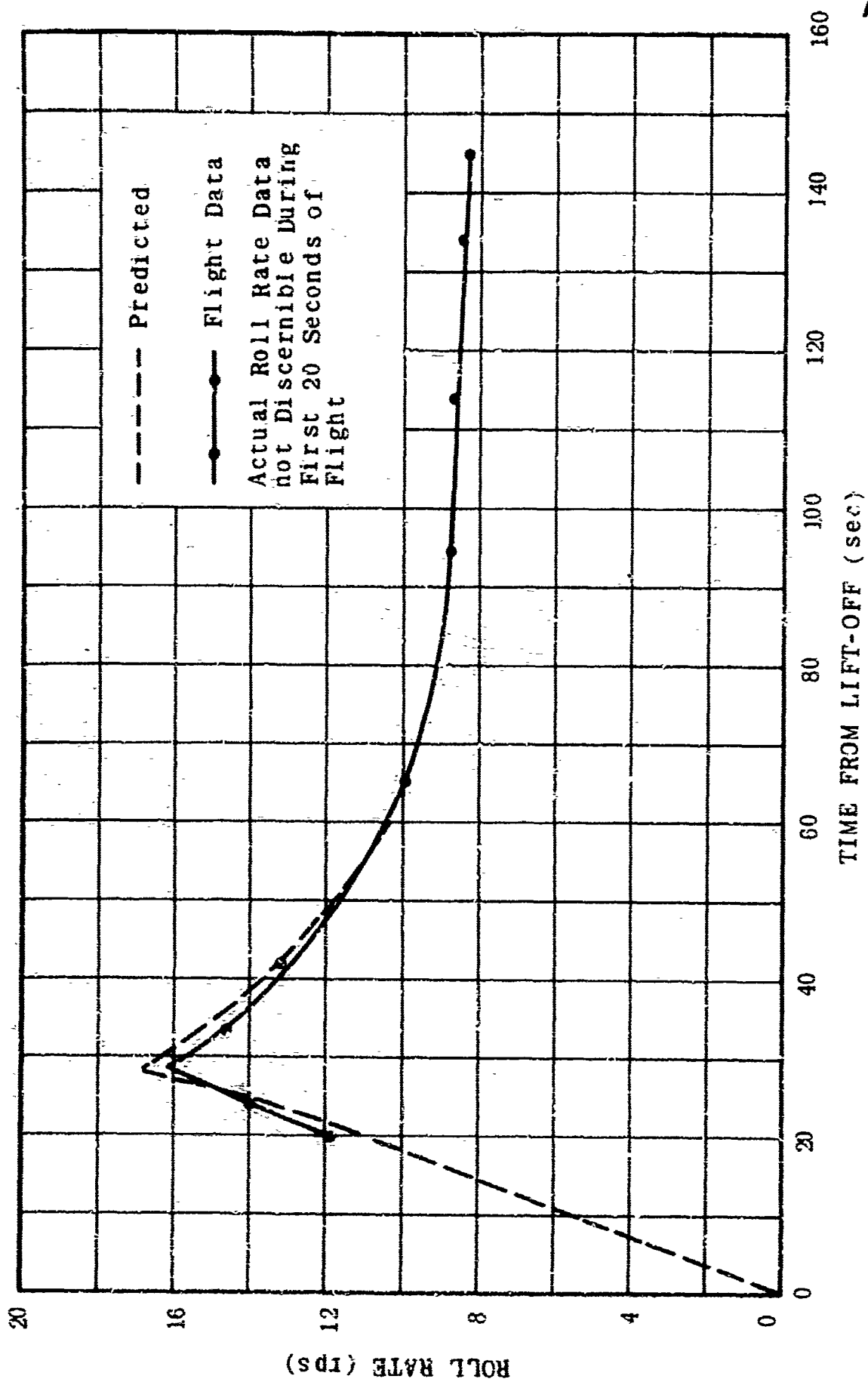


Figure 79

Frangible ARCAS Characteristic Drag Curve

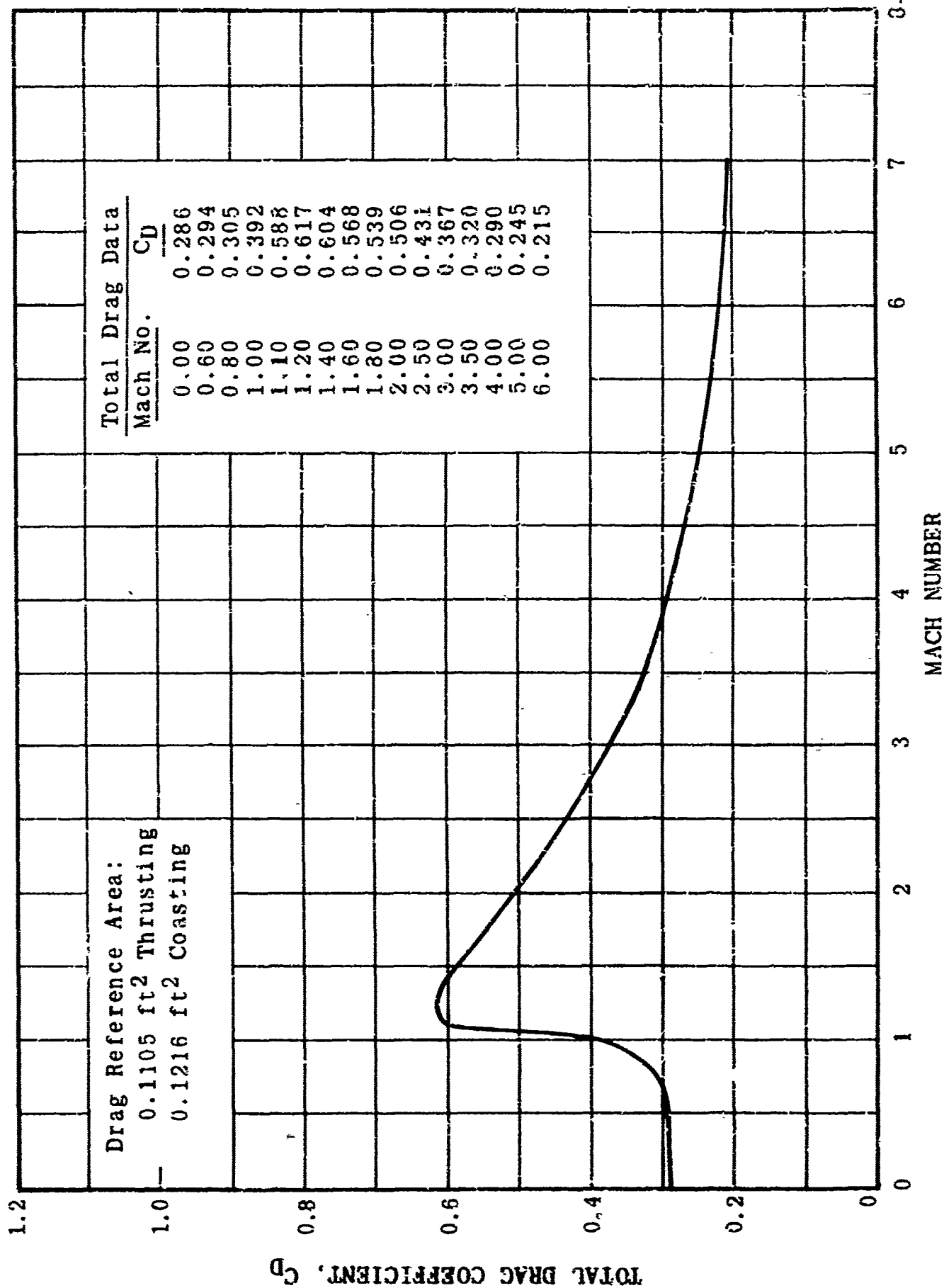


Figure 80

Frangible ARCAS Trajectory Profiles Critique Number 1

2551

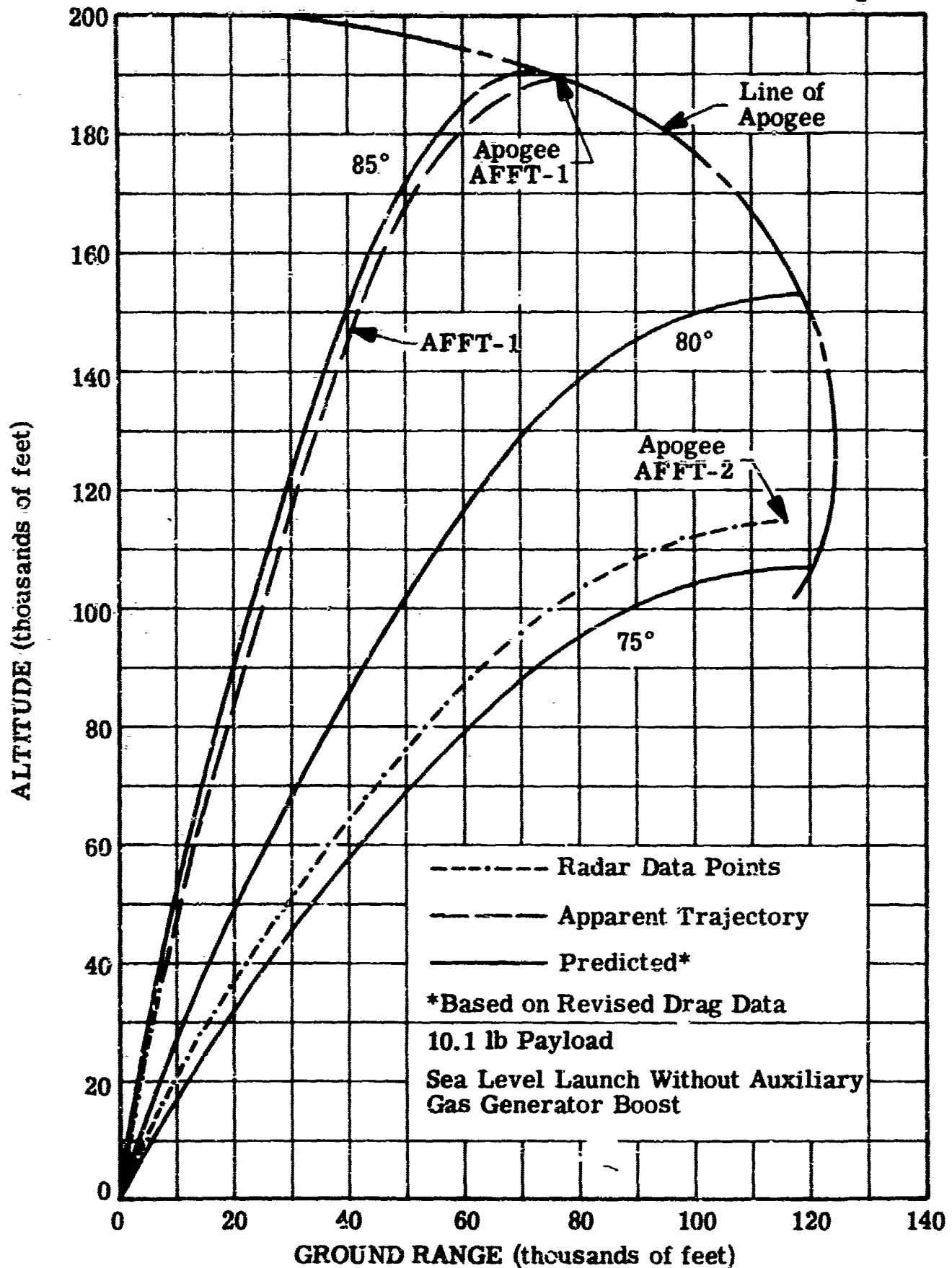


Figure 81

Payload Section Temperatures Versus Time for Flight Test AFTT-1

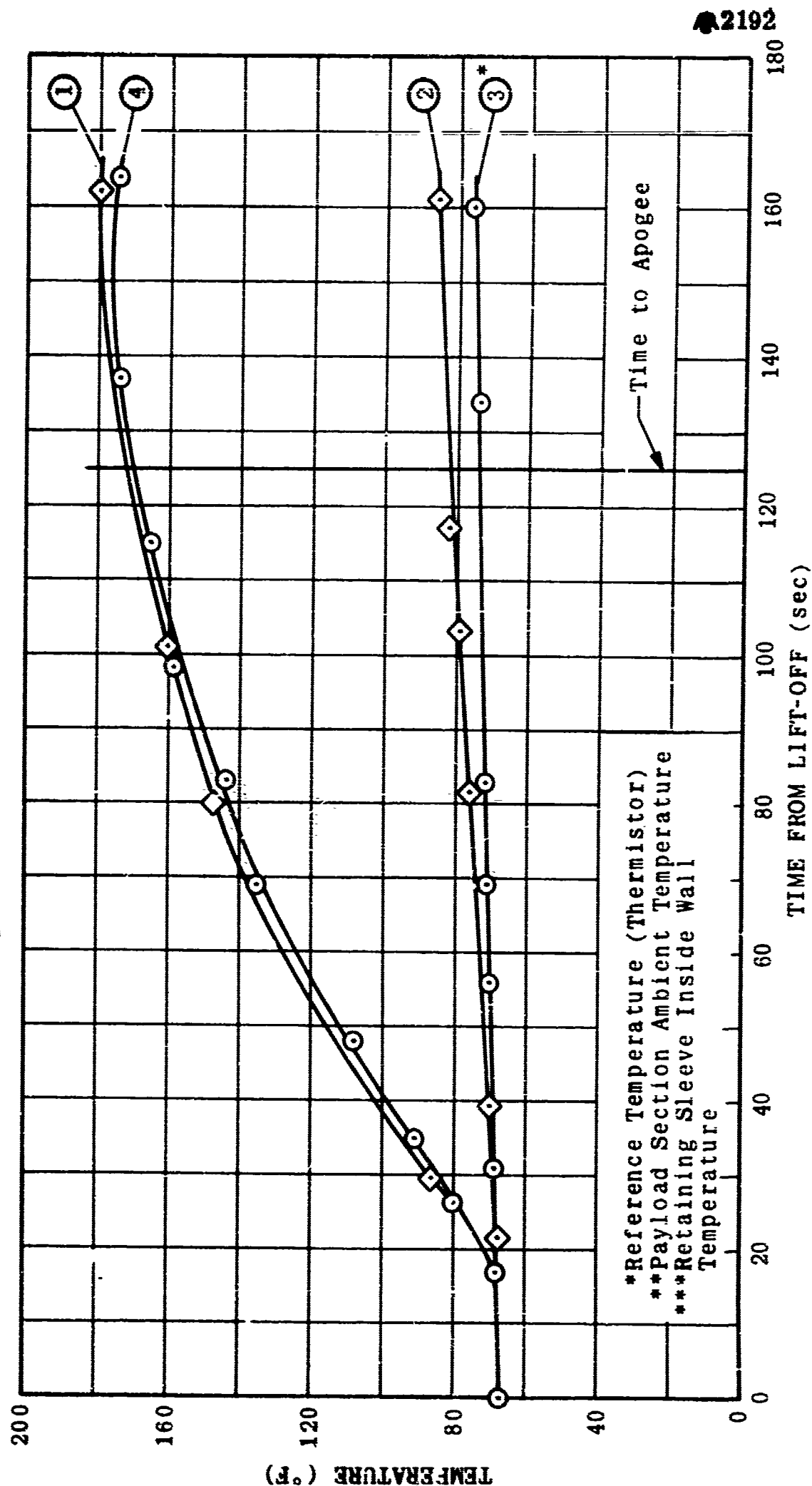
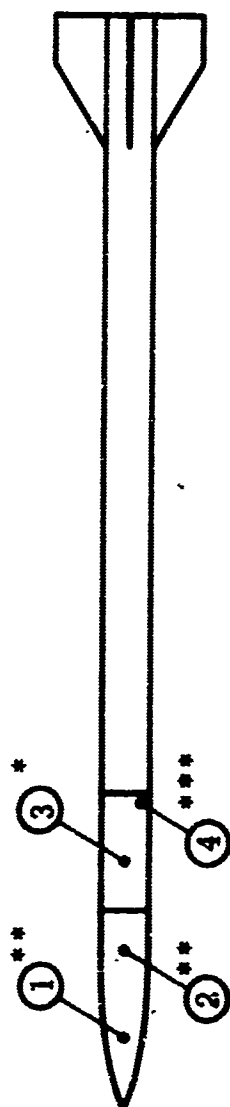


Figure 82

Frangible ARCAS Motor Case Skin Temperature Versus Flight Time Diagnostic Flight AFFT-2

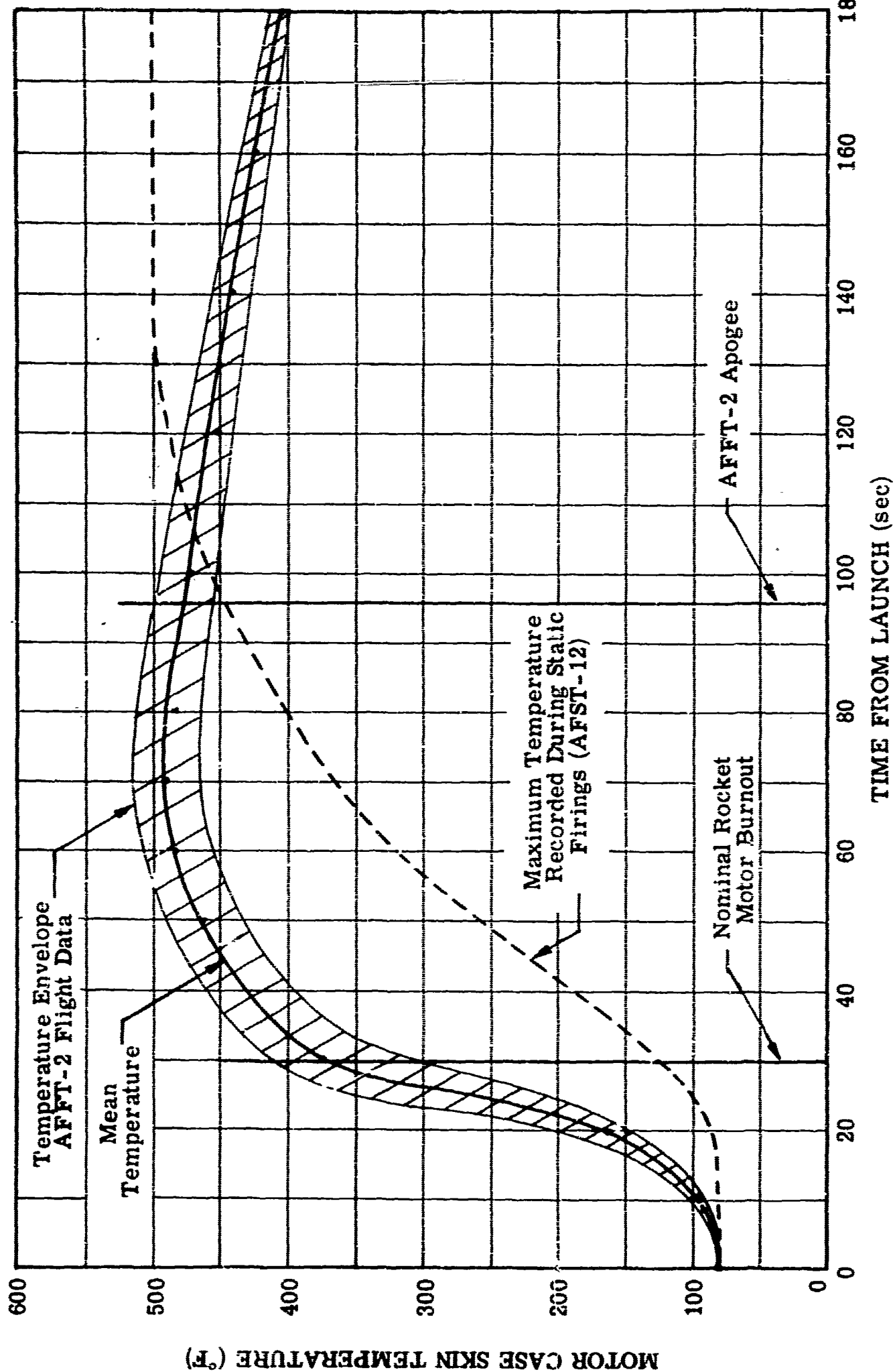
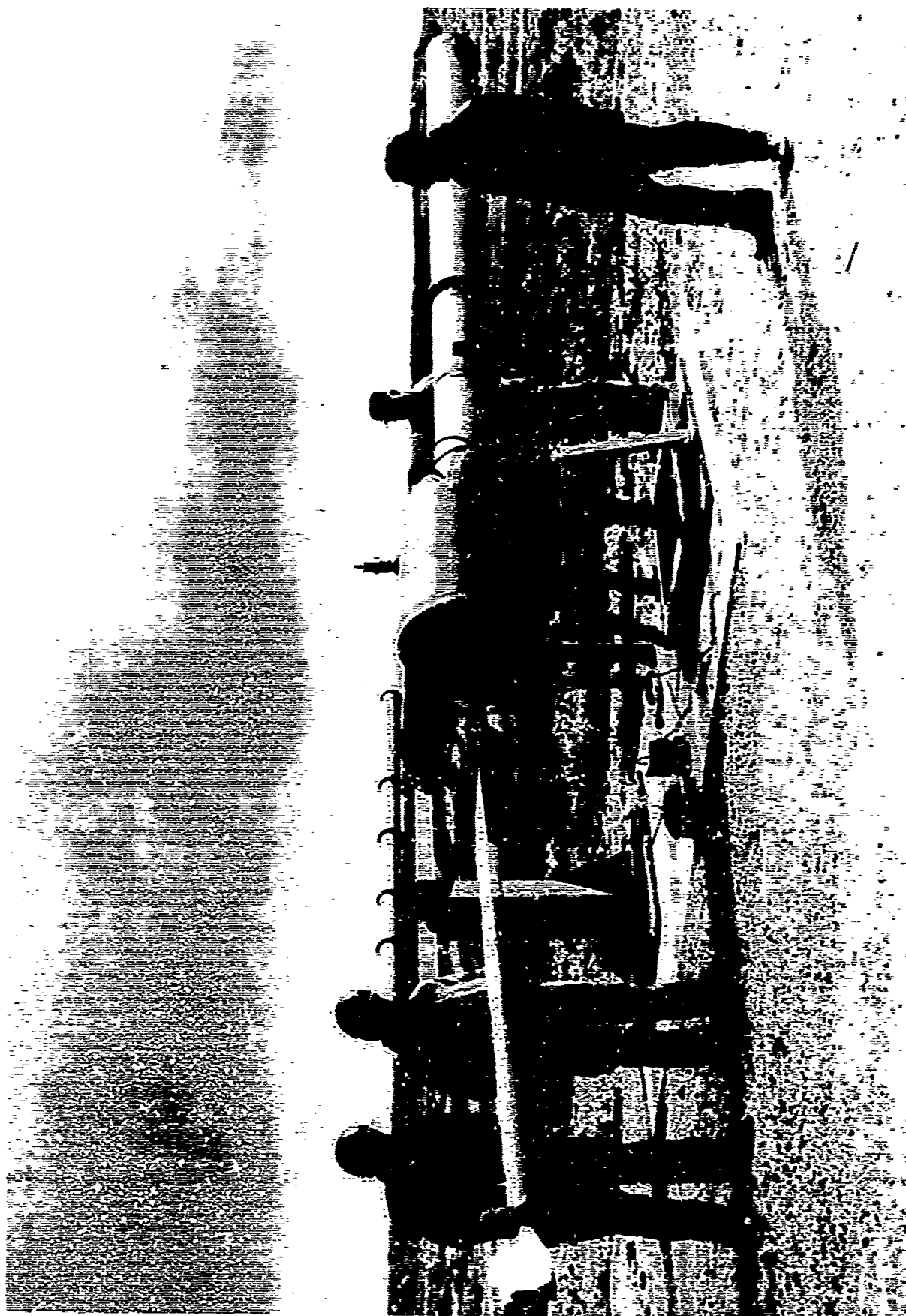


Fig. 83

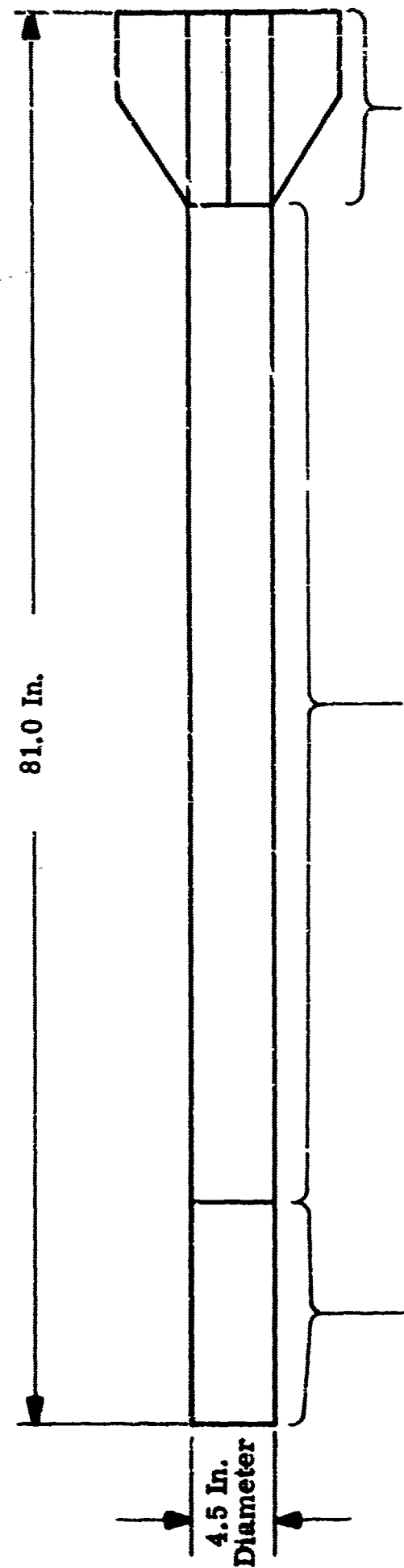
Fragible ARCAS Systems Vehicle Being Loaded into Launcher



0712
88722

Figure 84

Anticipated Fragmentation of the Frangible ARCAS Phase III Systems Vehicles



Parachute Container

	Weight (lb)	S (ft ²)	$\frac{W}{C_D S}$
Maximum	0.026	0.021	1.63
Average	0.010	0.010	1.32

Motor Case

	Weight (lb)	S (ft ²)	$\frac{W}{C_D S}$
Maximum	0.08	0.033	2.26
Average	0.040	0.041	0.98

Fin/Nozzle Section

Estimated Weight = 5.0 lbs

$$S = 0.73 \text{ ft}^2$$

$$\frac{W}{C_D S} = 6.85$$

2885

Figure 85

Frangible ARCAS Phase B (Fragmentation) Launch Hazard Area

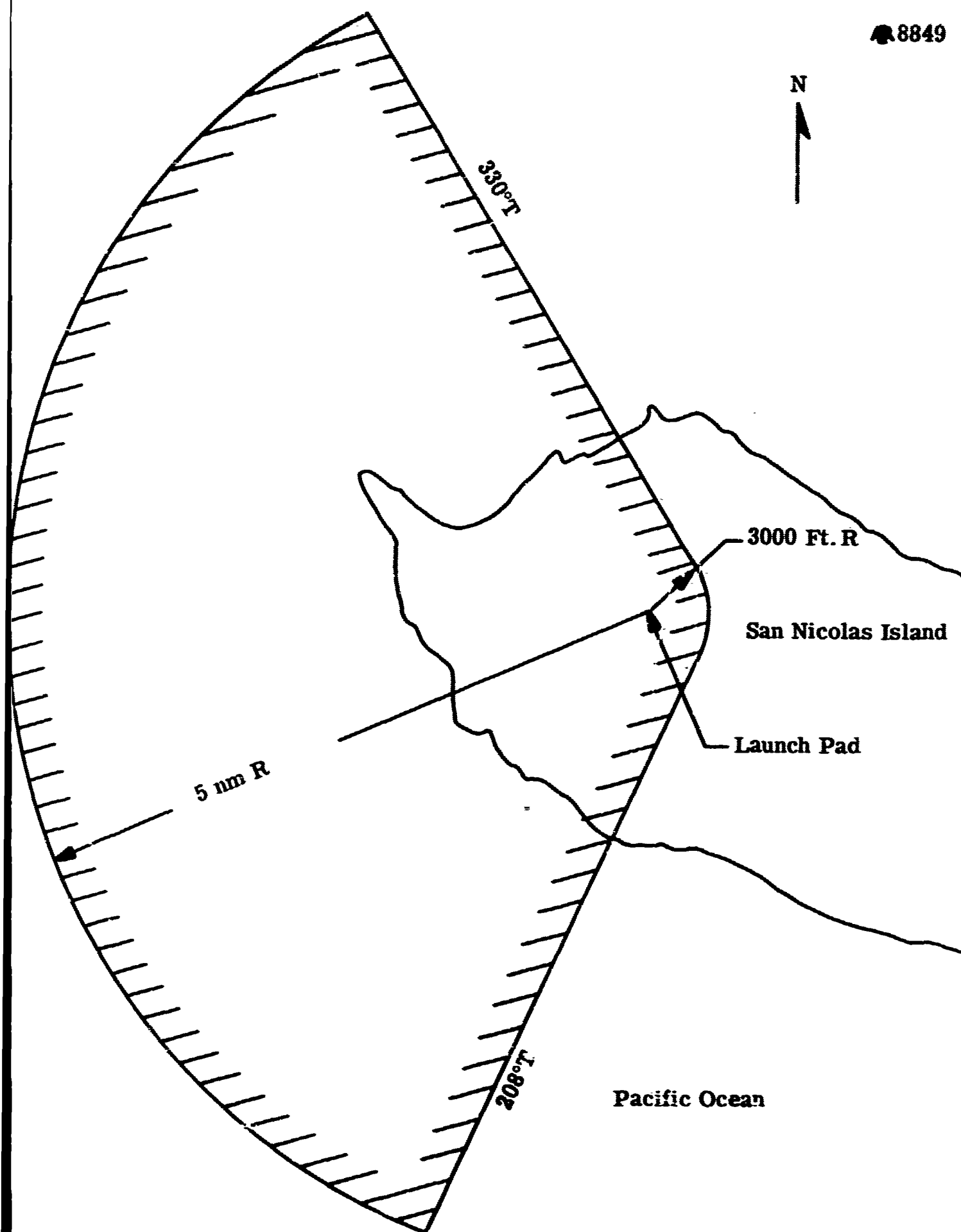


Figure 86

Frangible ARCAS Phase B (Fragmentation) Maximum Impact Area

6650

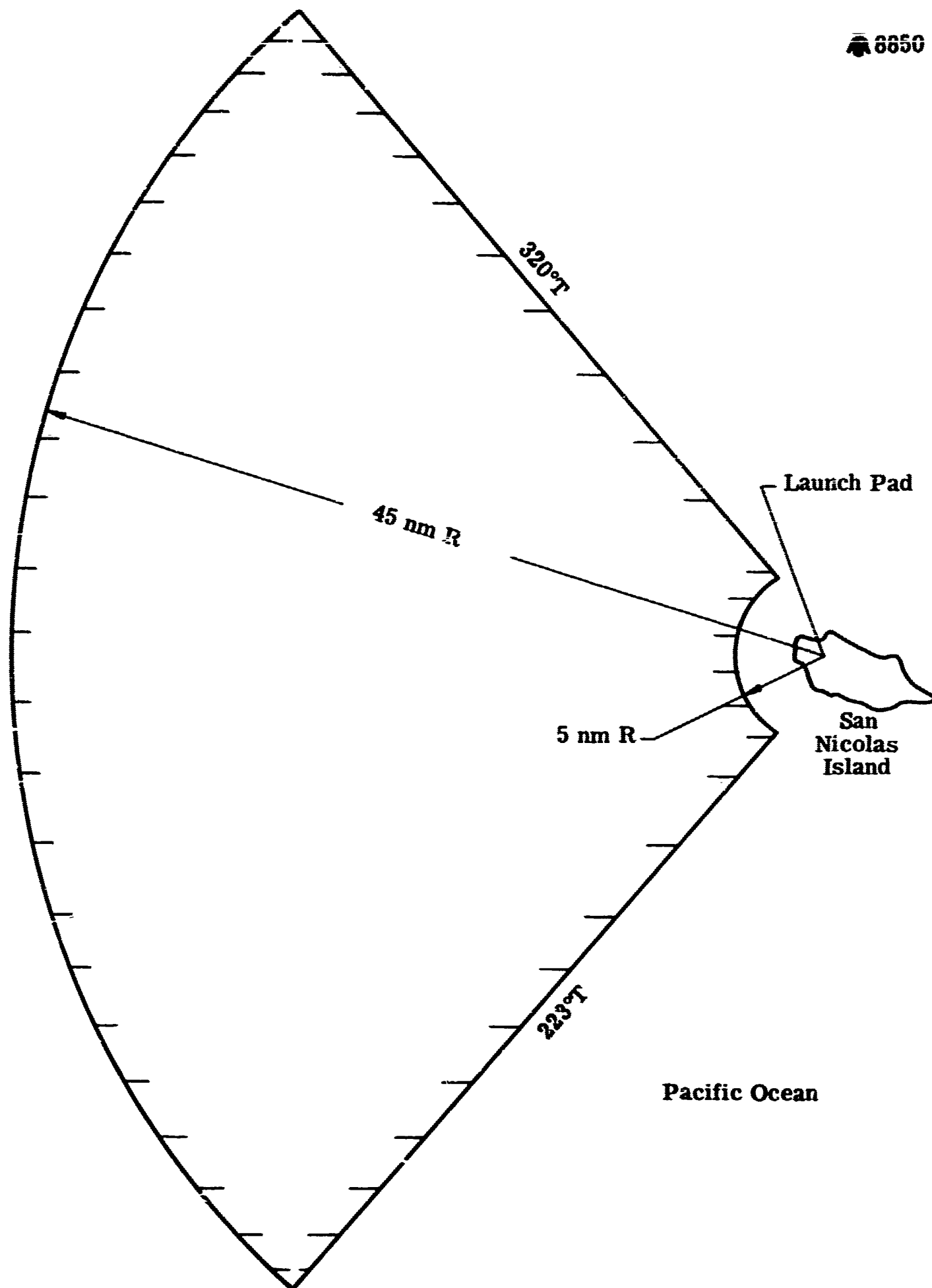


Figure 87

**Frangible ARCAS Systems Flight Test AFFT-4
Actual Sequence of Events
Phase III Vehicle Configuration**

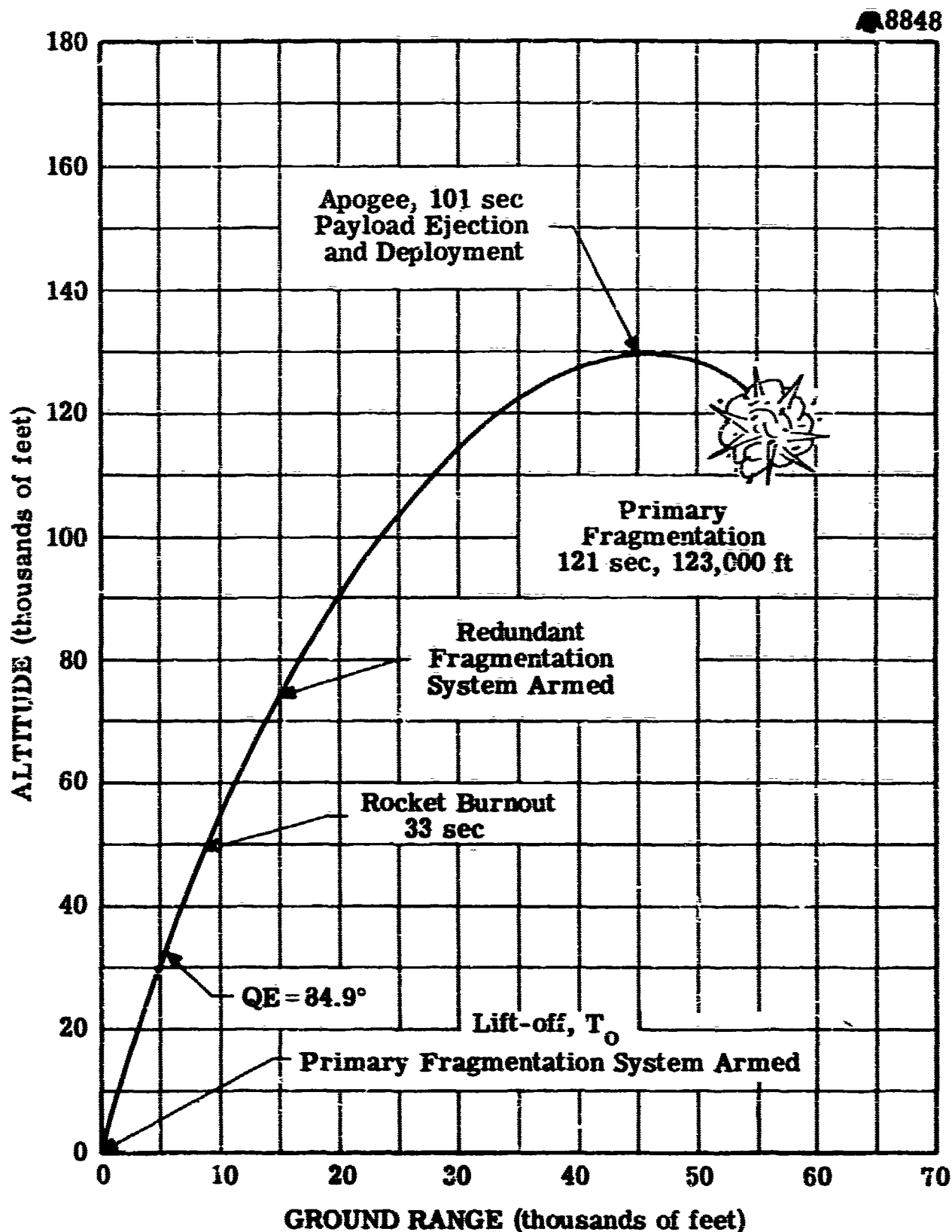


Figure 88

Nominal Trajectory Profiles to Apogee

8853

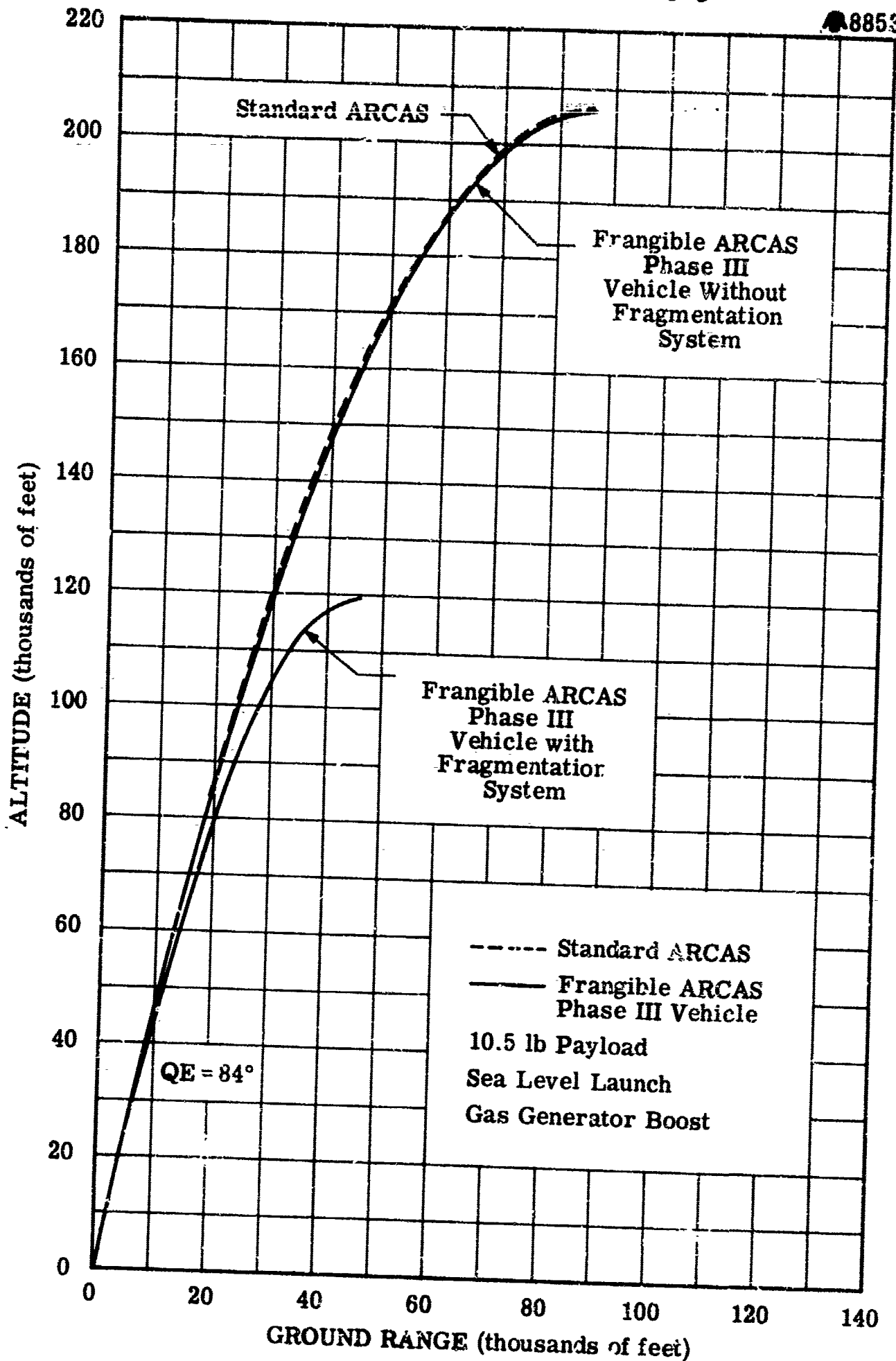


Figure 89

Frangible ARCAS Systems Vehicle Nominal Trajectory Profiles for Various Launch Angles

8851

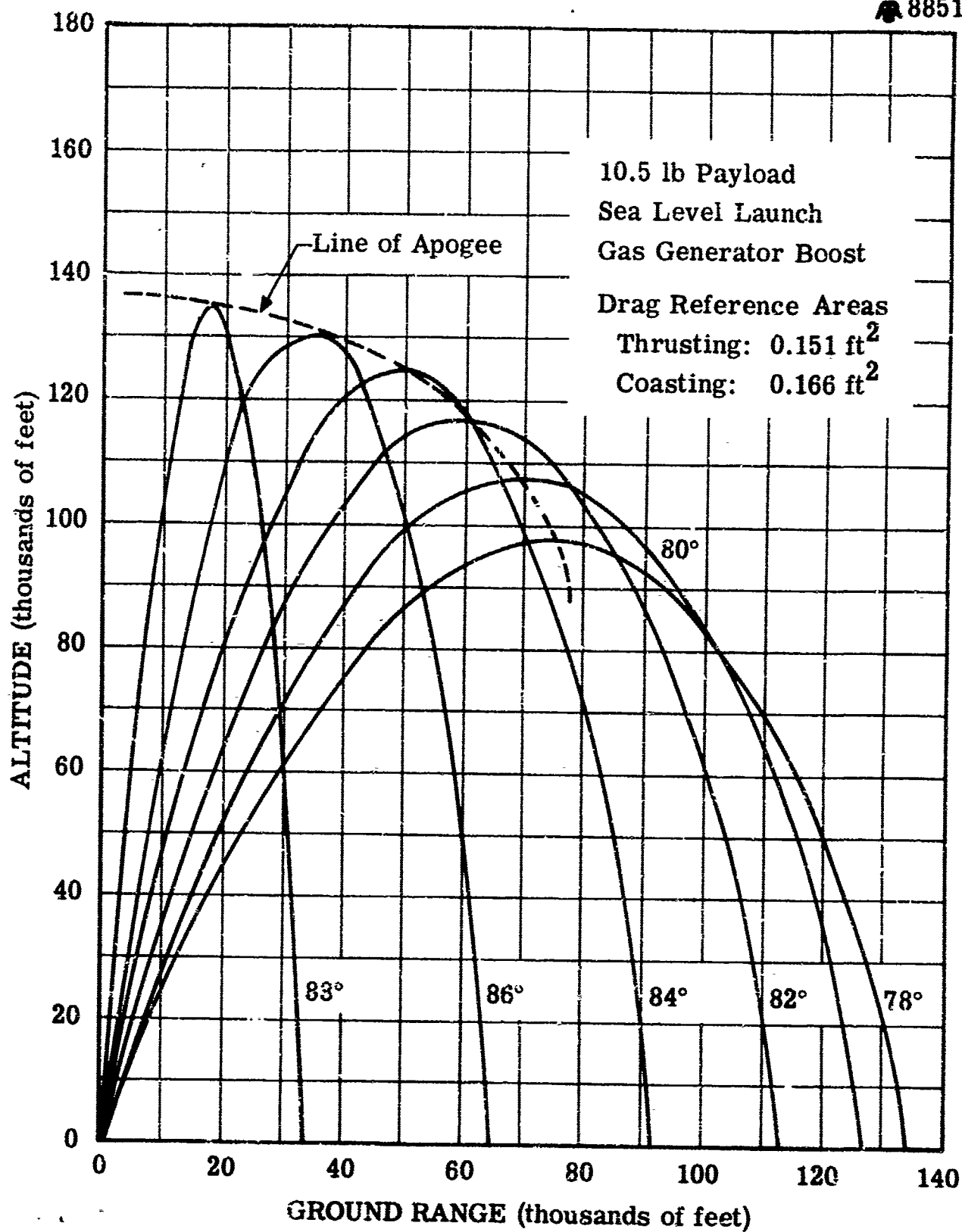


Figure 90

Frangible ARCAS Systems Vehicle Performance

8855

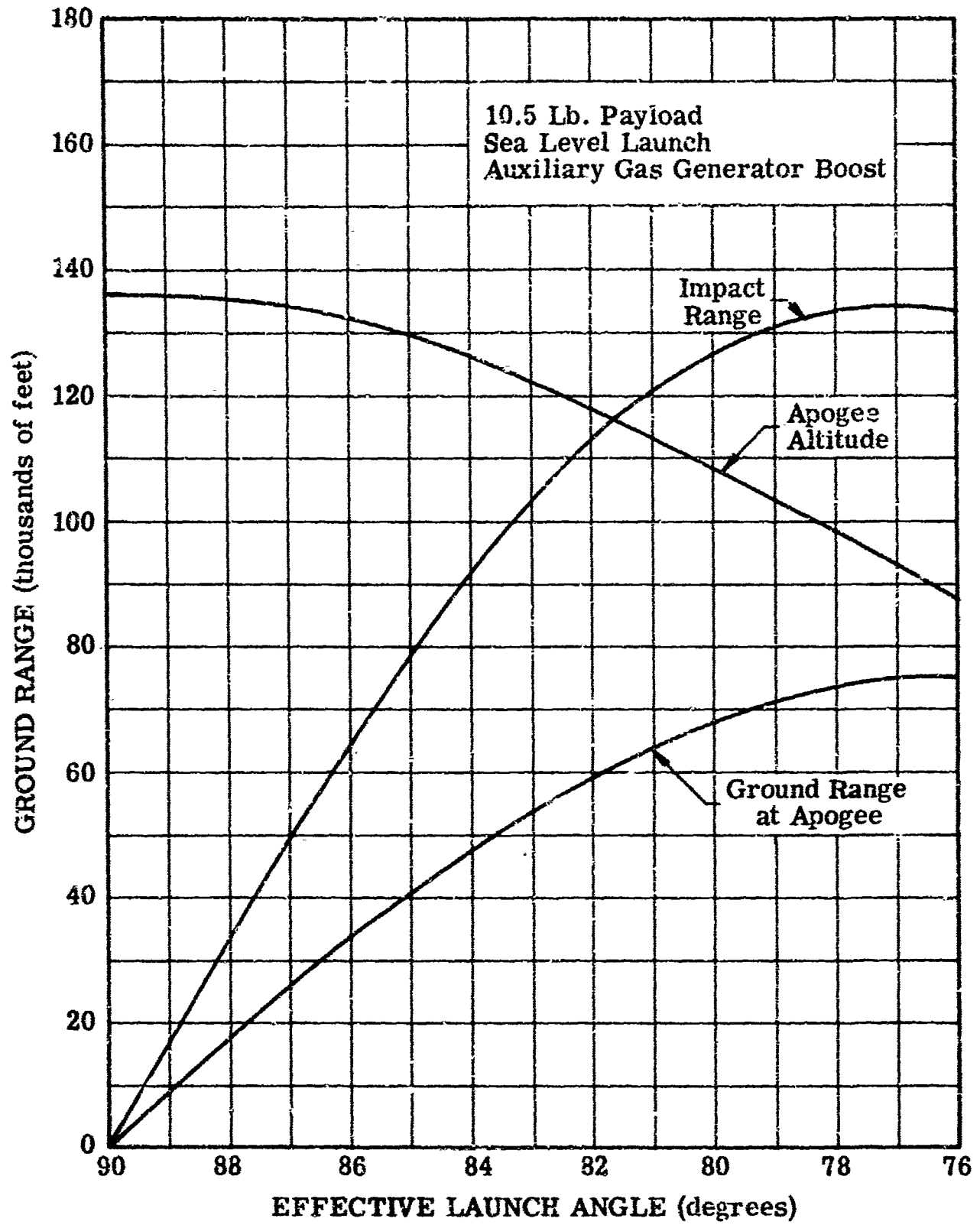


Figure 91

Frangible ARCAS Apogee Performance Versus Effective Launch Angle and Payload Weight

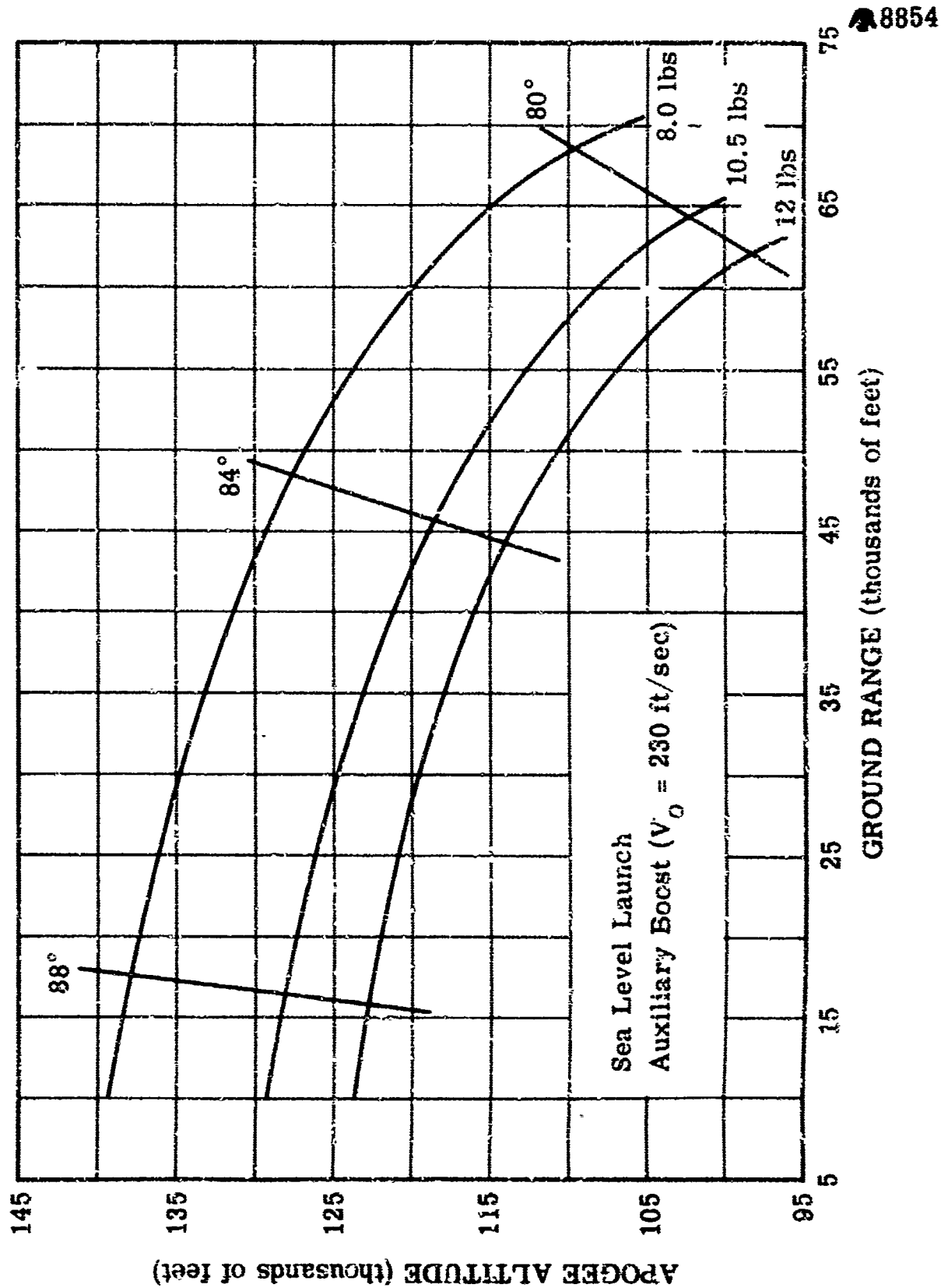


Figure 92

Frangible ARCAS Apogee Altitude Versus Payload Weight

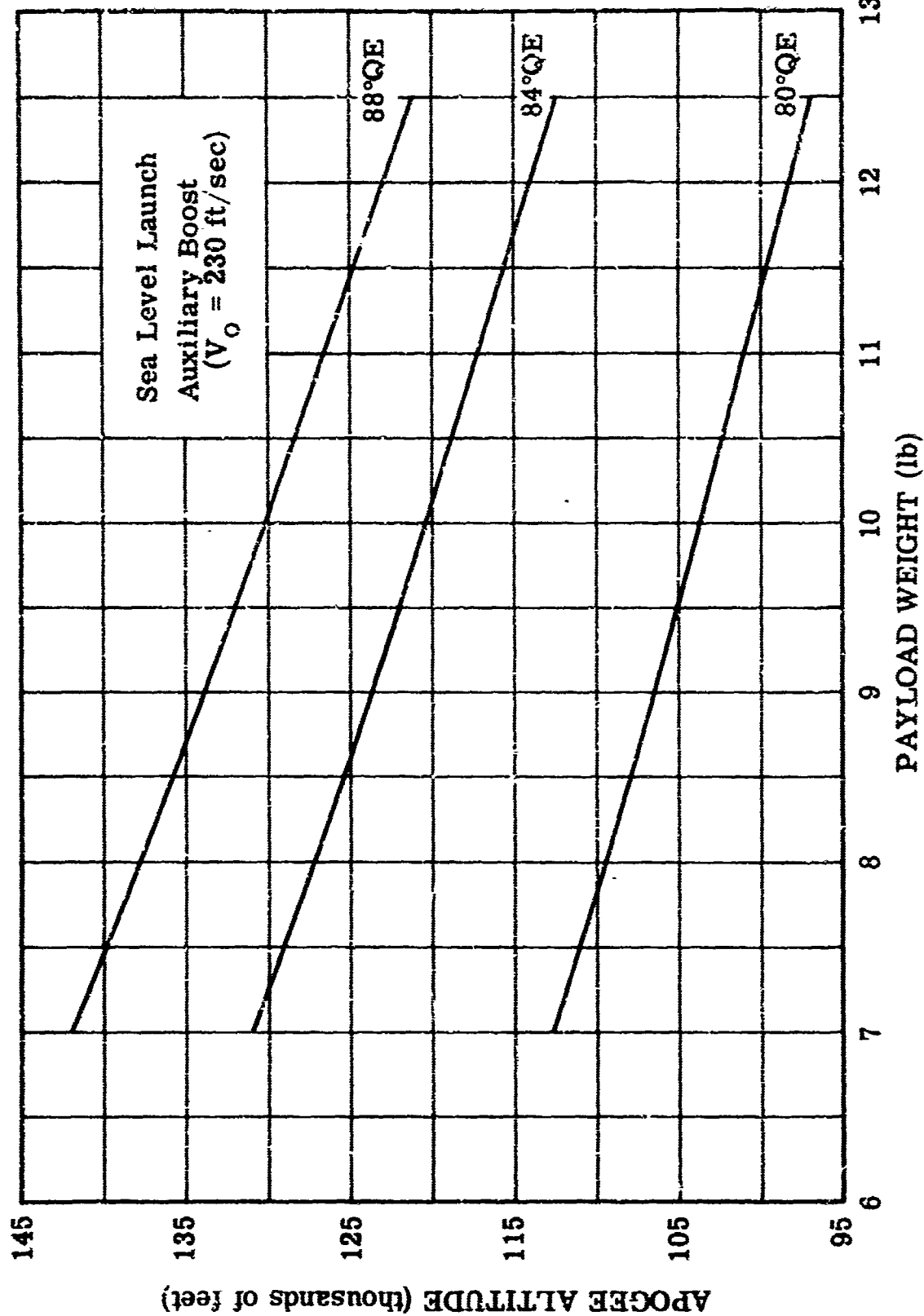
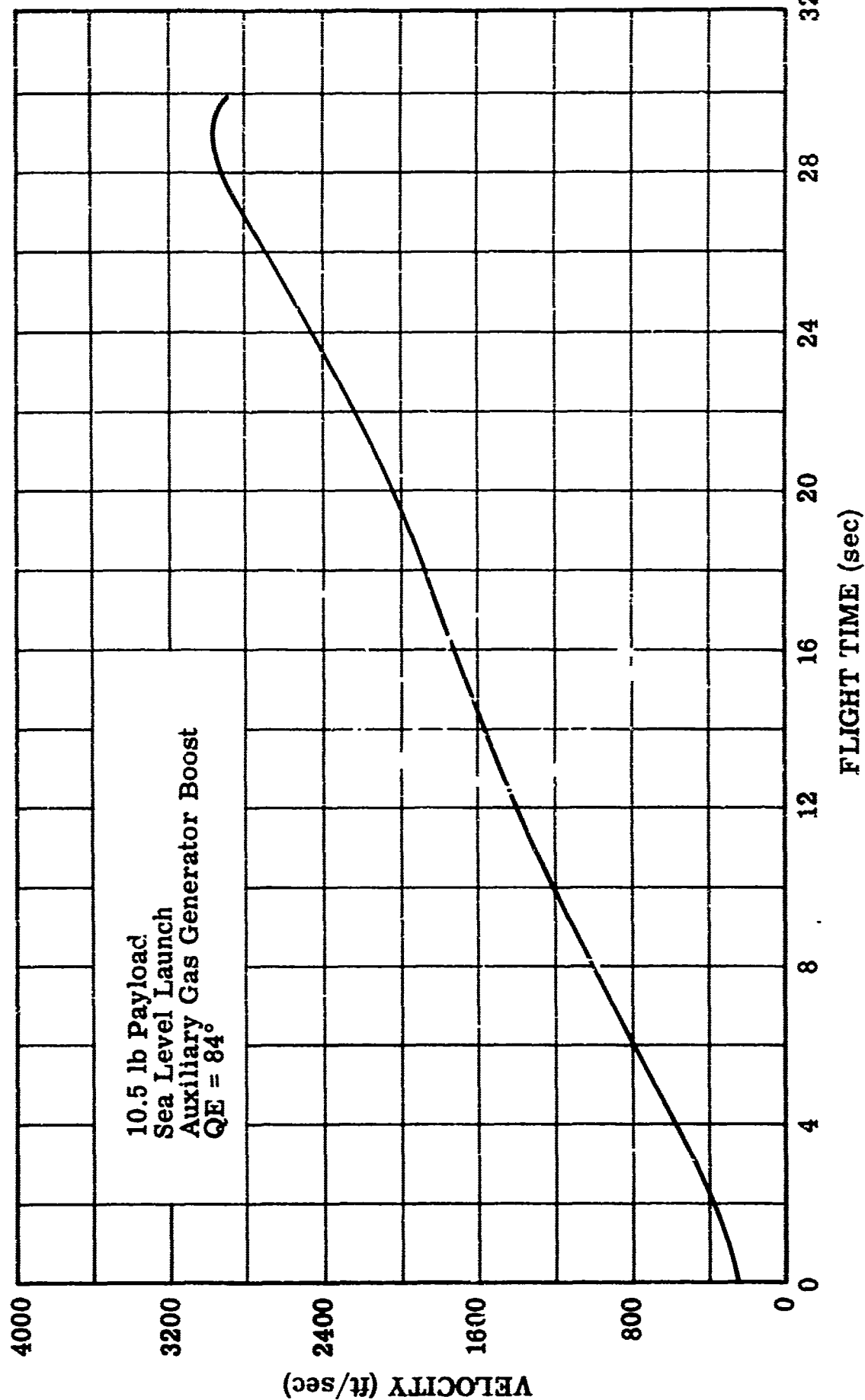


Figure 93

Frangible ARCAS Vehicle Velocity Versus Flight Time



8757

Figure 94

Frangible ARCAS Burnout Mach Number Versus Burnout Weight

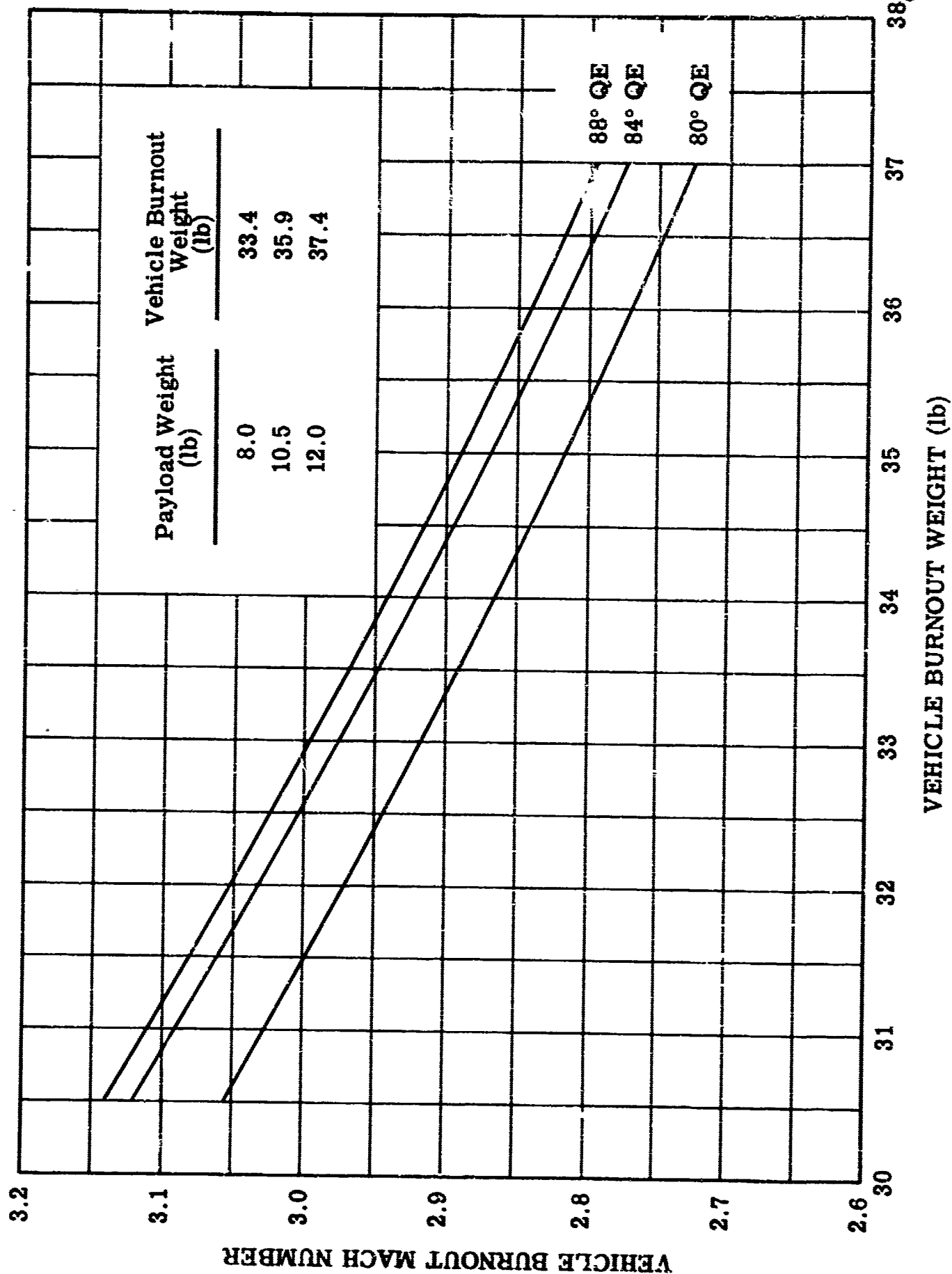


Figure 95

Apogee Altitude Versus Total Impulse, Burning Time and Motor Length

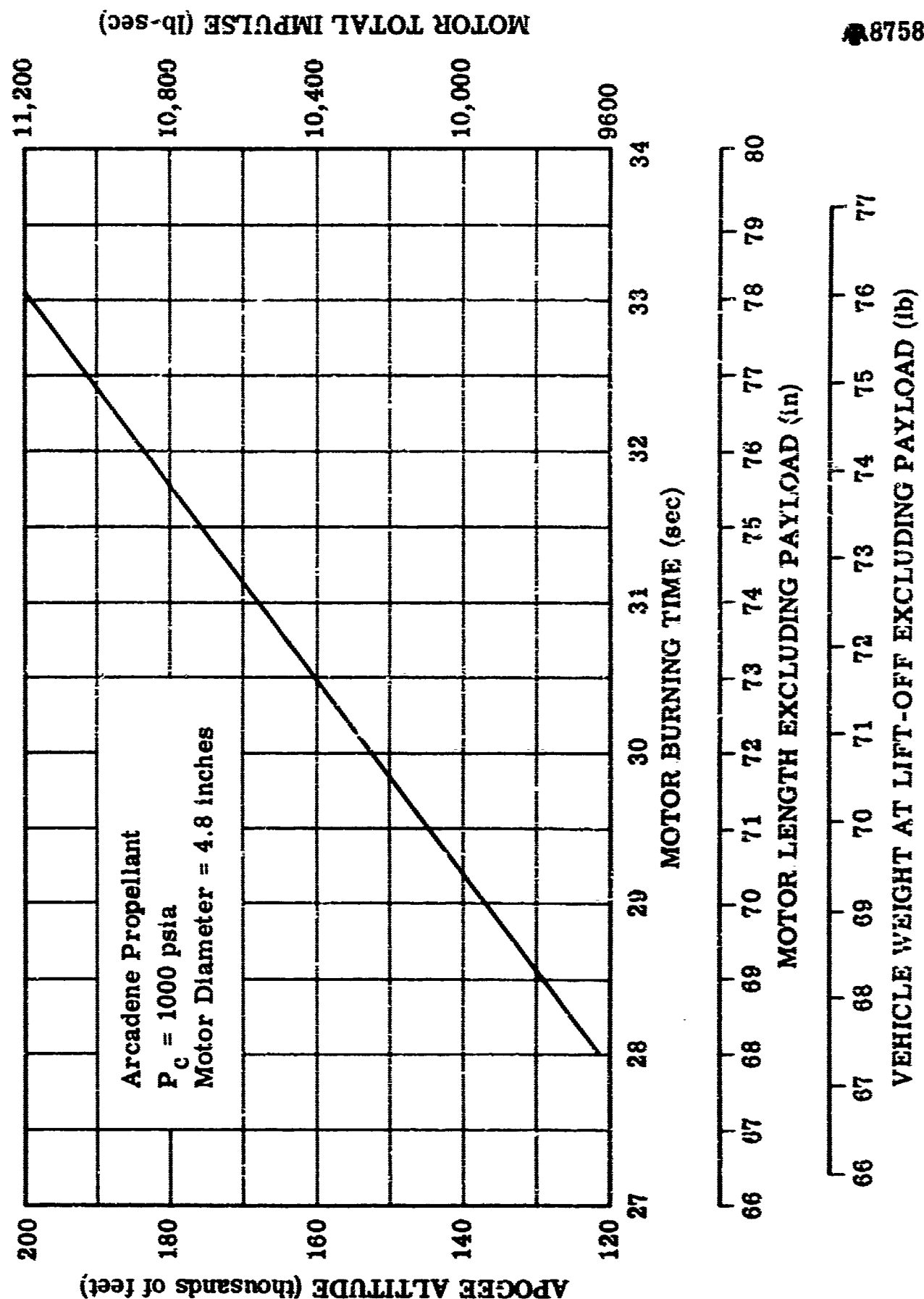


Figure 96

Comparison of Phase III and Modified Phase III Frangible ARCAS Vehicles

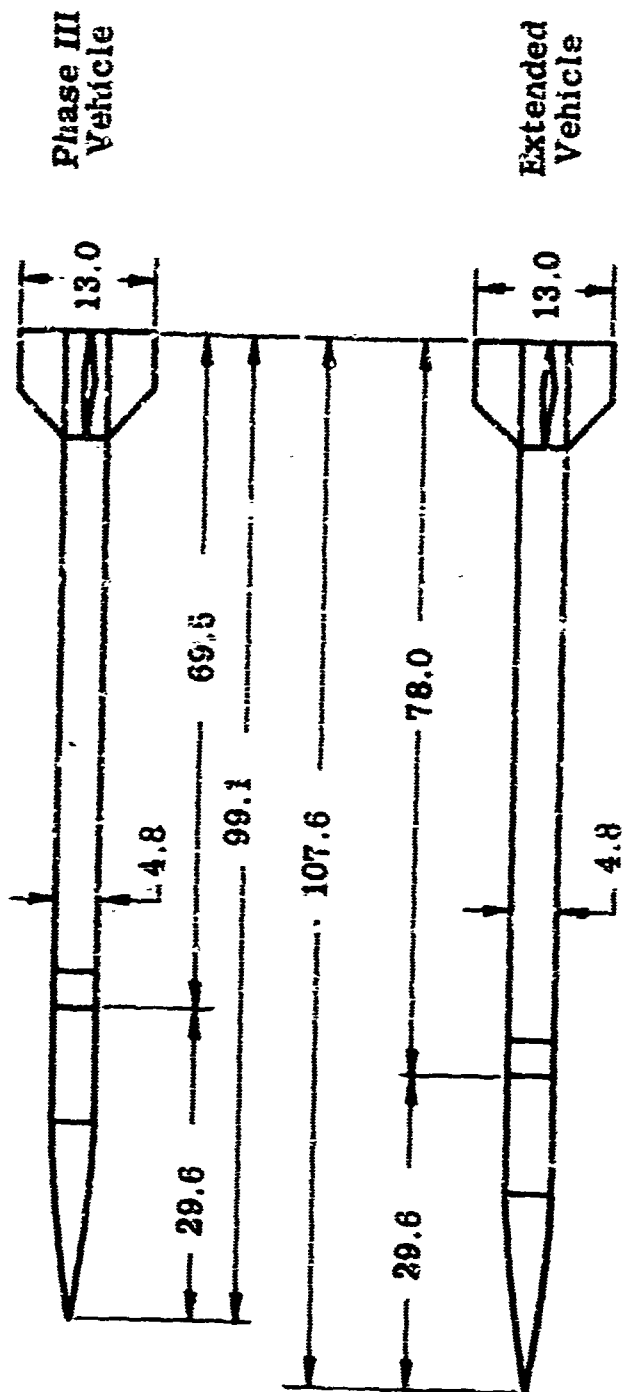


Figure 97

	Lift-Off Weight (Less Payload)	Burnout Weight (Less Payload)	Propellant	t_b (sec)	Apogee Altitude* (feet)
Phase III Vehicle	68.4	25.4	Arcite 373	30	119,000
Extended Vehicle	75.9	26.9	Arcadene	33	209,000

*10.5 Lb. Payload, Sea Level Launch, 84° QE

8847

Apogee Altitude Performance Versus Effective Launch Angle and Payload Weight
Extended Phase III Vehicle with Arcadene Propellant

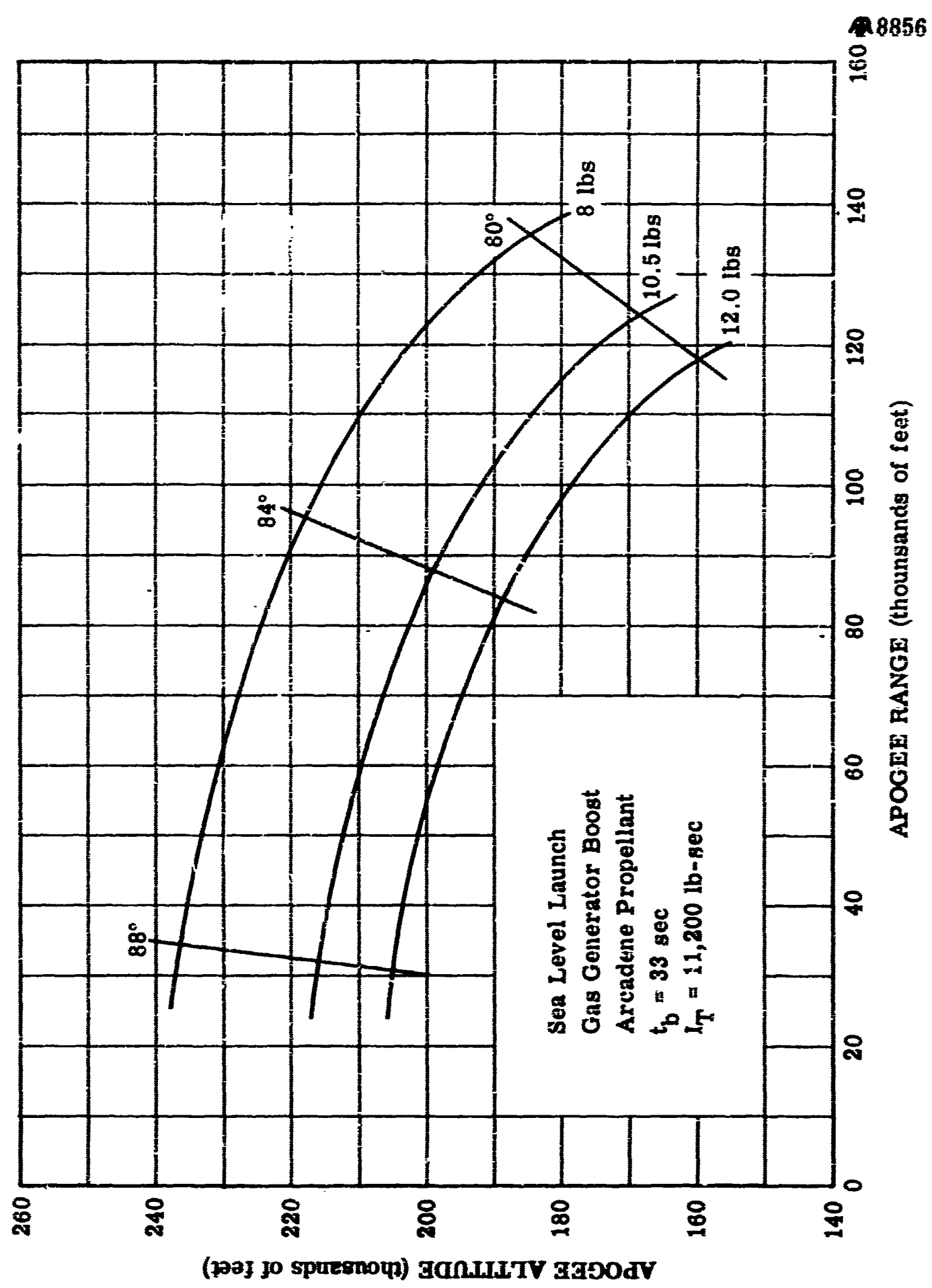


Figure 98

APPENDIX I
LONGITUDINAL ACCELERATION EFFECTS
ON THE REDUNDANT INITIATOR

PREPARED BY	B.R.T.	71 -64	SPACE/ARM WALLACE O. LEONARD, INC.	REPORT	1104
APPROVED BY			PASADENA, CALIFORNIA	PAGE	1 OF 2

ANALYSIS OF EFFECT OF HIGH LONGITUDINAL ACCELERATION LOADS
IMPOSED UPON THE ARMING MECHANISM OF THE MODEL 1046A AUTOMATIC
DESTRUCT INITIATOR.

1.0 PURPOSE:

THIS REPORT ANALYZES THE OPERATION OF THE ARMING AND FIRING MECHANISM OF THE MODEL 1046A AUTOMATIC DESTRUCT INITIATOR WHEN SUBJECTED TO HIGH LONGITUDINAL ACCELERATION LOADS, WITH THE PURPOSE OF DETERMINING IF ANY CONDITION EXISTS WHICH MIGHT RESULT IN PREMATURE OR INADVERTANT INITIATION OF THE ROCKET MOTOR DESTRUCT CHARGE.

2.0 POSITIVE LONGITUDINAL ACCELERATION:

A POSITIVE (ACTING IN A DIRECTION THAT CAUSES VELOCITY OF THE ROCKET TO BE INCREASED IN THE FORWARD DIRECTION) LONGITUDINAL ACCELERATION APPLIED TO THE INITIATOR CAUSES AN INERTIAL REACTION FORCE TO BE IMPARTED TO THE ARMING BIAS SPRING (12)*, ARMING SLEEVE (15), BELLOW FRONT PLATE (1-), FIRING CUP (17), AND BELLONS (21). THE INERTIAL FORCE (F_i) EXERTED BY THESE COMPONENTS IS THE PRODUCT OF THE MASS (M) OF THE COMPONENTS AND THE MAGNITUDE OF THE ACCELERATION FORCE (A). THE INERTIAL FORCE (F_i) IS RESISTED BY THE FORCE (F_s) OF THE ARMING BIAS SPRING (13) AND THE FORCE (F_a) DUE TO ATMOSPHERIC PRESSURE ACTING ON THE BELLONS (21), LESS THE STORED RETURN FORCE OF THE BELLONS (F_r).

THE NET FORCE (F_n) ACTING ON THE ARMING SYSTEM WHICH WOULD TEND TO CAUSE THE INITIATOR TO BECOME ARMED DUE TO INERTIAL FORCES IS:

$$F_n = MA - (F_s + F_a - F_r) \quad (2.1)$$

EQUATION 2.1 NEGLECTS THE EFFECT OF ANY DECREASE IN DYNAMIC PRESSURE RESULTING FROM INCREASING ALTITUDE.

* NUMBERS IN PARENTHESES () REFER TO ITEM NUMBERS OF SPACE/ARM DRAWING NO. 1046A-07.

PREPARED BY	B.R.T.	7-9-64	WALLACE O. LEONARD, INC.	REPORT	1104
APPROVED BY			PASADENA, CALIFORNIA	PAGE	2 OF 2

THE EFFECTIVE SPRUNG WEIGHT OF THE ARMING SYSTEM IS 0.0261 POUNDS DISTRIBUTED AS FOLLOWS:

ITEM NO.	ITEM	WEIGHT
13	ARMING BIAB SPRING	0.0006
15	ARMING SLEEVE	0.0046
16	BELLOWS FRONT PLATE	0.0042
17	FIRING CUP	0.0147
21	BELLOWS	0.0018
TOTAL		0.0261

SINCE $M = \frac{W}{G}$ WHERE W = WEIGHT IN POUNDS AND $G = 32.2 \text{ FT/SEC}^2$ THEN EQUATION 2.1 MAY BE WRITTEN:

$$F_N = \frac{WA}{G} - (F_S + F_A - F_B) \quad (2.2)$$

IF IT IS ASSUMED THAT THE INITIATOR IS IN THE SAFE POSITION AND THAT A POSITIVE LONGITUDINAL ACCELERATION OF 100 G IS APPLIED TO THE MECHANISM THE NET FORCE (F_N) THAT WOULD TEND TO ARM THE MECHANISM IS:

$$\begin{aligned}
 F_N &= \frac{0.0261(100)32.2}{32.2} - (0.15 - 9.9 - 2.69) \\
 &= 2.61 - 6.40 \\
 &= -3.79 \text{ POUNDS}
 \end{aligned}$$

SINCE THE RESULT IS A NEGATIVE QUANTITY IT IS OBVIOUS THAT A 100 G ACCELERATION WILL NOT EVER DISPLACE THE ARMING SYSTEM FROM THE SAFE POSITION.

THE STEADY STATE ACCELERATION REQUIRED TO DISPLACE THE ARMING SYSTEM FROM THE SAFE POSITION IS 245 G.

THE STEADY STATE ACCELERATION REQUIRED TO ARM THE MECHANISM IS 330 G.

APPENDIX II

**ANALYSIS OF THE DYNAMIC PRESSURE EFFECTS
OF THE REDUNDANT INITIATOR PRESSURE SENSING
MECHANISM DURING VEHICLE DESCENT**

APPENDIX II

ANALYSIS OF THE DYNAMIC PRESSURE EFFECTS ON THE REDUNDANT INITIATOR PRESSURE SENSING MECHANISM DURING VEHICLE DESCENT

G. K. Oss

Discussion

The back-up or redundant fragmentation charge initiation mechanism is to be activated by a pressure sensing element. This initiator will become armed during vehicle ascent at a predetermined atmospheric pressure and function, in the event of a failure of the primary initiator, by releasing a firing pin upon sensing a predetermined ambient pressure during vehicle descent.

Because of the gyroscopic stabilizing effect induced by the vehicle burnout roll rate of approximately 20 rps, the vehicle will tend to maintain its ascent attitude through apogee and descend in a sort of tail-first attitude until the aerodynamic forces become sufficient to restore the vehicle to the proper flight position as illustrated in Figure II-1. Previous static stability analyses of the EA 6 MOD 3 Arcas indicate that the vehicle will become aerodynamically unstable after payload ejection. This condition is experienced because of the rearward shift of the vehicle center of gravity induced by loss of the minimum payload weight of about 8.4 pounds required to maintain a static stability of at least one body diameter at burnout. Consequently, the rocket body will begin to tumble upon encountering aerodynamic restoring forces. It should be noted that while the vehicle descends at some angle of attack relative to the airflow, the pressure sensing orifice will be subjected to some magnitude of dynamic pressure in addition to ambient pressure due to the normal component of velocity on the vehicle. The purpose of this analysis was to determine what maximum error in destruct altitude may be experienced as a result of this dynamic pressure influence upon the pressure sensing element of the redundant initiator.

The nominal destruct altitude for the redundant initiator was originally set at 15,000 feet. Considering the limitations that would be imposed upon the vehicle with regard to launching locations because of FAA regulations, the destruct altitude was considerably increased. This analysis was based on a design destruct altitude of 50,000 to 70,000 feet. A minimum destruct altitude of 50,000 feet was selected in order to stay above the

altitude levels currently used by commercial and most military aircraft.

For the purposes of this analysis, the rocket body was assumed to be either aerodynamically stable or experience reasonably low rates of tumble. The analysis, then, may be considered accurate except for very high rates of tumble, which are not likely to be encountered with the Frangible Arcas vehicle.

Standard Arcas vehicle velocities were used to determine dynamic pressures since the performance of the Frangible Arcas will be nearly the same.

Analysis

As the rocket body descends with some angle of attack, as shown in Figure II-1, the redundant initiation mechanism will sense pressure ranging between something slightly less than ambient pressure, P_a , and total pressure, $P_a + \rho \frac{V^2}{2}$ (ambient pressure + dynamic pressure), as the pressure orifice is subjected to some component of free stream velocity during vehicle spinning and/or tumbling. The maximum condition would be represented by a constant vehicle descent attitude normal to the relative airflow such that the redundant initiator monitored total pressure at all points along the descent trajectory as illustrated in Figure II-2. Hence, a sensing of total pressure represents the maximum condition and was used to determine the maximum altitude that the redundant initiator could function. This altitude would, of course, be greater than the preselected destruct altitude based on ambient pressure, since the apparent ambient pressure (ambient pressure + dynamic pressure) is greater, which is representative of a lower actual altitude. A comparison of ambient and total pressures for the rocket body during descent is presented on Figure II-3. As shown by this graph, the intended destruct altitude limits of 50,000 to 70,000 feet could be increased to 94,000 to 112,000 feet under the maximum or total pressure sensing conditions. The upper limit of 112,000 feet, therefore, represents the altitude above which the redundant initiator could not be activated.

Since the rocket body will spin and/or tumble during descent, the total pressure sensing conditions described above will exist only as peak conditions as the pressure sensing orifice becomes oriented in a position

to be effected by dynamic pressure. Hence, the pressure-time relationship that will actually be experienced will be similar to the one illustrated on Figure II-4. Because the pressure sensing system will have some finite response time, it is unlikely that the mechanism could be activated by the peak conditions. The system will most likely respond at an apparent ambient pressure represented by the average of the pressure limits experienced. As shown by the trace on Figure II-3, the difference between ambient and total pressure during vehicle descent is generally much greater than the difference between zero pressure and ambient. Consequently, the apparent ambient pressure may be approximated by the average of the true ambient pressure and total pressure at any time during vehicle descent. A comparison of true ambient pressure and apparent ambient pressure is presented on Figure II-5. This comparison indicates that the intended destruct limits may be increased about 30,000 feet above the design altitude because of the effect of dynamic pressure on the pressure sensing system, assuming the response of the system will be such that the effective ambient pressure will be the average of the true ambient pressure and total pressure during vehicle descent. A tabulation of data used to plot the graphs on Figures II-3 and II-5 is presented on Table II-A.

Conclusions

Although the redundant initiation device will be designed to function at a predetermined ambient pressure during vehicle descent, the system may be activated at a higher altitude because the effect of dynamic pressure may result in an imposed total pressure greater than ambient. The effective destruct altitude is difficult to predict, but the analysis presented above establishes the limits of destruct altitude, included in the tabulation below.

Minimum Destruct Altitude	50,000 feet
Nominal Destruct Altitude	60,000 feet
Design Destruct Altitude Limits	50,000 to 70,000 feet
Probable Destruct Altitude Limits	81,000 to 100,000 feet
Maximum Destruct Altitude	112,000 feet

Although the design limits of destruct altitude may be considerably increased by the effects of dynamic pressure, the range of 50,000 feet minimum to 112,000 feet maximum is acceptable for fragmentation of the vehicle. There is no apparent reason at this time for reducing the destruct altitude limits, providing the minimum limit is sufficiently high to avoid safety hazards to aircraft, etc.

The effect of vehicle attitude during descent and response of the redundant initiation system to dynamic pressure can best be evaluated during flight tests, which are planned later in the program.

TABLE I-A

33264

Ambient Pressures

<u>Altitude (ft)</u>	<u>Absolute Pressure (psia)</u>
50,000	1.690
60,000	1.048
70,000	0.650

Dynamic and Total Pressures

<u>h (ft)</u>	<u>V (ft/sec)</u>	<u>ρ (lb-sec²/ft⁴)</u>	<u>$q = \frac{\rho V^2}{2}$ (psi)</u>	<u>P_a (psia)</u>	<u>$P_T = P_a + q$ (psia)</u>
160,000	2349	2.43×10^{-6}	0.047	0.015	0.062
138,000	2630	5.83×10^{-6}	0.140	0.033	0.173
113,000	2900	1.74×10^{-5}	0.508	0.091	0.599
77,000	3143	1.00×10^{-4}	3.440	0.466	3.906
49,000	2995	3.82×10^{-4}	11.900	1.770	13.670

Average Apparent Pressures, $\frac{P_T + P_a}{2}$

<u>h (ft)</u>	<u>P_T (psia)</u>	<u>P_a (psia)</u>	<u>$\frac{P_T + P_a}{2}$ (psia)</u>
160,000	0.062	0.015	0.039
138,000	0.173	0.033	0.103
113,000	0.599	0.091	0.345
77,000	3.906	0.466	2.186
49,000	13.670	1.770	7.720

Illustration of Vehicle Attitude Along a Free Flight Ballistic Trajectory

33087

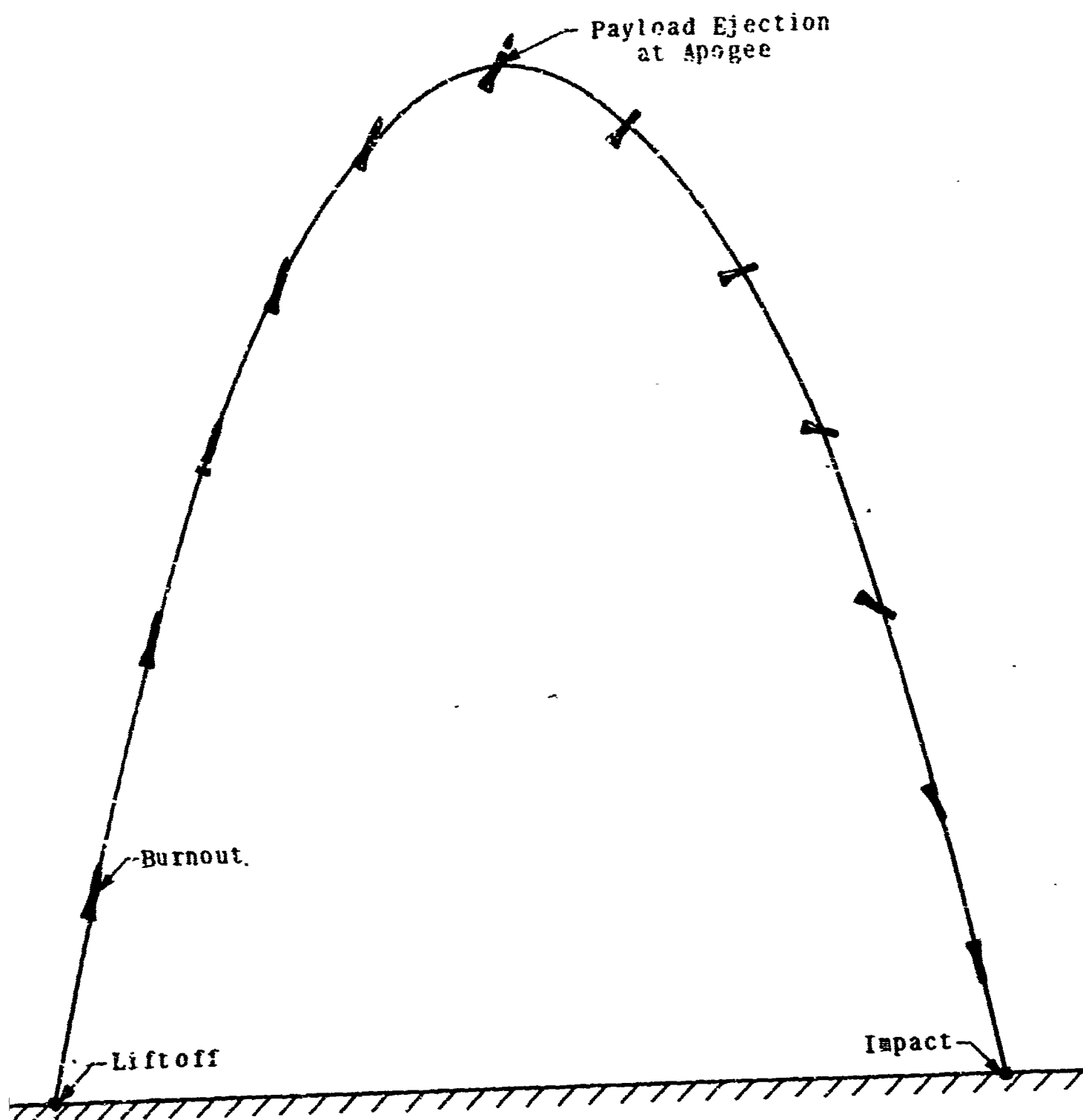


Figure II-1

Vehicle Descent Showing Altitude Normal to Relative Airflow

33093

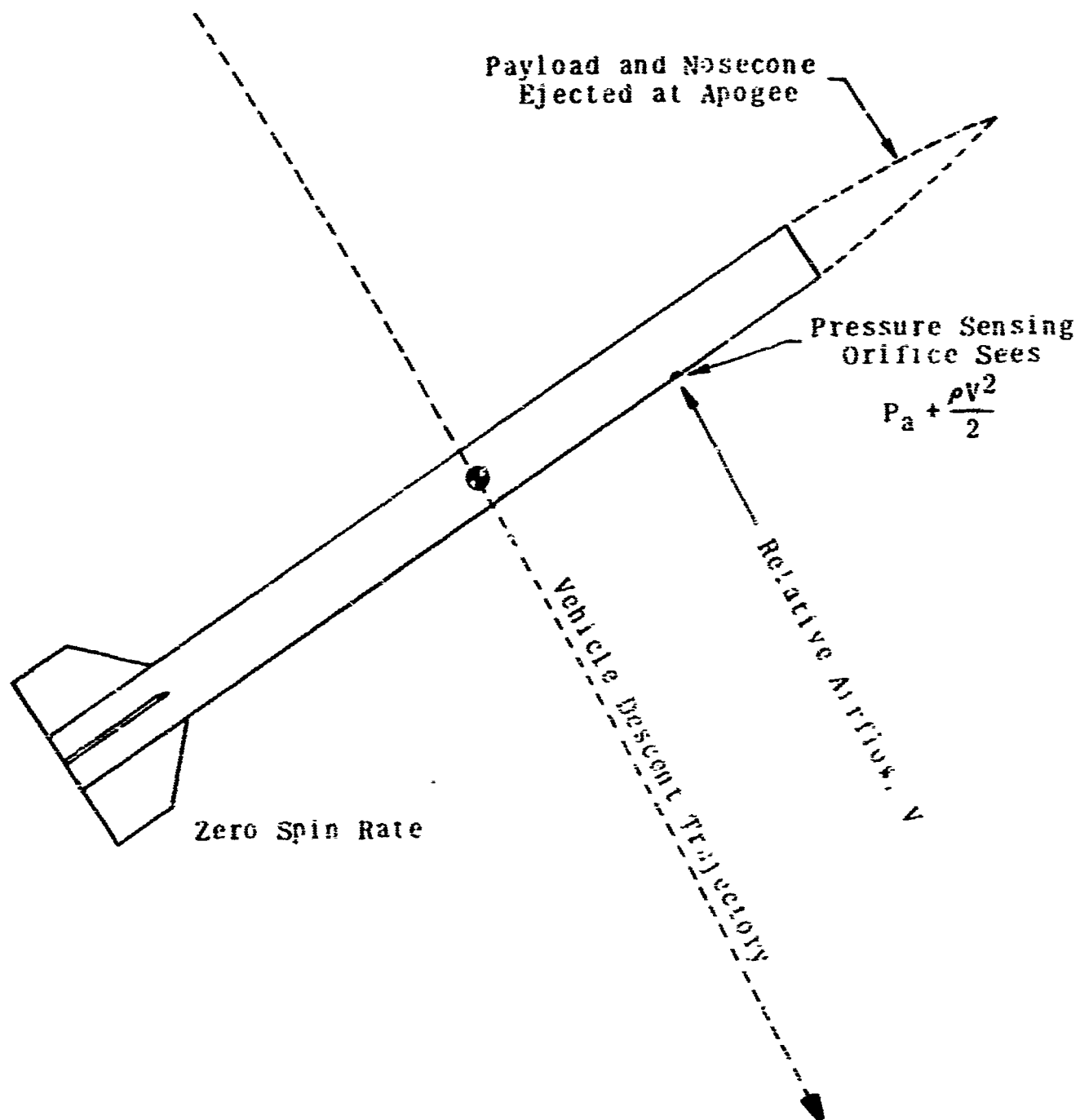


Figure K-2

Ambient and Total Pressures for the Frangible Arcas Vehicle During Descent

33089

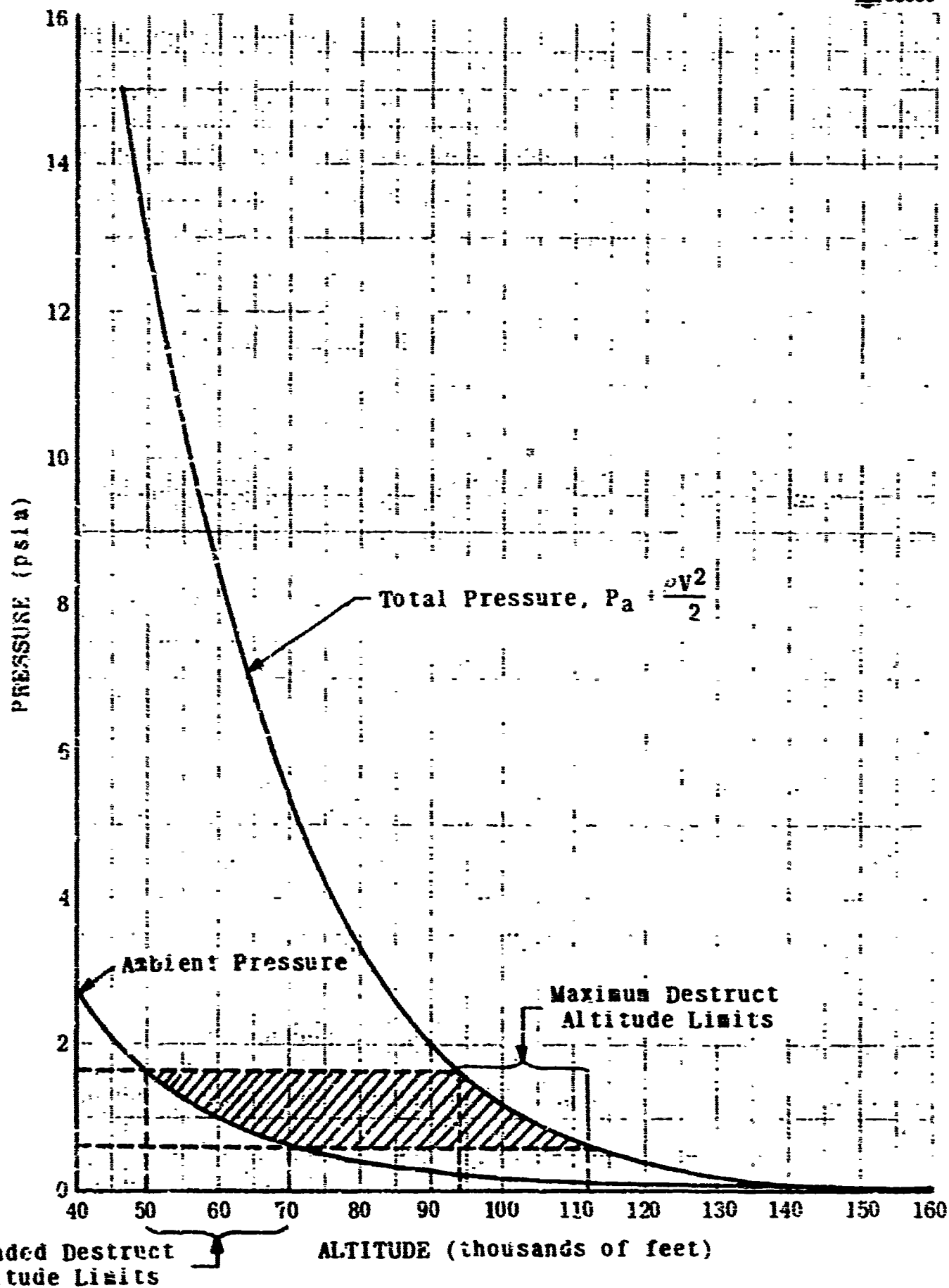


Figure II-3

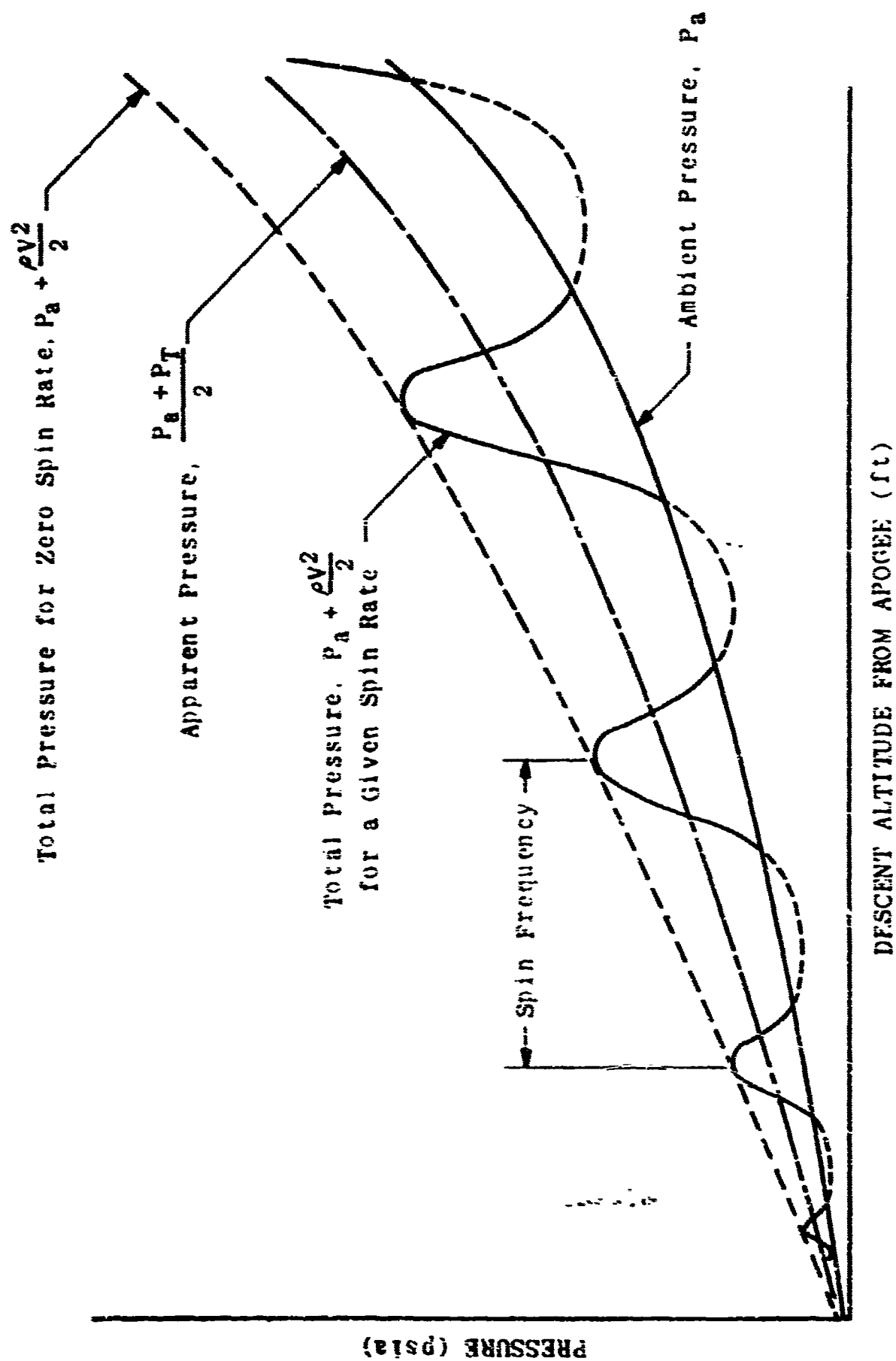


Figure I-4

Intend
Altit

Ambient and Apparent Ambient Pressures for the Frangible Arcas Vehicle During Descent

33088

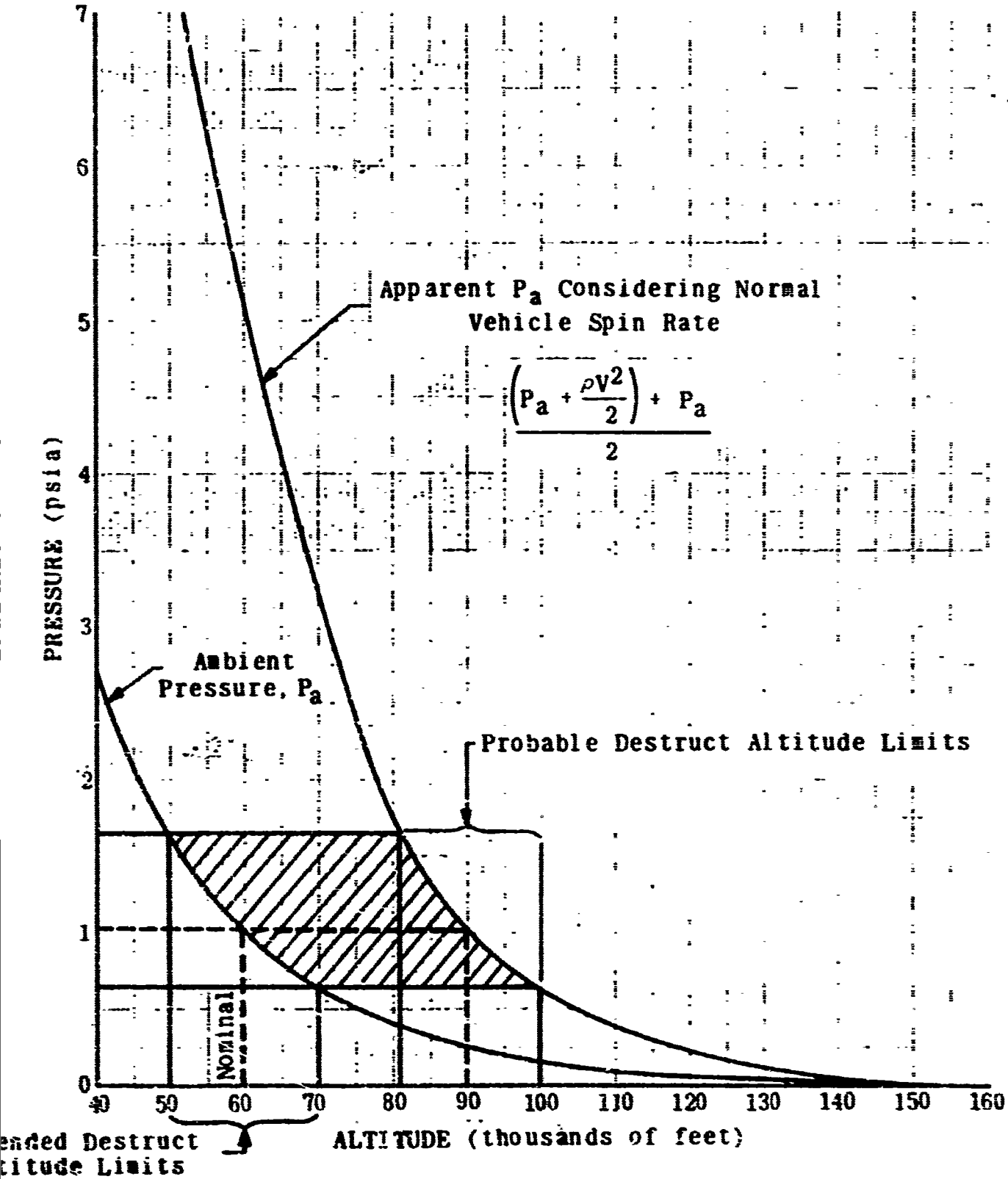


Figure E-5

ATLANTIC RESEARCH CORPORATION
ALEXANDRIA, VIRGINIA

FRANGIBLE ARCAS FLIGHT PERFORMANCE ANALYSIS

(DIAGNOSTIC VEHICLES)



G. K. Oss
Project Manager
Sounding Rocket Systems

19 February 1965

INTRODUCTION

Additional funding was made available in April 1964 to continue the Frangible Arcas development work which began in September 1962 under Bureau of Naval Weapons contract NOw 62-1106-c. The primary objective of the Frangible Arcas program is to demonstrate the feasibility of a frangible meteorological rocket system comparable in performance with the standard Arcas vehicle, but capable of self-induced fragmentation subsequent to payload ejection.

The design approach selected to achieve the required fragmentation capability utilizes materials and a configuration not heretofore evaluated on the systems level. Because of the necessity to evaluate various components of the vehicle systems with a minimum number of variables, a two-phase flight test program is being employed. Phase I consists of two flight tests of the final vehicle configuration, less the fragmentation system, to evaluate vehicle performance and monitor motor case temperatures in flight. Successful completion of these flight tests will provide the information to proceed with Phase II which will consist of two flight tests of the system vehicle for the purpose of evaluating payload ejection and vehicle fragmentation in flight.

Phase I of the flight test program was completed during January at PMR. Flight data obtained from the two units, listed below, were used to establish drag data which will more accurately characterize the Frangible Arcas systems vehicle configuration.

<u>Flight Unit</u>	<u>Op. No.</u>	<u>Date Flown</u>	<u>From</u>	<u>Payload</u>	<u>Payload Wt. (lbs)</u>
APFT-1	417156	12-16-64	SNI	Diagnostic	10.1
APFT-2	517613	1-20-65	Pt. Mugu	Diagnostic	10.1

The attached report presents a comparison of the flight data with that predicted and discusses significant portions of these data. The drag curve developed by this analysis is presented herein and will be used to predict performance of the systems flight vehicles.

TABLE OF CONTENTS

	<u>Page</u>
INTRODUCTION	1
SUMMARY	1
DIAGNOSTIC FLIGHT TESTS	1
AFFT-1 Flight Performance	1
AFFT-2 Flight Performance	3
FLIGHT PERFORMANCE SUMMARY	3
CRITIQUE	4
CONCLUSIONS	5

FRANGIBLE ARCAS FLIGHT PERFORMANCE ANALYSIS

SUMMARY

An analysis of the flight performance data obtained from the first two Frangible Arcas flight tests was performed to develop a more accurate drag curve to be used in predicting performance of the systems vehicle. Insufficient radar data were obtained from the first flight to construct a trajectory for the vehicle, but sufficient telemetry data were obtained to show that the flight was fully successful. The combination of this information with the data obtained from the second flight showed reasonably good agreement with the predicted vehicle performance, as tabulated below.

<u>Flight Unit</u>	<u>Payload Weight (lbs.)</u>	<u>Effective Apogee QE</u>	<u>Predicted Apogee Altitude (ft)</u>	<u>Actual Apogee Altitude (ft)</u>	<u>% Error</u>
AFFT-1	10.1	84.5*	200,000	190,000*	5.0%
AFFT-2	10.1	77.0*	140,000	114,373	18.3%

* Apparent apogee based on TM data

Although the vehicle performance data obtained from these flights were somewhat limited because of the failure to obtain sufficient radar coverage of the first flight, the analysis and critique of these flights established a new drag curve which provided predicted trajectory profiles that agree well with the actual trajectory data.

DIAGNOSTIC FLIGHT TESTS

Two diagnostic flight test vehicles, designed to monitor motor case skin temperatures in flight, were completed and shipped to PMR 19 November 1964. A photograph of these flight test units is shown on Figure 1. A tabulation of actual vehicle weights is presented on Table I. A discussion of the flight performance of each vehicle is presented below.

AFFT-1 Flight Performance

The first diagnostic flight vehicle was launched at an elevation setting computed to provide a launch elevation of 85.6 degrees. The vehicle was tracked by radar from about $T + 7$ to about $T + 27$ seconds at which time radar track was lost. A plot of radar data obtained is presented in comparison with the predicted trajectory profiles on Figure 2. An expanded scale plot for the early portion of the flight is presented on Figure 3. As observed from this comparison, the effective launch angle attained was about 85 degrees, which is in good agreement with the predicted angle. It may be noted, however, that the flight times at which the vehicle was to have reached various altitudes do not correlate well. It is highly unlikely that the velocity of the vehicle could truly have been such as to have behaved as the data indicate. A comparison of these data suggests an error in the time scale and/or magnitude of the radar trajectory data since various telemetry data indicate that the vehicle velocity and apogee performance attained were reasonably close to that predicted.

Short interval fade of the telemetry signal was experienced as the vehicle rolled during flight. This intermittent signal "drop-out" was produced by the changing orientation of the payload antenna as the vehicle rotated during flight. This inherent condition proved beneficial, however, since the roll rate of the vehicle was determined by observing the frequency of the signal fade. Since roll rate of the vehicle is directly proportional to its velocity, the velocity of the vehicle may be evaluated by monitoring the roll rate as a function of time. A comparison of the actual roll rate data with that predicted is presented on Figure 4. The agreement of these data shows that the velocity of the vehicle was close to that predicted.

Impact time for the vehicle was obtained from the telemetry data by observing the time of abrupt and complete loss of the telemetry signal. An impact time of 248 seconds after launch was recorded as compared to a predicted time of 254 seconds. The actual time to impact agrees with that predicted within less than 3% and is indicative of reasonably good agreement in apogee performance.

Two GMD-1 stations tracked the vehicle to provide back-up information for the radar data. A trajectory profile for the flight was constructed by the PMR Data Reduction staff utilizing these data in a computer program. The resulting trajectory is presented on Figure 5 in comparison with

predicted trajectory profiles at various launch angles. Although the accuracy of these data may have been impaired because the GMD-1 stations were located only about four miles apart, the resulting trajectory shows reasonably good performance as compared with that predicted and confirms the data presented above.

AFFT-2 Flight Performance

The second diagnostic flight vehicle was launched at an elevation setting computed to provide a launch elevation of 79 degrees. The vehicle was successfully tracked by FPS-16 radar throughout the flight. The actual trajectory achieved is presented on Figure 6 in comparison with the predicted trajectory profiles. As observed from this plot, an effective launch angle of about 77 degrees was achieved as compared to the predicted angle of 79 degrees. Trajectory performance of the vehicle appeared to be in relatively good agreement with the predicted data until after rocket motor burnout, at which time the vehicle diverged from the predicted path and achieved an apogee about 25,000 feet less than was predicted for a 77° QE.

The velocity achieved by the vehicle was less than that predicted with respect to both altitude and time as illustrated by the graphs on Figures 7 and 8 respectively. The latter plot revealed a point of significance in that the maximum velocity occurred about four seconds later than predicted. This phenomenon is characteristic of a motor burning time longer than that predicted, resulting in a lower than nominal thrust level for an extended period of time.

FLIGHT PERFORMANCE SUMMARY

Since the two subject flight vehicles carried the same gross payload weight, their trajectory profiles may be conveniently compared in a single graph as shown on Figure 9. As described above and observed from the comparative plot, the apogee performance of the diagnostic flight vehicles was somewhat less than that predicted. Insufficient radar coverage of the first flight was obtained to allow an adequate critique to be performed. Radar data obtained from the second flight, however, provided

good flight performance data. The second flight, therefore, provided the basis for the critique and development of a drag curve characteristic of the vehicle configuration. The apparent trajectory achieved by the first flight, based on vehicle velocity and impact time as observed from the telemetry data, was used as a method of checking the accuracy of the revised performance.

CRITIQUE

Failure of the vehicles to fully achieve the predicted peak altitude for their respective effective launch angles was most likely attributed to optimistic drag data assumed for the initial prediction of vehicle performance, since the vehicle weights and total impulse are accurately known. This conclusion is supported by comparison of the actual and predicted altitude vs. velocity curves on Figure 7. This comparison shows the actual velocity to be consistently less than the predicted value at all altitudes, which is characteristic of greater-than-predicted vehicle drag. The agreement of rate of decrease of vehicle velocity (deceleration) after rocket motor burnout as shown by Figure 8, however, indicates accurate drag data at the higher Mach numbers. Although the flight data show that the second vehicle experienced a burning time about four seconds longer than predicted, the reduced thrust level and resulting increase in gravity turn did not appear to be the most significant factor in decreased apogee performance experienced, since the ballistic trajectory did not deviate appreciably from the predicted curve until well after motor burnout.

Since the data presented above indicate that the most significant contributor to the optimistic prediction of vehicle performance was drag data, except at the higher Mach numbers, the drag curve which was used to characterize the vehicle configuration was modified as shown on Figure 10. This modification was predicated upon successful results obtained with the EV Arcas vehicle configuration which is characterized by this drag curve. Point-mass trajectories were computed utilizing the modified drag data. The resulting trajectories are presented on Figure 11 in comparison with the actual flight data obtained from the two diagnostic flight tests. As observed from this comparison, the new drag curve provided predicted trajectories

that more accurately describe the trajectories achieved. Comparison of the predicted and actual velocity data with respect to both altitude and time, Figures 12 and 13 respectively, show an improvement. The lower-than-nominal thrust level indicated by the increased burning time shown on Figure 13 may account for the deviation of the actual and predicted data on these last curves. The interplay of increased burning time, gravity turn and drag characteristics are extremely difficult to evaluate adequately with flight data from only one vehicle. Vehicle performance with respect to apogee altitude, however, shows good agreement between the prediction (critique) and actual flight data.

A comparison of actual and predicted times to impact, tabulated below, also shows relatively good agreement between the new predicted performance and that achieved.

Impact Time (sec)	AFPT-1	AFPT-2
Predicted *	247	210
Radar Data	No Data	202
Telemetry Data	248	205

* Based on revised performance data

CONCLUSIONS

Although the flight data available for the Frangible Arcas vehicle are limited, the performance data obtained from the two diagnostic flights indicated that the original assumptions of drag data were slightly optimistic.

Modification of the original drag data provided trajectories that agree well with the actual flight data. The use of the new drag curve should provide more accurate prediction of the Frangible Arcas systems vehicle performance.

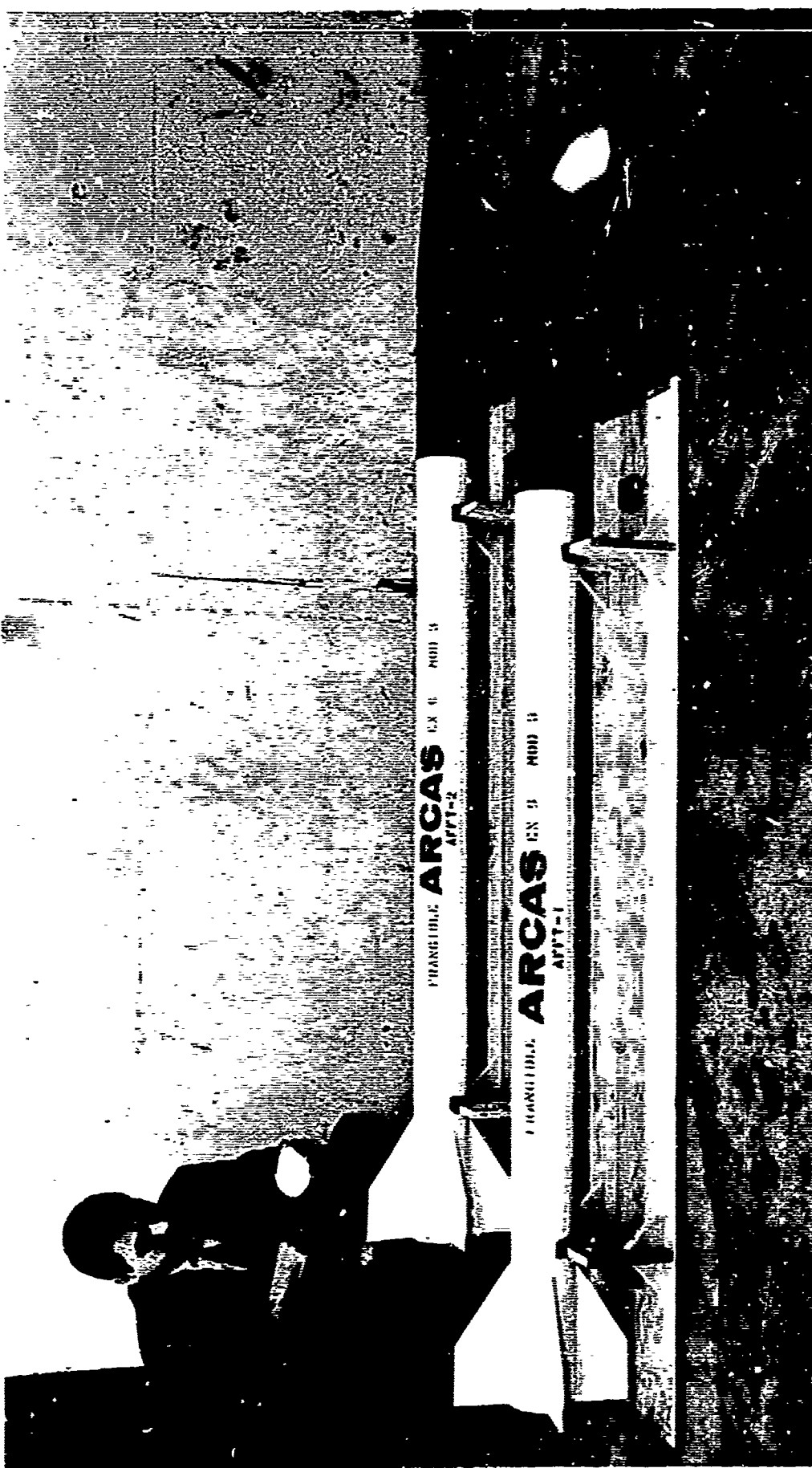
Although the new drag data presented herein represents the best data available at this time, its degree of accuracy cannot be fully evaluated without additional flight tests of the vehicle.

Table I
Tabulation of Actual Weights of Frangible Arcas
Diagnostic Flight Vehicles

2238

<u>Component Weights (lb)</u>	<u>AFFT-1</u>	<u>AFFT-2</u>
Motor Case Assembly	16.50	16.10
Fin Assembly	1.69	1.69
Fin Retaining Screws	0.03	0.03
Propellant Gr: in Assembly	42.69	42.13
Retaining Sleeve	1.93	1.93
Timer Assembly (Without Gas Generator)	0.60	0.60
	<u>63.44</u>	<u>62.48</u>
Diagnostic Payload	<u>10.10</u>	<u>10.10</u>
	73.54	72.58

Photograph of the Frangible ARCAS Diagnostic Flight Test Vehicles



34992

Figure 1

Frangible ARCAS Trajectory Profiles for 10.1 lb Payload
 Sea Level Launch Without Auxiliary Gas Generator Boost
 Diagnostic Flight AFFT-1

2144

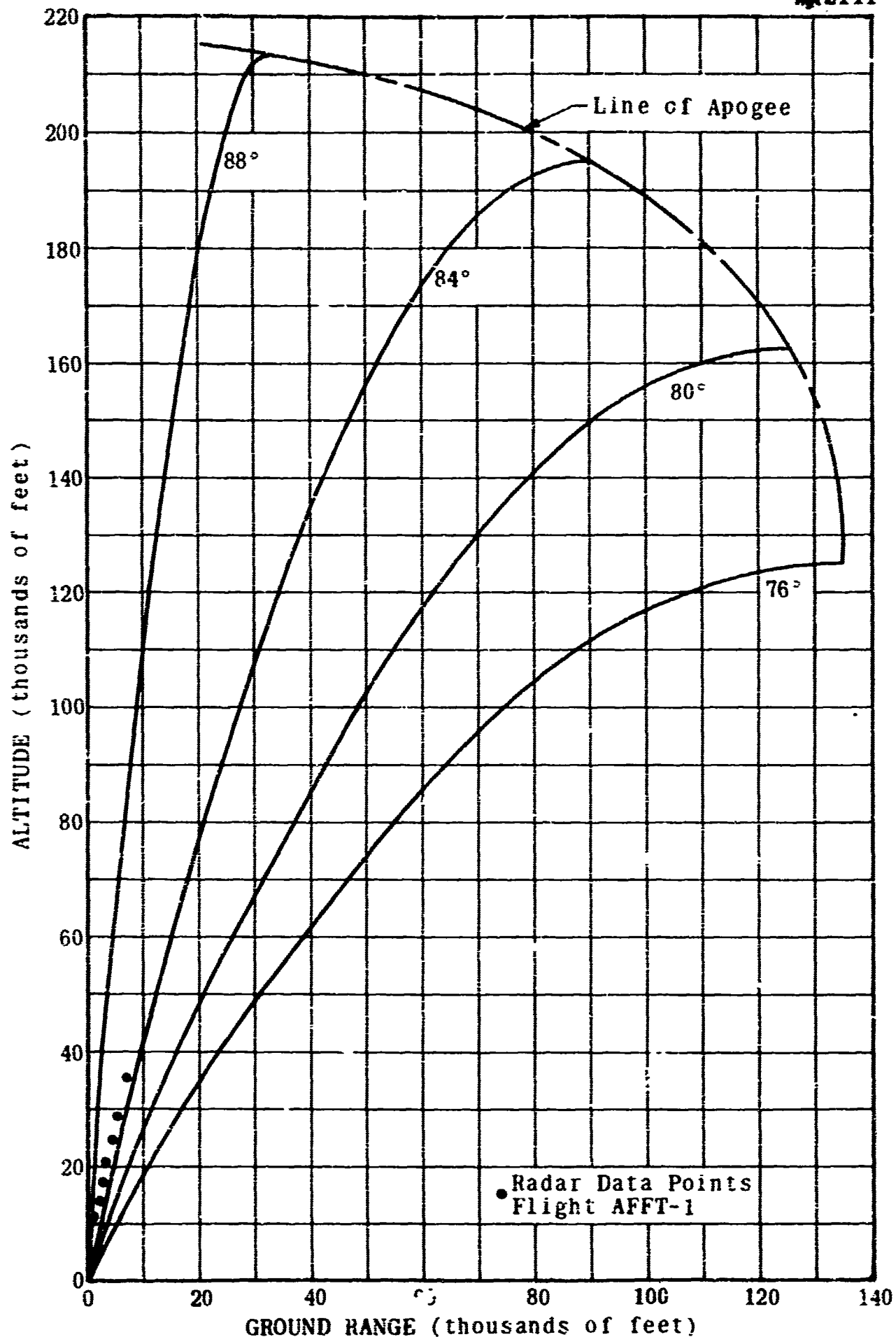


Figure 2

Frangible Arcas AFFT-1 Expanded Trajectory Profile

2191

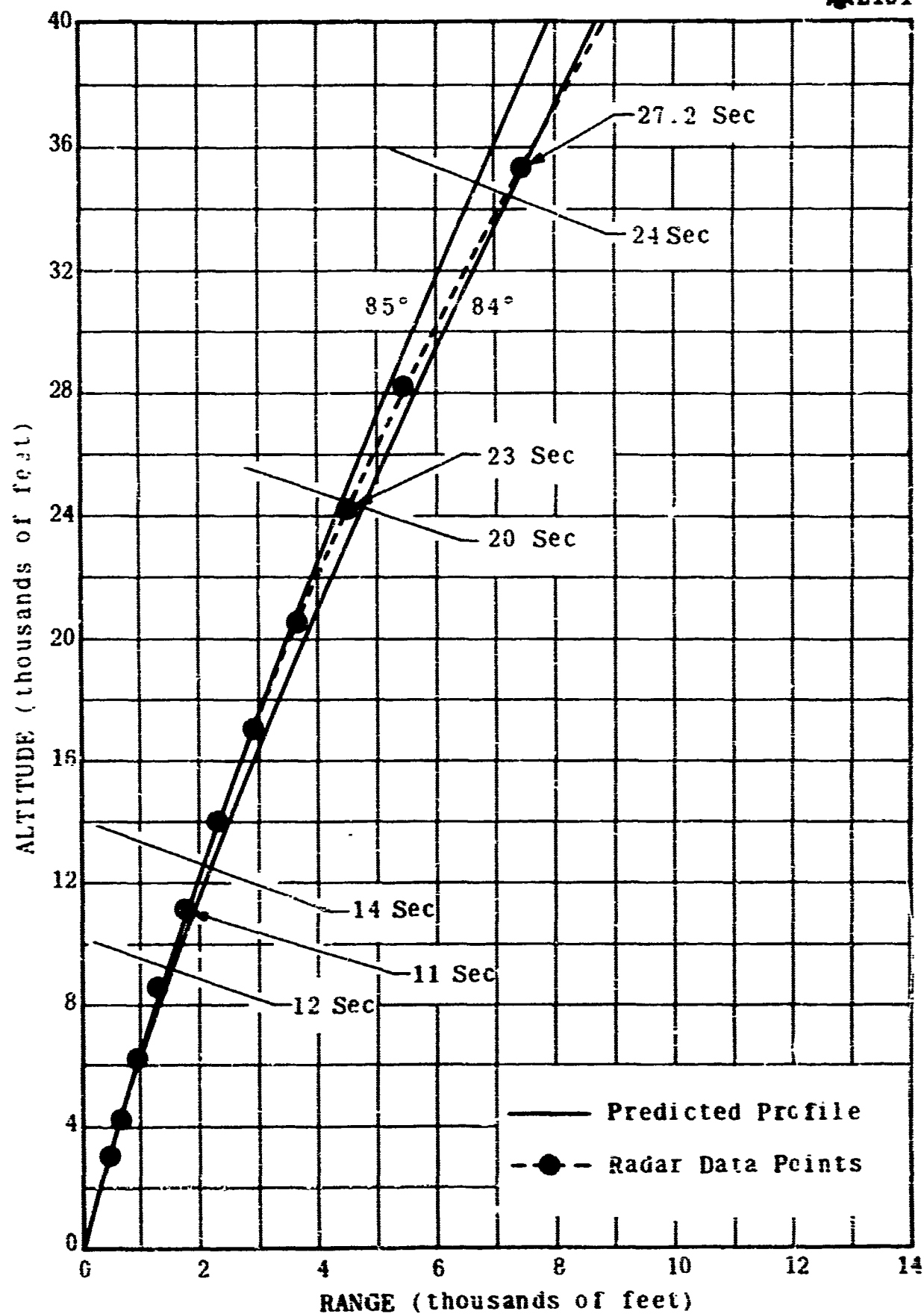


Figure 3

Roll Rate Versus Time Frangible Arcas Diagnostic Flight Test AFFT-1

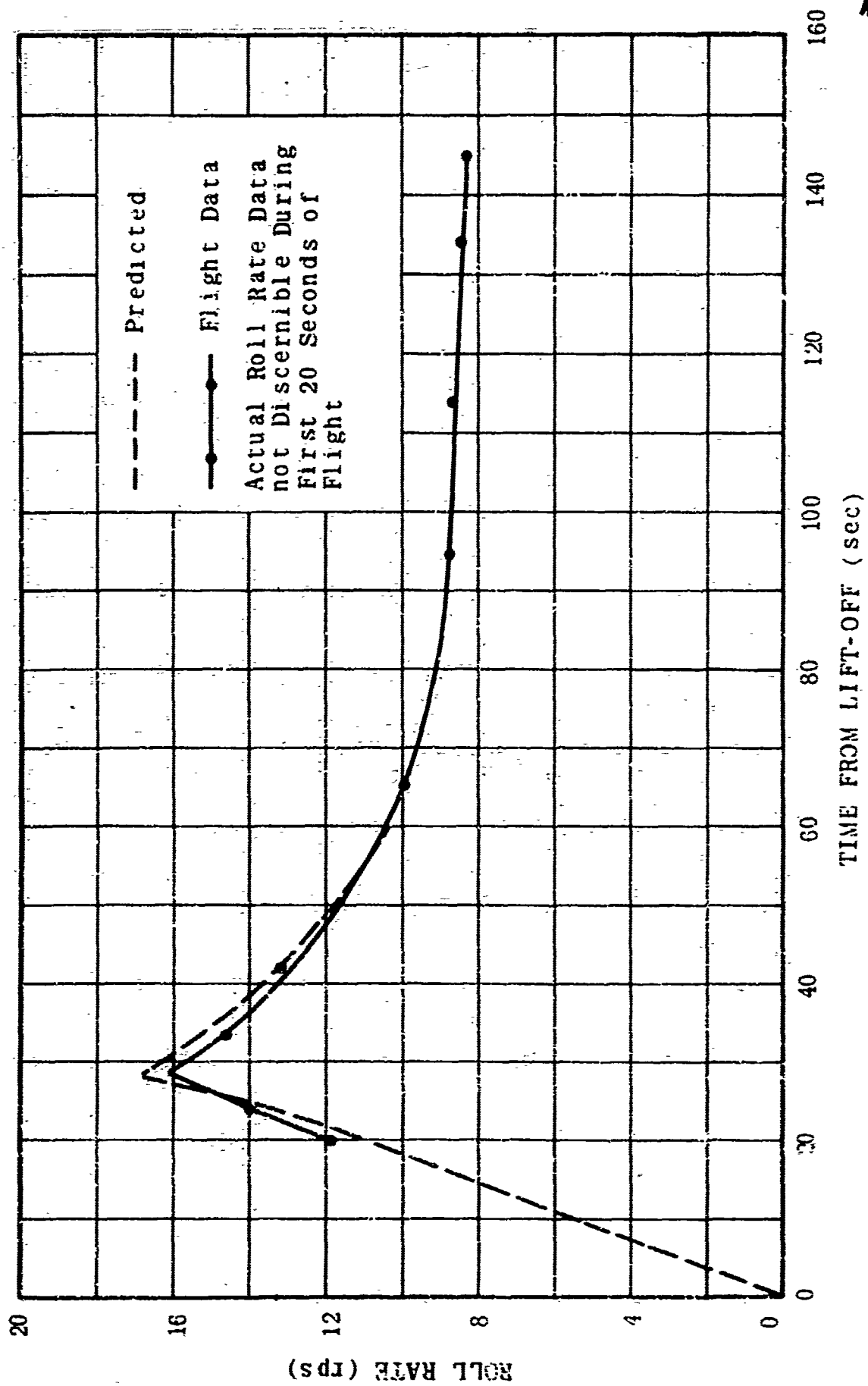


Figure 4

Frangible ARCAS Trajectory Profiles for 10.1 lb Payload Sea Level
Launch Without Auxiliary Gas Generator Boost

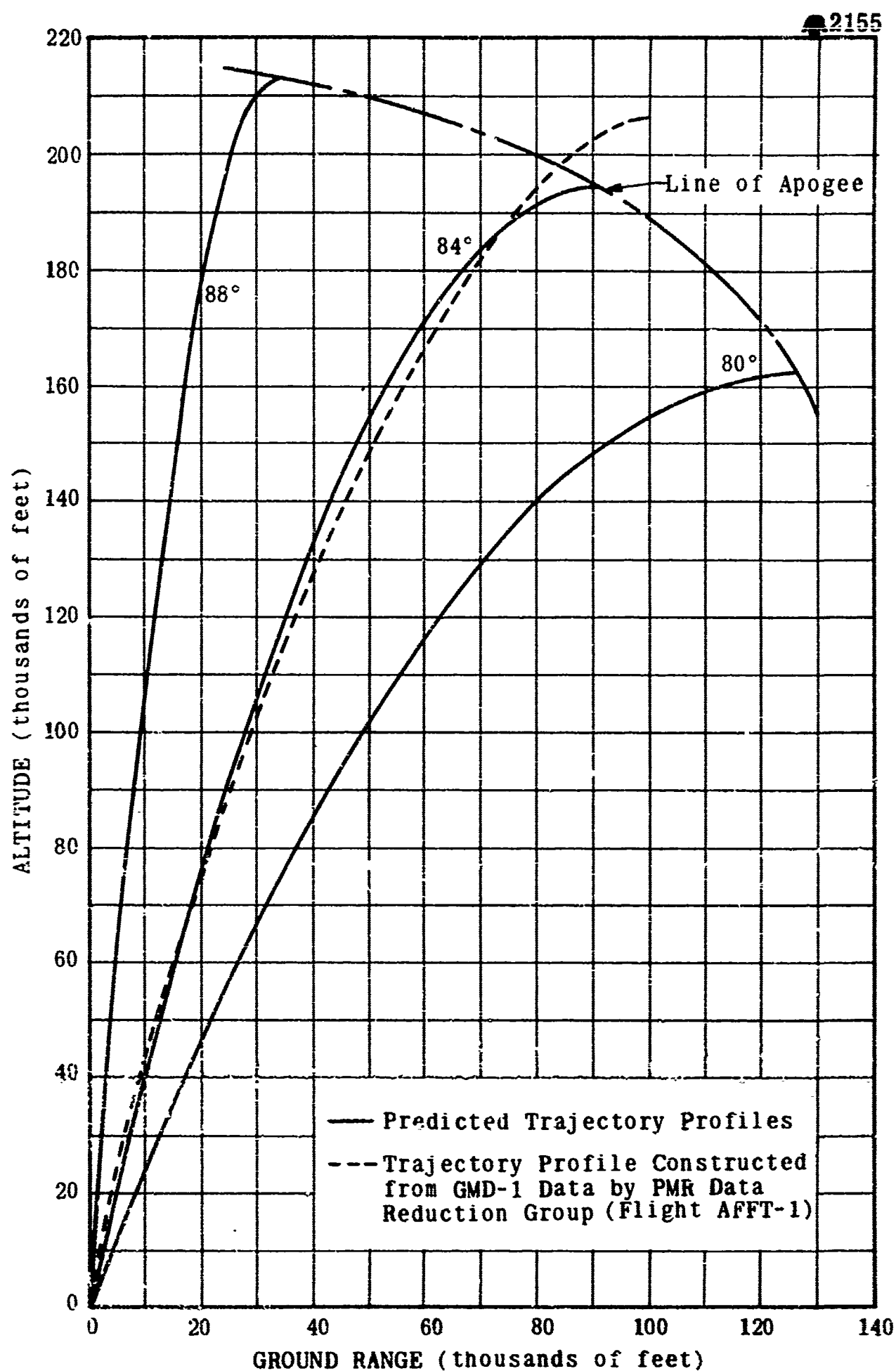


Figure 5

Frangible ARCAS Trajectory Profiles for 10.1 lb Payload
Sea Level Launch Diagnostic Flight AFFT-2
Without Auxiliary Gas Generator Boost

2483

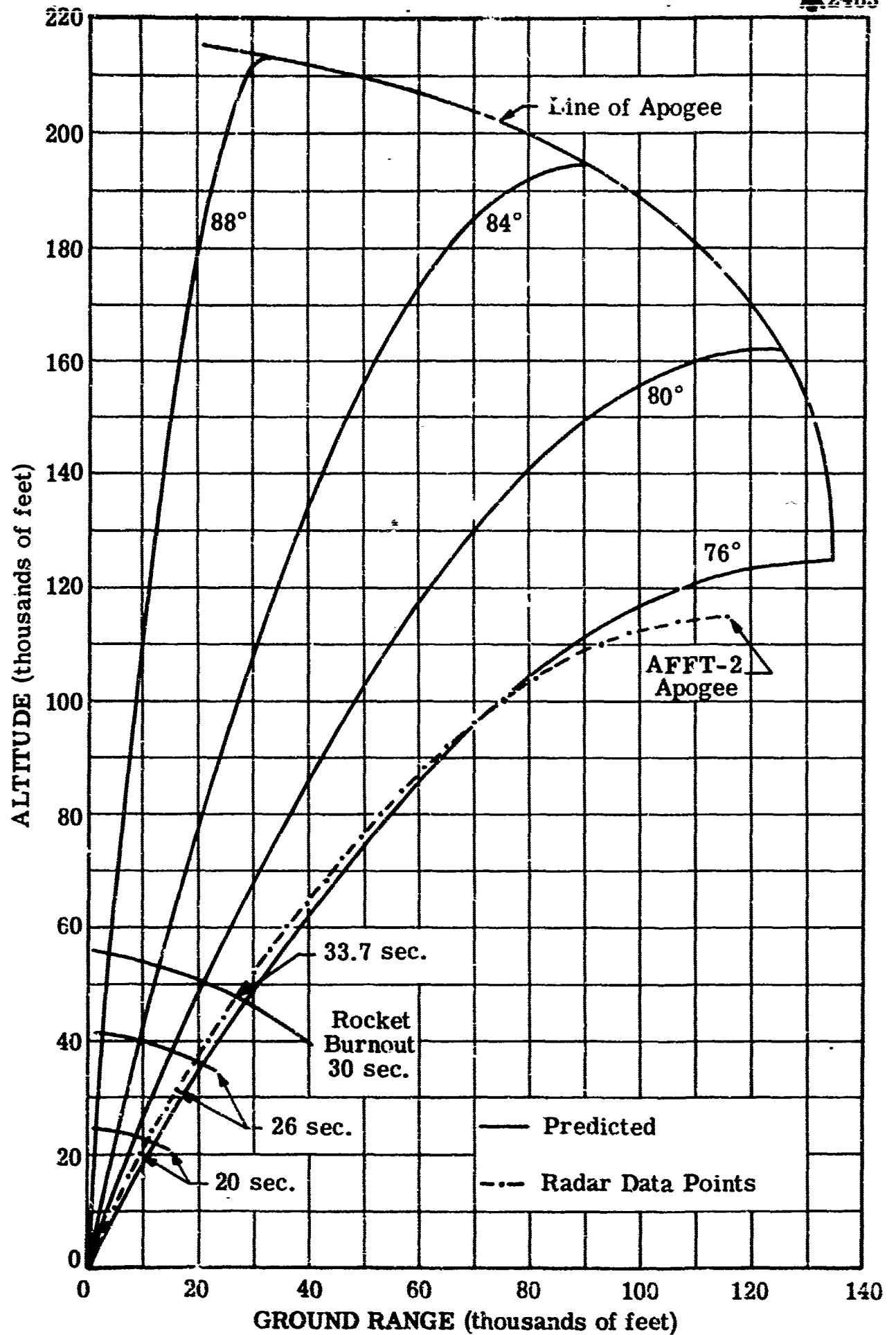


Figure 6

Frangible Arcas Altitude Versus Velocity
Diagnostic Vehicle AFFT-2

2485

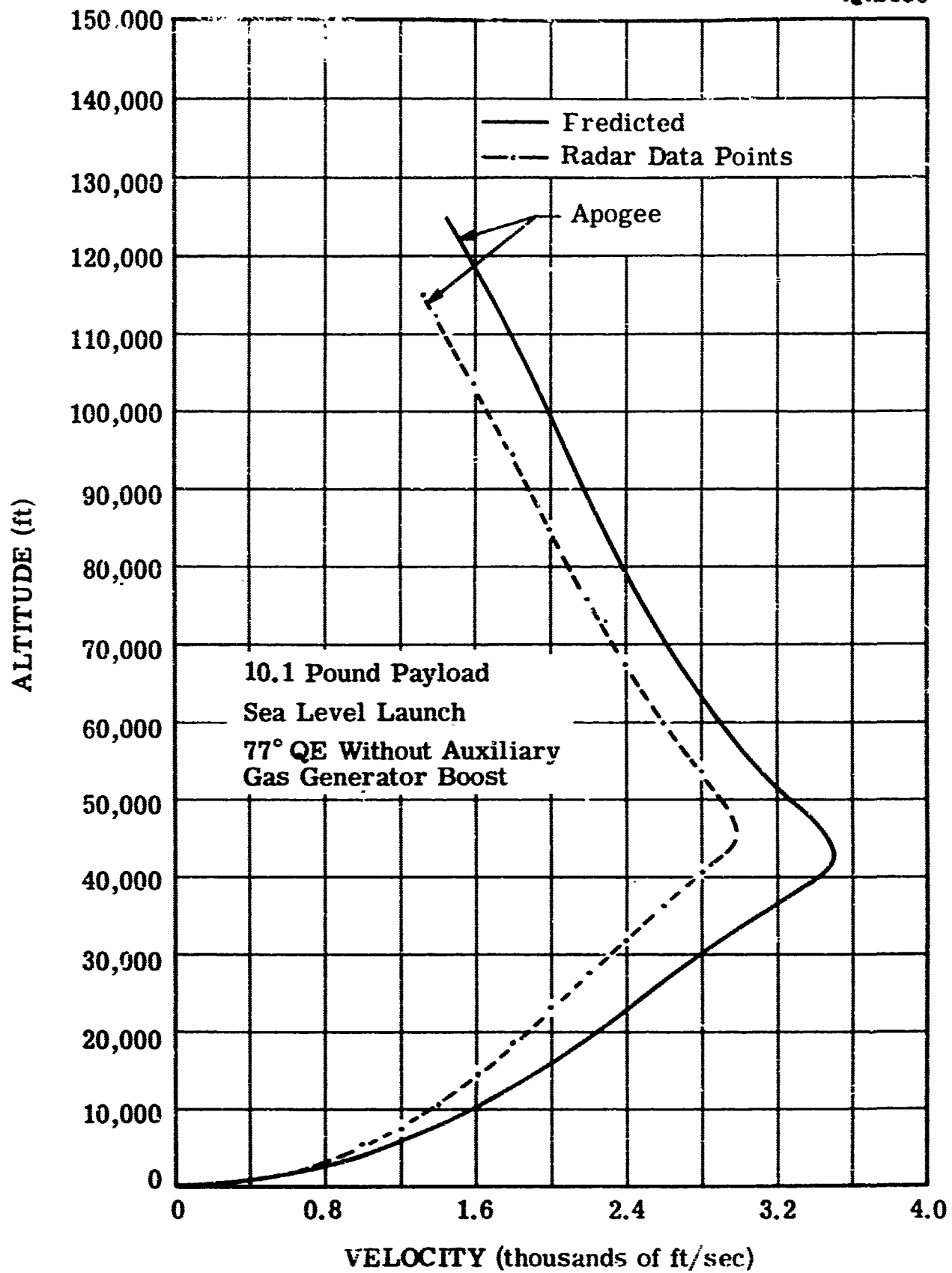


Figure 7

Frangible Arcas Velocity Versus Time
Diagnostic Vehicle AFFT-2

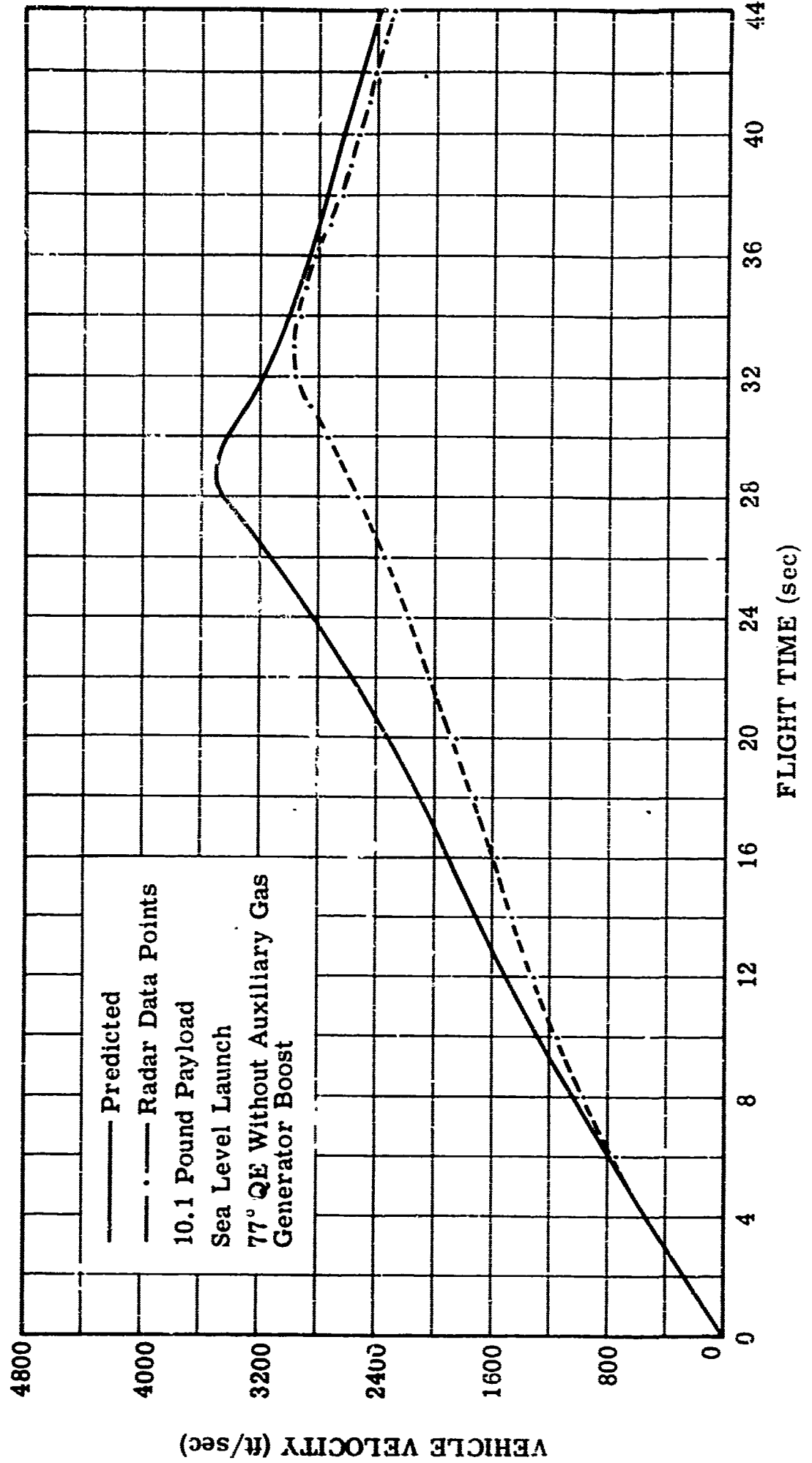


Figure 8

Frangible Arcas Trajectory Profiles for 10.1 Pound Payload Sea Level Launch
Diagnostic Vehicles AFFT-1 and AFFT-2 Without Auxiliary Gas Generator Boost

2553

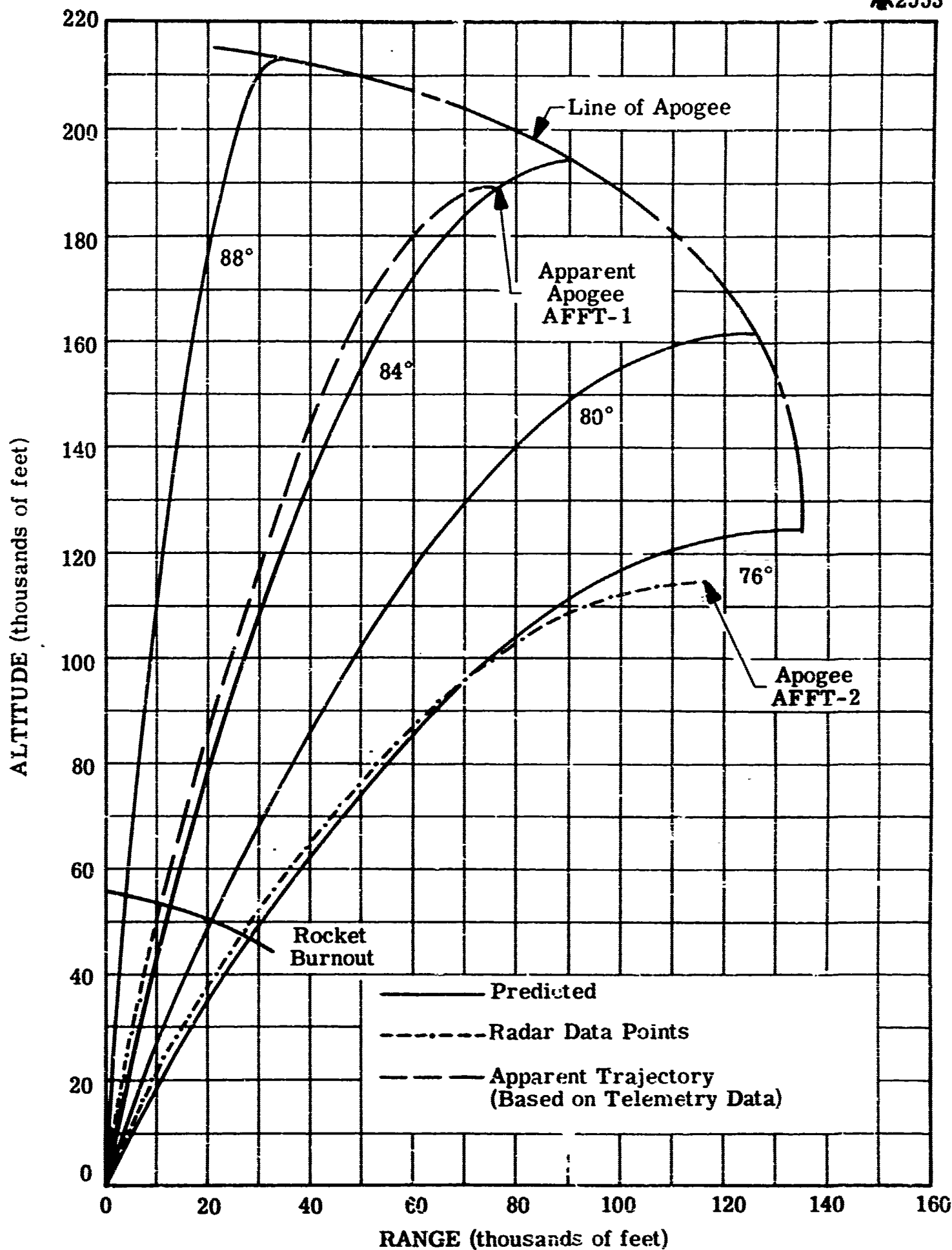


Figure 9

Frangible Arcas Drag Curve

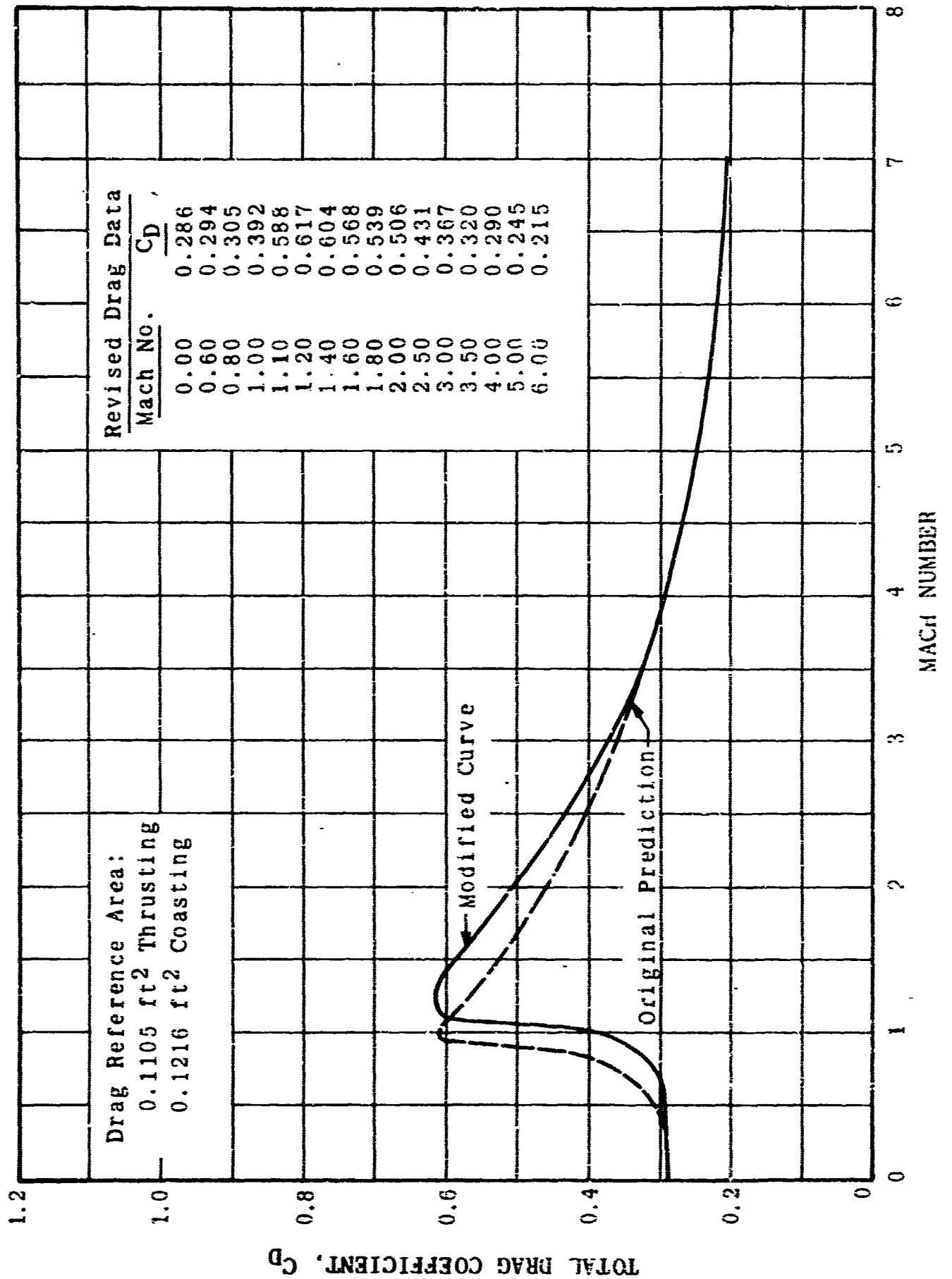


Figure 10

Frangible Arcas Trajectory Profiles Critique Number 1

2551

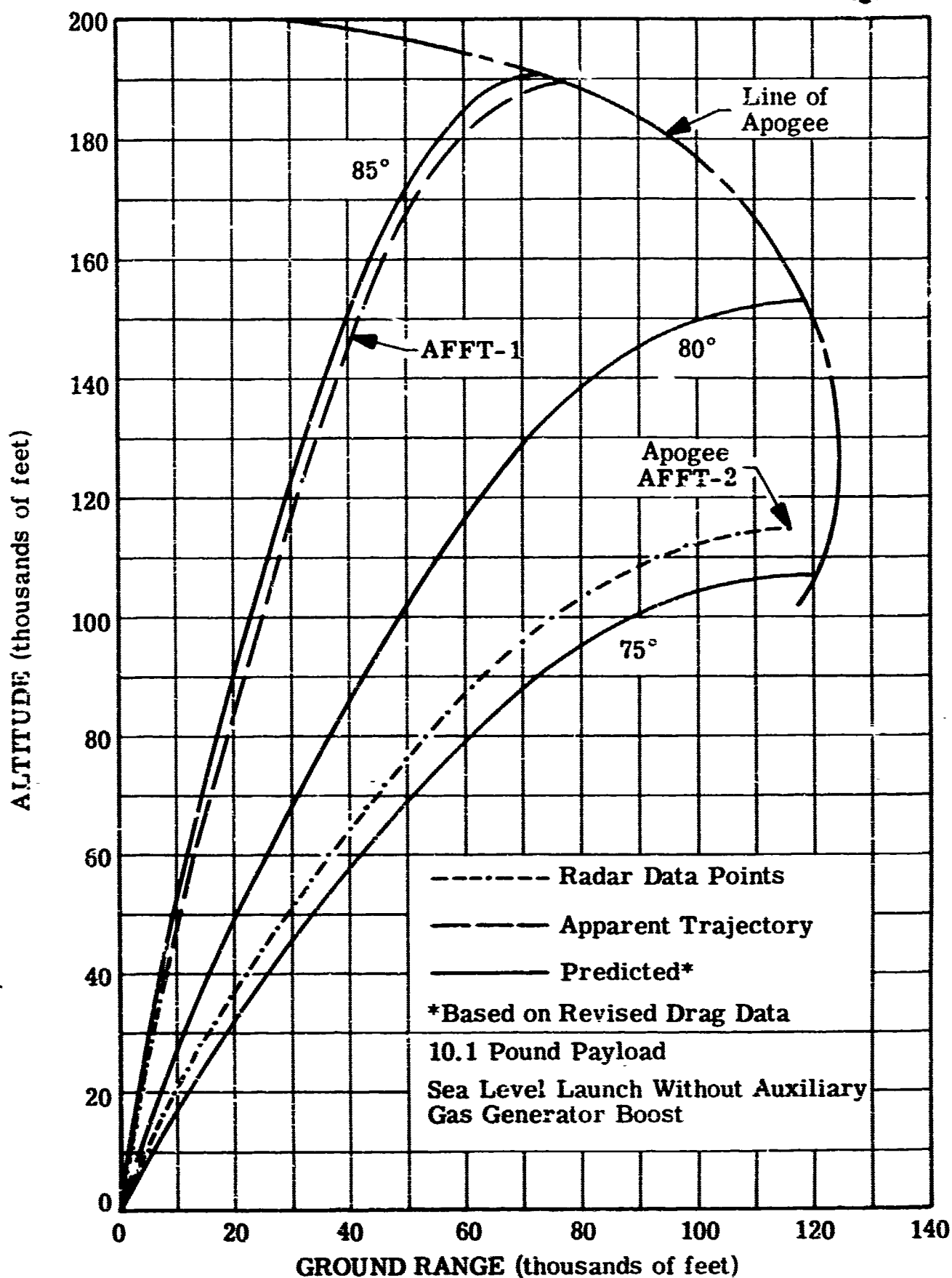


Figure 11

Frangible Arcas Altitude Versus Velocity Diagnostic Vehicle AFFT-2

2534

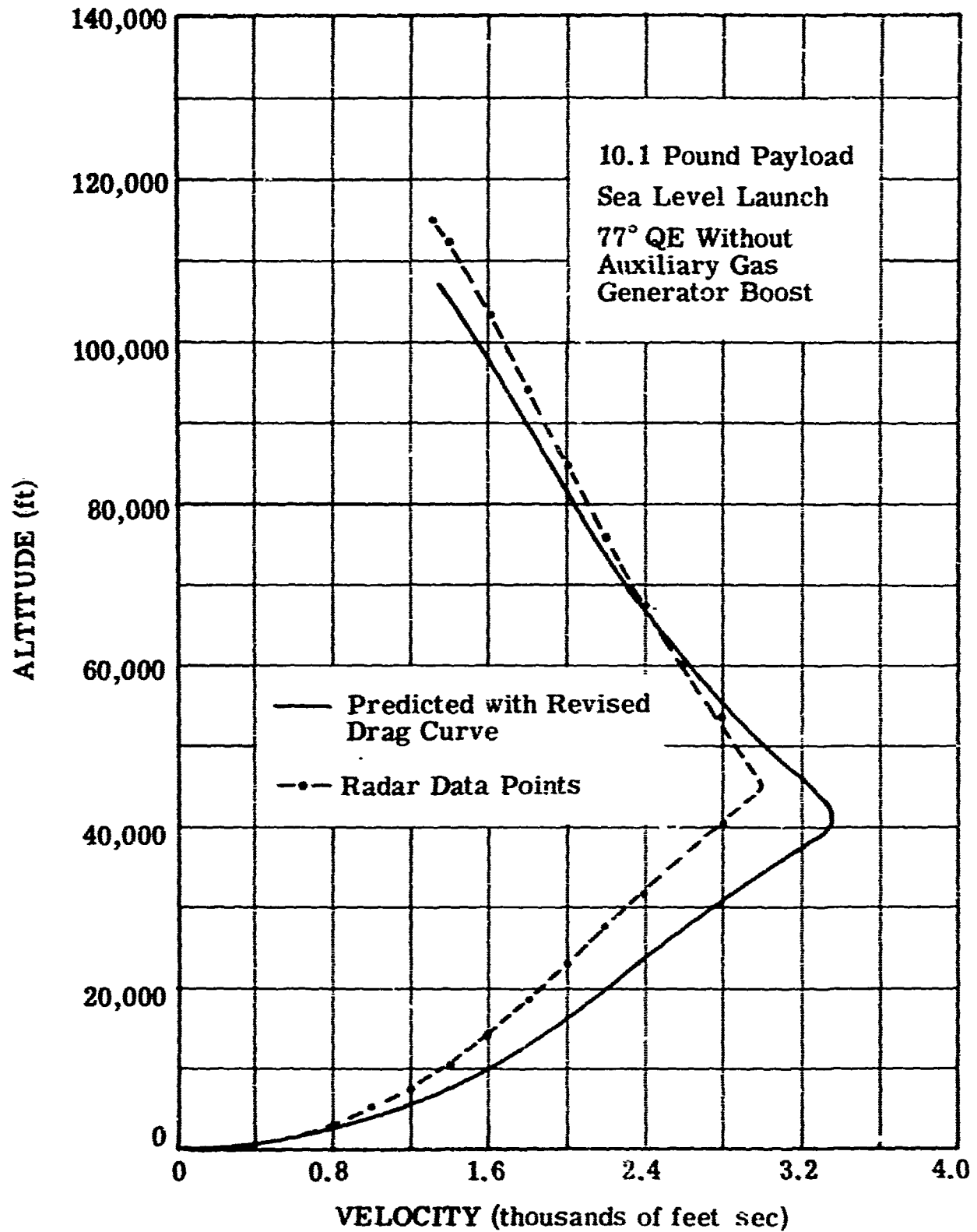


Figure 12

Drangible Arcas Velocity Versus Time Diagnostic Vehicle AFFT-2

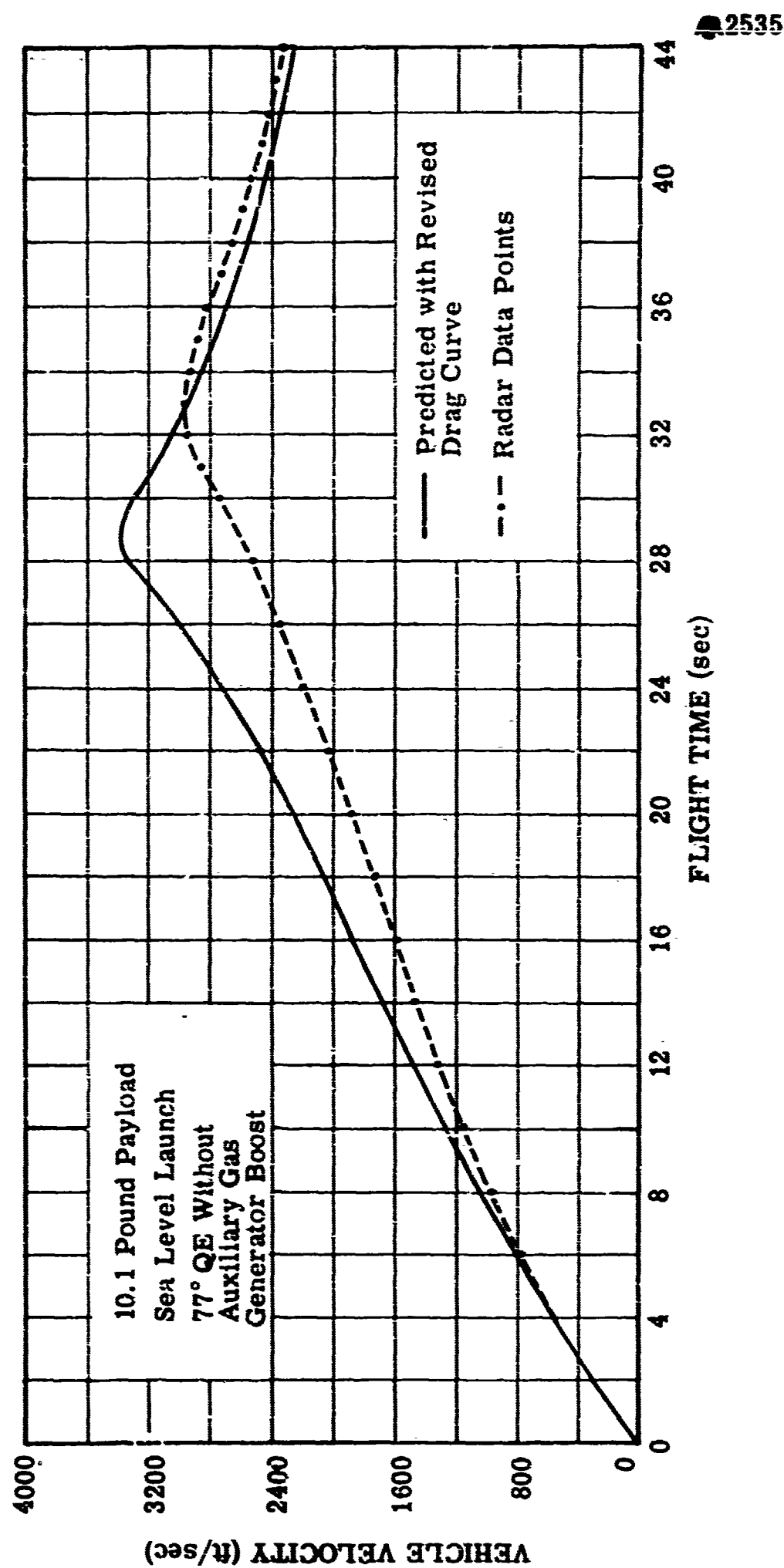


Figure 13

APPENDIX IV

FRANGIBLE ARCAS FLIGHT TEST RESULTS
(SYSTEMS VEHICLES)

TABLE OF CONTENTS

	<u>Page</u>
INTRODUCTION	IV-1
SUMMARY	IV-2
I. FABRICATION OF SYSTEMS VEHICLES	IV-3
II. FLIGHT TEST AFFT-3	IV-4
A. RESULTS	IV-4
B. FLIGHT DATA ANALYSIS	IV-6
C. AFFT-3 CRITIQUE	IV-7
D. CONCLUSIONS	IV-8
III. FLIGHT TEST AFFT-4	IV-8
A. RESULTS	IV-9
B. FLIGHT DATA ANALYSIS	IV-10
C. CONCLUSIONS	IV-11

INTRODUCTION

The primary objective of the Frangible ARCAS program was to demonstrate the feasibility of a frangible rocket system through flight test evaluation. In order to accomplish this objective a series of four flight tests were conducted. The first two flights consisted of the basic vehicle (no fragmentation system) which carried a payload designed to monitor motor case skin temperatures during flight. Both diagnostic flights were successful, thereby demonstrating airworthiness of the basic vehicle configuration, establishing skin temperatures during flight and providing the flight data required to establish a characteristic drag curve for the vehicle configuration.

The program was concluded with two flight tests of the systems vehicle. The purpose of these units was to demonstrate feasibility of the desired vehicle system by flight test evaluation and to provide flight test data for determination of the systems vehicle performance.

This report presents a detailed evaluation of the systems flight test data and compares predicted and actual flight performance.

SUMMARY

Phase III of the Frangible ARCAS program included the flight testing of two systems vehicles. The first flight was considered a "No Test" because of a malfunction experienced with the PMR modified launcher. Results of this flight, however, did indicate an increase in vehicle drag characteristics which was used to repredict the performance of the final flight unit.

The second and final flight test of the systems vehicle was successfully completed in December 1965. All systems functioned as programmed. Fragmentation was achieved twenty seconds after payload deployment at apogee. Radars tracked numerous pieces at various descent rates. The fragmented unit was tracked as a "cloud" which was observed to disperse as it descended.

GMD-1 telemetry data were lost shortly after liftoff, but successful payload deployment was observed by radar track and by physical recovery of the payload. The reason for telemetry signal loss is not readily apparent. The recovered Arcasonde payload was tested and found to function normally.

FRANGIBLE ARCAS FLIGHT TEST RESULTS (SYSTEMS VEHICLES)

I. FABRICATION OF SYSTEMS VEHICLES

Final assembly of the Frangible ARCAS systems vehicles for flights AFFT-3 and AFFT-4 was completed at PMR on 19 and 20 May, respectively. Final assembly consisted of incorporating the explosive fragmentation system into the rocket vehicle. The external sheet explosive was attached to the motor case by incorporating a silicone adhesive pressure sensitive fiberglass tape as a base material onto which the sheet explosive was fitted. The sheet explosive was then overwrapped with a layer of aluminum coated, silicone adhesive pressure sensitive tape. Upon installation of the explosive module and initiation units, the configuration was as illustrated on Figure 1. Application of the external explosive material and overwrap increased the original vehicle diameter by 0.10 inch. A tabulation of actual weight data for the two systems vehicles is presented below.

	<u>AFFT-3</u> <u>(lb)</u>	<u>AFFT-4</u> <u>(lb)</u>
Motor Case Assembly	16.80	16.10
Fin Assembly	1.70	1.70
Fin Retaining Screws	0.03	0.03
Propellant Grain Assembly	43.44	42.63
Retaining Sleeve and Module Housing	2.12	2.12
Mechanical Timer Assembly	0.70	0.70
Redundant Initiator Unit	0.31	0.31
Primary Modular Charge	2.08	2.09
Sheet Explosive and Overwrap	<u>2.29</u>	<u>2.32</u>
Total Vehicle Weight (Less Payload)	69.47	68.00

The systems vehicle AFFT-3 was fitted with an inert parachute section and an Arcasonde 1A telemetry payload. The payload was of the same weight and center of gravity location as the actual Arcasonde system, but an inert parachute section was utilized since payload ejection was not planned during the first fragmentation systems flight test. The payload was retained intentionally to provide a back-up method of detecting fragmentation in the event radar track of the vehicle was lost.

II. FLIGHT TEST AFFT-3

Since payload ejection was not planned with the first of two fragmentation systems vehicles and because some difficulty was experienced with one of the mechanical timers, the vehicle AFFT-3 was selected to evaluate the redundant initiator system. The primary objectives of the flight, therefore, were:

- a. To demonstrate vehicle fragmentation using the redundant initiator system.
- b. To evaluate the aerodynamic performance of the systems vehicle.

A. RESULTS

The flight test AFFT-3 was completed 19 May from the meteorological rocket launch complex at PMR's San Nicolas Island test site. Launcher settings and the effective azimuth and elevation angles for the flight are tabulated below:

	<u>Actual (degree)</u>	<u>Effective (degree)</u>
Launcher Elevation Setting	86	80.5
Launcher Azimuth Setting	263	290

Aerodynamic performance of the vehicle was satisfactory and radar track was maintained throughout the flight beginning at T + 18 seconds. Radar data, however, showed an abnormally low apogee altitude of about

69,000 feet as compared to the expected apogee of 135,000 feet and no evidence of fragmentation was indicated.

A post-test inspection of the launcher showed the access port cover plate (see Figure 2) to have been ejected during launch. It should be noted that the launcher imparts an initial velocity to the vehicle by a piston action created by pressure generated by the exhaust gases of the rocket motor. The normal ejection velocity attained by this technique is 150 ft/sec. When an auxiliary gas generator cartridge is incorporated to increase the internal launcher pressure, the initial velocity of the vehicle is increased to about 230 ft/sec. An access port was incorporated in the launch tube for use with the Frangible ARCAS systems vehicles. Although the use of this port was not mandatory, it was incorporated as an additional safety feature to allow final commit-to-arm of the explosive fragmentation system while the vehicle is in the launch position, thereby precluding the necessity for additional handling of the vehicle. Exposure of this port during launch, however, resulted in loss of the internal pressure and a corresponding decrease in the initial velocity imparted to the vehicle. The decrease in initial launch velocity resulted in an appreciable decrease in apogee altitude for the vehicle. Examination of the access port cover strap showed the connector to have failed from the loads experienced during launch.

Failure to achieve fragmentation of the vehicle was directly attributable to the altitude profile attained. The redundant initiator required exposure to atmospheric pressures equivalent to an altitude of between 70,000 and 100,000 feet to become armed. Since the maximum altitude attained was only 69,000 feet, the system did not become armed.

An analysis of the flight data shows the performance attained to be the result of an abnormally low initial launch velocity induced by failure of the access port cover strap on the Government modified launch tube during liftoff.

B. FLIGHT DATA ANALYSIS

An analysis of the flight data was performed to determine the actual launch velocity experienced and confirm that its effect on vehicle performance was in agreement with the flight data obtained with the vehicle AFFT-3. Failure of the access port cover plate, however, introduced two unknown parameters into the analysis; namely (1) the actual launch velocity attained, and (2) the effective launch angle attained. In order to approximate the magnitude of initial launch velocity, V_0 , a series of trajectories at various effective launch angles were compared with the actual ballistic trajectory achieved.

Figures 3 through 6 present a comparison of the actual flight trajectory to predicted trajectories at various effective launch angles for initial launch velocities of 150, 100, 60, and 40 ft/sec, respectively. An analysis of Figure 3 shows the predicted line of apogee to approach the actual apogee attained with a decrease in effective launch angle, but the QE required to provide apogee agreement does not coincide with the QE attained. It was concluded, therefore, that an initial launch velocity less than 150 ft/sec was experienced since no value of QE provides agreement. An analysis of Figure 4 provides the same conclusion for an initial launch velocity of 100 ft/sec. Figures 5 and 6 show reasonable agreement for launch velocities of 60 and 40 ft/sec although the predicted apogee altitudes were not fully attained.

The actual trajectory is presented in Figures 7 through 9 in comparison with predicted trajectories of various launch velocity and fixed QE. An analysis of these plots shows that any one of the following combinations of V_0 and QE approximately agree with the flight data.

<u>Initial Launch Velocity</u> (ft/sec)		<u>Effective Launch Angle</u> (degree)
90	at	78
60	at	80
20	at	82

It was noted, however, that the actual apogee altitude achieved was consistently less than predicted for these conditions by about 10 to 15 per cent. It was further observed that the vehicle velocity-time relationship (Figure 10) and altitude-velocity relationship (Figure 11) were consistently below that predicted. Although these relationships are characteristic of an error in the drag data, the drag curve established for the vehicle configuration during the diagnostic flights were believed to be accurate. Any error experienced as a result of drag, therefore, could be evaluated with respect to drag reference area. Although the normal characteristic reference area is that of the body cross section, it was considered likely that the effective drag reference area characterizing the Frangible ARCAS vehicle may be increased because of turbulent flow conditions, skin friction or other factors influencing vehicle drag as related to the sheet explosive overwrap.

C. AFFT-3 CRITIQUE

A series of trajectories were computed with the drag reference area increased from 0.126 ft^2 to 0.151 ft^2 . Figures 12 through 15 show the effect of initial launch velocity on apogee altitude and impact range at various effective launch angles. Although reasonable agreements are obtained in all cases presented, the degree of error experienced increases with launch velocities above 60 ft/sec. An analysis of these trajectories shows the conditions which most satisfactorily agree with the flight data is an initial launch velocity of 60 ft/sec at a QE of 80.5 degrees. A plot of vehicle velocity versus flight time (Figure 16) and altitude versus velocity (Figure 17), also show reasonably good agreement. A further adjustment in drag reference area during the powered phase of flight would provide a more accurate agreement between predicted and actual data. However, the accuracy attained on the basis of this one flight was considered sufficient to show that the decrease in vehicle performance was attributed to loss of the access port cover plate during launch. The data generated by this analysis also provide sufficient agreement with the flight data, as tabulated below, to indicate that the initial launch velocity experienced with the vehicle AFFT-3 was about 60 ft/sec.

	<u>Predicted</u>	<u>Actual</u>	<u>Per Cent Error</u>
Apogee Altitude, ft	70,000	68,602	-2.00
Apogee Range, ft	66,000	64,156	-2.80
Impact Range, ft	110,000	105,300	-4.30
Time to Apogee, sec	71.0	70.6	-0.60
Burnout Velocity, ft/sec	2660	2540	-4.50
Time to Impact, sec	157	159	+1.28

D. CONCLUSIONS

1. Although the AFFT-3 flight data analysis and critique showed the vehicle to have an apparent effective drag reference area somewhat greater than originally predicted, it provided conclusive evidence that the actual initial launch velocity experienced was only about 60 ft/sec as compared to the expected velocity of 230 ft/sec. Furthermore, the critique data showed the actual vehicle performance with a 60 ft/sec launch velocity to be as anticipated.

2. The launch parameters predicted and attained were:

	<u>Actual</u>	<u>Effective Predicted</u>	<u>Effective Attained</u>
Launcher Elevation Setting, deg	86	80.5	80.5
Launcher Azimuth Setting, deg	263	290	280
Launcher Velocity, ft/sec		230	60

III. FLIGHT TEST AFFT-4

This unit was the second and final systems vehicle to be flight tested in the program. It incorporated both the primary and the redundant fragmentation initiation systems. The payload consisted of a standard Arcasonde 1A telemetry package and a 15-foot diameter silk parachute with a nonreflective surface finish. A nonreflective parachute was used to aid in radar tracking of the spent rocket motor assembly after payload ejection since radar data was to be used for determining the fragmentation event.

Determination of successful payload ejection was to be determined primarily by GMD-1 tracking of the payload telemetry signal during descent.

The primary objective of this final flight test was to demonstrate the feasibility of a frangible meteorological rocket system, which was also the primary objective of the program. Secondary objectives of this flight were to evaluate general flight performance and aerodynamic characteristics of the systems vehicle.

A. RESULTS

The final flight test AFFT-4 was completed 21 December, 1965 at the meteorological rocket launch complex at PMR's San Nicolas Island test site. Radar data showed normal flight performance through an apogee altitude of 130,000 feet at which time payload ejection was observed. The payload telemetry signal was lost during vehicle ascent, consequently no GMD-1 data were obtained during payload descent. However, successful payload ejection was determined by both radar observation and physical recovery of the payload. Failure of the GMD-1 to maintain track is not readily apparent. It should be noted that the recovered payload was tested and found to function properly. Successful radar tracking of the descending rocket motor assembly was maintained after payload ejection.

Fragmentation was induced by the primary system (mechanical timer unit) at about $T + 121$ seconds at an altitude of 123,000 feet, or payload ejection plus 20 seconds, as programmed. One piece, undoubtedly the nozzle/fin section of the motor assembly, was tracked to impact at approximately the normal descent velocity. With the exception of this piece which was not expected to fragment, radar observation showed a "cloud" of particles with varying descent rates. Radar track of various pieces was maintained and the "cloud" was observed to disperse as it descended. Except for the extreme aft end of the vehicle, which was not prepared for fragmentation on this final unit, all indications were that the degree of fragmentation attained was the same as that achieved during tests conducted earlier in the program; i.e., less than 3.0 ft-lb of impact kinetic energy.

B. FLIGHT DATA ANALYSIS

An analysis of the flight data was conducted to compare the actual flight performance with that predicted. A plot of the actual trajectory profile is shown on Figure 18 in comparison with the predicted curves at various effective launch angles. This comparison shows good agreement between the actual and predicted data, which was based on an increased drag reference area as determined from the previous flight, AFFT-3. As observed from this comparison, the effective launch angle was 84.9 degrees and the flight data shows that the apogee altitude achieved was only about 1.8 per cent greater than that predicted. A comparison of actual and predicted vehicle velocity on Figure 19 shows the flight unit to lag the velocity profile predicted for a nominal burning time of 30 seconds. It should be noted, however, that the flight data show an actual burning time of about 33 seconds and a maximum velocity close to that predicted.

An increased motor burning time, which is characteristic of a conditioning temperature less than the 70°F nominal, produces a corresponding decrease in thrust. This condition is further characterized by the lag experienced in the vehicle velocity-altitude comparison shown on Figure 20.

The longer-than-nominal burning time was confirmed by comparing the actual vehicle velocity profile to that predicted for a 33-second burning time, Figure 19. Good agreement in all aspects of flight performance was achieved when the 33-second burning time was considered. It should be noted that this burning time corresponds to a conditioning temperature of about 40°F. A tabulation of predicted and actual flight parameters is presented below:

<u>Parameter</u>	<u>Burning time = 33 sec</u>	
	<u>Predicted</u>	<u>Actual^a</u>
Burnout Velocity, ft/sec	2867	2750
Burnout Altitude, ft	48,470	49,000
Apogee Altitude, ft	129,800	129,700
Apogee Range, ft	47,580	45,000
Time to Apogee, sec	102	101

a. AFFT-4 Radar Data.

A tabulation of vehicle performance data for a burning time of 33 seconds is presented on Table I. The actual trajectory profile for flight AFFT-4 showing the sequence of events and track of several fragmented particles is presented on Figure 21.

C. CONCLUSIONS

Ejection of the access port door from the launch tube during flight AFFT-3 provided an ejection velocity of only about 60 ft/sec and resulted in a significant reduction of vehicle performance. Although the flight was considered a "No Test," the increase in vehicle drag characteristics derived from the flight data provided accurate predicted performance for the second systems vehicle.

Flight performance of the second and final systems vehicle (Flight AFFT-4) was close to that predicted considering the 33-second burning time experienced. The 33-second burning time was attributed to a motor conditioning temperature of about 40°F.

The successful performance of the systems flight test vehicle AFFT-4 demonstrated the feasibility of a frangible meteorological rocket vehicle. Radar data indicated fragmentation as programmed.

Table I.

INITIAL TRAJECTORY PARAMETER VALUES									
TRAJECTORY NO. 1									
STAGE 1 MISSILE PARAMETERS									
STAGE 2 MISSILE PARAMETERS									
STAGE 3 MISSILE PARAMETERS									
STAGE 4 MISSILE PARAMETERS									
STAGE 5 MISSILE PARAMETERS									
STAGE 6 MISSILE PARAMETERS									
STAGE 7 MISSILE PARAMETERS									
STAGE 8 MISSILE PARAMETERS									
STAGE 9 MISSILE PARAMETERS									
STAGE 10 MISSILE PARAMETERS									
STAGE 11 MISSILE PARAMETERS									
STAGE 12 MISSILE PARAMETERS									
STAGE 13 MISSILE PARAMETERS									
STAGE 14 MISSILE PARAMETERS									
STAGE 15 MISSILE PARAMETERS									
STAGE 16 MISSILE PARAMETERS									
STAGE 17 MISSILE PARAMETERS									
STAGE 18 MISSILE PARAMETERS									
STAGE 19 MISSILE PARAMETERS									
STAGE 20 MISSILE PARAMETERS									
STAGE 21 MISSILE PARAMETERS									
STAGE 22 MISSILE PARAMETERS									
STAGE 23 MISSILE PARAMETERS									
STAGE 24 MISSILE PARAMETERS									
STAGE 25 MISSILE PARAMETERS									
STAGE 26 MISSILE PARAMETERS									
STAGE 27 MISSILE PARAMETERS									
STAGE 28 MISSILE PARAMETERS									
STAGE 29 MISSILE PARAMETERS									
STAGE 30 MISSILE PARAMETERS									
STAGE 31 MISSILE PARAMETERS									
STAGE 32 MISSILE PARAMETERS									
STAGE 33 MISSILE PARAMETERS									
STAGE 34 MISSILE PARAMETERS									
STAGE 35 MISSILE PARAMETERS									
STAGE 36 MISSILE PARAMETERS									
STAGE 37 MISSILE PARAMETERS									
STAGE 38 MISSILE PARAMETERS									
STAGE 39 MISSILE PARAMETERS									
STAGE 40 MISSILE PARAMETERS									
STAGE 41 MISSILE PARAMETERS									
STAGE 42 MISSILE PARAMETERS									
STAGE 43 MISSILE PARAMETERS									
STAGE 44 MISSILE PARAMETERS									
STAGE 45 MISSILE PARAMETERS									
STAGE 46 MISSILE PARAMETERS									
STAGE 47 MISSILE PARAMETERS									
STAGE 48 MISSILE PARAMETERS									
STAGE 49 MISSILE PARAMETERS									
STAGE 50 MISSILE PARAMETERS									
STAGE 51 MISSILE PARAMETERS									
STAGE 52 MISSILE PARAMETERS									
STAGE 53 MISSILE PARAMETERS									
STAGE 54 MISSILE PARAMETERS									
STAGE 55 MISSILE PARAMETERS									
STAGE 56 MISSILE PARAMETERS									
STAGE 57 MISSILE PARAMETERS									
STAGE 58 MISSILE PARAMETERS									
STAGE 59 MISSILE PARAMETERS									
STAGE 60 MISSILE PARAMETERS									
STAGE 61 MISSILE PARAMETERS									
STAGE 62 MISSILE PARAMETERS									
STAGE 63 MISSILE PARAMETERS									
STAGE 64 MISSILE PARAMETERS									
STAGE 65 MISSILE PARAMETERS									
STAGE 66 MISSILE PARAMETERS									
STAGE 67 MISSILE PARAMETERS									
STAGE 68 MISSILE PARAMETERS									
STAGE 69 MISSILE PARAMETERS									
STAGE 70 MISSILE PARAMETERS									
STAGE 71 MISSILE PARAMETERS									
STAGE 72 MISSILE PARAMETERS									
STAGE 73 MISSILE PARAMETERS									
STAGE 74 MISSILE PARAMETERS									
STAGE 75 MISSILE PARAMETERS									
STAGE 76 MISSILE PARAMETERS									
STAGE 77 MISSILE PARAMETERS									
STAGE 78 MISSILE PARAMETERS									
STAGE 79 MISSILE PARAMETERS									
STAGE 80 MISSILE PARAMETERS									
STAGE 81 MISSILE PARAMETERS									
STAGE 82 MISSILE PARAMETERS									
STAGE 83 MISSILE PARAMETERS									
STAGE 84 MISSILE PARAMETERS									
STAGE 85 MISSILE PARAMETERS									
STAGE 86 MISSILE PARAMETERS									
STAGE 87 MISSILE PARAMETERS									
STAGE 88 MISSILE PARAMETERS									
STAGE 89 MISSILE PARAMETERS									
STAGE 90 MISSILE PARAMETERS									
STAGE 91 MISSILE PARAMETERS									
STAGE 92 MISSILE PARAMETERS									
STAGE 93 MISSILE PARAMETERS									
STAGE 94 MISSILE PARAMETERS									
STAGE 95 MISSILE PARAMETERS									
STAGE 96 MISSILE PARAMETERS									
STAGE 97 MISSILE PARAMETERS									
STAGE 98 MISSILE PARAMETERS									
STAGE 99 MISSILE PARAMETERS									
STAGE 100 MISSILE PARAMETERS									
STAGE 101 MISSILE PARAMETERS									
STAGE 102 MISSILE PARAMETERS									
STAGE 103 MISSILE PARAMETERS									
STAGE 104 MISSILE PARAMETERS									
STAGE 105 MISSILE PARAMETERS									
STAGE 106 MISSILE PARAMETERS									
STAGE 107 MISSILE PARAMETERS									
STAGE 108 MISSILE PARAMETERS									
STAGE 109 MISSILE PARAMETERS									
STAGE 110 MISSILE PARAMETERS									
STAGE 111 MISSILE PARAMETERS									
STAGE 112 MISSILE PARAMETERS									
STAGE 113 MISSILE PARAMETERS									
STAGE 114 MISSILE PARAMETERS									
STAGE 115 MISSILE PARAMETERS									
STAGE 116 MISSILE PARAMETERS									
STAGE 117 MISSILE PARAMETERS									
STAGE 118 MISSILE PARAMETERS									
STAGE 119 MISSILE PARAMETERS									
STAGE 120 MISSILE PARAMETERS									
STAGE 121 MISSILE PARAMETERS									
STAGE 122 MISSILE PARAMETERS									
STAGE 123 MISSILE PARAMETERS									
STAGE 124 MISSILE PARAMETERS									
STAGE 125 MISSILE PARAMETERS									
STAGE 126 MISSILE PARAMETERS									
STAGE 127 MISSILE PARAMETERS									
STAGE 128 MISSILE PARAMETERS									
STAGE 129 MISSILE PARAMETERS									
STAGE 130 MISSILE PARAMETERS									
STAGE 131 MISSILE PARAMETERS									
STAGE 132 MISSILE PARAMETERS									
STAGE 133 MISSILE PARAMETERS									
STAGE 134 MISSILE PARAMETERS									
STAGE 135 MISSILE PARAMETERS									
STAGE 136 MISSILE PARAMETERS									
STAGE 137 MISSILE PARAMETERS									
STAGE 138 MISSILE PARAMETERS									
STAGE 139 MISSILE PARAMETERS									
STAGE 140 MISSILE PARAMETERS									
STAGE 141 MISSILE PARAMETERS									
STAGE 142 MISSILE PARAMETERS									
STAGE 143 MISSILE PARAMETERS									
STAGE 144 MISSILE PARAMETERS									
STAGE 145 MISSILE PARAMETERS									
STAGE 146 MISSILE PARAMETERS									
STAGE 147 MISSILE PARAMETERS									
STAGE 148 MISSILE PARAMETERS									
STAGE 149 MISSILE PARAMETERS									
STAGE 150 MISSILE PARAMETERS									
STAGE 151 MISSILE PARAMETERS									
STAGE 152 MISSILE PARAMETERS									
STAGE 153 MISSILE PARAMETERS									
STAGE 154 MISSILE PARAMETERS									
STAGE 155 MISSILE PARAMETERS									
STAGE 156 MISSILE PARAMETERS									
STAGE 157 MISSILE PARAMETERS									
STAGE 158 MISSILE PARAMETERS									
STAGE 159 MISSILE PARAMETERS									
STAGE 160 MISSILE PARAMETERS									
STAGE 161 MISSILE PARAMETERS									
STAGE 162 MISSILE PARAMETERS									
STAGE 163 MISSILE PARAMETERS									
STAGE 164 MISSILE PARAMETERS									
STAGE 165 MISSILE PARAMETERS									
STAGE 166 MISSILE PARAMETERS									
STAGE 167 MISSILE PARAMETERS									
STAGE 168 MISSILE PARAMETERS									
STAGE 169 MISSILE PARAMETERS									
STAGE 170 MISSILE PARAMETERS									
STAGE 171 MISSILE PARAMETERS									
STAGE 172 MISSILE PARAMETERS									
STAGE 173 MISSILE PARAMETERS									
STAGE 174 MISSILE PARAMETERS									
STAGE 175 MISSILE PARAMETERS									
STAGE 176 MISSILE PARAMETERS									
STAGE 177 MISSILE PARAMETERS									
STAGE 178 MISSILE PARAMETERS									
STAGE 179 MISSILE PARAMETERS									
STAGE 180 MISSILE PARAMETERS									
STAGE 181 MISSILE PARAMETERS									
STAGE 182 MISSILE PARAMETERS									
STAGE 183 MISSILE PARAMETERS									
STAGE 184 MISSILE PARAMETERS									
STAGE 185 MISSILE PARAMETERS									
STAGE 186 MISSILE PARAMETERS									
STAGE 187 MISSILE PARAMETERS									
STAGE 188 MISSILE PARAMETERS									
STAGE 189 MISSILE PARAMETERS									
STAGE 190 MISSILE PARAMETERS									
STAGE 191 MISSILE PARAMETERS									
STAGE 192 MISSILE PARAMETERS									
STAGE 193 MISSILE PARAMETERS									
STAGE 194 MISSILE PARAMETERS									
STAGE 195 MISSILE PARAMETERS									
STAGE 196 MISSILE PARAMETERS									
STAGE 197 MISSILE PARAMETERS									
STAGE 198 MISSILE PARAMETERS									
STAGE 199 MISSILE PARAMETERS									
STAGE 200 MISSILE PARAMETERS									
STAGE 201 MISSILE PARAMETERS									
STAGE 202 MISSILE PARAMETERS									
STAGE 203 MISSILE PARAMETERS									
STAGE 204 MISSILE PARAMETERS									
STAGE 205 MISSILE PARAMETERS									
STAGE 206 MISSILE PARAMETERS									
STAGE 207 MISSILE PARAMETERS									
STAGE 208 MISSILE PARAMETERS									
STAGE 209 MISSILE PARAMETERS									
STAGE 210 MISSILE PARAMETERS									
STAGE 211 MISSILE PARAMETERS									
STAGE 212 MISSILE PARAMETERS									
STAGE 213 MISSILE PARAMETERS									
STAGE 214 MISSILE PARAMETERS									
STAGE 215 MISSILE PARAMETERS									
STAGE 216 MISSILE PARAMETERS									
STAGE 217 MISSILE PARAMETERS									
STAGE 218 MISSILE PARAMETERS									
STAGE 219 MISSILE PARAMETERS									
STAGE 220 MISSILE PARAMETERS									
STAGE 221 MISSILE PARAMETERS									
STAGE 222 MISSILE PARAMETERS									
STAGE 223 MISSILE PARAMETERS									
STAGE 224 MISSILE PARAMETERS									
STAGE 225 MISSILE PARAMETERS									
STAGE 226 MISSILE PARAMETERS									
STAGE 227 MISSILE PARAMETERS									
STAGE 228 MISSILE PARAMETERS									
STAGE 229 MISSILE PARAMETERS									
STAGE 230 MISSILE PARAMETERS									
STAGE 231 MISSILE PARAMETERS									
STAGE 232 MISSILE PARAMETERS									
STAGE 233 MISSILE PARAMETERS									
STAGE 234 MISSILE PARAMETERS									
STAGE 235 MISSILE PARAMETERS									
STAGE 236 MISSILE PARAMETERS									
STAGE 237 MISSILE PARAMETERS									
STAGE 238 MISSILE PARAMETERS									
STAGE 239 MISSILE PARAMETERS									
STAGE 240 MISSILE PARAMETERS									
STAGE 241 MISSILE PARAMETERS									
STAGE 242 MISSILE PARAMETERS									
STAGE 243 MISSILE PARAMETERS									
STAGE 244 MISSILE PARAMETERS									
STAGE 245 MISSILE PARAMETERS									
STAGE 246 MISSILE PARAMETERS									
STAGE 247 MISSILE PARAMETERS									
STAGE 248 MISSILE PARAMETERS									
STAGE 249 MISSILE PARAMETERS									
STAGE 250 MISSILE PARAMETERS									
STAGE 251 MISSILE PARAMETERS									
STAGE 252 MISSILE PARAMETERS									
STAGE 253 MISSILE PARAMETERS									
STAGE 254 MISSILE PARAMETERS									
STAGE 255 MISSILE PARAMETERS									
STAGE 256 MISSILE PARAMETERS									
STAGE 257 MISSILE PARAMETERS									
STAGE 258 MISSILE PARAMETERS									
STAGE 259 MISSILE PARAMETERS									
STAGE 260 MISSILE PARAMETERS									
STAGE 261 MISSILE PARAMETERS									
STAGE 262 MISSILE PARAMETERS									
STAGE 263 MISSILE PARAMETERS									
STAGE 264 MISSILE PARAMETERS									
STAGE 265 MISSILE PARAMETERS									
STAGE 266 MISSILE PARAMETERS									
STAGE 267 MISSILE PARAMETERS									
STAGE 268 MISSILE PARAMETERS									
STAGE 269 MISSILE PARAMETERS									
STAGE 270 MISSILE PARAMETERS									
STAGE 271 MISSILE PARAMETERS									
STAGE 272 MISSILE PARAMETERS									
STAGE 273 MISSILE PARAMETERS									
STAGE 274 MISSILE PARAMETERS									
STAGE 275 MISSILE PARAMETERS									
STAGE 276 MISSILE PARAMETERS									
STAGE 277 MISSILE PARAMETERS									
STAGE 278 MISSILE PARAMETERS									
STAGE 279 MISSILE PARAMETERS									
STAGE 280 MISSILE PARAMETERS									
STAGE 281 MISSILE PARAMETERS									
STAGE 282 MISSILE PARAMETERS									
STAGE 283 MISSILE PARAMETERS									
STAGE 284 MISSILE PARAMETERS									
STAGE 285 MISSILE PARAMETERS									
STAGE 286 MISSILE PARAMETERS									
STAGE 287 MISSILE PARAMETERS									
STAGE 288 MISSILE PARAMETERS									
STAGE 289 MISSILE PARAMETERS									
STAGE 290 MISSILE PARAMETERS									
STAGE 291 MISSILE PARAMETERS									
STAGE 292 MISSILE PARAMETERS									
STAGE 293 MISSILE PARAMETERS									
STAGE 294 MISSILE PARAMETERS									
STAGE 295 MISSILE PARAMETERS									
STAGE 296 MISSILE PARAMETERS									
STAGE 297 MISSILE PARAMETERS									
STAGE 298 MISSILE PARAMETERS									
STAGE 299 MISSILE PARAMETERS									
STAGE 300 MISSILE PARAMETERS									
STAGE 301 MISSILE PARAMETERS									
STAGE 302 MISSILE PARAMETERS									
STAGE 303 MISSILE PARAMETERS									
STAGE 304 MISSILE PARAMETERS									
STAGE 305 MISSILE PARAMETERS									
STAGE 306 MISSILE PARAMETERS									
STAGE 307 MISSILE PARAMETERS									
STAGE 308 MISSILE PARAMETERS									
STAGE 309 MISSILE PARAMETERS									
STAGE 310 MISSILE PARAMETERS									
STAGE 311 MISSILE PARAMETERS									
STAGE 312 MISSILE PARAMETERS									
STAGE 313 MISSILE PARAMETERS									
STAGE 314 MISSILE PARAMETERS									
STAGE 315 MISSILE PARAMETERS									
STAGE 316 MISSILE PARAMETERS									
STAGE 317 MISSILE PARAMETERS									
STAGE 318 MISSILE PARAMETERS									
STAGE 319 MISSILE PARAMETERS									
STAGE 320 MISSILE PARAMETERS									
STAGE 321 MISSILE PARAMETERS									
STAGE 322 MISSILE PARAMETERS									
STAGE 323 MISSILE PARAMETERS									
STAGE 324 MISSILE PARAMETERS									
STAGE 325 MISSILE PARAMETERS									
STAGE 326 MISSILE PARAMETERS									
STAGE 327 MISSILE PARAMETERS									
STAGE 328 MISSILE PARAMETERS									
STAGE 329 MISSILE PARAMETERS									
STAGE 330 MISSILE PARAMETERS									
STAGE 331 MISSILE PARAMETERS									
STAGE 332 MISSILE PARAMETERS									
STAGE 333 MISSILE PARAMETERS									
STAGE 334 MISSILE PARAMETERS									
STAGE 335 MISSILE PARAMETERS									
STAGE 336 MISSILE PARAMETERS									
STAGE 337 MISSILE PARAMETERS									
STAGE 338 MISSILE PARAMETERS									
STAGE 339 MISSILE PARAMETERS									
STAGE 340 MISSILE PARAMETERS									
STAGE 341 MISSILE PARAMETERS									
STAGE 342 MISSILE PARAMETERS									
STAGE 343 MISSILE PARAMETERS									
STAGE 344 MISSILE PARAMETERS									
STAGE 345 MISSILE PARAMETERS									
STAGE 346 MISSILE PARAMETERS									
STAGE 347 MISSILE PARAMETERS									
STAGE 348 MISSILE PARAMETERS									
STAGE 349 MISSILE PARAMETERS									
STAGE 350 MISSILE PARAMETERS									
STAGE 351 MISSILE PARAMETERS									
STAGE 352 MISSILE PARAMETERS									
STAGE 353 MISSILE PARAMETERS									
STAGE 354 MISSILE PARAMETERS									
STAGE 355 MISSILE PARAMETERS									
STAGE 356 MISSILE PARAMETERS									
STAGE 357 MISSILE PARAMETERS									
STAGE 358 MISSILE PARAMETERS									
STAGE 359 MISSILE PARAMETERS									
STAGE 360 MISSILE PARAMETERS									
STAGE 361 MISSILE PARAMETERS									
STAGE 362 MISSILE PARAMETERS									
STAGE 363 MISSILE PARAMETERS									
STAGE 364 MISSILE PARAMETERS									
STAGE 365 MISSILE PARAMETERS									
STAGE 366 MISSILE PARAMETERS									
STAGE 367 MISSILE PARAMETERS									
STAGE 368 MISSILE PARAMETERS									
STAGE 369 MISSILE PARAMETERS									
STAGE 370 MISSILE PARAMETERS									
STAGE 371 MISSILE PARAMETERS									
STAGE 372 MISSILE PARAMETERS									
STAGE 373 MISSILE PARAMETERS									
STAGE 374 MISSILE PARAMETERS									
STAGE 375 MISSILE PARAMETERS									
STAGE 376 MISSILE PARAMETERS									
STAGE 377 MISSILE PARAMETERS									
STAGE 378 MISSILE PARAMETERS									
STAGE 379 MISSILE PARAMETERS									
STAGE 380 MISSILE PARAMETERS									
STAGE 381 MISSILE PARAMETERS									
STAGE 382 MISSILE PARAMETERS									
STAGE 383 MISSILE PARAMETERS									
STAGE 384 MISSILE PARAMETERS									
STAGE 385 MISSILE PARAMETERS									
STAGE 386 MISSILE PARAMETERS									
STAGE 387 MISSILE PARAMETERS									
STAGE 388 MISSILE PARAMETERS									
STAGE 389 MISSILE PARAMETERS									
STAGE 390 MISSILE PARAMETERS									
STAGE 391 MISSILE PARAMETERS									
STAGE 392 MISSILE PARAMETERS									
STAGE 393 MISSILE PARAMETERS									
STAGE 394 MISSILE PARAMETERS									
STAGE 395 MISSILE PARAMETERS									
STAGE 396 MISSILE PARAMETERS									
STAGE 397 MISSILE PARAMETERS									
STAGE 398 MISSILE PARAMETERS									
STAGE 399 MISSILE PARAMETERS									
STAGE 400 MISSILE PARAMETERS									
STAGE 401 MISSILE PARAMETERS									
STAGE 402 MISSILE PARAMETERS									
STAGE 403 MISSILE PARAMETERS									
STAGE 404 MISSILE PARAMETERS									
STAGE 405 MISSILE PARAMETERS									
STAGE 406 MISSILE PARAMETERS									
STAGE 407 MISSILE PARAMETERS									
STAGE 408 MISSILE PARAMETERS									
STAGE 409 MISSILE PARAMETERS									
STAGE 410 MISSILE PARAMETERS									
STAGE 411 MISSILE PARAMETERS									
STAGE 412 MISSILE PARAMETERS									
STAGE 413 MISSILE PARAMETERS									
STAGE 414 MISSILE PARAMETERS									
STAGE 415 MISSILE PARAMETERS									
STAGE 416 MISSILE PARAMETERS									
STAGE 417 MISSILE PARAMETERS									
STAGE 418 MISSILE PARAMETERS									
STAGE 419 MISSILE PARAMETERS									
STAGE 420 MISSILE PARAMETERS									
STAGE 421 MISSILE PARAMETERS									
STAGE 422 MISSILE PARAMETERS									
STAGE 423 MISSILE PARAMETERS									
STAGE 424 MISSILE PARAMETERS									
STAGE 425 MISSILE PARAMETERS									
STAGE 426 MISSILE PARAMETERS									
STAGE 427 MISSILE PARAMETERS									
STAGE 428 MISSILE PARAMETERS									
STAGE 429 MISSILE PARAMETERS									
STAGE 430 MISSILE PARAMETERS									
STAGE 431 MISSILE PARAMETERS									
STAGE 432 MISSILE PARAMETERS									
STAGE 433 MISSILE PARAMETERS									
STAGE 434 MISSILE PARAMETERS									
STAGE 435 MISSILE PARAMETERS									
STAGE 436 MISSILE PARAMETERS									
STAGE 437 MISSILE PARAMETERS									
STAGE 438 MISSILE PARAMETERS									
STAGE 439 MISSILE PARAMETERS									
STAGE 440 MISSILE PARAMETERS									
STAGE 441 MISSILE PARAMETERS									
STAGE 442 MISSILE PARAMETERS									
STAGE 443 MISSILE PARAMETERS									
STAGE 444 MISSILE PARAMETERS									
STAGE 445 MISSILE PARAMETERS									
STAGE 446 MISSILE PARAMETERS									
STAGE 447 MISSILE PARAMETERS									
STAGE 448 MISSILE PARAMETERS									
STAGE 449 MISSILE PARAMETERS									
STAGE 450 MISSILE PARAMETERS									
STAGE 451 MISSILE PARAMETERS									
STAGE 452 MISSILE PARAMETERS									
STAGE 453 MISSILE PARAMETERS									
STAGE 454 MISSILE PARAMETERS									
STAGE 455 MISSILE PARAMETERS									
STAGE 456 MISSILE PARAMETERS									
STAGE 457 MISSILE PARAMETERS									
STAGE 458 MISSILE PARAMETERS									
STAGE 459 MISSILE PARAMETERS									
STAGE 460 MISSILE PARAMETERS									
STAGE 461 MISSILE PARAMETERS									
STAGE 462 MISSILE PARAMETERS									
STAGE 463 MISSILE PARAMETERS									
STAGE 464 MISSILE PARAMETERS									
STAGE 465 MISSILE PARAMETERS									
STAGE 466 MISSILE PARAMETERS									
STAGE 467 MISSILE PARAMETERS									
STAGE 468 MISSILE PARAMETERS									
STAGE 469 MISSILE PARAMETERS									
STAGE 470 MISSILE PARAMETERS									
STAGE 471 MISSILE PARAMETERS									
STAGE 472 MISSILE PARAMETERS									
STAGE 473 MISSILE PARAMETERS									
STAGE 474 MISSILE PARAMETERS									
STAGE 475 MISSILE PARAMETERS									
STAGE 476 MISSILE PARAMETERS									
STAGE 477 MISSILE PARAMETERS									
STAGE 478 MISSILE PARAMETERS									
STAGE 479 MISSILE PARAMETERS									
STAGE 480 MISSILE PARAMETERS									
STAGE 481 MISSILE PARAMETERS									
STAGE 482 MISSILE PARAMETERS									
STAGE 483 MISSILE PARAMETERS									
STAGE 484 MISSILE PARAMETERS									
STAGE 485 MISSILE PARAMETERS									
STAGE 486 MISSILE PARAMETERS									
STAGE 487 MISSILE PARAMETERS									
STAGE 488 MISSILE PARAMETERS									
STAGE 489 MISSILE PARAMETERS									
STAGE 490 MISSILE PARAMETERS									
STAGE 491 MISSILE PARAMETERS									
STAGE 492 MISSILE PARAMETERS									
STAGE 493 MISSILE PARAMETERS									
STAGE 494 MISSILE PARAMETERS									
STAGE 495 MISSILE PARAMETERS									
STAGE 496 MISSILE PARAMETERS									
STAGE 497 MISSILE PARAMETERS									
STAGE 498 MISSILE PARAMETERS									
STAGE 499 MISSILE PARAMETERS									
STAGE 500 MISSILE PARAMETERS									
STAGE 501 MISSILE PARAMETERS									
STAGE 502 MISSILE PARAMETERS									
STAGE 503 MISSILE PARAMETERS									
STAGE 504 MISSILE PARAMETERS									
STAGE 505 MISSILE PARAMETERS									
STAGE 506 MISSILE PARAMETERS									
STAGE 507 MISSILE PARAMETERS									
STAGE 508 MISSILE PARAMETERS									
STAGE 509 MISSILE PARAMETERS									
STAGE 510 MISSILE PARAMETERS									
STAGE 511 MISSILE PARAMETERS									
STAGE 512 MISSILE PARAMETERS									
STAGE 513 MISSILE PARAMETERS									
STAGE 514 MISSILE PARAMETERS									
STAGE 515 MISSILE PARAMETERS									
STAGE 516 MISSILE PARAMETERS									
STAGE 517 MISSILE PARAMETERS									
STAGE 518 MISSILE PARAMETERS									
STAGE 519 MISSILE PARAMETERS									
STAGE 520 MISSILE PARAMETERS									
STAGE 521 MISSILE PARAMETERS									
STAGE 522 MISSILE PARAMETERS									
STAGE 523 MISSILE PARAMETERS									
STAGE 524 MISSILE PARAMETERS									
STAGE 525 MISSILE PARAMETERS									
STAGE 526 MISSILE PARAMETERS									
STAGE 527 MISSILE PARAMETERS									
STAGE 528 MISSILE PARAMETERS									
STAGE 529 MISSILE PARAMETERS									
STAGE 530 MISSILE PARAMETERS									
STAGE 531 MISSILE PARAMETERS									
STAGE 532 MISSILE PARAMETERS									
STAGE 533 MISSILE PARAMETERS									
STAGE 534 MISSILE PARAMETERS									
STAGE 535 MISSILE PARAMETERS									
STAGE 536 MISSILE PARAMETERS									
STAGE 537 MISSILE PARAMETERS									
STAGE 538 MISSILE PARAMETERS									
STAGE 539 MISSILE PARAMETERS									
STAGE 540 MISSILE PARAMETERS									
STAGE 541 MISSILE PARAMETERS									
STAGE 542 MISSILE PARAMETERS									
STAGE 543 MISSILE PARAMETERS									
STAGE 544 MISSILE PARAMETERS									
STAGE 545 MISSILE PARAMETERS									
STAGE 546 MISSILE PARAMETERS									
STAGE 547 MISSILE PARAMETERS									
STAGE 548 MISSILE PARAMETERS									
STAGE 549 MISSILE PARAMETERS									
STAGE 550 MISSILE PARAMETERS									
STAGE 551 MISSILE PARAMETERS									
STAGE 552 MISSILE PARAMETERS									
STAGE 553 MISSILE PARAMETERS									
STAGE 554 MISSILE PARAMETERS									
STAGE 555 MISSILE PARAMETERS									
STAGE 556 MISSILE PARAMETERS									
STAGE 557 MISSILE PARAMETERS									
STAGE 558 MISSILE PARAMETERS									
STAGE 559 MISSILE PARAMETERS									
STAGE 560 MISSILE PARAMETERS									
STAGE 561 MISSILE PARAMETERS									
STAGE 562 MISSILE PARAMETERS									
STAGE 563 MISSILE PARAMETERS									
STAGE 564 MISSILE PARAMETERS									
STAGE 565 MISSILE PARAMETERS									
STAGE 566 MISSILE PARAMETERS									

Table I. (Cont'd)

93.0000	-15.8	603.9	128432	29.64	42886	1.704, 00	.58	.0	35.90	.0023	2748.2
97.2000	-9.6	550.0	129406	17.47	45077	1.314, 00	.53	.0	35.90	.0018	2748.4
97.4000	-9.1	549.1	129438	16.83	45181	1.305, 00	.53	.0	35.90	.0018	2748.5
97.6000	-8.9	546.3	129469	16.20	45285	1.296, 00	.53	.0	35.90	.0017	2748.5
97.8000	-8.6	544.5	129499	15.55	45390	1.288, 00	.53	.0	35.90	.0017	2748.5
98.0000	-8.2	542.8	129527	14.91	45494	1.280, 00	.52	.0	35.90	.0017	2748.5
98.2000	-7.9	541.2	129555	14.26	45598	1.272, 00	.52	.0	35.90	.0017	2748.5
98.4000	-7.5	539.7	129581	13.61	45702	1.265, 00	.52	.0	35.90	.0017	2748.5
98.6000	-7.2	538.2	129606	12.95	45807	1.258, 00	.52	.0	35.90	.0017	2748.5
98.8000	-6.8	536.8	129629	12.29	45911	1.252, 00	.52	.0	35.90	.0017	2748.5
99.0000	-6.5	535.5	129651	11.62	46015	1.245, 00	.52	.0	35.90	.0017	2748.5
99.2500	-6.1	534.2	129672	10.96	46119	1.240, 00	.52	.0	35.90	.0017	2748.6
99.4000	-5.7	533.0	129692	10.29	46224	1.234, 00	.51	.0	35.90	.0017	2748.6
99.6000	-5.4	531.9	129710	9.61	46328	1.229, 00	.51	.0	35.90	.0017	2748.6
100.000	-4.6	529.9	129743	8.26	46536	1.220, 00	.51	.0	35.90	.0017	2748.5
100.600	-3.5	527.5	129783	6.21	46849	1.209, 00	.51	.0	35.90	.0016	2748.6
101.000	-2.7	526.3	129803	4.83	47057	1.203, 00	.51	.0	35.90	.0016	2748.7
101.600	-1.6	525.0	129824	2.76	47370	1.197, 00	.51	.0	35.90	.0016	2748.7
102.000	-.8	524.5	129832	1.37	47579	1.195, 00	.51	.0	35.90	.0016	2748.7
103.400	1.9	525.2	129818	-3.48	48308	1.202, 00	.51	.0	35.90	.0016	2748.8
105.40		532.8	129691		49350						

APPROX. CONDITIONS

Table I. (Cont'd)

TRAJECTORY NO. 1

FEB 8,66

TB = 33 SEC.

FRANGIBLE ARCAS

TIME THRUST MACH = CD

STAGE 1

.000	286.00	.000	.28600
32.000	286.00	.600	.29400
33.000	.00	.800	.30500
.000	.00	1.000	.39200
.000	.00	1.100	.58800
.060	.00	1.200	.61700
.000	.00	1.400	.60400
.000	.00	1.600	.56800
.000	.00	1.800	.53900
.000	.00	2.000	.50600
.000	.00	2.500	.43100
.000	.00	3.000	.36700
.000	.00	3.500	.32000
.000	.00	4.000	.29000
.000	.00	5.000	.24500
.000	.00	6.000	.21500
.000	.00	8.000	.21500

STAGE 2

.00	.286
.60	.294
.80	.305
1.00	.392
1.10	.588
1.20	.617
1.40	.604
1.60	.568
1.80	.539
2.00	.506
2.50	.431
3.00	.367
3.50	.320
4.00	.290
5.00	.245
6.00	.215
8.00	.215

Frangible ARCAS Forward Section Assembly

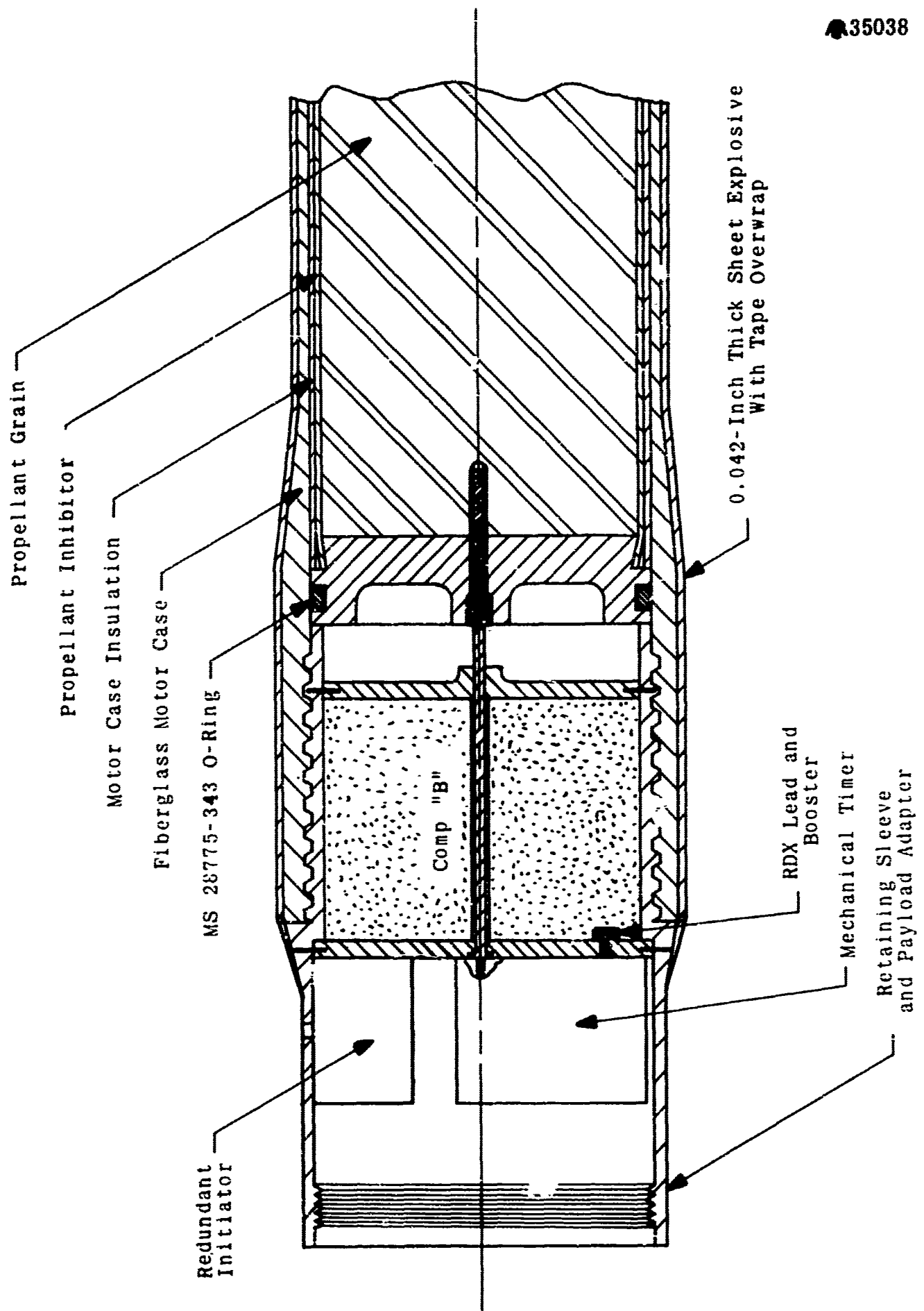


Figure 1

Illustration of Modification to the Standard ARCAS Launch Tube to Provide Access Port

2116

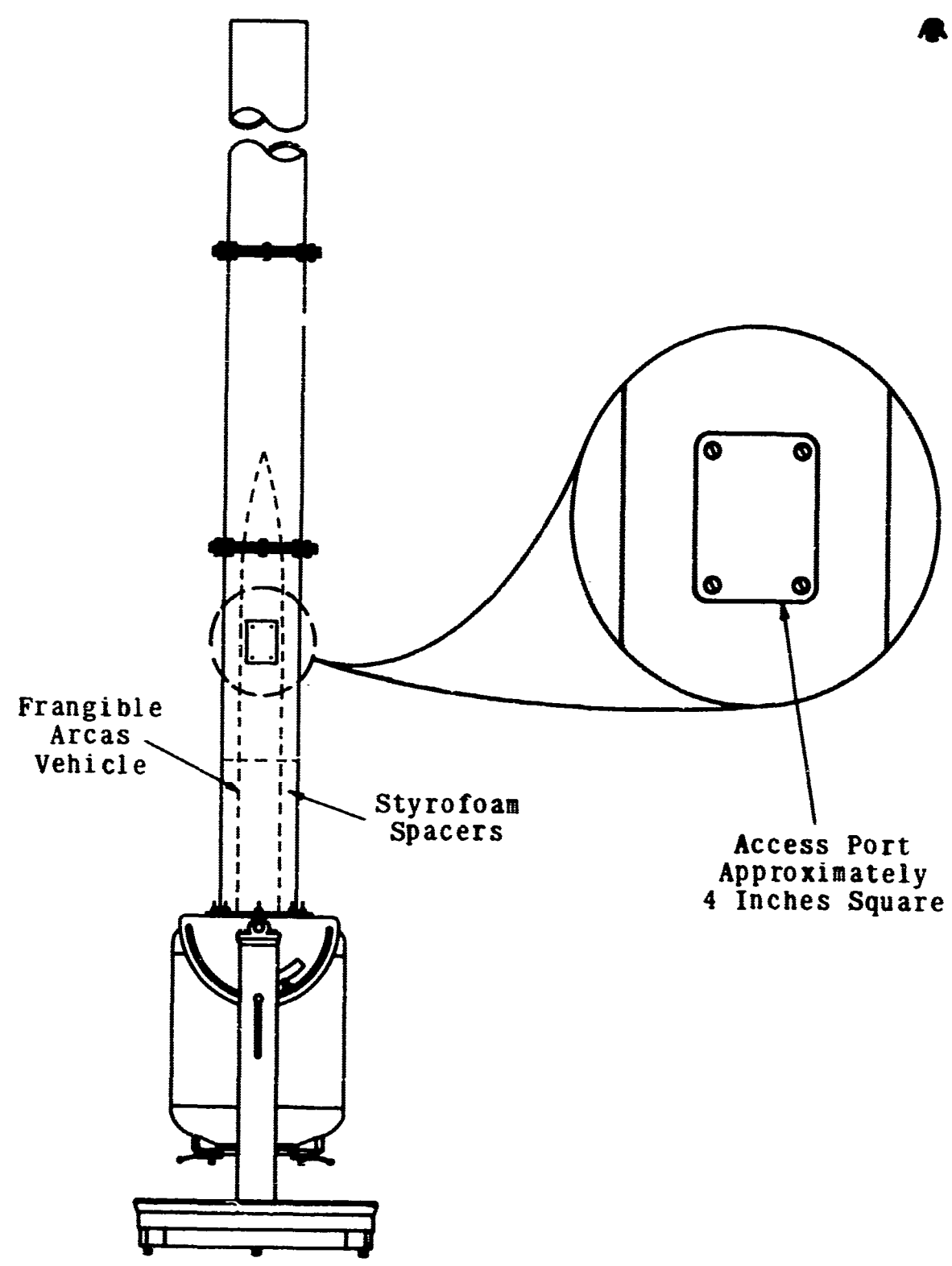


Figure 2

Frangible ARCAS Launcher Malfunction Critique Flight Test AFFT-3

5240

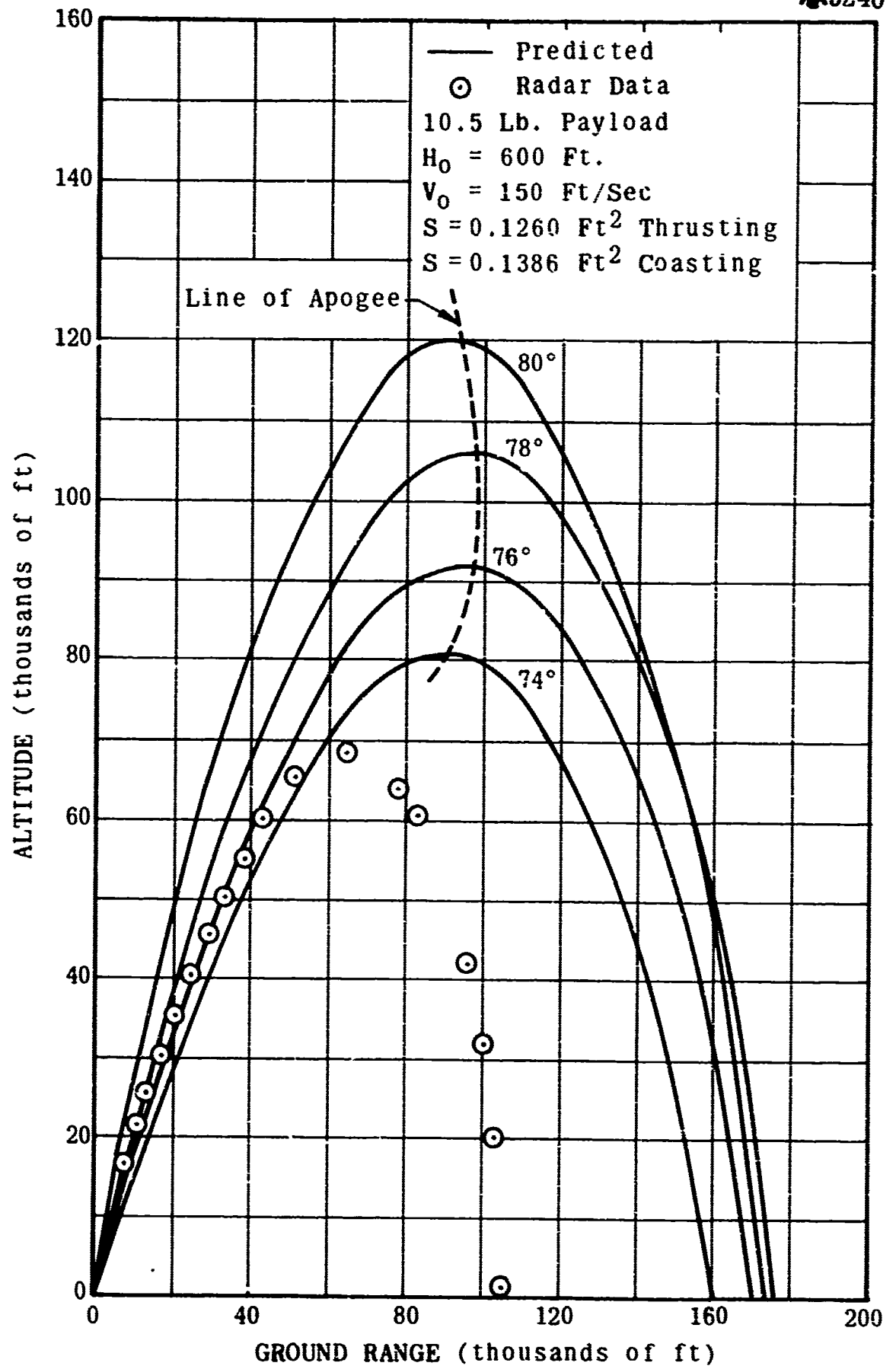


Figure 3

Frangible ARCAS Launcher Malfunction Critique Flight Test AFFT-3

5254

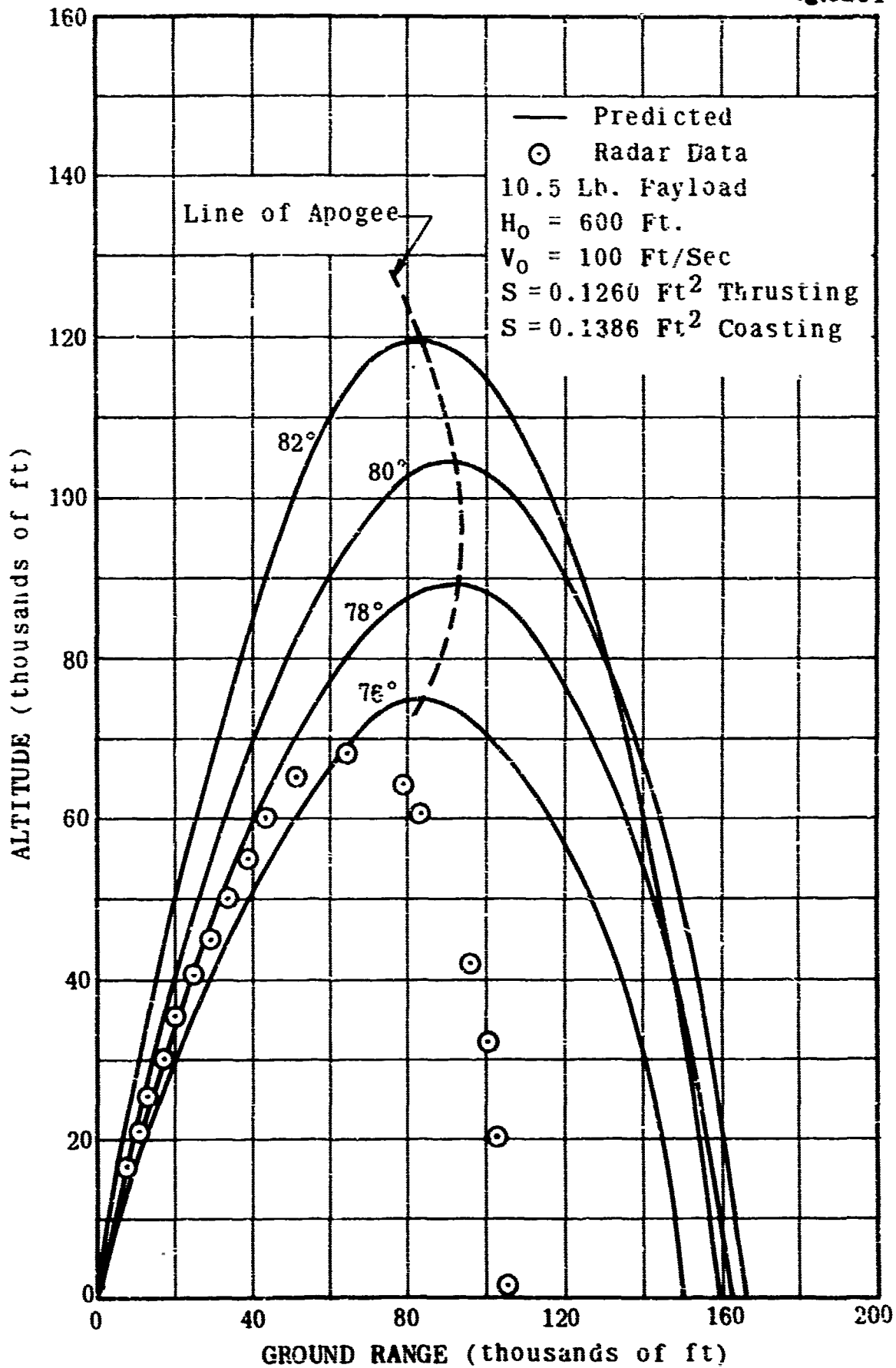


Figure 4

Frangible ARCAS Launcher Malfunction Critique Flight Test AFFT-3

5253

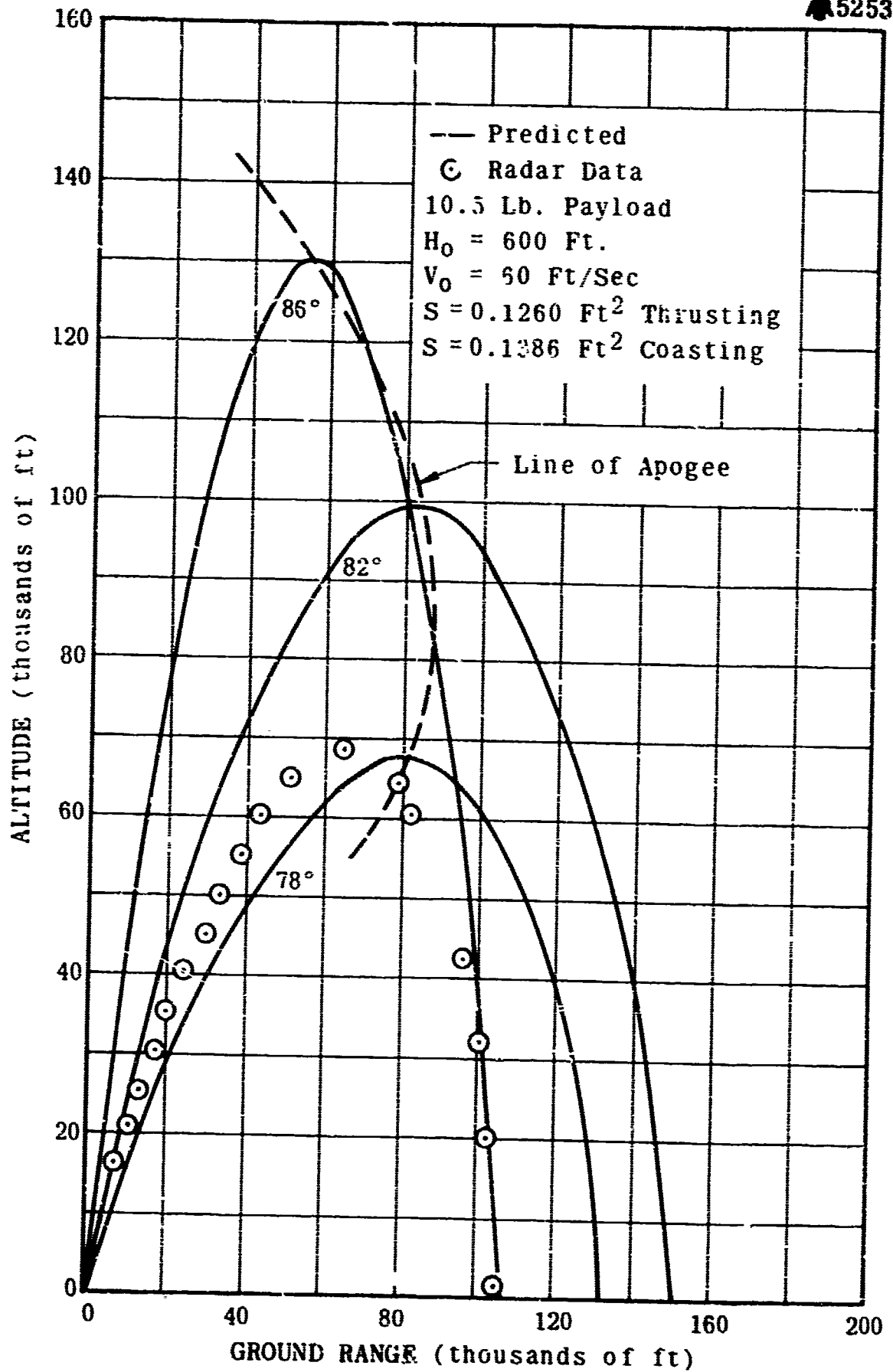


Figure 5

Frangible ARCAS Launcher Malfunction Critique Flight Test AFFT-3

5252

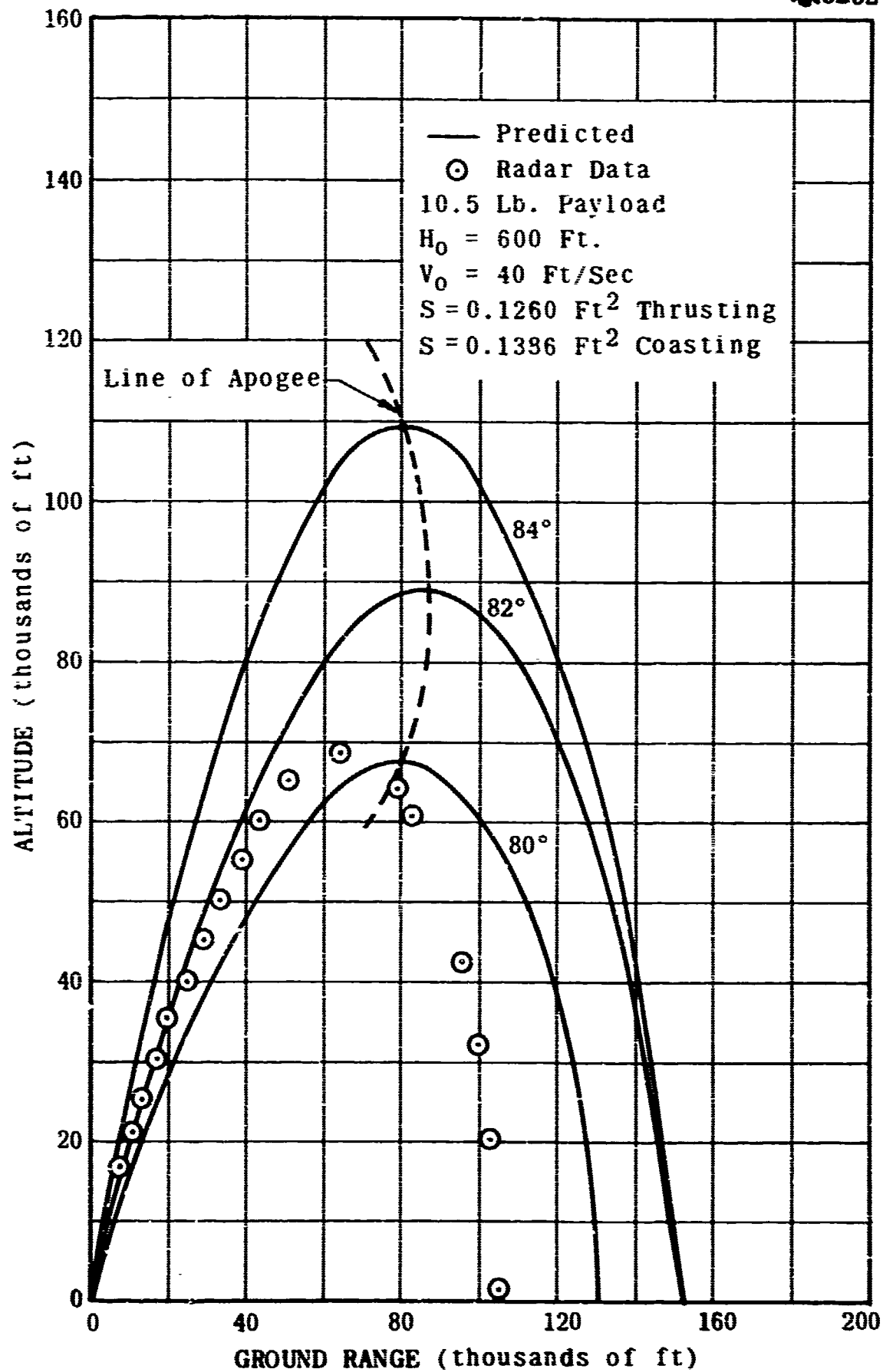


Figure 6

Frangible ARCAS Launcher Malfunction Critique Flight Test AFFT-3

5251

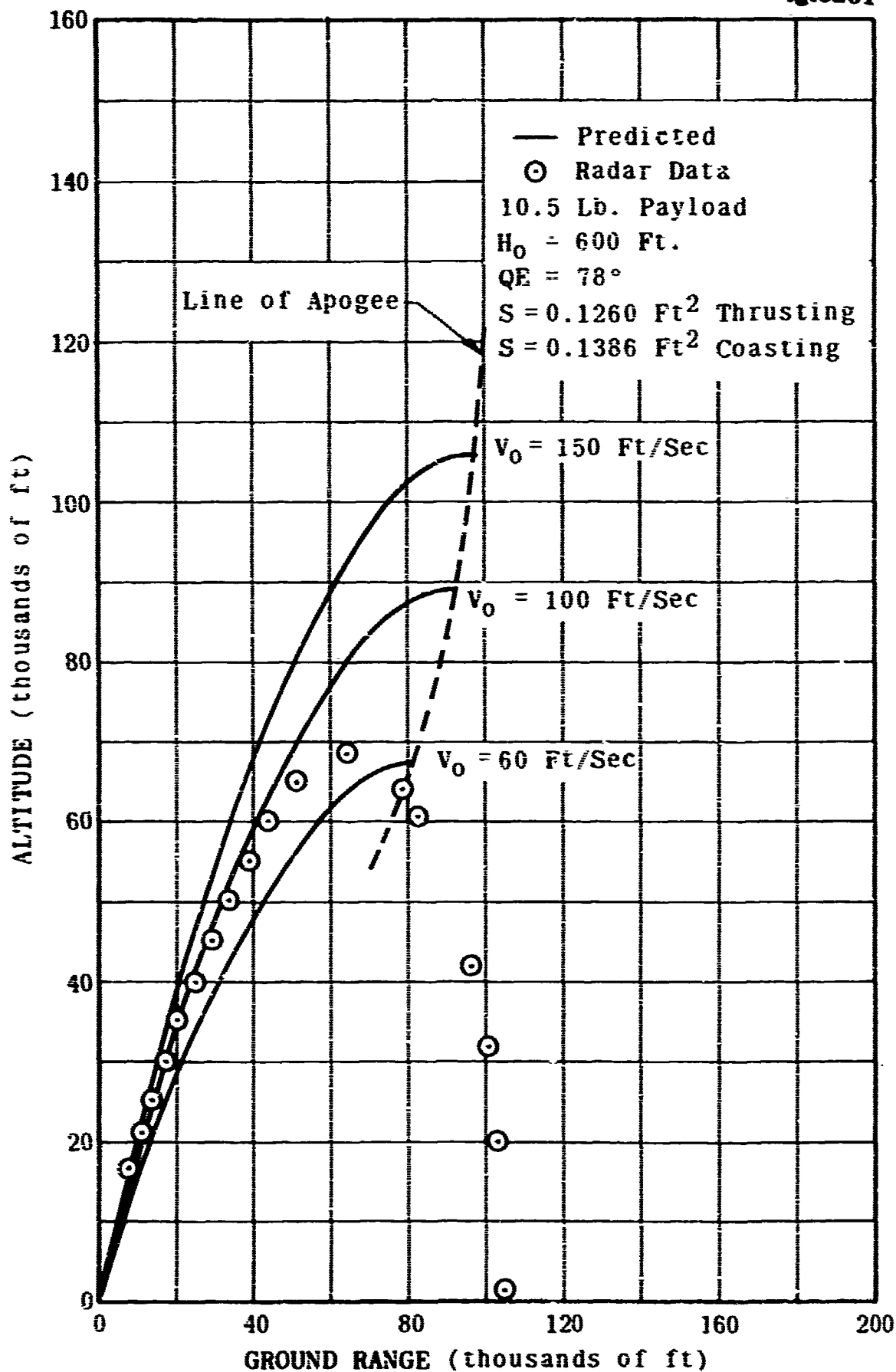


Figure 7

Frangible ARCAS Launcher Malfunction Critique Flight Test AFFT-3

5250

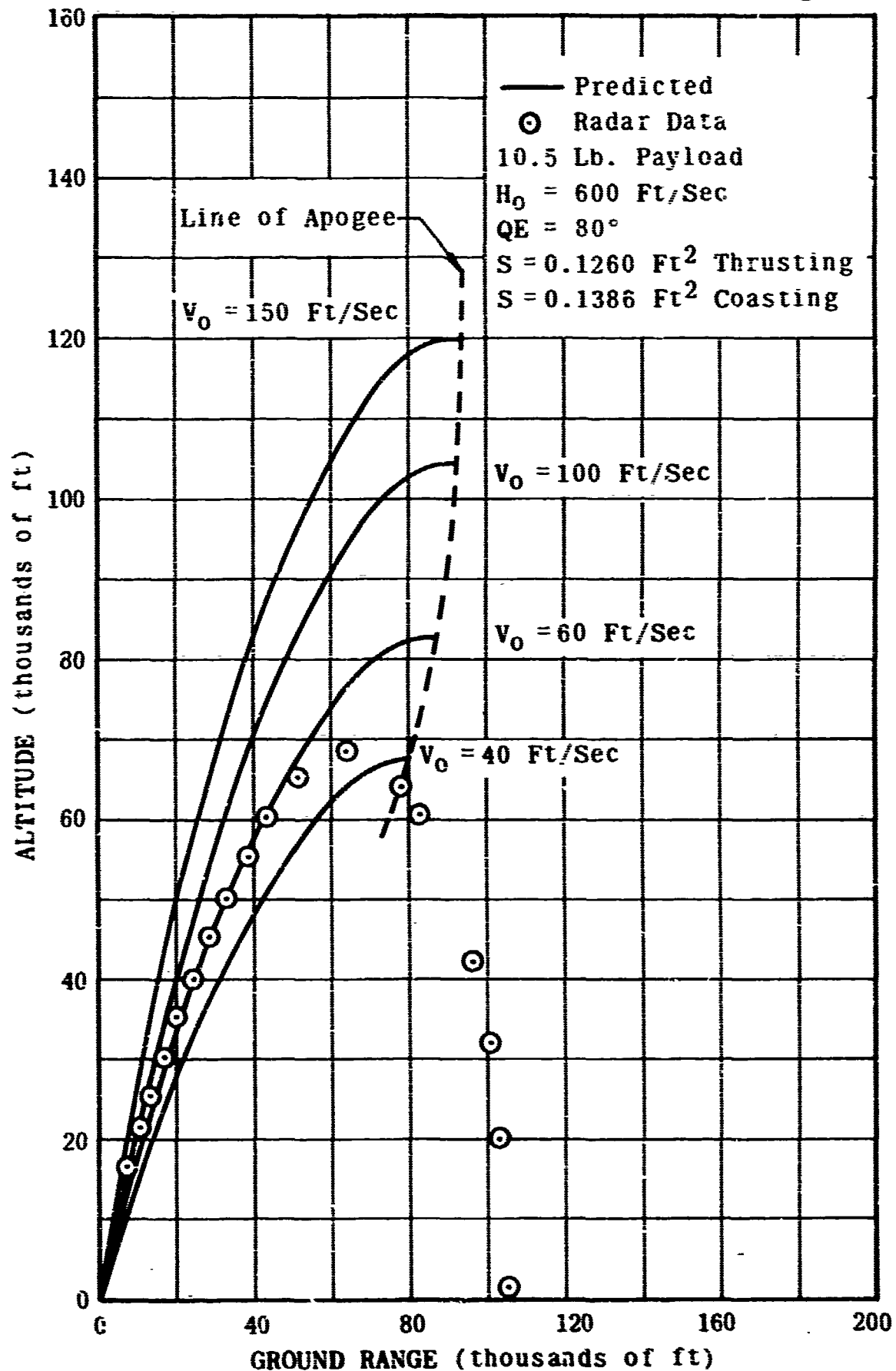


Figure 8

Frangible ARCAS Launcher Malfunction Critique Flight Test AFFT-3

5249

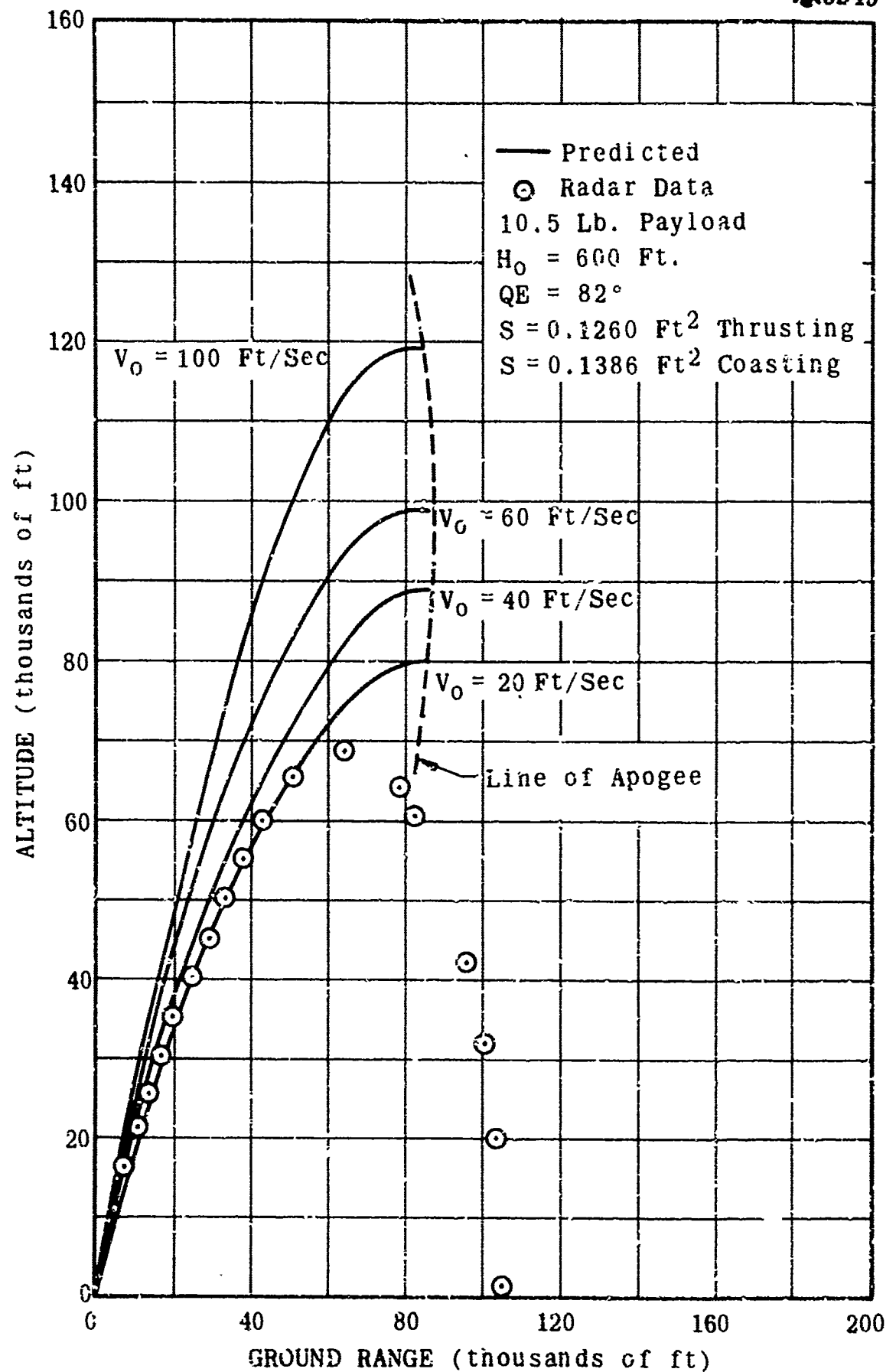


Figure 9

Frangible ARCAS Vehicle Velocity Versus Flight Time Flight Test AFFT-3

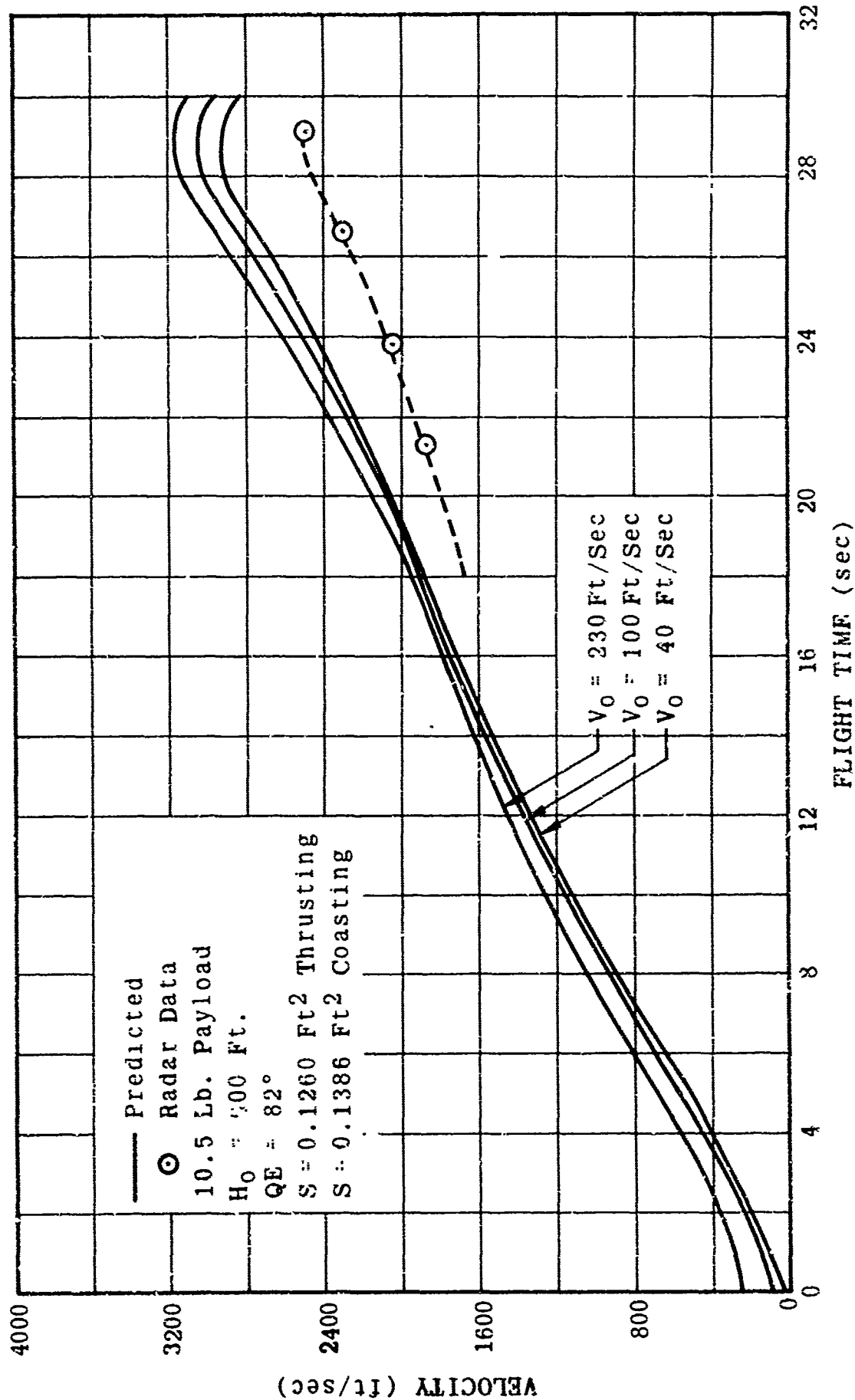


Figure 10

Frangible APCAS Launcher Malfunction Critique Flight Test AFFT-3

5241

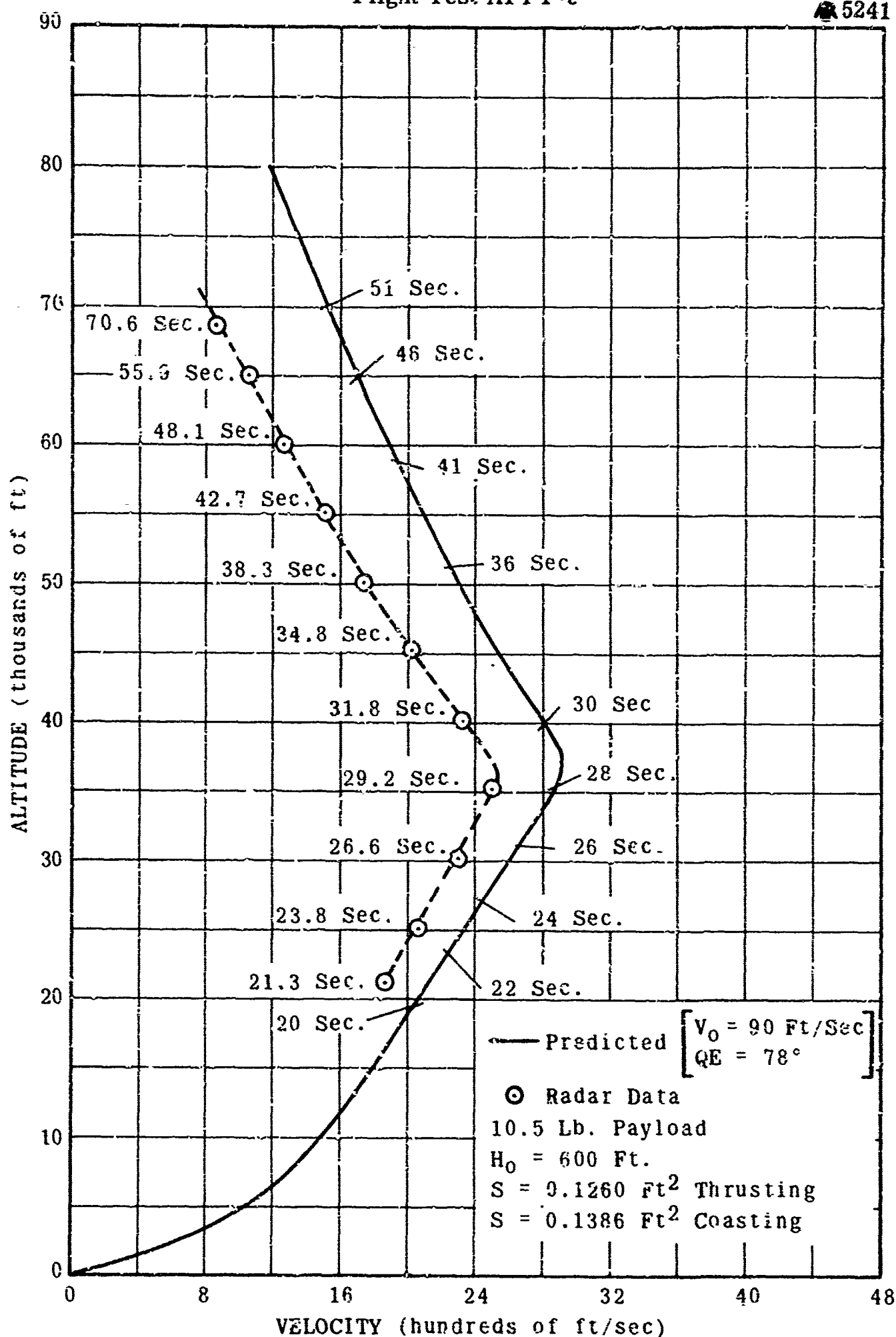


Figure 11

Frangible ARCAS Flight Test AFFT-3 Critique

5247

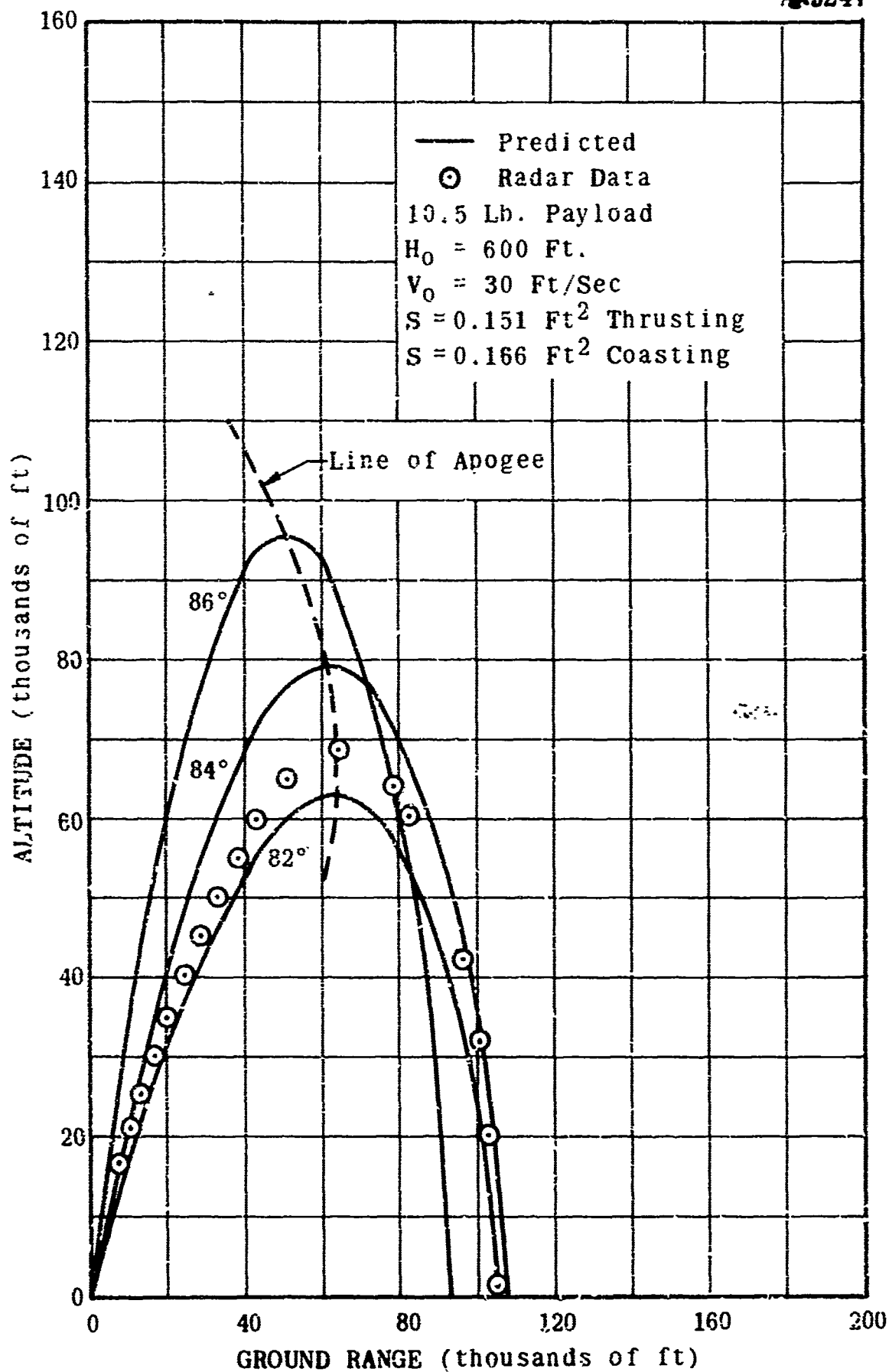


Figure 12

Frangible ARCAS Flight Test AFFT-3 Critique

5246

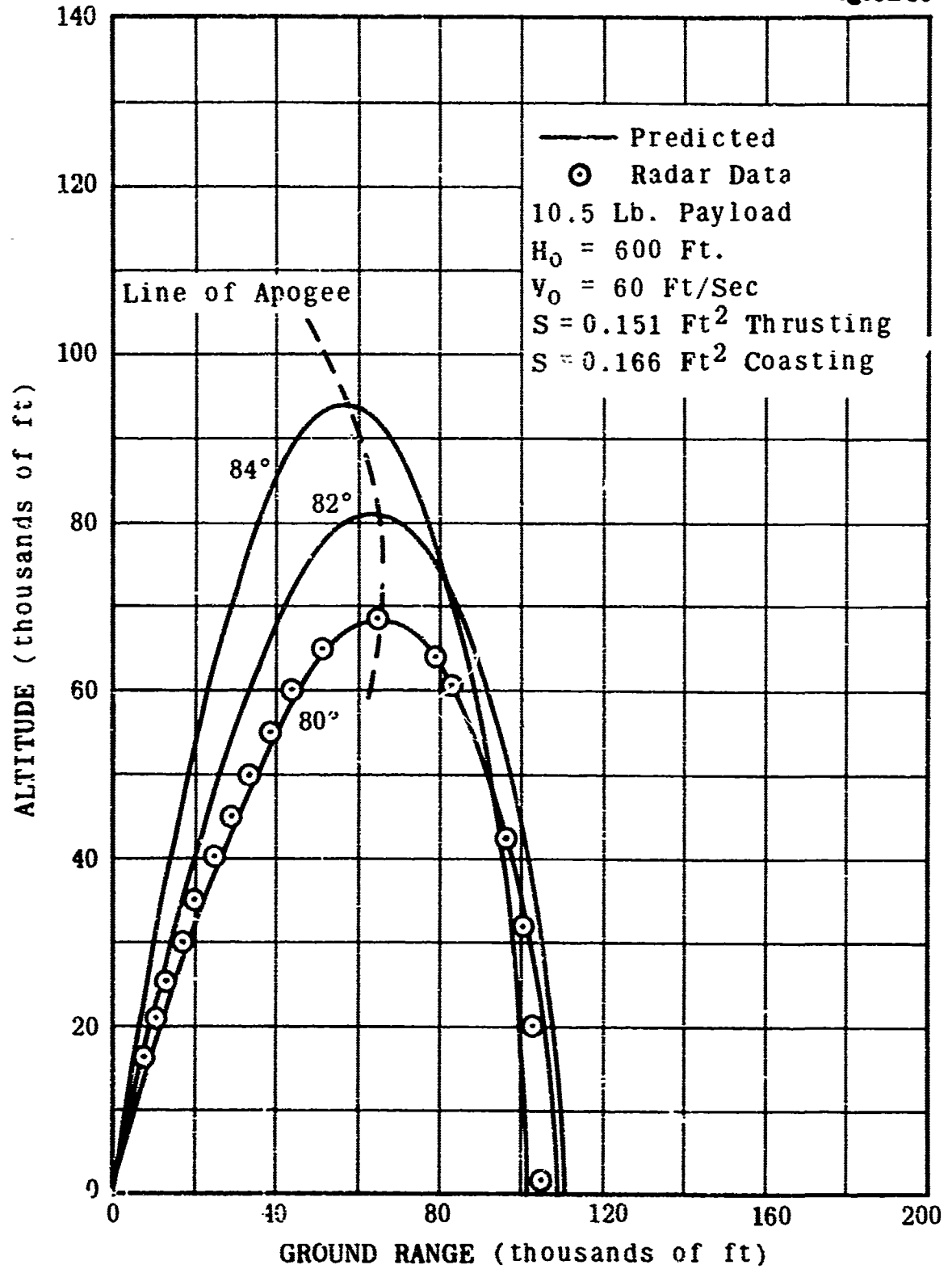


Figure 13

Frangible ARCAS Flight Test AFFT-3 Critique

5245

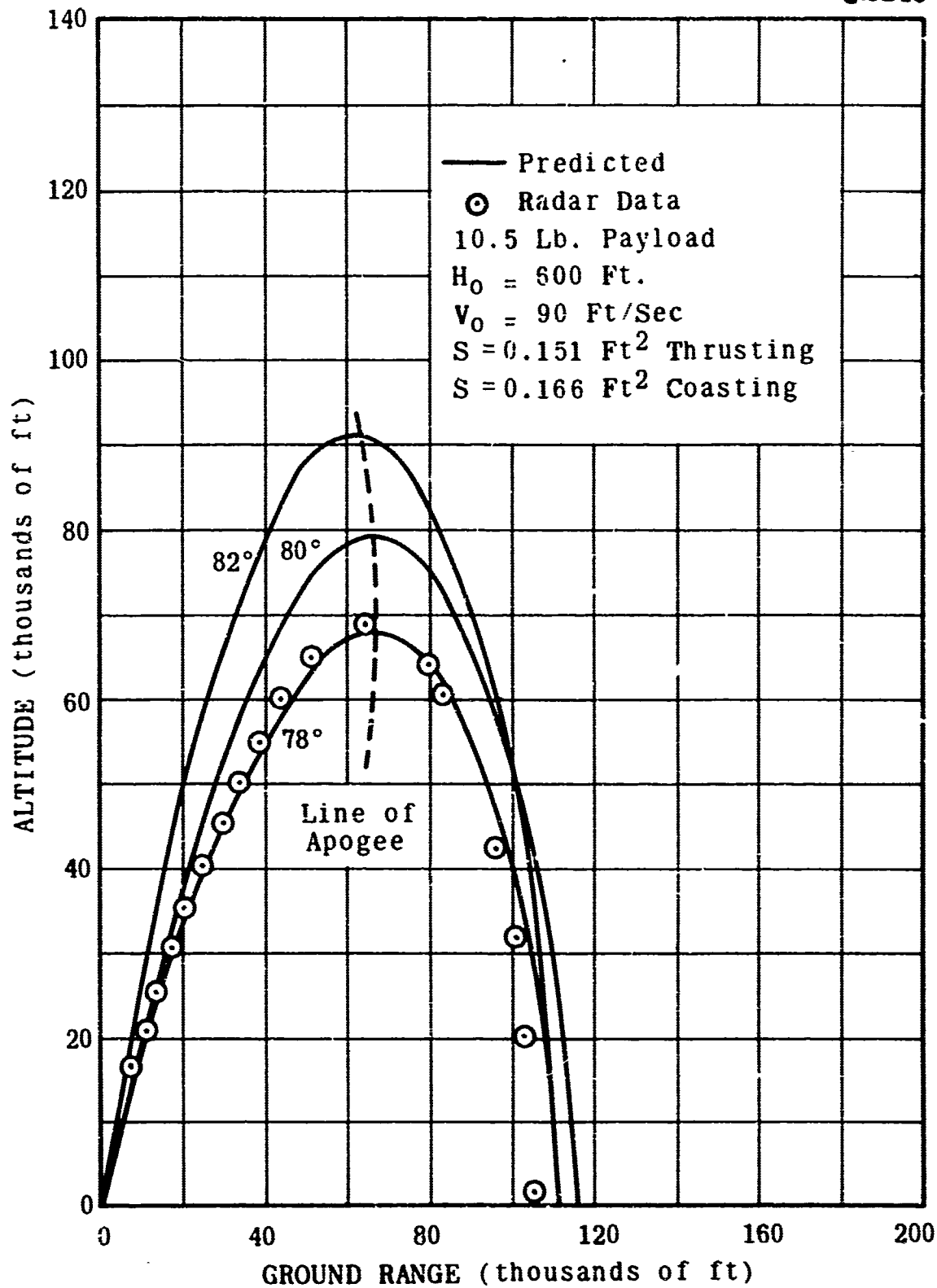


Figure 14

Managible ARCAS Flight Test AFFT-3 Critique

5243

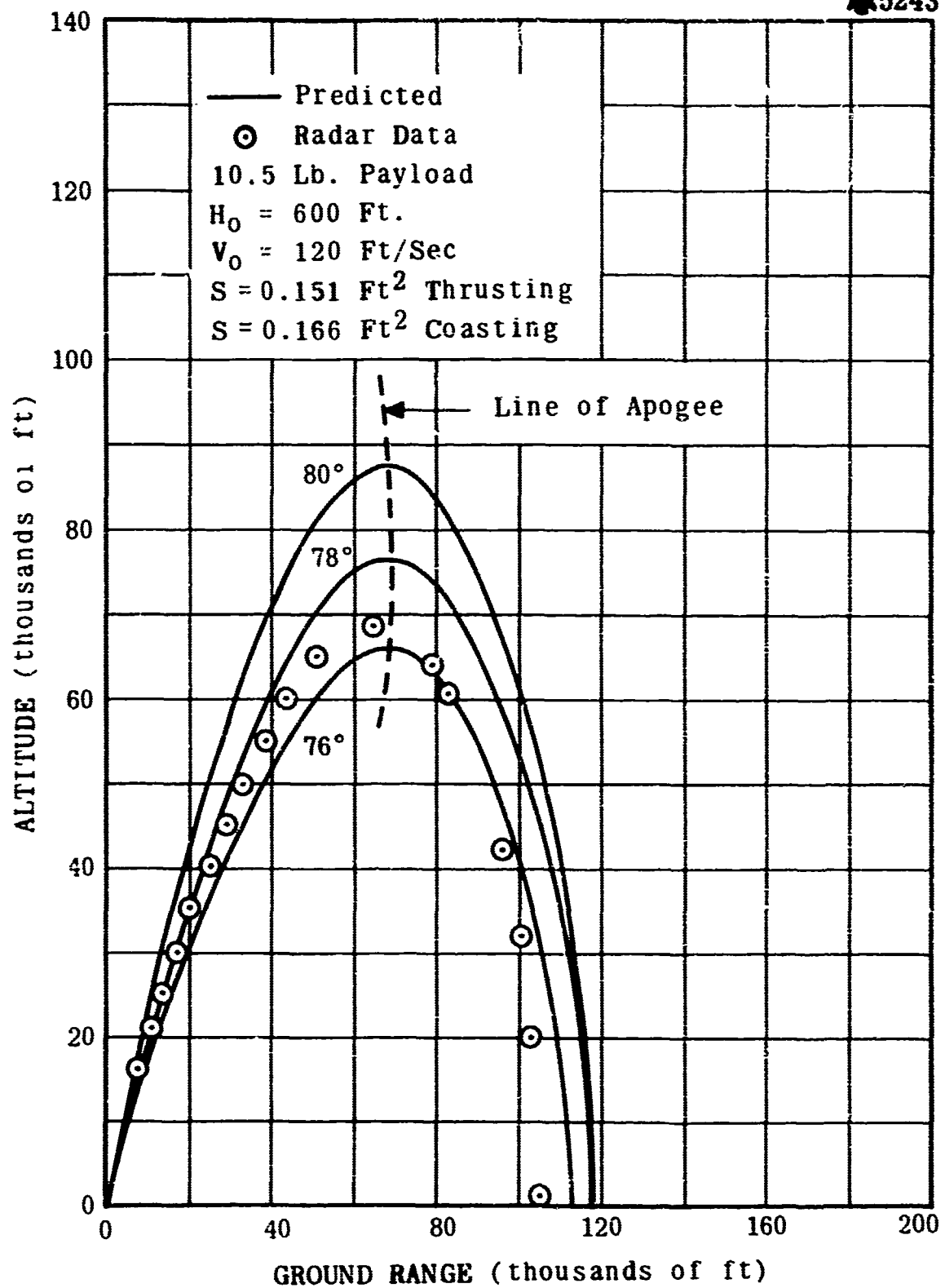
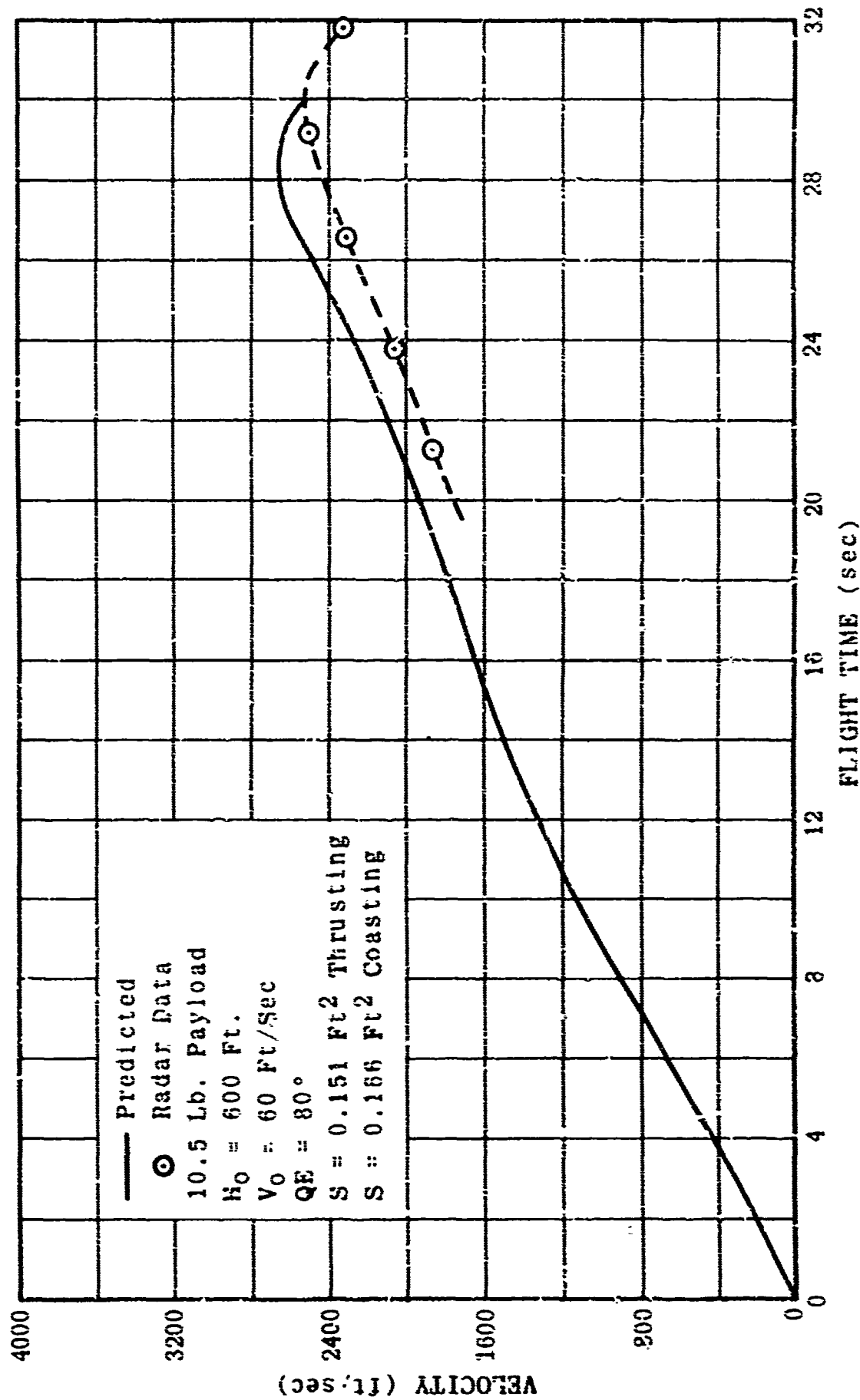


Figure 15

Frangible ARCAS Flight Test AFFT-3 Critique



5244

Figure 16

Frangible ARCAS Flight Test AFFT-3 Critique

5242

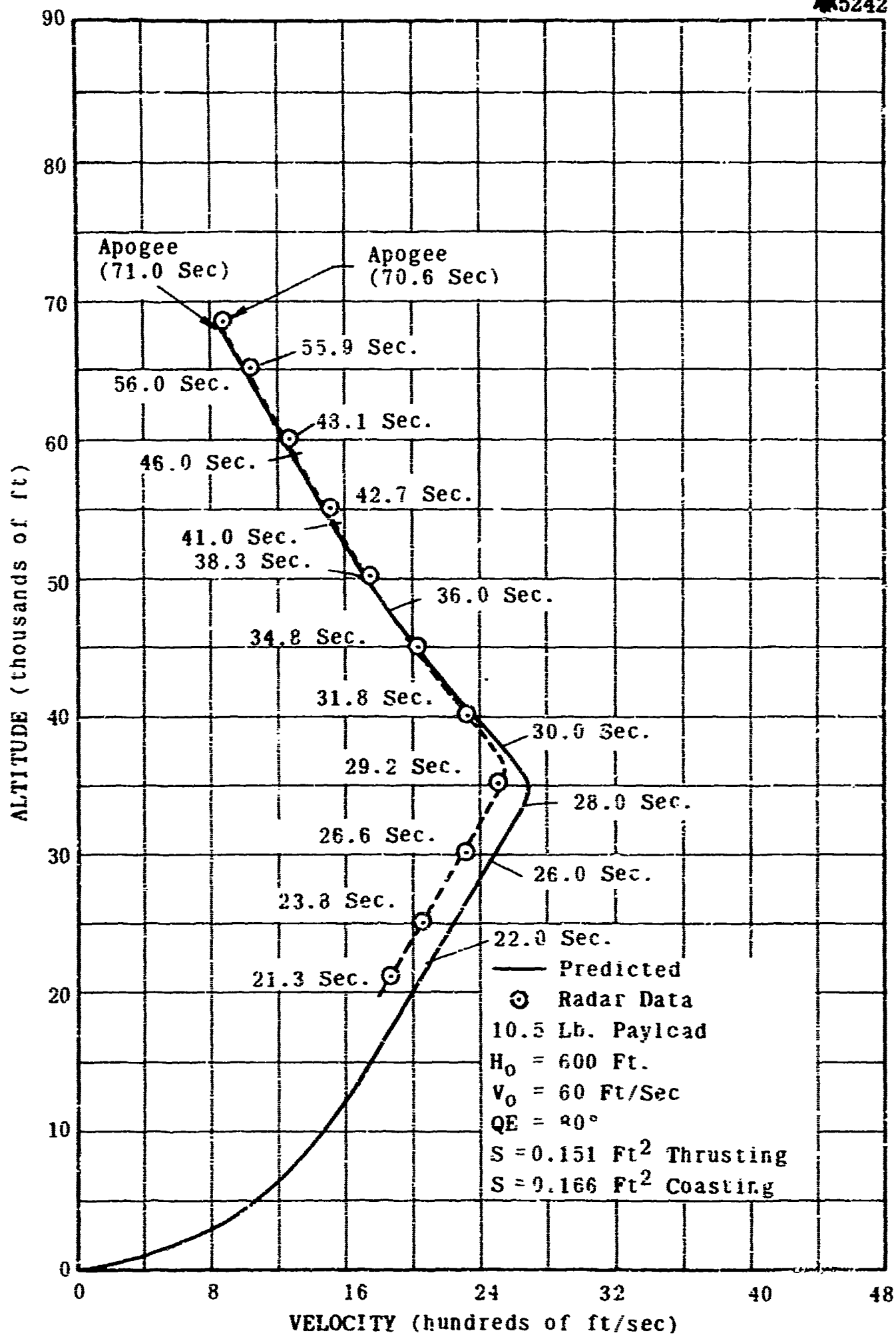


Figure 17

Frangible ARCAS Trajectory Profiles Phase III Systems Vehicle

8779

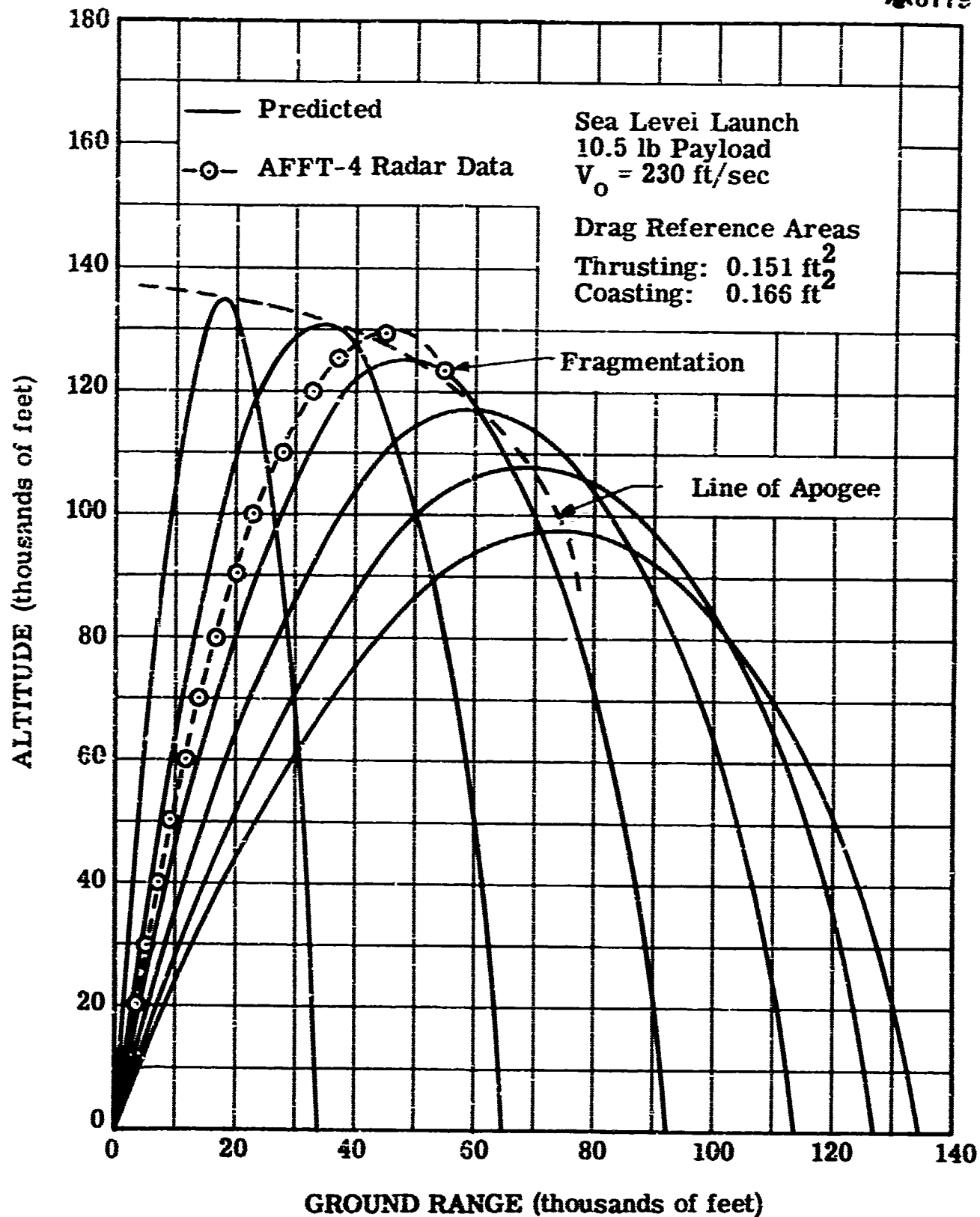


Figure 18

Frangible ARCAS Velocity Versus Flight Time

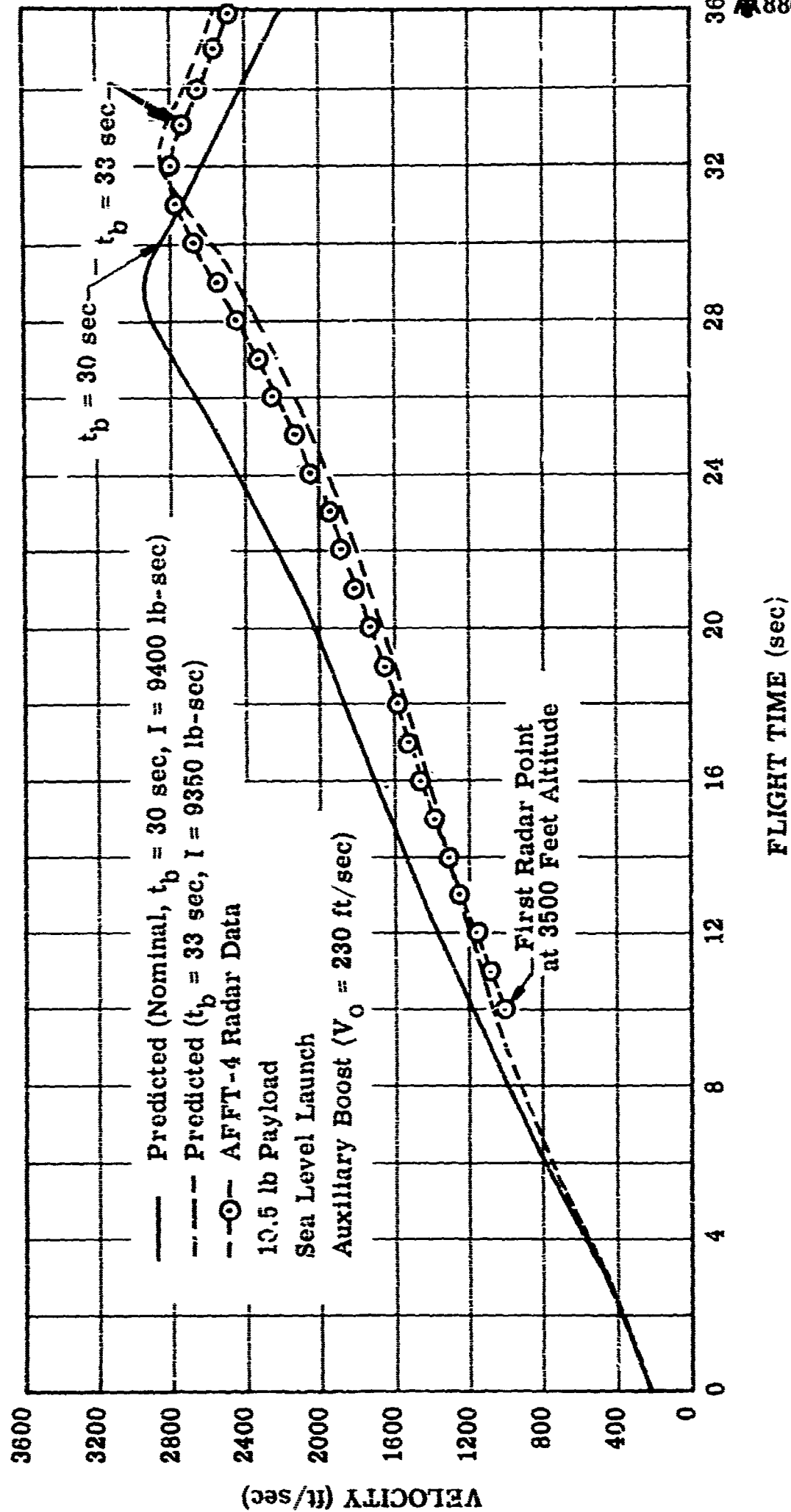


Figure 19

Frangible ARCAS Altitude Versus Vehicle Velocity

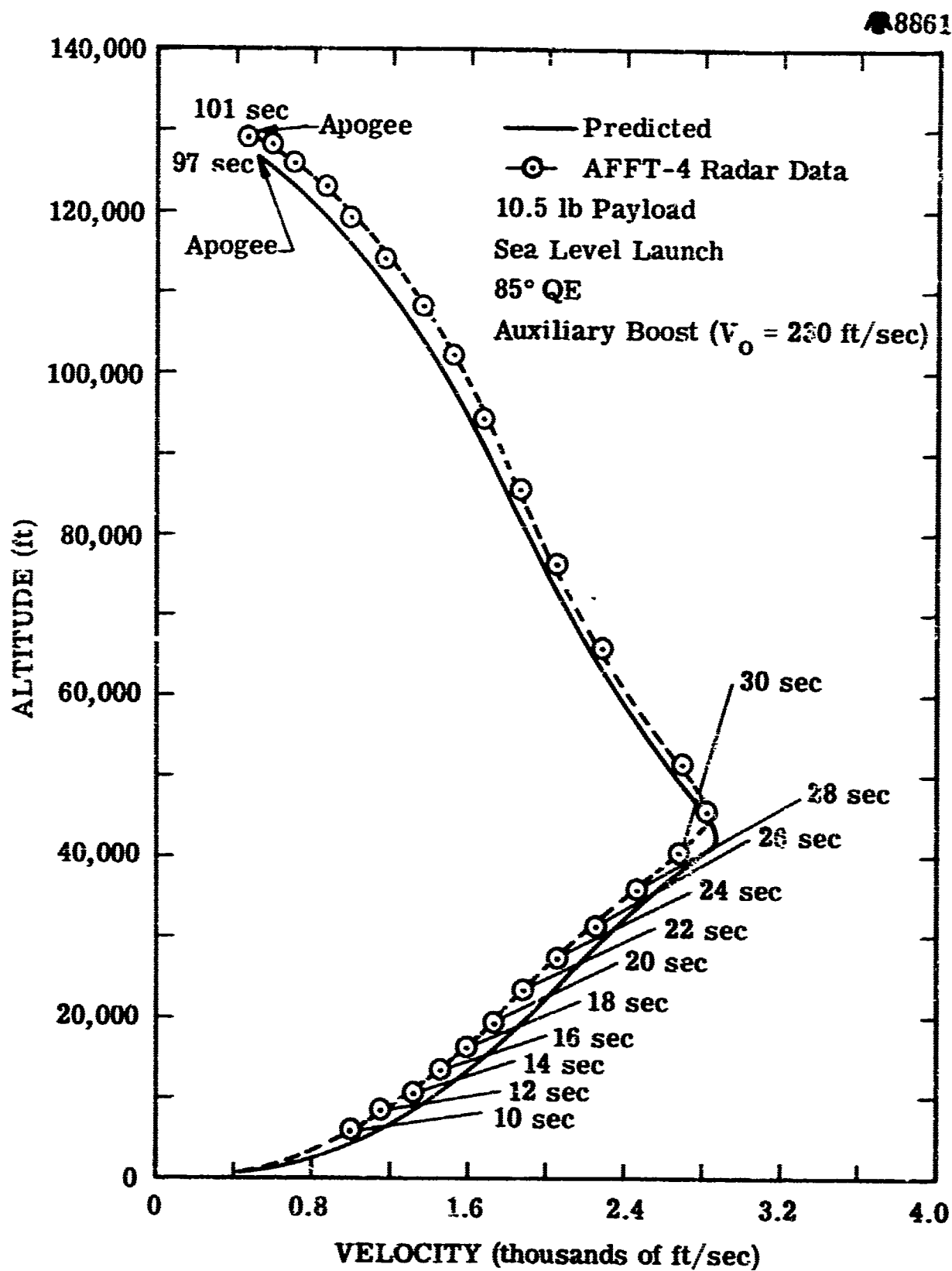


Figure 20

Frangible ARCAS Trajectory Profile Flight Test AFFT-4

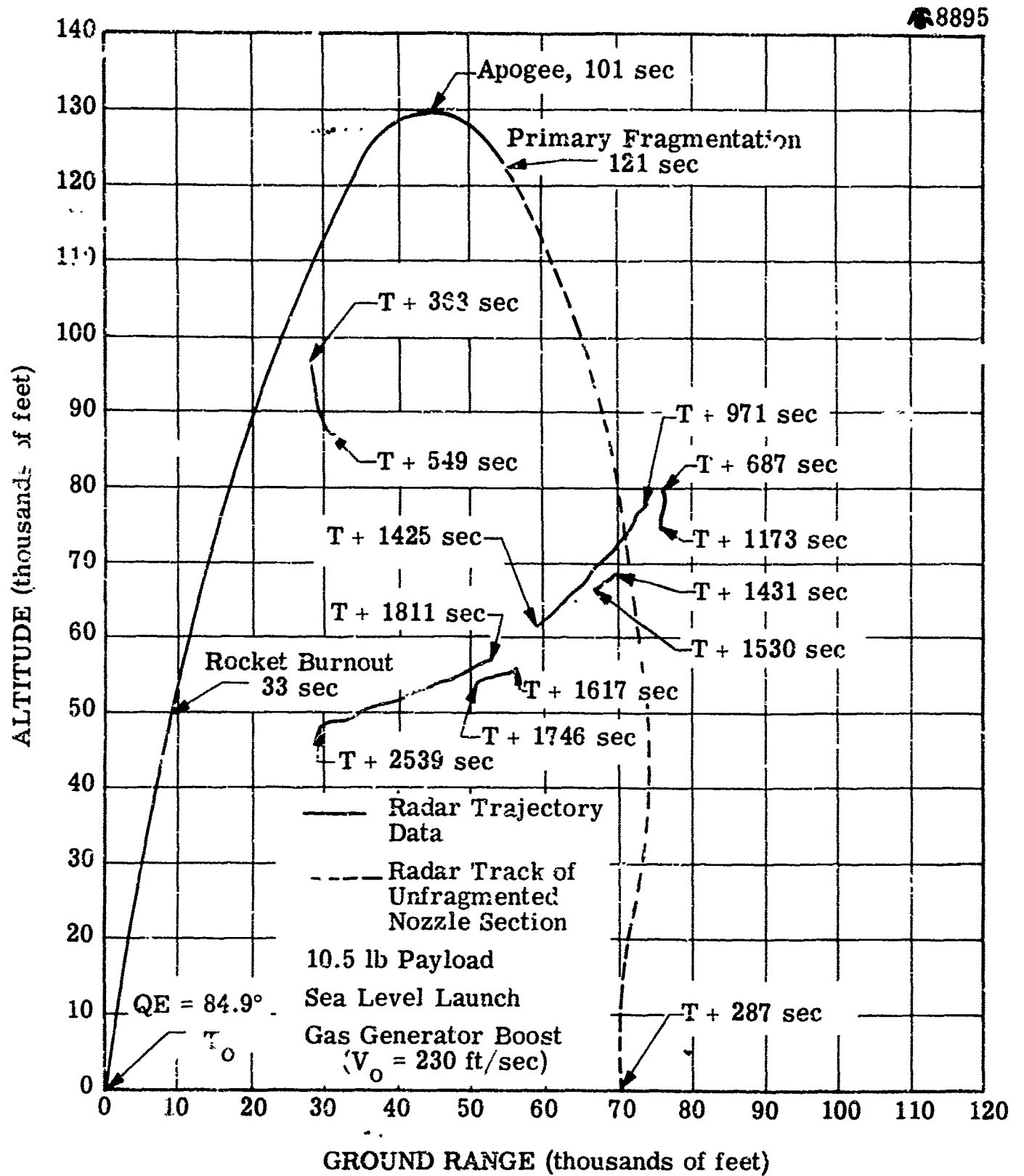


Figure 21

Unclassified

Security Classification

DOCUMENT CONTROL DATA - R&D		
(Security classification of title, body of abstract and indexing annotation must be entered when the overall report is classified)		
1. ORIGINATING ACTIVITY (Corporate author) Atlantic Research Corporation Shirley Highway at Edsall Road Alexandria, Virginia		2a. REPORT SECURITY CLASSIFICATION UNCLASSIFIED
3. REPORT TITLE Development of the Frangible ARGAS Meteorological Rocket Vehicle		2b. GROUP
4. DESCRIPTIVE NOTES (Type of report and inclusive dates) Final Scientific Report, April 1964-December 1965 Approved: 16 March 66		
5. AUTHOR(S) (Last name, first name, initial) Oss, George K.		
6. REPORT DATE 15 February 1966	7a. TOTAL NO. OF PAGES 245	7b. NO. OF REFS 0
8a. CONTRACT OR GRANT NO. AF19 (628)-4033	9a. ORIGINATOR'S REPORT NUMBER(S) TRPL 8895	
b. PROJECT AND TASK NO. 6670, 03	9b. OTHER REPORT NO(S) (Any other numbers that may be assigned this report) AFCRL 66-157	
c. DOD ELEMENT 62405394		
d. DOD SUBELEMENT 681000		
10. AVAILABILITY/LIMITATION NOTICES Distribution of this document is unlimited.		
11. SUPPLEMENTARY NOTES	12. SPONSORING MILITARY ACTIVITY Air Force Cambridge Research Labs, Office of Aerospace Research (CRE) United States Air Force Bedford, Massachusetts	
13. ABSTRACT <p>Development of the Frangible ARGAS vehicle was successfully completed and demonstrated during this program. Two of seven static tests completed during this program, designated Phase III, included successful fragmentation of the spent rocket motor assembly to particle sizes yielding kinetic impact energy levels less than 3.0 ft-lbs. Further analysis showed that maximum energy levels of 1.5 ft-lbs. could be achieved with the existing configuration with only minor modification of the nozzle section.</p> <p>Four flight tests were conducted during the program, two of which included all systems. The initial tests established the flight temperature environment experienced by the explosive fragmentation system. The first systems flight was considered a "No Test" because of a malfunction induced by the government modified launcher. The final flight test successfully demonstrated vehicle performance, payload ejection at apogee and subsequent vehicle fragmentation as programmed. This flight test fulfilled the primary objective of the program by demonstrating the feasibility of a frangible meteorological rocket system.</p>		

DD FORM 1473
1 JAN 64

Unclassified

Security Classification

Unclassified

Security Classification

14.	KEY WORDS	LINK A		LINK B		LINK C	
		ROLE	WT	ROLE	WT	ROLE	WT
	Frangible ARCAS Fragmentation Particle Sizes Impact Kinetic Energy Temperature Environment Explosive Flight Test Demonstrated Objective Feasibility Meteorological Rocket System						

INSTRUCTIONS

1. **ORIGINATING ACTIVITY:** Enter the name and address of the contractor, subcontractor, grantee, Department of Defense activity or other organization (*corporate author*) issuing the report.
- 2a. **REPORT SECURITY CLASSIFICATION:** Enter the overall security classification of the report. Indicate whether "Restricted Data" is included. Marking is to be in accordance with appropriate security regulations.
- 2b. **GROUP:** Automatic downgrading is specified in DoD Directive 5200.10 and Armed Forces Industrial Manual. Enter the group number. Also, when applicable, show that optional markings have been used for Group 3 and Group 4 as authorized.
3. **REPORT TITLE:** Enter the complete report title in all capital letters. Titles in all cases should be unclassified. If a meaningful title cannot be selected without classification, show title classification in all capitals in parenthesis immediately following the title.
4. **DESCRIPTIVE NOTES:** If appropriate, enter the type of report, e.g., interim, progress, summary, annual, or final. Give the inclusive dates when a specific reporting period is covered.
5. **AUTHOR(S):** Enter the name(s) of author(s) as shown on or in the report. Enter last name, first name, middle initial. If military, show rank and branch of service. The name of the principal author is an absolute minimum requirement.
6. **REPORT DATE:** Enter the date of the report as day, month, year, or month, year. If more than one date appears on the report, use date of publication.
- 7a. **TOTAL NUMBER OF PAGES:** The total page count should follow normal pagination procedures, i.e., enter the number of pages containing information.
- 7b. **NUMBER OF REFERENCES:** Enter the total number of references cited in the report.
- 8a. **CONTRACT OR GRANT NUMBER:** If appropriate, enter the applicable number of the contract or grant under which the report was written.
- 8b, 8c, & 8d. **PROJECT NUMBER:** Enter the appropriate military department identification, such as project number, subproject number, system numbers, task number, etc.
- 9a. **ORIGINATOR'S REPORT NUMBER(S):** Enter the official report number by which the document will be identified and controlled by the originating activity. This number must be unique to this report.
- 9b. **OTHER REPORT NUMBER(S):** If the report has been assigned any other report numbers (*either by the originator or by the sponsor*), also enter this number(s).

10. **AVAILABILITY/LIMITATION NOTICES:** Enter any limitations on further dissemination of the report, other than those imposed by security classification, using standard statements such as:

- (1) "Qualified requesters may obtain copies of this report from DDC."
- (2) "Foreign announcement and dissemination of this report by DDC is not authorized."
- (3) "U. S. Government agencies may obtain copies of this report directly from DDC. Other qualified DDC users shall request through _____."
- (4) "U. S. military agencies may obtain copies of this report directly from DDC. Other qualified users shall request through _____."
- (5) "All distribution of this report is controlled. Qualified DDC users shall request through _____."

If the report has been furnished to the Office of Technical Services, Department of Commerce, for sale to the public, indicate this fact and enter the price, if known.

11. **SUPPLEMENTARY NOTES:** Use for additional explanatory notes.
12. **SPONSORING MILITARY ACTIVITY:** Enter the name of the departmental project office or laboratory sponsoring (*paying for*) the research and development. Include address.
13. **ABSTRACT:** Enter an abstract giving a brief and factual summary of the document indicative of the report, even though it may also appear elsewhere in the body of the technical report. If additional space is required, a continuation sheet shall be attached.

It is highly desirable that the abstract of classified reports be unclassified. Each paragraph of the abstract shall end with an indication of the military or security classification of the information in the paragraph, represented as (TS), (S), (C), or (U).

There is no limitation on the length of the abstract. However, the suggested length is from 150 to 225 words.

14. **KEY WORDS:** Key words are technically meaningful terms or short phrases that characterize a report and may be used as index entries for cataloging the report. Key words must be selected so that no security classification is required. Identifiers, such as equipment model designation, trade name, military project code name, geographic location, may be used as key words but will be followed by an indication of technical context. The assignment of links, rules, and weights is optional.

Unclassified

Security Classification